National Nanotechnology Coordinated Infrastructure (NNCI)

Research and Education Highlights

Year 9 (October 2023 – September 2024)

National Nanotechnology Coordinated Infrastructure

NSF

Table of Contents

National Nanotechnology Coordinated Infrastructure

Center for Nanoscale Systems (CNS)

National Nanotechnology Coordinated Infrastructure

On-chip multi-degree-of-freedom control of two-dimensional materials

Two-dimensional materials (2DM) and their heterostructures offer tunable electrical and optical properties, primarily modifiable through electrostatic gating and twisting. Although electrostatic gating is a well-established method for manipulating 2DM, achieving real-time control over interfacial properties remains challenging in exploring 2DM physics and advanced quantum device technology. Current methods, often reliant on scanning microscopes, are limited in their scope of application, lacking the accessibility and scalability of electrostatic gating at the device level. Here introduced is an on-chip platform for 2DM with in situ adjustable interfacial properties, using a microelectromechanical system (MEMS). This platform comprises compact and cost-effective devices with the ability of precise voltage-controlled manipulation of 2DM, including approaching, twisting and pressurizing actions. This technology is demonstrated by creating synthetic topological singularities, such as merons, in the nonlinear optical susceptibility of twisted hexagonal boron nitride (h-BN). A key application of this technology is the development of integrated light sources with real-time and wide-range tunable polarization. Furthermore, a quantum analogue that can generate entangled photon pairs with adjustable entanglement properties is predicted. This work extends the abilities of existing technologies in manipulating low-dimensional quantum materials and paves the way for new hybrid two- and three-dimensional devices, with promising implications in condensed-matter physics, quantum optics and related fields.

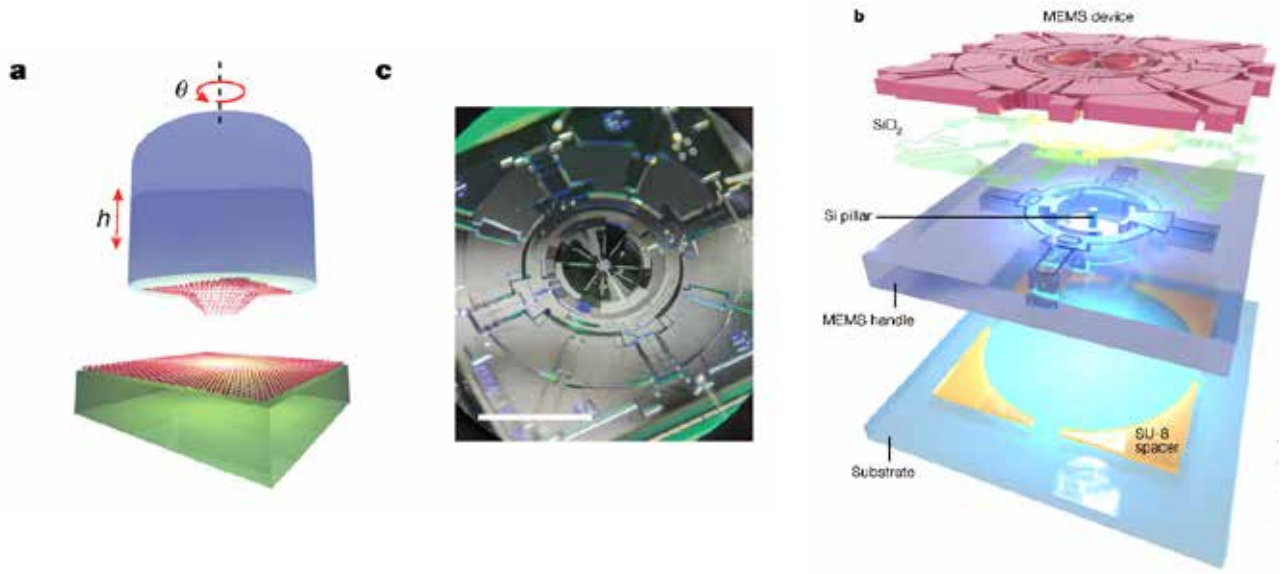

Fig. 1: MEGA2D, an on-chip MEMS platform for twisting 2D materials. ***a****, Illustration of the high-level idea of controlling the stacking in 2DM heterostructures using nanomechanical systems. We wish to control the twist angle θ and distance h between two 2DM independently.* ***b****, Exploded schematic of the main components in a MEGA2D device.* ***c,*** *Photograph of a fully assembled MEGA2D device. Scale bar, 2 mm*

Haoning Tang, Yiting Wang, Xueqi Ni, Kenji Watanabe, Takashi Taniguchi, Pablo Jarillo-Herrero, Shanhui Fan, Eric Mazur, Amir Yacoby & Yuan Ca;
School of Engineering and Applied Sciences, Harvard, National Institute for Materials Science, Tsukuba, Japan, Department of Physics, MIT, Department of Applied Physics and Ginzton Laboratory, Stanford University, Department of Physics, Harvard, Society of Fellows, Harvard, Department of Electrical Engineering and Computer Science, University of California-Berkeley.

This work was supported by NSF Award # ECCS-2025158. *Nature* Vol 632, 29 August 2024

National Research Priority: NSF - Quantum Leap

National Nanotechnology Coordinated Infrastructure

Center for Nanoscale Systems, Harvard University

Ultrafast high-endurance memory based on sliding ferroelectrics

The persistence of voltage-switchable collective electronic phenomena down to the atomic scale has extensive implications for area- and energy-efficient electronics, especially in emerging nonvolatile memory technology. We investigate the performance of a ferroelectric field-effect transistor (FeFET) based on sliding ferroelectricity in bilayer boron nitride at room temperature. Sliding ferroelectricity represents a different form of atomically thin two-dimensional (2D) ferroelectrics, characterized by the switching of out-of-plane polarization through interlayer sliding motion. We examined the FeFET device employing monolayer graphene as the channel layer, which demonstrated ultrafast switching speeds on the nanosecond scale and high endurance exceeding 10 11 switching cycles, comparable to state-of-the-art FeFET devices. These characteristics highlight the potential of 2D sliding ferroelectrics for inspiring next-generation nonvolatile memory technology.

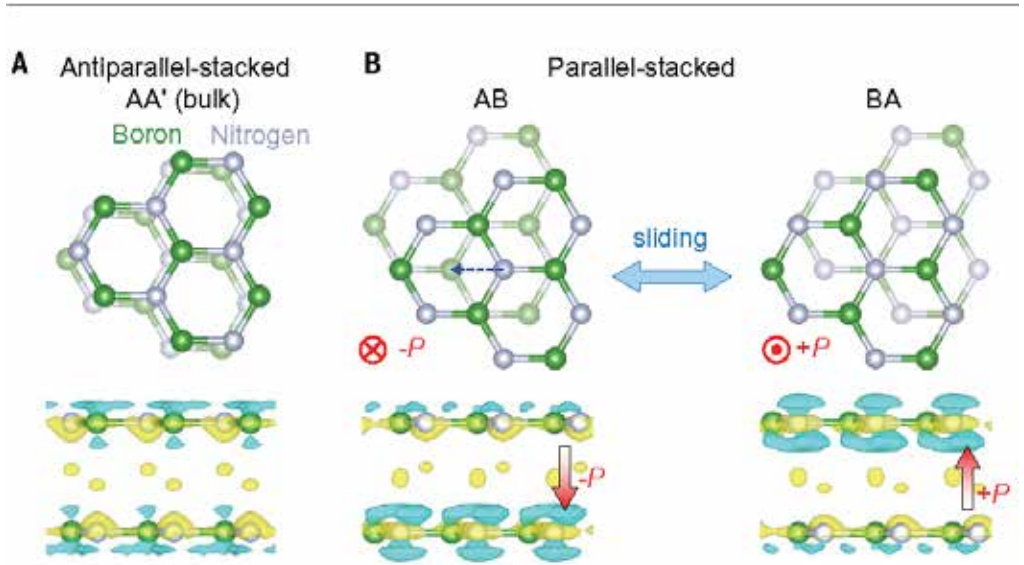

Fig. 1. Basic characteristics of a ferroelectric field-effect transistor based on sliding ferroelectrics. (A) Schematic of the crystal structure of antiparallel-stacked bilayer boron nitride with AA' stacking. Nitrogen and boron atoms are displayed in silver and green, respectively. The bottom panel shows the differential charge distribution mapping. The yellow and blue region corresponds to the increased negative and positive charge as compared to a monolayer, respectively. The figures are drawn using VESTA (44). (B) Schematic of the crystal structures of parallel-stacked bilayer boron nitride. AB and BA stacking creates out-of-plane ferroelectric polarization in opposite directions, which can be switched by the interlayer sliding motion, denoted by the dotted blue line.

Kenji Yasuda, Evan Zalys-Geller, Xirui Wang, Daniel Bennett, Suraj S. Cheema, Kenji Watanabe, Takashi Taniguchi, Efthimios Kaxiras, Pablo Jarillo-Herrero, Raymond Ashoori1*; *Department of Physics, MIT, 2School of Applied and Engineering Physics, Cornell University, John A. Paulson School of Engineering and Applied Sciences, Harvard University. Research Laboratory of Electronics, MIT, 5Research Center for Electronic and Optical Materials, National Institute for Materials Science, Tsukuba, Japan; Research Center for Materials Nanoarchitectonics, National Institute for Materials Science, Tsukuba, Japan; Department of Physics, Harvard.*

This work was supported by NSF Award # ECCS-2025158. *Science* Vol 385, (53-56) 2024

National Research Priority: NSF - Quantum Leap

National Nanotechnology Coordinated Infrastructure

Center for Nanoscale Systems
Harvard University
FAS • SEAS

Metasurface-enabled single-shot and complete Mueller matrix imaging

When light scatters off an object, its polarization, in general, changes—a transformation described by the object's Mueller matrix. Mueller matrix imaging is an important technique in science and technology to image the spatially varying polarization response of an object of interest, to reveal rich information otherwise invisible to traditional imaging. Here we conceptualize, implement and demonstrate a compact Mueller matrix imaging system—composed of a metasurface to produce structured polarization illumination and a metasurface for polarization analysis—that can, in a single shot, acquire all 16 components of an object's spatially varying Mueller matrix over an image. Our implementation, which is free of any moving parts or bulk polarization optics, should enable and empower applications in real-time medical imaging, material characterization, machine vision, target detection and other important areas.

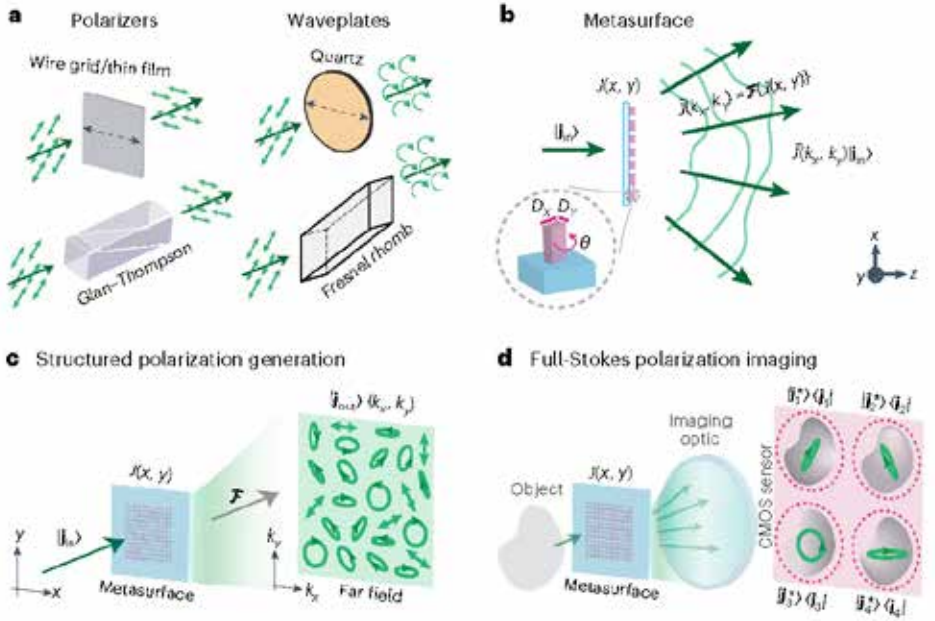

Fig. 1 | Conventional polarization optics versus metasurfaces. ***a,*** *Examples of conventional polarization optics; owing to their bulk polarization response.* ***b****, A metasurface—which can be described by a spatially varying Jones matrix distribution J(x, y), and a far-field polarization response. Each nanopillar provides three degrees of freedom—pillar length DX, pillar width DY and pillar orientation θ; the metasurface, composed of thousands of such nanopillars, has many degrees of freedom that can be optimized for the desired polarization response.* ***c****, A metasurface can be used for 'structured polarization' generation, where, for an incident polarization state || jin⟩, the far-field output || jout⟩ (kx, ky), given by J̃(kx, ky) || jin⟩, follows a user-specified polarization distribution. d, A metasurface can also be designed to function as a polarization analyser with a Jones matrix response; ~J =||j∗(kx, ky)⟩⟨j(kx, ky)||, in the far field. A (periodic) metasurface—which splits the incoming light into its first four diffraction orders, and simultaneously analyses for four different polarization states—alongside an imaging lens and a sensor, can perform full-Stokes imaging.*

Aun Zaidi, Noah A. Rubin, Maryna L. Meretska, Lisa W. Li , Ahmed H. Dorrah 1, Joon-Suh Park 1 & Federico Capasso; *John A. Paulson School of Engineering and Applied Sciences, Harvard University, Department of Electrical and Computer Engineering, University of California-San Diego, 3Institute of Nanotechnology, Karlsruhe Institute of Technology.*

This work was supported by NSF Award # ECCS-2025158. *Nature Photonics* Vol 18, July 2024

Silk fibroin as a surfactant for water-based nanofabrication

Water-based processing plays a crucial role in high technology, especially in electronics, material sciences and life sciences, with important implications in the development of high-quality reliable devices, fabrication efficiency, safety and sustainability. At the micro- and nanoscale, water is uniquely enabling as a bridge between biological and technological systems. However, new approaches are needed to overcome fundamental challenges that arise from the high surface tension of water, which hinders wetting and, thus, fabrication at the bio–nano interface. Here we report the use of silk fibroin as a surfactant to enable water-based processing of nanoscale devices. Even in minute quantities (for example, 0.01 w/v%), silk fibroin considerably enhances surface coverage and outperforms commercial surfactants in precisely controlling interfacial energy between water-based solutions and hydrophobic surfaces. This effect is ascribed to the amphiphilic nature of the silk molecule and its adaptive adsorption onto substrates with diverse surface energy, facilitating intermolecular interactions between unlikely pairs of materials. The approach's versatility is highlighted by manufacturing water-processed nanodevices, ranging from transistors to photovoltaic cells. Its performance is found to be equivalent to analogous vacuum-processed devices, underscoring the utility and versatility of this approach for water-based nanofabrication.

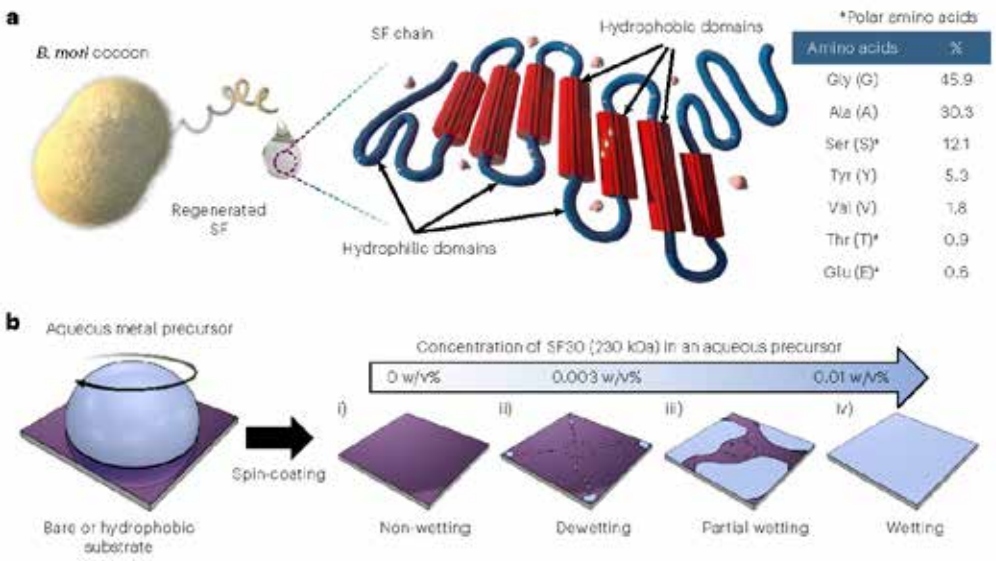

Fig. 1 | SF as a natural surfactant. a, Schematic diagram illustrating amphiphilicity of regenerated SF chain. b, Schematic illustration of the improvement in surface coverage achieved by spin-coating a metal hydrate solution with increasing concentrations of SF.

Taehoon Kim 1, Beom Joon Kim 1, Giorgio E. Bonacchini2, Nicholas A. Ostrovsky-Snider 1 & Fiorenzo G. Omenetto*; Silklab, Department of Biomedical Engineering, Tufts University, Istituto Italiano di Tecnologia, Department of Physics, Tufts University, Department of Electrical and Computer Engineering, Tufts University.*

This work was supported by NSF Award # ECCS-2025158. *Nature Nanotechnology* Vol 19, October 2024

Electrical manipulation of telecom color centers in silicon

Silicon color centers have recently emerged as promising candidates for commercial quantum technology, yet their interaction with electric fields has yet to be investigated. In this paper, we demonstrate electrical manipulation of telecom silicon color centers by implementing novel lateral electrical diodes with an integrated G center ensemble in a commercial silicon on insulator wafer. The ensemble optical response is characterized under application of a reverse-biased DC electric field, observing both 100% modulation of fluorescence signal, and wavelength redshift of approximately 1.24 ± 0.08 GHz/V above a threshold voltage. Finally, we use G center fluorescence to directly image the electric field distribution within the devices, obtaining insight into the spatial and voltage-dependent variation of the junction depletion region and the associated mediating effects on the ensemble. Strong correlation between emitter-field coupling and generated photocurrent is observed. Our demonstration enables electrical control and stabilization of semiconductor quantum emitters.

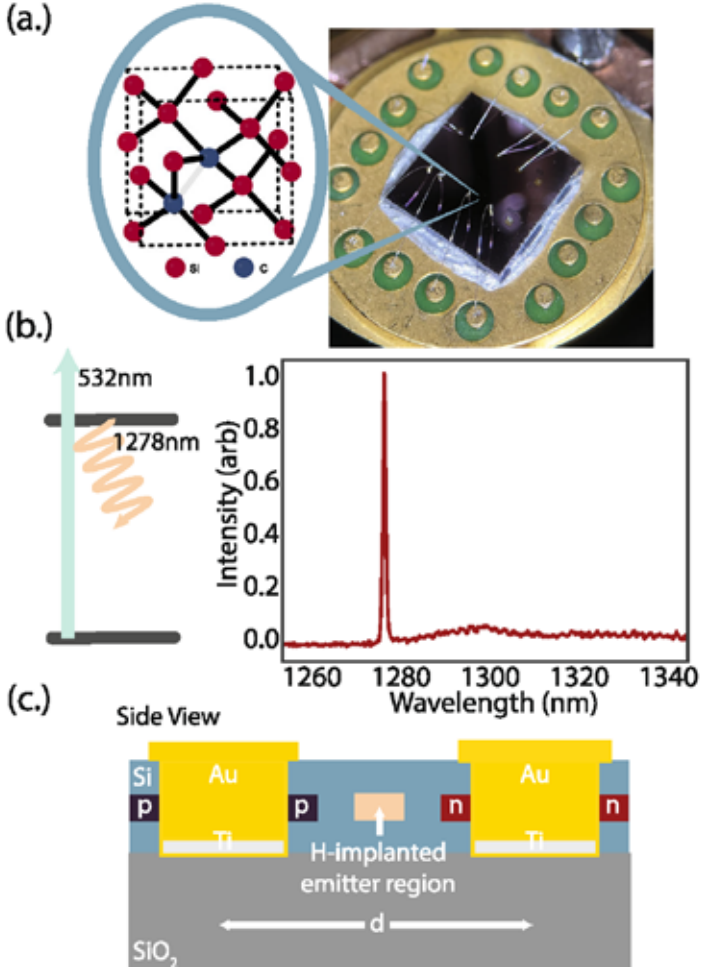

*Fig. 1 | Diode-integrated silicon G centers. **A** Carbon-related silicon color centers are integrated into lateral p+-p-n+ junctions (diodes) fabricated in silicon on insulator and electrically driven by a wire-bonded 16-pin helium cryostat connector. **b** The color centers are optically excited by a 532 nmlaser and fluoresce at 1278 nm in the telecommunication O-Band. **c** Side profile of fabricated diodes. P- and n-doping is achieved via ion implantation, and hydrogen is locally incorporated to selectively form G centers at the junction center.*

Aaron M. Day, Madison Sutula, Jonathan R. Dietz, Alexander Raun, Denis D. Sukachev, Mihir K. Bhaskar & Evelyn L. Hu; *John A. Paulson School of Engineering and Applied Sciences, Harvard, Department of Physics, Harvard, AWS Center for Quantum Networking.*

This work was supported by NSF Award # ECCS-2025158. *Nature Communications* Vol 15, 29 (2024)

National Research Priority: NSF - Quantum Leap

National Nanotechnology Coordinated Infrastructure

Center for Nanoscale Systems, Harvard University

Telecom Networking with a Diamond Quantum Memory

Practical quantum networks require interfacing quantum memories with existing channels and systems that operate in the telecom band. Here we demonstrate low-noise, bidirectional quantum frequency conversion that enables a solid-state quantum memory to directly interface with telecom-band systems. In particular, we demonstrate conversion of visible-band single photons emitted from a silicon-vacancy (SiV) center in diamond to the telecom O band, maintaining low noise (g2(0) < 0.1) and high indistinguishability (V = 89 ± 8%). We further demonstrate the utility of this system for quantum networking by converting telecom-band time-bin pulses, sent across a lossy and noisy 50-km deployed fiber link, to the visible band and entangling them with a diamond quantum memory with fidelity F ≥ 87 2.5%. These results demonstrate the viability of SiV quantum memories integrated with telecom band systems for scalable quantum networking applications

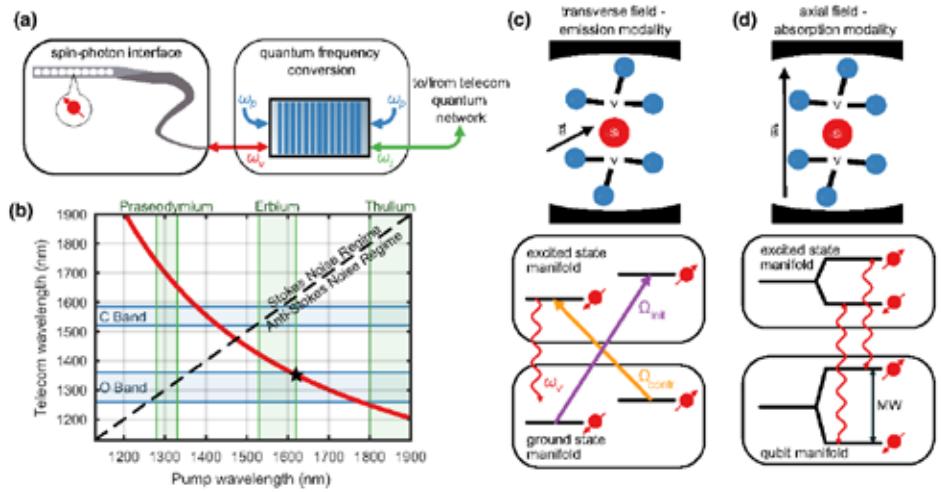

FIG. 1. (a) Quantum networks based on a spin-photon interface with a single atomlike defect center such as silicon-vacancy centers in diamond coupled to a nanophotonic cavity. Such memories often exhibit visible emission frequencies ωv, necessitating quantum frequency conversion (QFC) to a telecom frequency ωt mediated by a pump at ωp . (b) The parameter space for low-noise QFC using a single $\chi^{(2)}$-based conversion step. The red line indicates conversion schemes that can be performed for the SiV's 737-nm transition, the blue shaded regions indicate the low-loss telecom O and C bands, and green shaded regions indicate what conversion processes can be easily pumped given common gain materials. The black star indicates our conversion scheme. (c) SiV emission modality: an SiV in an overcoupled cavity and a transverse external magnetic field can be driven coherently with alternating initialization (Winit) and control optical pulses (Wcontr) to emit single photons near 737 nm (ωv). (d) SiV absorption modality: an SiV in a critically coupled cavity and an axial external magnetic field exhibits spin-conserving optical transitions that yield spin-dependent cavity reflectivity, enabling entanglement with an incoming photonic qubit at ω_v.

Eric Bersin, Madison Sutula, Yan Qi Huan, Aziza Suleymanzade, Daniel R. Assumpcao, Yan-Cheng Wei, Pieter-Jan Stas, Can M. Knaut, Erik N. Knall, Carsten Langrock, Neil Sinclair, Ryan Murphy, Ralf Riedinger , Matthew Yeh ,C.J. Xin, Saumil Bandyopadhyay , Denis D. Sukachev , Bartholomeus Machielse, David S. Levonian, Mihir K. Bhaskar, Scott Hamilton, Hongkun Park, Marko Lonˇcar, Martin M. Fejer , P. Benjamin Dixon, Dirk R. Englund, and Mikhail D. Lukin; *Lincoln Laboratory, MIT, Department of Electrical Engineering and Computer Science, MIT, Department of Physics, Harvard, John A. Paulson School of Engineering and Applied Sciences, Harvard, Ginzton Laboratory, Stanford University, Institut für Laserphysik und Zentrum für Optische Quantentechnologien, Universität Hamburg, The Hamburg Centre for Ultrafast Imaging, AWS Center for Quantum Networking, Department of Chemistry and Chemical Biology, Harvard.*

This work was supported by NSF Award # ECCS-2025158. *PRX QUANTUM* 5, 010303 (2024)

National Research Priority: NSF - Quantum Leap

National Nanotechnology Coordinated Infrastructure

Center for Nanoscale Systems Harvard University FAS • SEAS

Quantum metric nonlinear Hall effect in a topological antiferromagnetic heterostructure

Quantum geometry in condensed-matter physics has two components: the real part quantum metric and the imaginary part Berry curvature. Whereas the effects of Berry curvature have been observed through phenomena such as the quantum Hall effect in two-dimensional electron gases and the anomalous Hall effect (AHE) in ferromagnets, the quantum metric has rarely been explored. Here, we report a nonlinear Hall effect induced by the quantum metric dipole by interfacing even layered MnBi2 Te4 with black phosphorus. The quantum metric nonlinear Hall effect switches direction upon reversing the antiferromagnetic (AFM) spins and exhibits distinct scaling that is independent of the scattering time. Our results open the door to discovering quantum metric responses predicted theoretically and pave the way for applications that bridge nonlinear electronics with AFM spintronics.

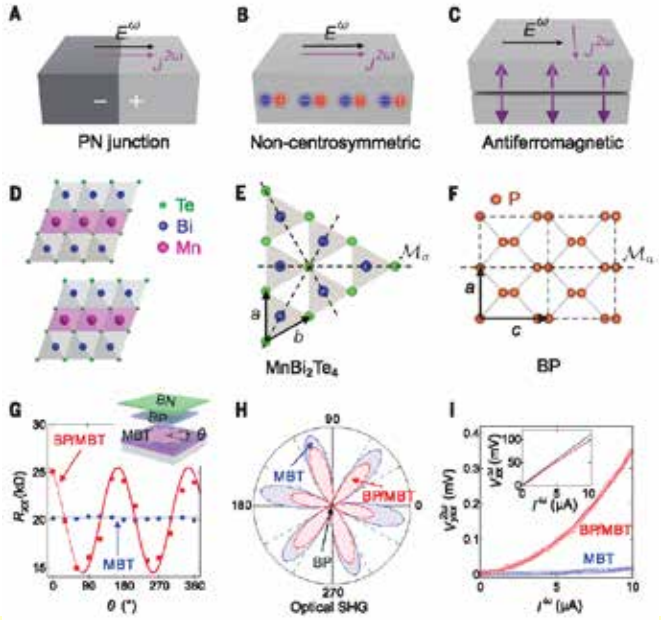

Fig. 1. Spin-induced electrical nonlinearity in PT-symmetric antiferromagnets and introduction to our sample. (A and B) Nonlinear electrical transport in PN junctions and noncentrosymmetric conductors (charge-induced electrical nonlinearity). (C) Nonlinear electrical transport in PT-symmetric AFMs (spininduced electrical nonlinearity). (D to F) Lattice structures of the MnBi2Te4 and BP. (G and H) Angle-resolved resistance and optical SHG measurements of a 6SL MnBi2Te4 before and after being interfaced with BP. (I) The nonlinear Hall signal $V^{2w}{}_{yxx}$ before and after being interfaced with BP at B = 0 T. Inset: The linear longitudinal voltage $V^{w}{}_{xx}$ before and after being interfaced with BP.

Anyuan Gao, Yu-Fei Liu, Jian-Xiang Qiu, Barun Ghosh, Thaís V. Trevisan, Yugo Onishi, Chaowei Hu,Tiema Qian, Hung-Ju Tien, Shao-Wen Chen, Mengqi Huang, Damien Bérubé, Houchen Li,Christian Tzschaschel, Thao Dinh, Zhe Sun, Sheng-Chin Ho, Shang-Wei Lien, Bahadur Singh,Kenji Watanabe, Takashi Taniguchi, David C. Bell, Hsin Lin, Tay-Rong Chang, Chunhui Rita Du, Arun Bansil, Liang Fu, Ni Ni, Peter P. Orth, Qiong Ma, Su-Yang Xu*; *Department of Chemistry and Chemical Biology, Harvard, 2Department of Physics, Harvard, Department of Physics, Northeastern University, Department of Physics and Astronomy, Iowa State University, ,Ames National Laboratory, ,Department of Physics, MIT, Department of Physics and Astronomy and California NanoSystems Institute, UCLA, Department of Physics, National Cheng Kung University, Department of Physics, UCSD, Department of Physics, Boston College, Department of Condensed Matter Physics and Materials Science, Tata Institute of Fundamental Research, International Center for Materials Nanoarchitectonics, National Institute for Materials Science, Harvard John A. Paulson School of Engineering and Applied Sciences, Center for Nanoscale Systems, Harvard, Institute of Physics, Academia Sinica, Center for Quantum Frontiers of Research and Technology (QFort), Physics Division National Center for Theoretical Sciences, Canadian Institute for Advanced Research.*

This work was supported by NSF Award # ECCS-2025158. *Science* **381**, (181-186) July 2023

Cornell Nanoscale Science and Engineering Facility (CNF)

National Nanotechnology Coordinated Infrastructure

Magnetically Programmed Diffractive Robotics

A new class of magnetically controlled microscopic robots (microbots) that operate at the visible-light diffraction limit was developed. These robots, termed diffractive robots, were realized by combining nanometer-thick mechanical membranes, programmable nanomagnets, and diffractive optical elements. The untethered diffractive microbots are small enough to diffract visible light and flexible enough to undergo complex reconfigurations in millitesla-scale magnetic fields.

The diffractive robots were tested for applications including sub-diffractive imaging using a novel variant of Structured Illumination Microscopy (Robot-SIM), tunable diffractive optical elements for beam steering and focusing, and force sensing with piconewton sensitivity. This platform thus offers a powerful new tool for high-resolution imaging, tunable optics, and ultra-small force sensing, merging robotics and optical technologies at the microscale.

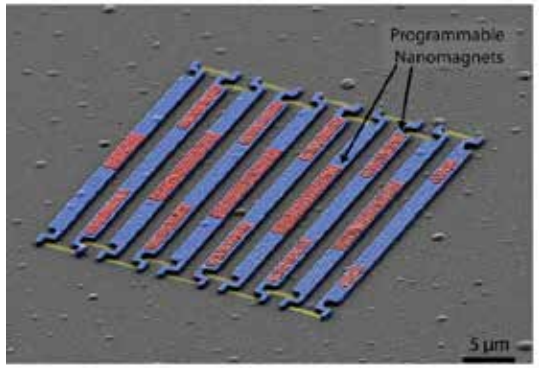

Top: False color SEM image of a diffractive robot, consisting of silicon oxide hinges (yellow), programmable cobalt nanomagnets (red), and rigid silicon oxide panels (blue).

Bottom: (a) SEM image of 2D resolution markers. **(b)** Micrograph of diffractive robot near markers, **(c)** Robot-SIM reconstruction of the markers using the diffractive robot.

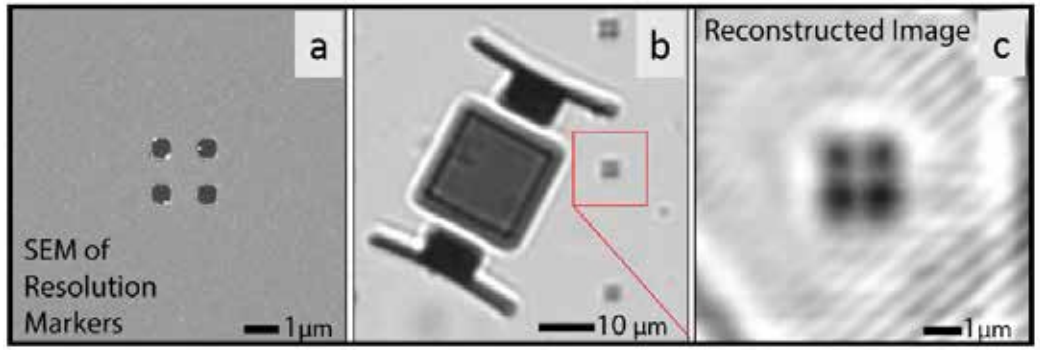

C. Smart, T. G. Pearson, Z. Liang, M. X. Lim, M. Abdelrahman, F. Monticone, I. Cohen, and P. L. McEuen, Cornell University. This work was performed, in part, at Cornell NanoScale Facility, an NNCI member supported by NSF grant NNCI-2025233.

This work was funded by the National Science Foundation and Alfred P. Sloan Foundation. *Science* **386**, No.6725 (2024).

National Research Priority: NSF – Growing Convergence Research

National Nanotechnology Coordinated Infrastructure

CNF Cornell NanoScale Science and Technology Facility

Microwave Frequency Acoustic Resonators for Quantum Applications

Bulk acoustic wave and surface acoustic wave devices are being developed for applications in quantum acoustics, to be measured using superconducting qubits as single phonon sources and detectors. To this end, low temperature mechanical performance of oriented aluminum nitride (AlN) thin films, deposited on silicon and sapphire substrates, is being evaluated. The goal is to quantify loss in these devices at low temperatures and low phonon excitation powers.

The oriented AlN films were grown by reactive sputter deposition at CNF and lithographically patterned at the University of Chicago's Pritzker Nanofabrication Facility. The pattern defines either surface acoustic wave transducers or bulk wave acoustic resonators in the microwave frequency band (1 – 10 GHz). We show that AlN films can be integrated on double-side polished silicon wafers to make high quality factor (1 – 10 million Q) bulk acoustic wave resonators.

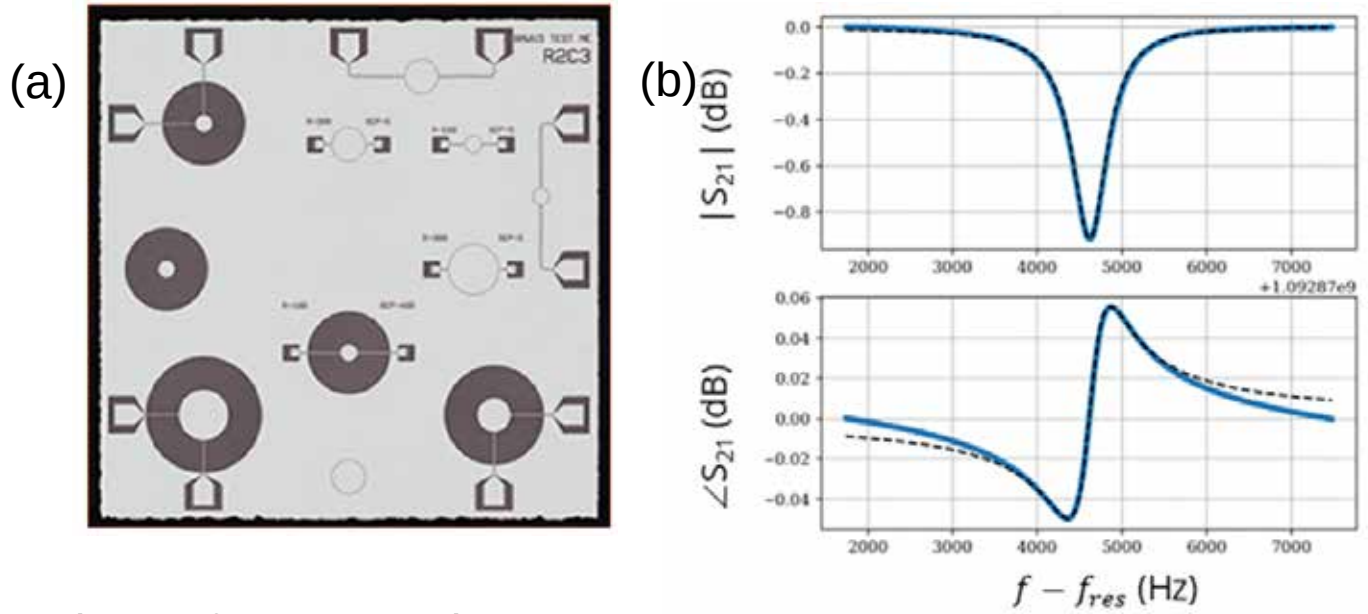

Microwave frequency acoustic resonators.
(a) Optical micrograph of a set of bulk acoustic wave resonators; silver is aluminum metallization and darker regions are underlying aluminum nitride on silicon.
(b) Vector network analyzer measurements of a bulk acoustic wave resonance, with a mechanical quality factor of ~ 2 million measured at 3 GHz and temperature of 3 K.

E. Dumur, K. J. Satzinger, G. A. Peairs, M.H. Chou, A. Bienfait, H.-S. Chang, C. R. Conner, J. Grebel, R. G. Povey, Y. P. Zhong, A. N. Cleland, Pritzker School of Molecular Engineering, University of Chicago. The work was performed, in part, at Cornell NanoScale Facility, an NNCI member supported by NSF grant NNCI-2025233.

This work was funded by the Air Force Office of Scientific Research. *Appl. Phys. Lett*. 124, 052201 (2024).

National Nanotechnology Coordinated Infrastructure

National Research Priority: NSF – Quantum Leap

CNF Cornell NanoScale Science and Technology Facility

Resistivity Scaling of Porous MoP Narrow Lines for Interconnects

The resistivity scaling of copper interconnects with decreasing dimensions remains a major challenge in the continued downscaling of integrated circuits, which causes increased signal delays and power consumption in the circuits. Previously we showed that MoP nanowires show resistivity values comparable to copper at ~ 35 nm width [1]; however, our previous synthesis method is not compatible with standard semiconductor processing.

Here, we use electron beam lithography and reactive ion etching to fabricate narrow lines out of topological metal MoP with tunable line width and thickness to investigate its resistivity scaling effect at the nanoscale. We first make large area flakes of MoP by converting MoS_2 flakes to MoP. The developed process is more adoptable to processing conditions in industry. We find that this conversion creates nanoscale pores in MoP, and the resistivity of the resulting narrow MoP lines correlates strongly with the porosity [2].

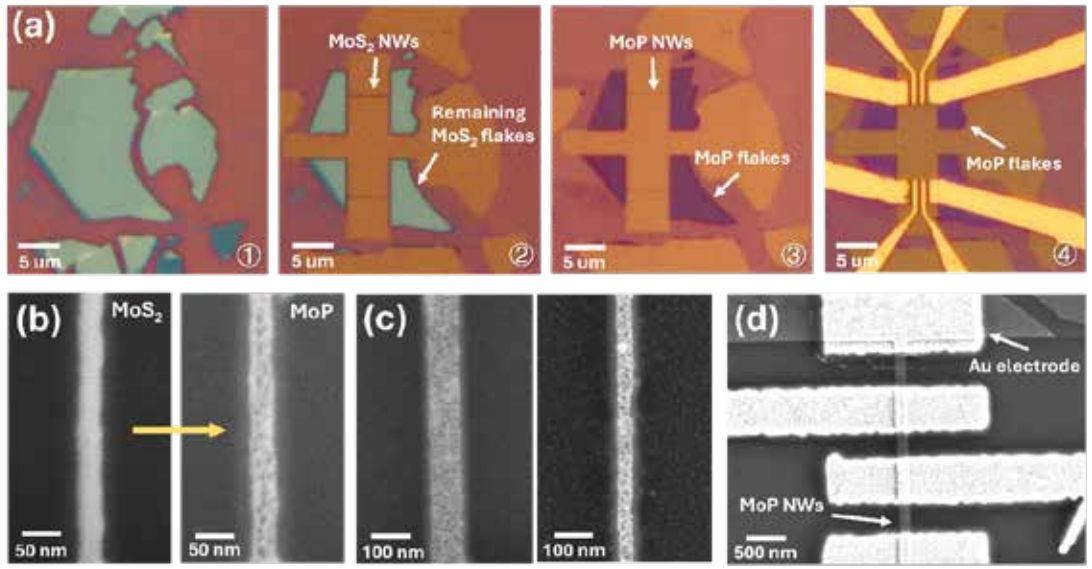

Fabrication process to make narrow MoP lines to study resistivity scaling.
(a) Optical images of exfoliated MoS_2 flakes (1), narrow MoS_2 lines after RIE (2), converted narrow MoP lines (3), and after electrode deposition (4). (b) SEM images of a MoS_2 and MoP line before and after conversion. (c) SEM images of porous MoP lines with different widths. (d) SEM image of a 4-point probe device on a MoP nano line.

H. J. Han, et. al., Cornell University. This work was performed, in part, at Cornell NanoScale Facility, an NNCI member supported by NSF grant NNCI-2025233.

This work was supported by SRC JUMP2.0 SUPREME and NSF GRFP #2139899. *Advanced Materials* 35, e2208965 (2023), *APL Materials* 12, 121113 (2024),

National Research Priority: DoD - Microelectronics and Advanced Materials

National Nanotechnology Coordinated Infrastructure

CNF Cornell NanoScale Science and Technology Facility

High-Density, Integrated, Multi-Functional Neural Probe for Small Animals

Micro-fabricated neural probes serve as an important tool for probing neural activities. There is an increasing need to develop a high-density, multi-functional probing device to monitor electrical and electrochemical signals from neurons in physiological environment with minimum invasion and long operation time.

Here, using CNF, a high-density neural interface was fabricated on conformable parylene-C substrate, with a small cross-section of 3 x 126 μm^2, which ensures minimal damage to brain tissues. A light-weight wireless high-channel count head stage coated with the parylene film was developed to achieve wireless neural activity recording in rodents during unrestrained behavior. Using the high-density, integrated, multi-functional neural probe, high-quality data from freely moving rodents in naturalistic environment was successfully recorded.

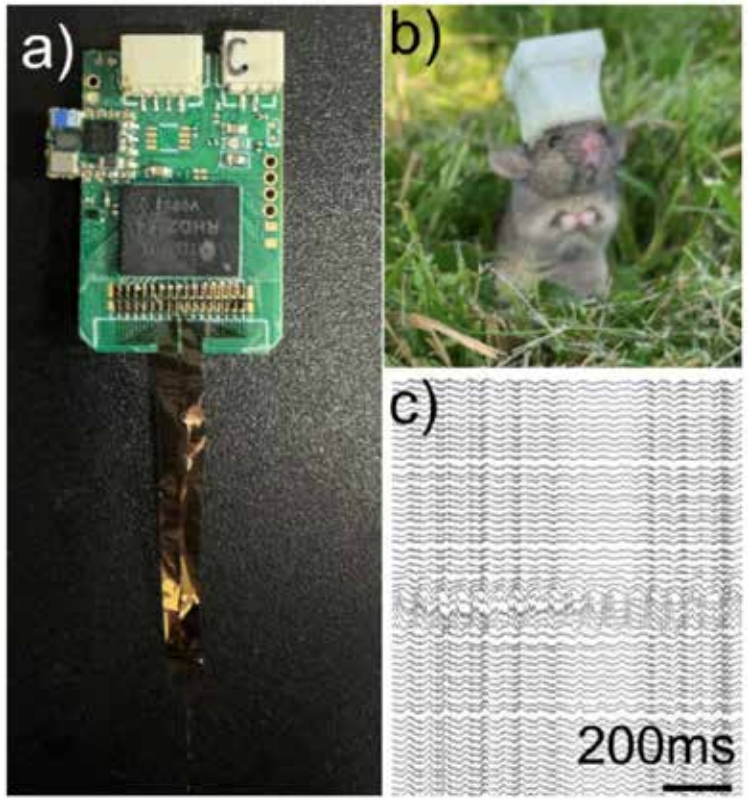

Figure on right: Wireless electrophysiology system to study unbounded animal behavior. (a) Assembled wireless device with microelectrodes. (b) A mouse with 3D printed carrier for wireless head stage. (c) recorded high quality electrophysiology data during animal locomotion.

A. O. Gonzalez, A. Fernandez-Ruiz, L. Karaba, J. Park, Z. Zhao, Neurobiology and Behavior, Cornell University. The work was performed, in part, at Cornell NanoScale Facility, an NNCI member supported by NSF grant NNCI-2025233.

This work was funded by NIH DP2MH136496, R00MH120343, and R00MH122582.

National Research Priority: NSF – Understanding the Rules of Life

On-Chip Cell Transportation and Rotation Using Vibration-Induced Flow

The Cornell Nanoscale Facility was used to fabricate a flow system for cell manipulation based on vibration-induced flow. Micropillar arrays were fabricated on photoresist using photolithography, such that a piezoelectric stage can be used to create circular vibration. This on-chip device allows manipulation of large cells by the applied flow velocity near the micropillar arrays.

Using this system, we control the mouse oocytes' transportation, rotation, and manipulation. A circular vibration with two sinusoidal wave signals was generated by controlling the piezoelectric stage. The current spiral design generates a flow pattern that moves the mouse oocyte cells to the center of the chip, achieving easy detection and collection of the cells.

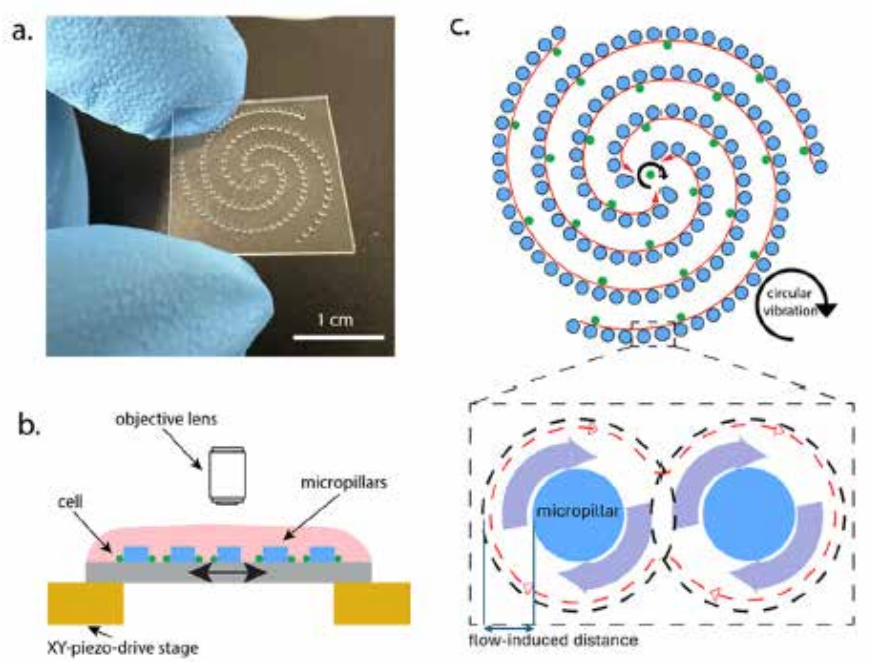

Fabricated vibration-induced flow chip.
(a) Optical micrograph of micropillars arranged in a spiral pattern. **(b)** Experimental set-up, where a piezoelectric stage will generate a flow pattern on the device. **(c)** Schematic of cell transportation using the vibration-induced flow.

A. Favakeh, A. Mokhtrare, and A. Abbaspourrad, Department of Food Science, Cornell University. The work was performed, in part, at Cornell NanoScale Facility, an NNCI member supported by NSF grant NNCI-2025233.

National Research Priority: NSF – Understanding the Rules of Life

New High-Resolution Resists for EUV Lithography

Continued miniaturization of device feature sizes in integrated circuits requires new light sources with smaller wavelengths than what is currently available. The frontier effort is in the development of an extreme ultraviolet (EUV) lithography. This requires development of new photoresists as current photoresists are inadequate for EUV lithography due to their poor absorption of EUV and diffusion of molecules that degrade resolution, among others.

A single-component monomolecular resist composed solely of polypeptoids was developed for EUV lithography. The polypeptoids include phenol derivatives that change solubility upon exposure to EUV. Thus, the developed photoresist platform is patternable under EUV lithography and removes the need for photoacid generators (PAGs) or other additives in the resist formulation. This innovation addresses problems related to uneven PAG distribution and tackles environmental, health, and regulatory concerns associated with PAGs.

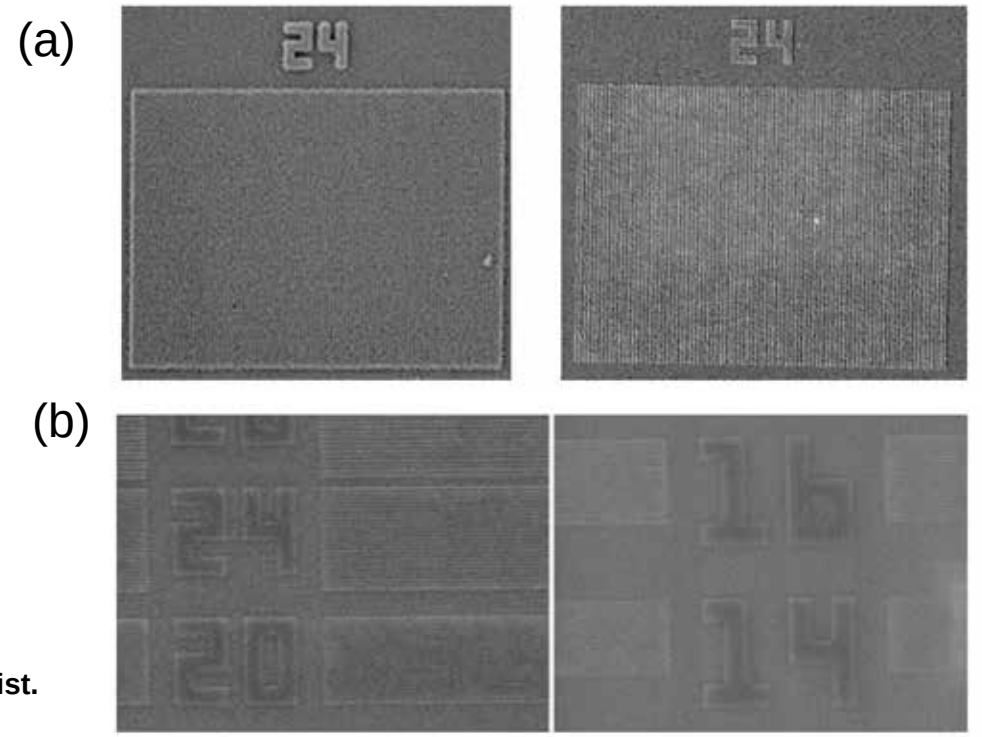

(a) 24-nm half-pitch electron-beam patterns of the polypeptoid resist.
Left: with 10 wt% PAG. Right: without PAG.
(b) EUV patterns generated from the polypeptoid resist.
Left: with 10 wt% PAG. Right: without PAG.

C. Yuan, E. Yoshida, C. Adams, R. A. Segalman, C. K. Ober, Dept. of Materials Science and Engineering, Cornell University. The work was performed, in part, at Cornell NanoScale Facility, an NNCI member supported by NSF grant NNCI-2025233.

This work was funded by the U.S. Department of Energy, Office of Science, Basic Energy Sciences. *SPIE Advances in Patterning Materials and Processes* XLI 12957, 129570S (2024).

Potential Silicon Dioxide Etch Gas with Low Global Warming Potential

Currently, fluorocarbon (FC) and hydrofluorocarbon (HFC) gases are the primary choice for high aspect ratio etching of dielectric materials due to many desirable attributes in terms of their tunability, etching performance, and availability in high purity. Nevertheless, they have a high global warming potential (GWP), greater than 600 (GWP of 1 is set to the heating of the earth by 1 ton of CO_2 over a set period). Thus, alternative etch gases with lower GWP are urgently needed.

Working with EFC Gases & Advanced Materials, CNF conducted systematic etching experiments on SiO_2 blank wafers and patterned wafers using low-GWP hydrofluoroolefins (HFOs). HOFs are proven to have much lower GWP values compared to the common FC and HFC etch gases. Systematic etching results show that HFO 1,3,3,3-Tetrafluoropropene ($C_3H_2F_4$) has a comparable etching rate and better selectivity than legacy etch gases CHF_3 or $CH2F_2$ under the same etching conditions using an Oxford PlasmaLab 100 inductively coupled plasma (ICP) reactive ion etch (RIE) system.

Etch Gas	SiO_2 Etch Rate (nm/min)	Selectivity
$C_3H_2F_4$	206.3	6.04
CHF_3/O_2	182.5	1.51
CH_2F_2	158.7	2.24

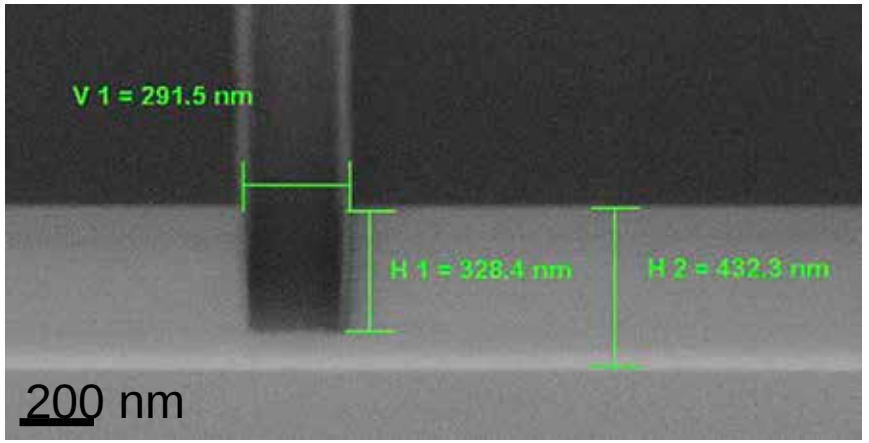

Top: Table summary of etching results of low GWP etch gas $C_3H_2F_4$. **Bottom:** 300 nm SiO_2 line, etched with $C_3H_2F_4$ for 120 seconds.

A. J. Windsor, J. C. Clark, G. McMurdy, E. A. Joseph, R. G. Syvret, R. J. Olson Jr., J. J. Cha, Cornell University and EFC Gases & Advanced Materials. This work was performed, in part, at Cornell NanoScale Facility, an NNCI member supported by NSF grant NNCI-2025233.

National Research Priority: Sustainable Semiconductor Manufacturing

Fabrication of High-Resistivity Silicon Interposers (REU research)

Recent advancements in semiconductor technology requires heterogeneous integration of chiplets on an interposer, which is typically made of polymers, glass, or doped silicon. In this work, high-resistivity (> 1 kΩ·cm) silicon interposers were fabricated and characterized for millimeter-wave applications, using etching and metallization of through-silicon vias (TSVs).

A complete process flow for the fabrication of high-quality TSVs for use on high-resistivity silicon interposers has been developed and verified. The TSVs were patterned for radio frequency (RF) characterization to form grounded coplanar waveguides. The waveguides were probed up to 40 GHz, which showed an insertion loss of 2 dB/mm and a return loss of 26 dB at 40 GHz. The measured insertion loss is too high and is attributed to the insufficient amount of a metal layer at the front side of TSVs.

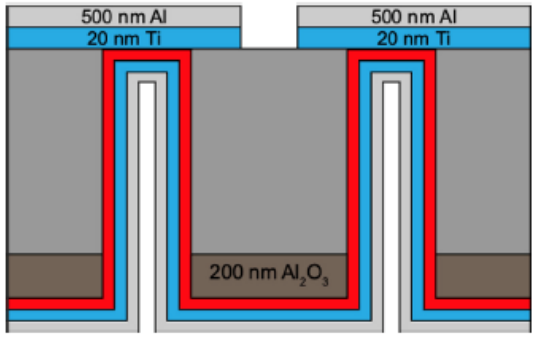

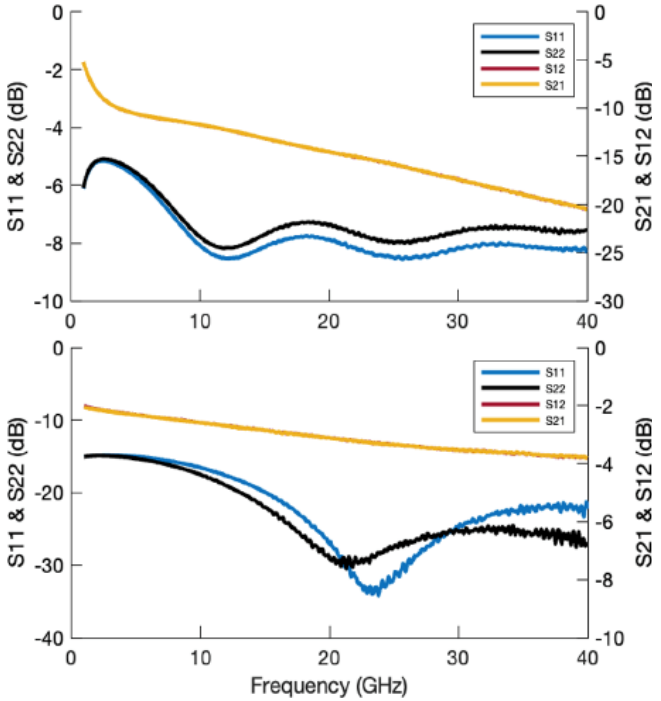

Top: Cross-sectional geometry of through-silicon vias.
Right: S-parameters of 2146 µm grounded coplanar waveguide for doped silicon (top panel) and high-resistivity silicon (bottom panel) up to 40 GHz.

By G. Lemaster (Brown University); X. Wang, Y. Ding, J. Hwang (Cornell University). This summer REU work was supported by the REU program hosted by the Cornell NanoScale Facility, and performed, in part, at CNF, an NNCI member supported by NSF grant NNCI-2025233.

National Research Priority: DoD - Microelectronics and Heterointegration

Metamaterial Spectrometer: A Low SWaP, Robust, High Performance Hyperspectral Sensor (Industry Research)

Plasmonic chips with a metamaterial surface were fabricated to enable Extraordinary Optical Transmission (EOT), a phenomenon unique to metastructures, in which light is transmitted through apertures much smaller than the incident wavelength at anomalously large intensities relative to the predictions from conventional aperture theory.

Phoebus Optoelectronics has extensively used the resources of the Cornell. Nanoscale Facility to develop a hyperspectral imaging system. This system uses a metasurface to target precisely very narrow spectral bands of interest, enabling a significant reduction in the size and number of optical components compared to the current state-of-the-art imaging systems. The immediate goal is to detect and image trace gases in the Earth's atmosphere in the midwave infrared, while minimizing dependence on the angle of incidence of light upon the sensor.

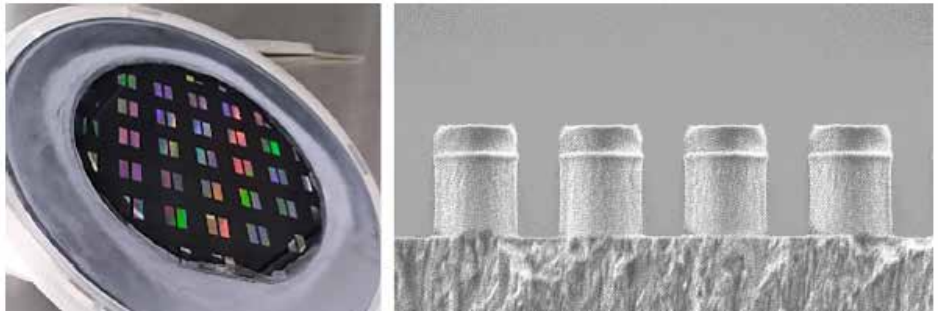

Left: Wafer, lithographically patterned with optical metastructures.
Right: SEM image of the etched pillars with near-vertical sidewalls.

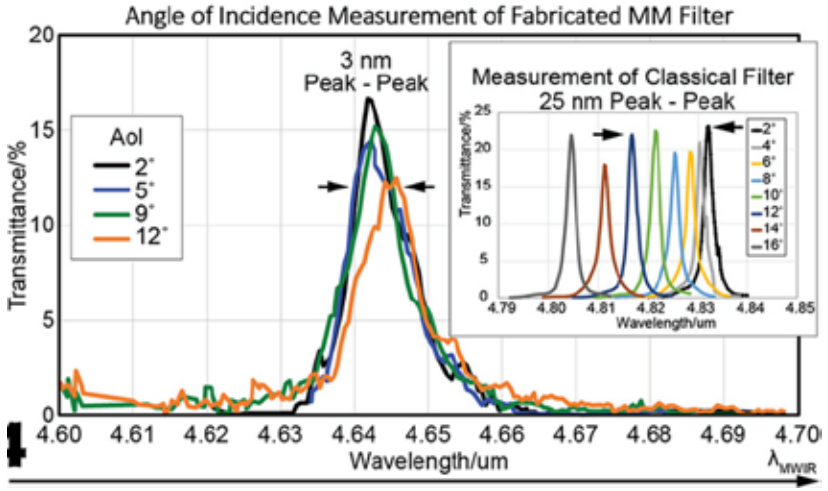

Optical performance of fabricated metamaterial filter. The measurement shows that the transmission is independent of the angle of incidence up to a cone of 12 °(f/2.4). Inset shows the same measurement performed on a classical Fabry-Pérot filter, which shows the shifts of the transmission wavelengths as a function of incident angle.

This work was carried out by Phoebus Optoelectronics LLC. The work was performed, in part, at Cornell NanoScale Facility, an NNCI member supported by NSF grant NNCI-2025233.

This work was funded by the National Aeronautics and Space Administration (NASA).

System-On-Foil (Industry Research)

Lux Semiconductors Inc. is developing a new system-level advanced packaging technology, System-on-Foil, designed to overcome limitations on current packaging technologies. This architecture integrates a patterned metal core substrate, which facilitates high-speed signal transmission between redistribution layers on the top and backside.

Copper transmission lines are patterned using silicon wafer toolsets to achieve interposer-like densities, enabling high bandwidth, low latency routing for chiplet-based heterogeneous integration. The rigid metal substate allows for thicker dielectric layers that enable low loss, high speed transmission lines, leveraging the metal substrate as reference ground. The fabricated thin metal foil interposers were integrated with traditional and flexible hybrid electronics to demonstrate the technology.

(a)

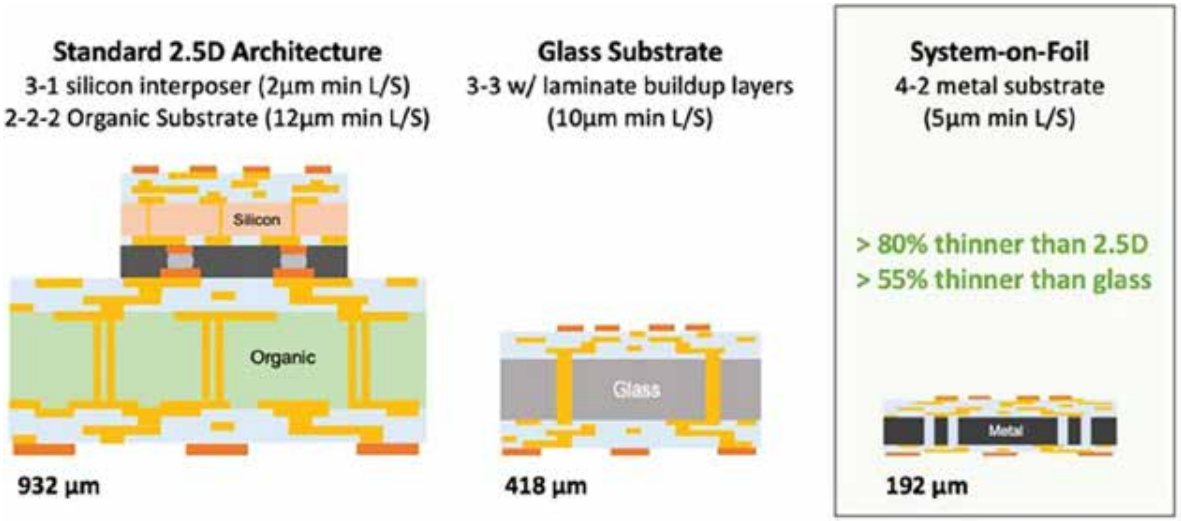

(b)

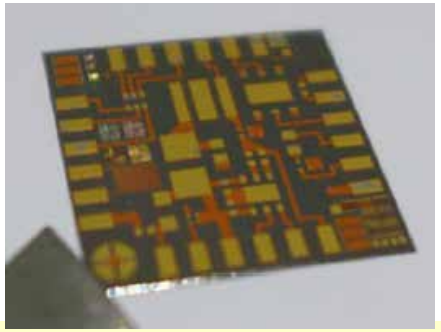

System-on-foil for advanced packaging technology. **(a)** Schematic comparisons of different advanced packaging technologies. In contrast to standard 2.5D architecture or glass substrate, the system-on-foil solution is much thinner, facilitating high-speed signal transmission between redistribution layers and providing flexibility. **(b)** Completed metal foil interposer.

Lux Semiconductors Inc. The work was performed, in part, at Cornell NanoScale Facility, an NNCI member supported by NSF grant NNCI-2025233.

This work was funded by the SNF SBIR program.

National Research Priority: DoD - Microelectronics and Heterointegration

National Nanotechnology Coordinated Infrastructure

CNF Cornell NanoScale Science and Technology Facility

Kentucky Multi-Scale Manufacturing and Nano Integration Node (KY Multiscale)

National Nanotechnology Coordinated Infrastructure

Interrogation of Tumor Biophysical, Ultrastructural, and ECM Signatures via AFM and SEM

Glioblastoma (GBM) is a highly aggressive and invasive brain cancer, carrying a median survival of 15 months. This poor prognosis is due, in part, to its resistance to therapy through tumor adaptations mediated by the tumor microenvironment (TME). Efforts to describe the tumor-protective cues in the TME may aid in the development of strategies to combat resistance. Emerging work has indicated that tumor biophysical properties are significant modulators of tumor evolution; however, these parameters are poorly described in GBM. Here, we investigate the mechanical, ultrastructural, and ECM characteristics of tumors in patient-matched GBM core and rim. Using AFM, SEM, and microscopy techniques, we find that GBM core is abnormally stiff and dense with high ECM components while rim tissue possess characteristics that resemble normal brain and are soft, more porous, with lower ECM when compared to core. These data suggest that the stiff core participates in tumor adaptations through pro-malignant mechanotransduction while the rim provides more permissive routes for GBM invasion. These novel insights support the development of TME targeting therapies that alter tumor mechanics.

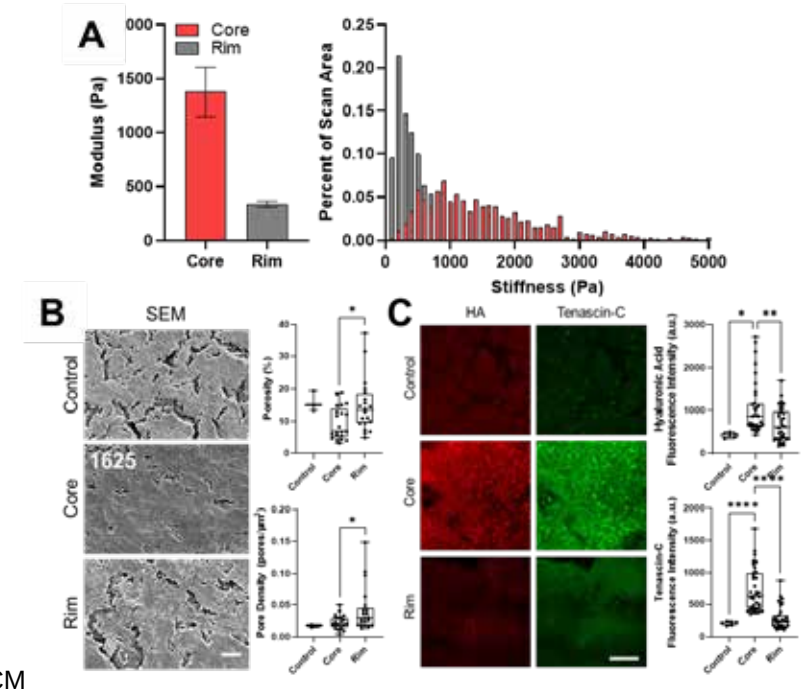

GBM core and rim exhibit unique mechanical ultrastructural, and ECM signatures. (A-C) GBM core displays a median stiffness of ~ 1.3 kPa and possess low porosity and elevated ECM while GBM rim is soft (~ 400 Pa), porous, and exhibits lower levels of ECM components.

Mahaffey BJ, Fowler ZP, Lung Z, Dang V, Lee H, Johnson AM, Munoz MA, Goodin DA, Frieboes HB, Williams BJ, Chen J. Research was performed at University of Louisville MicroNano Technology Center (MNTC) and was supported by NSF NNCI Award #2025075.

Mahaffey and Fowler et al *APL Bioeng*. 8, 036101 (2024)

National Research Priority: NSF – Understanding the Rules of Life

National Nanotechnology Coordinated Infrastructure

KY MULTISCALE
The NSF NNCI Multi-Scale Manufacturing & Nano Intergration Node

CO_2 Conversion to Methyl Formate in a Flow Electrolyzer with Mixed Propylene Carbonate/Methanol Catholyte

CO_2 electroreduction in non-aqueous solvents being pursued to expand the suite of products that can be made with high selectivity. CO_2 reduction in alcohols coupled with in-situ esterification can produce esters such as methyl formate but needs to be translated to a high-performance flow electrolyzer. However, alcohols wet and flood porous electrodes, thus impeding reactor performance. In this work, methanol was mixed with higher surface tension propylene carbonate as a catholyte for a gas-fed CO_2 flow electrolyzer that avoided cathode flooding. With 10 vol % methanol in 90 vol % propylene carbonate, 63% faradaic efficiency for methyl formate ester product was sustained without cathode flooding.

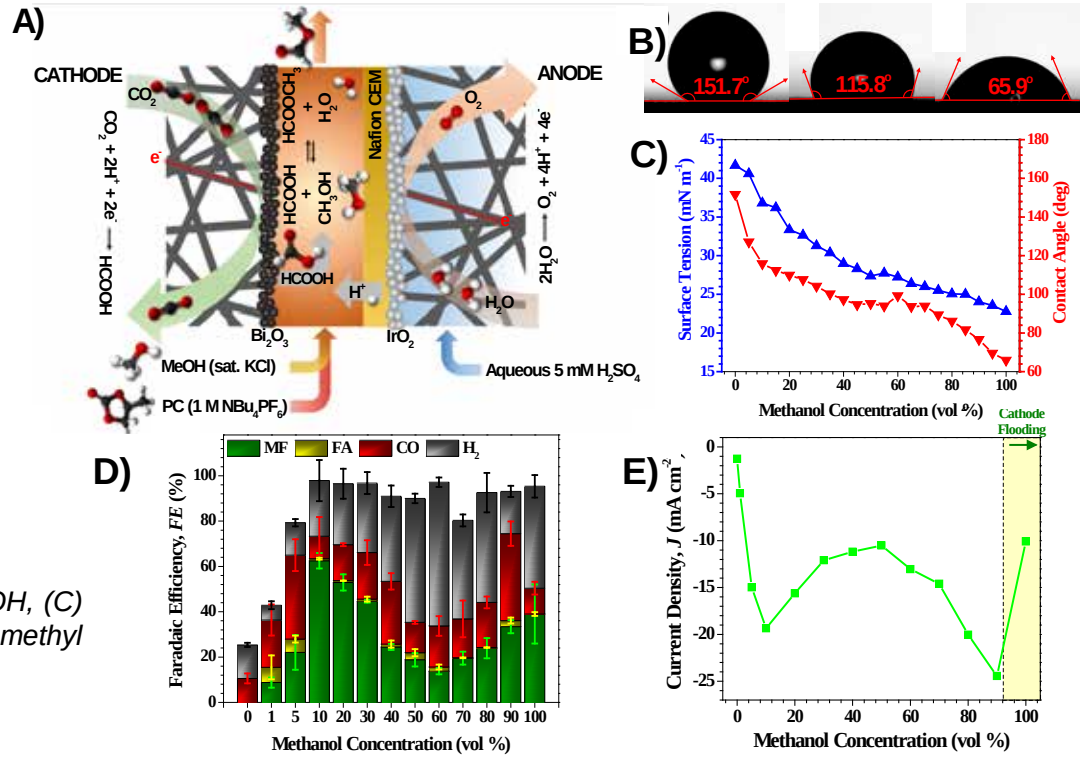

(A) Flow cell schematic, (B) contact angles from pure PC to pure MeOH, (C) mixed catholyte properties, (D) resulting product distribution, and (E) methyl formate current densities.

Uttarwar, S., Hofsommer, D., Hartman, C., Nkurunziza, F., Gautam, M., Paxton, W., Grapperhaus, C., and Spurgeon, J. Research was performed at the University of Louisville Conn Center for Renewable Energy Research and the MicroNanoTechnology Center (MNTC).

ACS Sust. Chem. Eng. DOI:10.1021/acssuschemeng.4c04699

National Research Priority: Energy and Climate

Electrokinetic Particle Trapping in Microfluidic Wells Using Conductive Nanofiber Mats

The goal of this research is to improve filtration by incorporating conductive nanofibers to enhance dielectrophoresis (DEP) trapping forces. These nanoscale features greatly increase the gradient of the electric field-squared, which is the primary driver of DEP forces. This study specifically looked at the influence of the applied AC frequency in trapping. Fluorescent microspheres (1 μm) were trapped at various electric field frequencies between 30 kHz and 1 MHz. Digital images of each well were analyzed to quantify particle trapping. DEP trapping by the CNF mats was greater at all tested frequencies than that of the control of no applied field, and the greatest trapping was observed at a frequency of 600 kHz, where electrothermal flow is more significantly weakened than DEP. Theoretical analysis and measured impedance spectra indicate that this result was due to a combination of the frequency dependence of DEP and capacitive behavior of the well-based device.

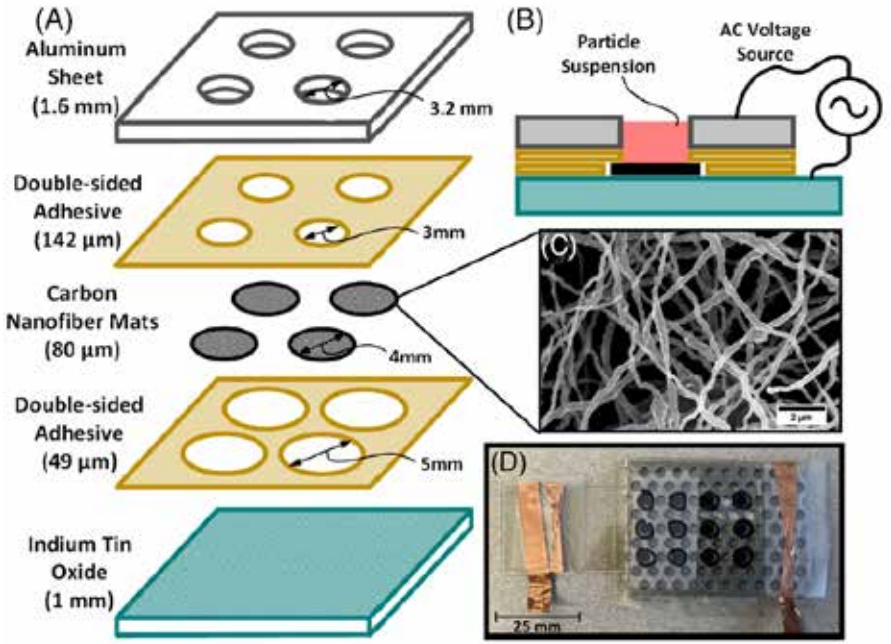

(A and B) Exploded view and cross-section view, respectively, of the well-based device schematic used for dielectrophoretic particle trapping. (C) A scanning electron microscopy (SEM) image of the conductive carbon nanofiber (CNF) mat. (D) An image from the top side of one of the assembled devices.

J. Hunter West, Tonoy K. Mondal, and Stuart J. Williams. Research was performed at the University of Louisville MicroNanoTechnology Center (MNTC) and was supported by NSF NNCI Award #2025075.

This work was funded by MCA Award #2121008. *Electrophoresis* (2024), DOI: 10.1002/elps.202400051.

National Research Priority: NSF – Growing Convergence Research

National Nanotechnology Coordinated Infrastructure

KY MULTISCALE
The NSF NNCI Multi-Scale Manufacturing & Nano Intergration Node

Device Model for a Solid-State Barocaloric Refrigerator

Solid-state refrigeration offers a promising alternative to vapor compression systems, with devices based on magnetocaloric, electrocaloric, and elastocaloric effects showing high efficiency and environmental benefits. However, barocaloric cooling systems, which rely on entropy change from applied hydrostatic pressure, have not been fully realized despite their potential. This work presents a thermodynamic and heat transfer model for a barocaloric refrigerator, simulating thermal transport and heat exchange during a reversed Brayton cycle. We evaluate the Specific Cooling Power (SCP) and Coefficient of Performance (COP) of a device using Nitrile Butadiene Rubber (NBR) as the refrigerant, assessing the impact of cycle frequency, applied pressure, temperatures, and heat transfer coefficient. Results show that a barocaloric refrigerator with a 2.4 K temperature span and 0.1 GPa pressure can achieve an SCP of 0.024 W/g at 10 mHz and a COP of 5.5 at 1 mHz, outperforming conventional systems. We also examine how material properties like bulk modulus, heat capacity, and thermal conductivity affect performance, highlighting the trade-off between maximizing the barocaloric response and improving thermal transport. This work underscores the potential of soft barocaloric materials for solid-state cooling.

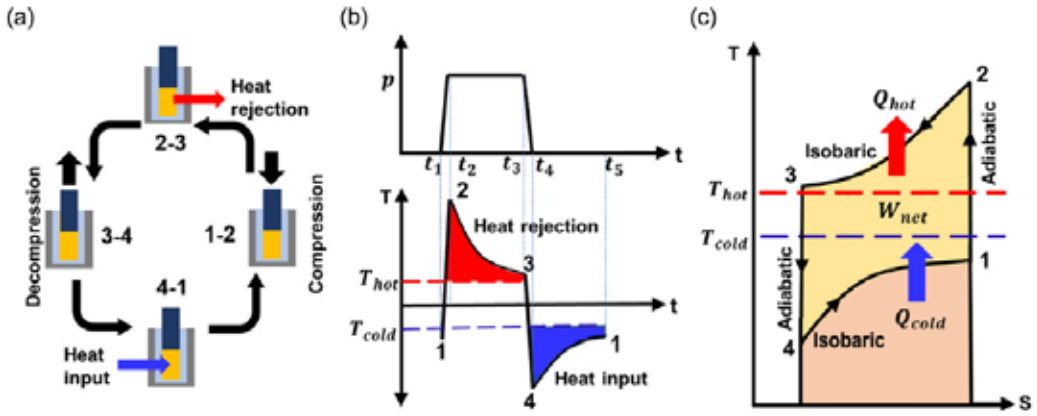

Barocaloric (BC) refrigeration uses the reversed Brayton cycle. a) Schematic of BC cooling cycle. b) Time sequence of hydrostatic pressure and BC material temperature. c) T–S diagram of the BC cycle.

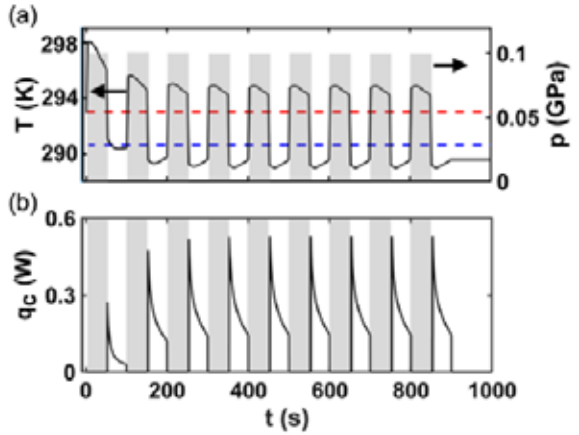

Transient simulation results for multiple cycles: a) Center-line refrigerant core temperature, and b) heat transfer rate from the cold reservoir to the refrigerant during cycle operation.

Naveen Weerasekera, Huan Jiang, Yanyu Chen, Gamini Sumanasekera, and Bikram Bhatia. Work used core facilities at the University of Louisville Conn Center of Energy Research.

Supported by NASA Kentucky award# 80NSSC20M0047. *Energy Technology* 2401057 (2024)

National Research Priority: NSF – Growing Convergence Research

National Nanotechnology Coordinated Infrastructure

KY MULTISCALE
The NSF NNCI Multi-Scale Manufacturing & Nano Intergration Node

The Effects of Thickness, Polarization, and Strain on Vibrational Modes of 2D Fe_3GeTe_2

In recent years, Fe_3GeTe_2 (FGT) has attracted significant attention as a layered magnetic material with a notably high Curie temperature and ferromagnetic ordering even at monolayer thickness. In this study, we investigated the effects of thickness (Fig. a), light polarization (Fig. b), and strain (Fig. c) on the Raman spectra of two-dimensional (2D) FGT crystals synthesized via chemical vapor transport. It was found that increasing FGT thickness influences the position, separation, and relative intensity of the A^1_g and E^2_g Raman modes. Angle-resolved polarized Raman spectroscopy reveals the complete disappearance of the A^1_g mode in the crossed polarization direction, while the intensities of the A^1_g and E^2_g modes in parallel polarization and the E^2_g mode in crossed polarization remain constant at all angles. These findings align with Raman tensor analysis, providing clear evidence for the unambiguous assignment of the A^1_g and E^2_g peaks, thus resolving previous ambiguities in the literature. Additionally, we explored the effect of strain on few-layer FGT deposited on polyethylene terephthalate. Under tensile and compressive bending, the Raman peak positions exhibited notable downshifts and upshifts, respectively. This demonstrates the potential for modulating the magnetic properties of FGT through strain engineering.

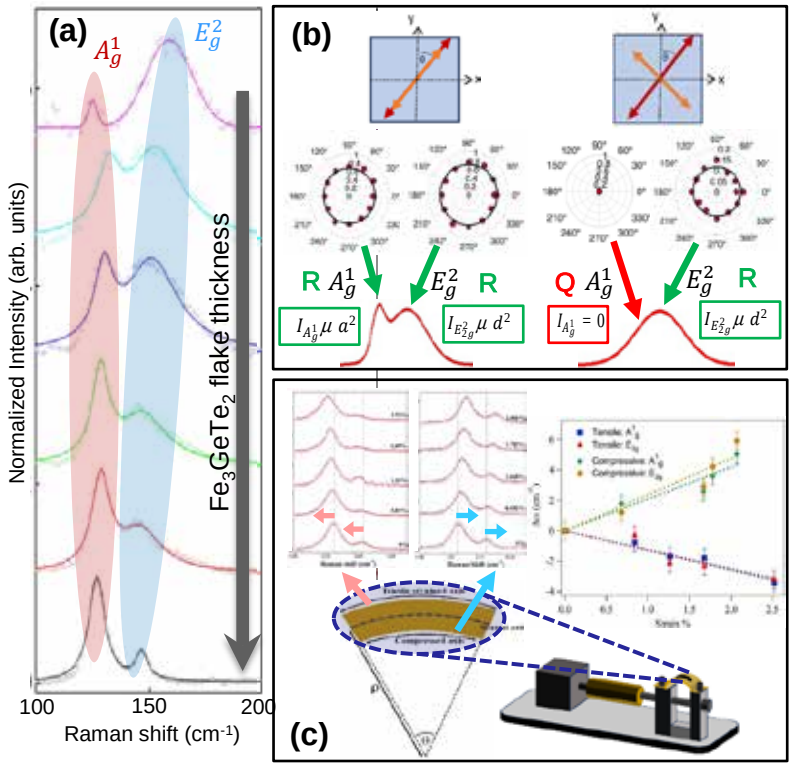

(a) Thickness, (b) light polarization, and (c) strain effects on Raman spectra of Fe_3GeTe_2.

H. Weerahennedige, M. Irziqat, D. Vithanage, H. Weerarathne, Z. Ronau, Jacek B Jasinski, Gamini Sumanasekera. Research was performed at the University of Louisville Conn Center for Renewable Energy Research.

Supported by DOE BES Award # DE-SC0024131. Results published in Weerahennedige et al., *Surfaces and Interfaces 51, 104797 (2024).*

National Research Priority: NSF – Growing Convergence Research

National Nanotechnology Coordinated Infrastructure

KY MULTISCALE
The NSF NNCI Multi-Scale Manufacturing & Nano Intergration Node

ARPRS Study of Arsenic-Phosphorus Alloys and Identification of As-P Vibrational Modes

Recently, angle-resolved polarized Raman spectroscopy (ARPRS) has emerged as a versatile technique for the in-depth characterization of layered and/or two-dimensional (2D) materials. In this research, ARPRS was used to analyze the anisotropic vibrational properties of arsenic-phosphorus layered alloys and investigate the local distribution of As and P atoms in these materials. The experimental setup is shown in Fig. a. The results reveal a clear polarization dependence in the Raman intensity of the P-P, As-P, and As-As modes, which is corroborated by first-principles calculations. Furthermore, the As-P Raman peak observed around 350 cm^{-1} is identified as a linear combination of two in-plane vibrations (i.e., A_g^2 and B_{2g}), explaining the measured butterfly-shaped polar plots (Fig. b). The significance of this work lies in demonstrating that ARPRS can effectively analyze the structure and local atomic distribution of these alloys. These materials, analogues of phosphorene, exhibit similar unique and technologically relevant properties but offer improved environmental stability, making them more suitable for practical applications compared to phosphorene.

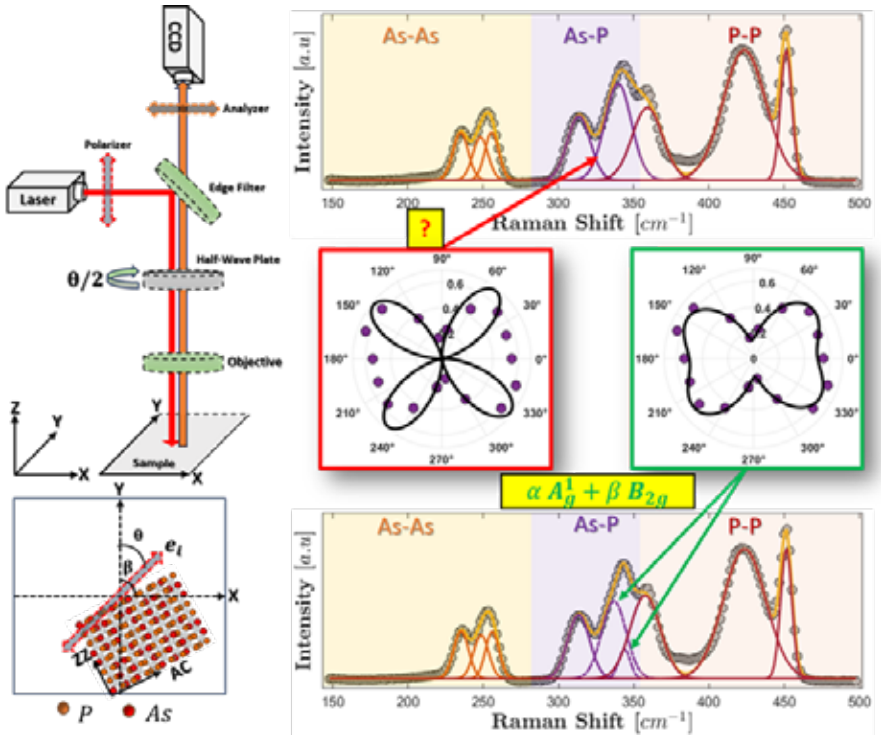

(left) Schematic of the ARPRS experimental setup. (right) ARPRS-based analysis of the As-P Raman peak observed around 350 cm^{-1}.

Irziqat, M., Weerahennedige, H., Vithanage, D., Tasnim, K. J., Musa, M.R.K., Weerarathne, H., Sumanasekera, G., Jasinski, J.B., and Yu, M. Research was performed at the University of Louisville Conn Center for Renewable Energy Research.

Supported by DOE BES Award # DE-SC0024131. Irziqat, et al., *J. Alloys Compd.* 992, 174609 (2024).

National Research Priority: NSF – Understanding the Rules of Life

National Nanotechnology Coordinated Infrastructure

KY MULTISCALE
The NSF NNCI Multi-Scale Manufacturing & Nano Intergration Node

Expanding the Solvent Diversity and Perovskite Compatibility of SnO2 Inks

Tin oxide (SnO2) is an attractive electron transport material (ETM) for perovskite solar cells (PSCs) due to its optoelectronic properties, low-temperature solution processability, cost, and stability. However, solvent incompatibilities have largely limited its application to devices with SnO2 deposited below the perovskite. To expand its utility in other device structures, including inverted PSCs and tandem devices, alternate deposition strategies are needed. This study addresses the solvent scope and perovskite compatibility of acetate-stabilized yttrium-doped SnO2 (Y:SnO2) dispersions. We show that dispersions in several lower alcohols and select polar aprotic solvents can be directly deposited on perovskite using scalable and low-temperature processes. Further, they are compatible with various perovskite formulations, including those with mixed cations and mixed anions. The study expands the applicability of SnO2 as a solution-processible and cost-effective ETM as an alternative to fullerene-based organic ETMs and serves as a guide for its use in PSCs and tandem devices.

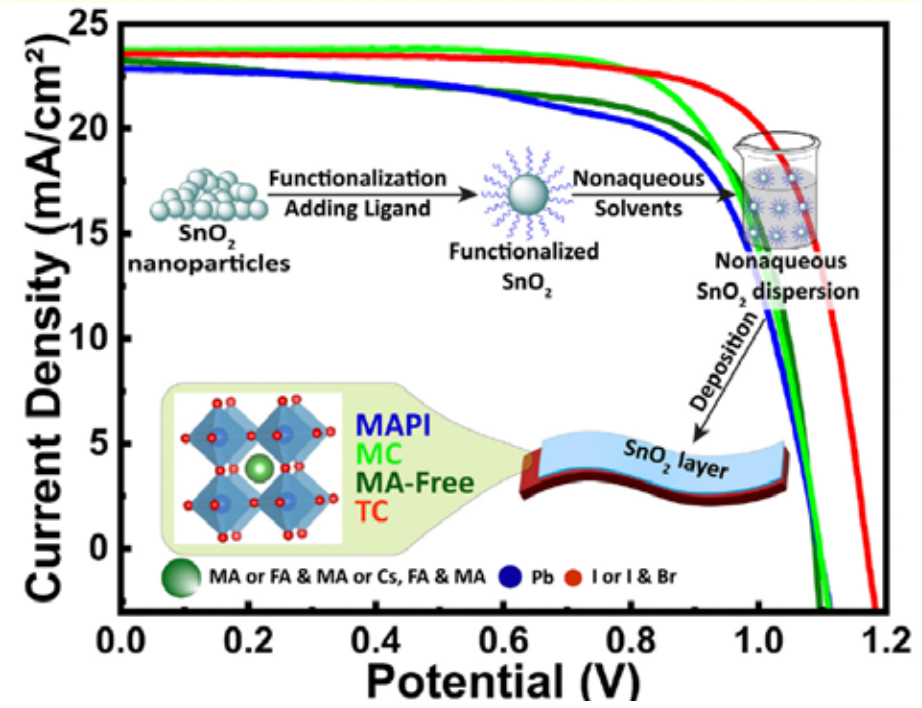

Photovoltaic performance of devices built with synthesized SnO2 using 4 separate perovskite absorber layers.

Sashil Chapagain, Peter J. Armstrong, Rojita Panta, Narayan Acharya, Thad Druffel, and Craig A. Grapperhaus Research was performed at the University of Louisville Conn Center for Renewable Energy Research.

Supported by DOE SETO Award DE-EE0008752. *iScience* DOI: 10.1016/j.isci.2024.110964.

National Research Priority: NAE Grand Challenge – Make Solar Energy Economical

National Nanotechnology Coordinated Infrastructure

KY MULTISCALE
The NSF NNCI Multi-Scale Manufacturing & Nano Intergration Node

High-temperature Operation and Low Loss Contacts for Perovskite Solar Cells

A team of researchers, including users of both SHyNE and KY Multiscale, recently reported two remarkable breakthroughs for perovskite solar cells. First, they discovered that fluorinated ammonium ligands can passivate perovskite interfaces while minimizing reaction with the perovskite itself. As a result, they achieved a certified power conversion efficiency (PCE) exceeding 24% and maintained 85% of the original PCE even after operating under challenging conditions (85 ° C and 50% relative humidity) for over 1500 hours. This work was reported in *Science* (Park et al., *Science*, 381, 2023) in July 2023. Soon thereafter, the team discovered that low loss contacts could be formed for inverted perovskite solar cells (PSC) using engineered self-assembled monolayers on textured substrates. This work, published in *Nature* in October (Park et al. *Nature* 624, 2023), enabled both enhanced light management and carrier extraction and ultimately yielded a certified power conversion efficiency (PCE) of 24.8%. In addition, the PCE surpassed 24% even after 1000 hours of accelerated aging, making it one of the most stable PSCs reported to date. The figure at right shows the structure of the inverted PSC, its certified performance, and x-ray photoelectron spectroscopy data from KY Multiscale confirming the nature of the novel low-loss contact.

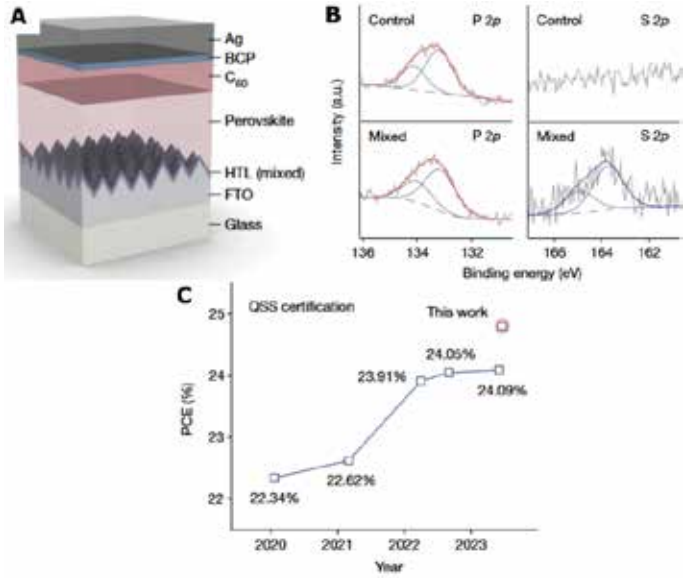

(A) Inverted perovskite solar cell with a mixed self-assembled monolayer serving as the hole transport layer (HTL) on a textured substrate for light management. (B) XPS measurements confirmed the mixed nature of the monolayer HTL. (C) The resulting solar cell achieved a certified power conversion efficiency of 24.8%. Adapted from Park et al. Nature 624 (2023).

This research used KY Multiscale and SHyNE facilities.

Park, SM et al. *Science*, v.381, p.6654, 2023 and Park, SM et al. *Nature*, v.624, p.7991, 2023.

National Research Priority: NSF – Growing Convergence Research

National Nanotechnology Coordinated Infrastructure

KY MULTISCALE
The NSF NNCI Multi-Scale Manufacturing & Nano Intergration Node

Microscale Geometry Influences Mechanical Properties of 3D Printed Aerospace Alloys

A team of KY Multiscale researchers led by Professor Paul Rottmann at the University of Kentucky recently showed that the microstructure and mechanical properties of additively manufactured Iconel 718 are strongly influenced by the geometry of the 3D printed part. The work, published in Sept. 2023 (Varney et al. *Materialia* 31 2023) showed that parts with wall dimensions on the microscale exhibited reduced ductility but increased overall strength compared to their bulk counterparts. This effect was related to difference in cooling rate and nucleation site density for the microscale features. This study indicates that the local geometry of additive parts must be considered to predict the microstructure and mechanical properties of this critical alloy. The figure at right shows the change in surface texture and dramatic change in grain structure between microscale and bulk printed features.

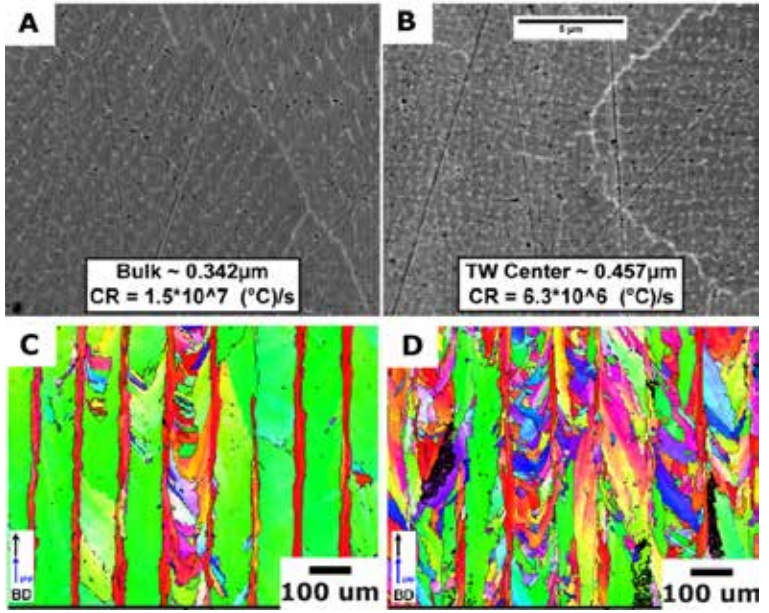

Bulk (A) and thin-wall (B) additively manufactured Iconel 718 exhibit different dendrite spacing related to their cooling rates. Electron backscatter diffraction maps reveal columnar grains oriented along the build direction in bulk samples (C) and highly stochastic grain structure in thin wall samples (D). Adapted from Varney et al. Materialia (2023).

Paul Rottmann, Materials Science and Engineering, University of Kentucky. This research used the KY Multiscale EMC center.

Materialia 31 (2023) 101867.

National Research Priority: NSF – Growing Convergence Research

National Nanotechnology Coordinated Infrastructure

KY MULTISCALE
The NSF NNCI Multi-Scale Manufacturing & Nano Intergration Node

High Hole Mobility Fiber Organic Electrochemical Transistors for next-Generation Adaptive Neuromorphic bio-Hybrid Technologies

Organic electrochemical transistors (OECT) can serve as active electronics in low-cost, wearable systems and for neuromorphic technologies. Researcher at the University of Kentucky recently demonstrated that poly(3,4-ethylene-dioxythiophene):polystyrene sulfonate (PEDOT:PSS) fibers are a promising material system for OECTs. Specifically, their transistors exhibited *record high hole mobilities,* stable contacts, and high mobility-capacitance products (a key figure of merit). Neuromorphic electronics formed from the fibers were responsive to the presence of dopamine and closely matched the geometry of the neuronal axon terminal.

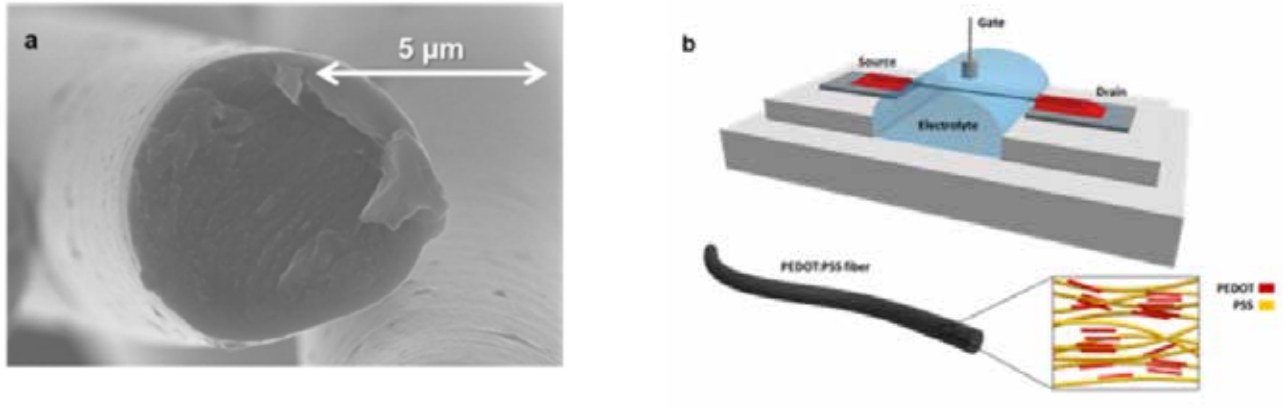

PEDOT:PSS fibers (a) exhibit extremely high hole mobility and can be used to form organic electrochemical transistors (b). These transistors subsequently formed the basis for neuromorphic devices that are responsive to the neurotransmitter dopamine.

Alexandra Paterson, Materials Science and Engineering, Univ. Kentucky. Work performed in part at KY Multiscale.

Support from NSF OIA 1849213. Paula Alarcon-Espejo et al. *Advanced Materials* 36.11 (2024): 2305371.

National Research Priority: NSF – Growing Convergence Research

National Nanotechnology Coordinated Infrastructure

KY MULTISCALE
The NSF NNCI Multi-Scale Manufacturing & Nano Intergration Node

Mid-Atlantic Nanotechnology Hub (MANTH)

National Nanotechnology Coordinated Infrastructure

Exciton-Polariton Photovoltaics for Energy Harvesting

- Excitonic photovoltaics (PVs) offer a route to create significantly thinner solar energy harvesting devices and low power sensors at lower cost.
- Poor excitonic transport plagues excitonic PV efficiency but exciton-polaritons are hybrid light-matter states that can exhibit long range transport.
- Transition metal dichalcogenides (TMDs) are van der Waals materials with large complex refractive indices, enabling strong absorption in very thin structures. Certain TMDs such as WS_2 show strong exciton resonances at room temperature, even in bulk form.
- These results offer a route to improve efficiencies of optoelectronics based on high refractive index excitonic nanomaterials.

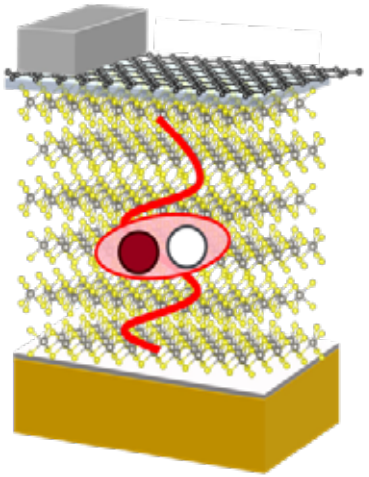

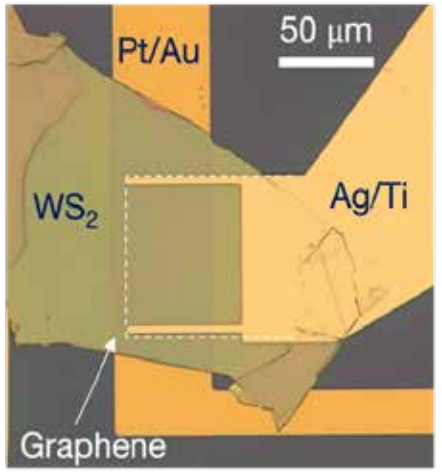

Above: schematic of TMD device, and an optical microscope image of an actual one. Right: Evidence of enhancement of internal quantum efficiency (IQE) and internal power conversion efficiency (IPCE).

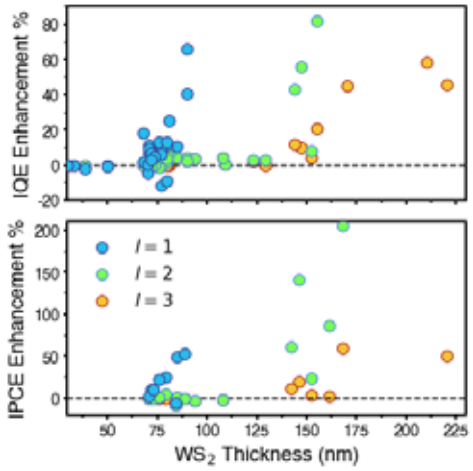

This research was supported in part by the Air Force Office of Scientific Research (AFOSR) FA2386-20-1-4074 and FA2386-21-1-4063. Alfieri et al., *Adv. Optical Mater.* 2023, 11, 2202011.

Characterizing the Structure and Composition of Lithium Ion Batteries

- Understanding the structure and composition of lithium-ion batteries is crucial due to their widespread use in portable electronics and their potential for efficient energy storage.
- In this study, Penn researchers, including Singh Center Director Eric Stach, used advanced microscopy techniques to examine lithium metal, a material used in high-energy density batteries and can be easily damaged during sample preparation for microscopic analysis.
- To overcome this challenge, a technique called "cryogenic lift-out" was developed at the Singh Center and used to prepare thin samples of lithium metal for examination using advanced transmission electron microscopy techniques.

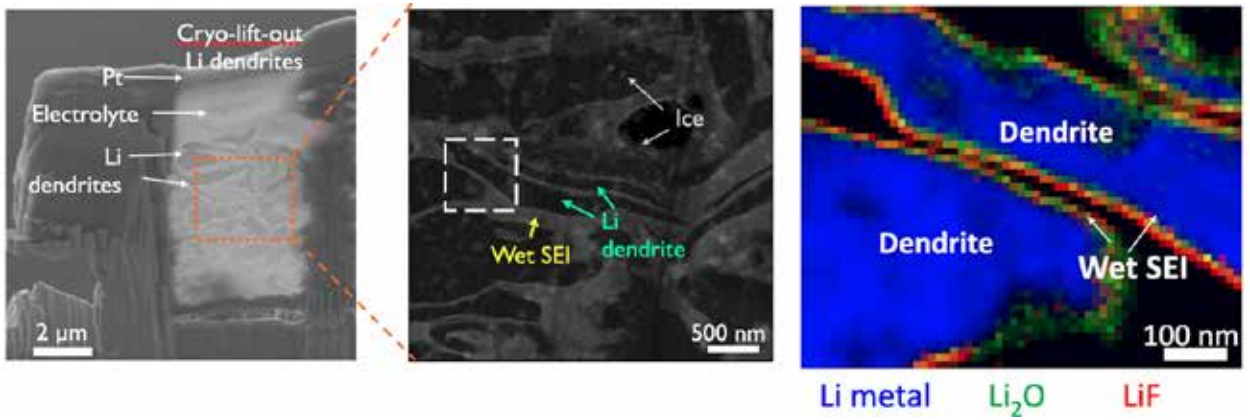

Left: Focused ion beam image of a sample prepared by cryogenic liftout. Middle: electron microscope image from the orange boxed region showing lithium dendrites and frozen ("wet") solid electrolyte interphase. Right: False color imaging showing the composition of the region in the white box, by electron energy loss spectroscopy.

H. Koh, E., Detsi and E.A Stach, *Microscopy and Microanalysis* 29 (4), 1350-1356 (2023) 10.1093/micmic

Nanopore Sensors for Space Exploration – Industry Research

- Researchers at Goeppert LLC are developing nanopore sensors that can enable new discoveries in future NASA missions searching for life on other planets and moons.
- Nanopores, just a few nanometers wide,are fabricated in thin silicon nitride membranes.
- When a voltage is applied across the membrane, molecules traversing through the nanopore briefly disrupt the ionic current flow.
- Careful analysis of these signals allows extremely sensitive detection and characterization of single molecules like DNA.

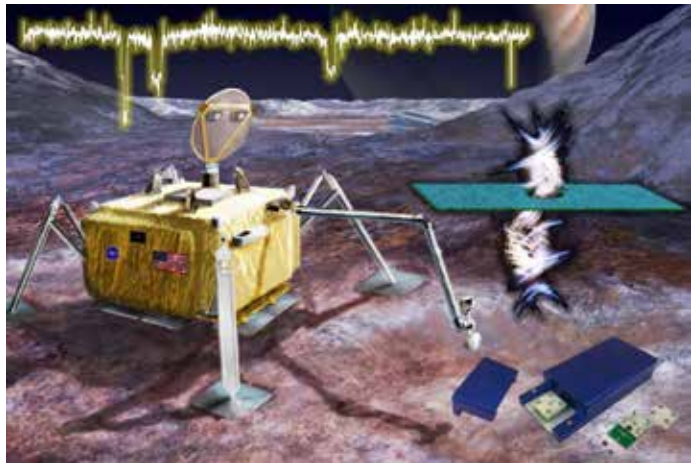

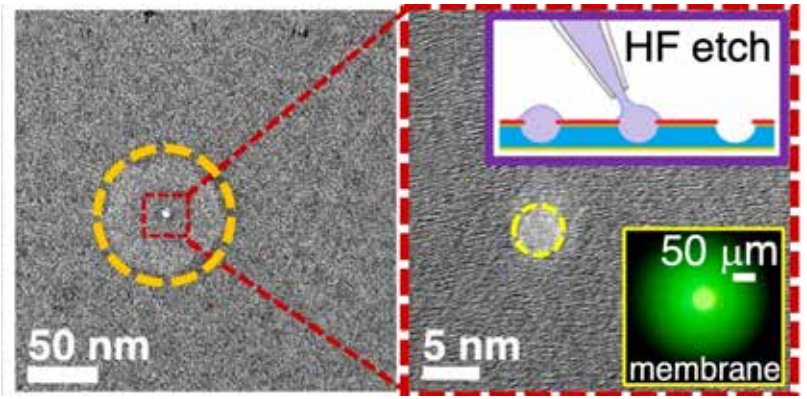

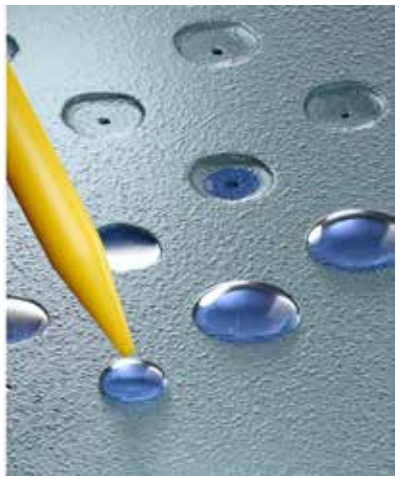

Xia, Z., Patchin, M., McKay, C. P. & Drndic, M., *Astrobiology* (2022) doi:10.1089/ast.2021.0051

National Research Priority: NSF – Understanding the Rules of Life

Structural Phase Patterning of MoS_2 – External Academic Research

- Finding ways to protect our technology from intellectual theft has become increasingly important, including the need to bolster the protection of hardware.
- To aid this endeavor, we propose an alternative method of making MOSFETs by utilizing the structural phases of molybdenum di-sulfide (MoS_2), which can be either a **semiconductor or metal**, enabling di-material logic gates which could substantially fortify device security.
- MoS_2 is a transition metal di-chalcogenide that behaves as a semiconductor in its natural phase (2H). Upon being irradiated with electrons from an electron beam, the crystal will shift to the 1T phase and transitioning the semiconductor into a metal.
- The MoS_2 flakes were profiled at MANTH by Atomic Force Microscopy (AFM) and Kelvin Probe Force Microscopy (KPFM) to map out the difference in work function between the surface and the AFM tip. Brighter areas in the image on the right correspond to a higher work function.

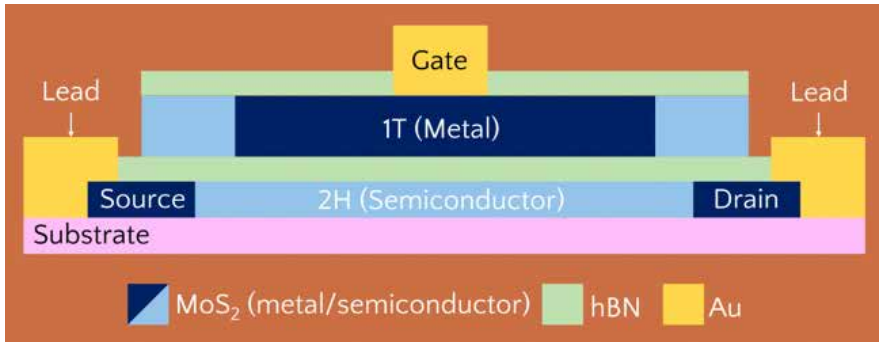

Above: Schematic of a device where MoS2 acts as both a metal and a semiconductor. Below: KPFM image and relationship of work function and beam exposure dose.

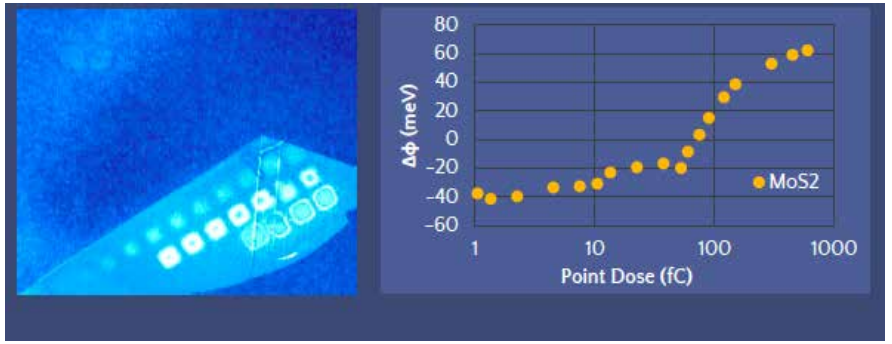

Christopher Barnes and Scott Dietrich, West Chester University and Villanova University. Work performed in part at MANTH.

Biodegradation of Bio-Packaging Materials for Electronic Devices

- CONVERGENCE OF ELECTRONICS, AGRICULTURE, AND ENVIRONMENT
- The degradation behavior of sustainable bio-packaging materials for electronic devices under different operational conditions, such as burying them in top-surface soil, compost, and transparent gel, has been investigated by a group at Penn led by Prof. Mark Allen.
- The objective of these researchers is to develop eco-friendly packaging solutions for electronics in the agricultural sector that provide real-time feedback on soil heterogeneity during crop growth.
- A total of 52 electronic device samples, waxed and unwaxed, were buried in 3 different environments: top surface soil, compost, and “clear soil” (potassium polyacrylate), and held at different temperatures
- This study provides practical insights into the development of eco-friendly packaging solutions for the agricultural sector.

Left: Biodegradable soil sensors used in the experiment. Right: The degradation testbed in operation.

National Research Priority: NSF – Understanding the Rules of Life and Growing Convergence Research

Full Wafters with a High-Performance 2D Semiconductor for Integration on Si

- The semiconductor industry today is responding to a threefold mandate: increasing computing power, decreasing chip sizes and managing power in densely packed circuits. To meet these demands, the industry must look beyond silicon
- One of the biggest shortcomings of silicon is that it can only be made so thin because its material properties are fundamentally limited to three dimensions [3D]. For this reason, two-dimensional [2D] semiconductors have become an object of interest to scientists, engineers and nanoelectronics manufacturers.
- Growth of two-dimensional (2D) indium monoselenide (InSe) over 2-in wafers was demonstrated using pulsed metal-organic chemical vapor deposition (MOCVD) at temperatures below 500 C, a temperature compatible with
eventual integration of the material onto Si devices.
- In addition, the synthesized InSe exhibits gate-tunable electrical transport and field- effect mobility comparable to those of single-crystalline flakes. These findings suggest that MOCVD-grown InSe could serve as an effective channel material for electronics.

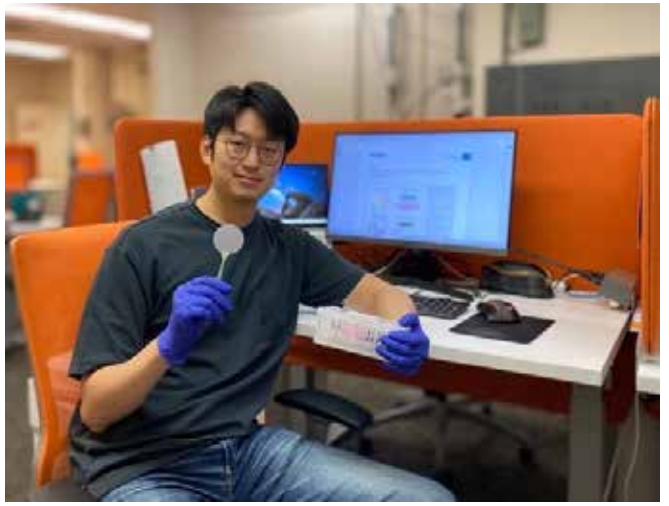

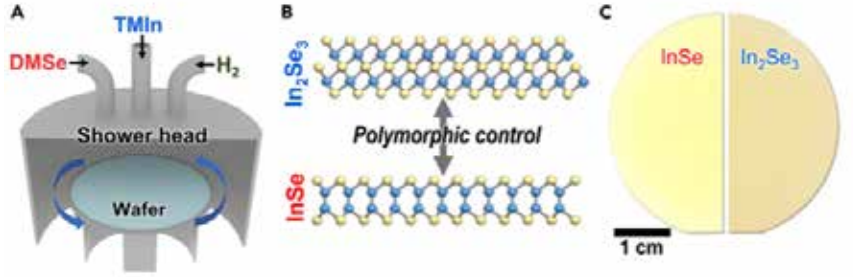

Collaborators include those from U Penn Engineering, Brookhaven National Laboratory, KBR Inc., and the Air Force Research Laboratory. Work performed in part at MANTH.

Song, Seunguk et al., *Matter*. 6.10 (2023): 3483–3498.

Midwest Nanotechnology Infrastructure Corridor (MiNIC)

National Nanotechnology Coordinated Infrastructure

NSF

Zero-Dimensional Valley-Chiral Modes in a Graphene Point Junction

It has been shown that the valley degree of freedom can be manipulated in two-dimensional (2D) materials in a field of low-dissipation quantum electronics called “valleytronics.” It has been shown that valley-polarized current can been realized at the boundary between two regions of bilayer graphene with different atomic or electrostatic configuration. However, the demanding fabrication and operation requirements limit device reproducibility and scalability toward more advanced valleytronic circuits.

In this work, the group of Ke Wang at the University of Minnesota demonstrated a point junction device where a valley-chiral zero-dimensional (0D) PN junction can be configured to be capable of carrying electrical current with an estimated valley polarization of ~80%. This work provides a building block in manipulating valley quantum numbers for scalable valleytronics.

This work was supported by NSF Award No. DMR-1944498. K. Davydov, X. Zhang, W. Ren, M. Coles, L. Kline, B. Zucker, K. Watanabe, T. Taniguchi, and K. Wang, *Sci. Adv.* **10**, eadp6296 (2024).

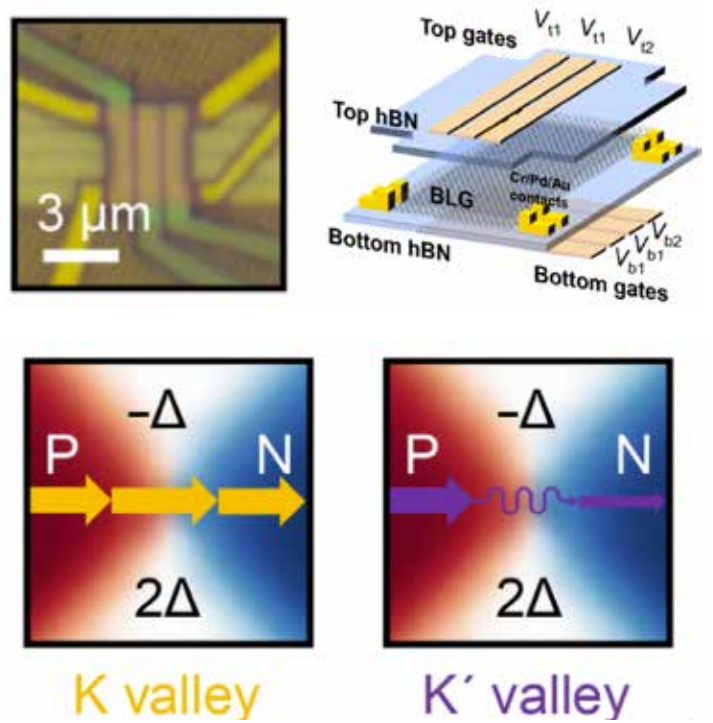

Top: Optical image of a backgated 0D PN junction device with multiple horizontal bottom gates and vertical top gates. Bottom: Conductivity results showing how barriers from the K and K' valleys contribute equally to the measured tunneling current across the junction without valley chirality.

National Research Priority: NSF – Quantum Leap

Gate-Tunable Superconducting Diode Effect in a Three-Terminal Josephson Device

The phenomenon of non-reciprocal critical current in a Josephson device, termed the Josephson diode effect, has garnered much interest in recent years. However, fabrication of the diode is challenging and requires inversion symmetry breaking, typically obtained by spin-orbit interactions.

In this work, the Pribiag group at the University of Minnesota, in collaboration with UCSB, reported observation of the Josephson diode effect in a three-terminal Josephson device based upon an InAs quantum well 2DEG proximitized by an epitaxial aluminum superconducting layer.

Electron-beam lithography was used to fabricate the nanoscale devices, and showed that the diode efficiency in can be tuned by a small out-of-plane magnetic field or by electrostatic gating. The work work showed that Josephson diodes could serve as gate-tunable building blocks for the design of topologically protected qubits for error-resistant quantum computing.

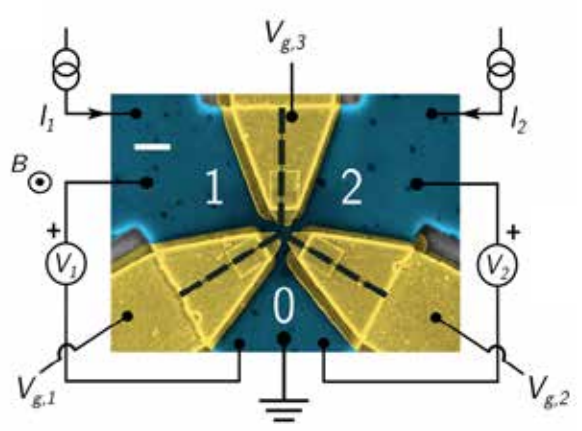

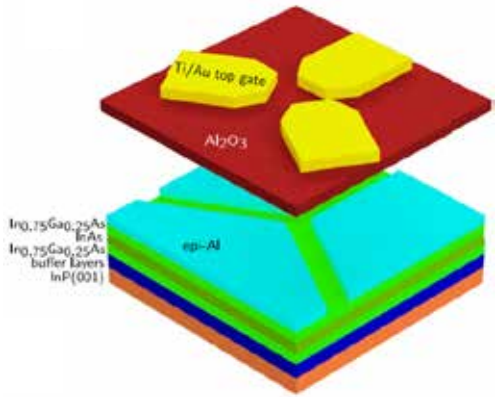

Top: Color enhanced SEM image and Bottom: 3D schematic of a Josephson diode showing layered heterostructure design.

This work was supported by DOE Award No. Department of Energy under Award No. DE-SC0019274 M. Gupta, G. V. Graziano, M. Pendharkar, J. T. Dong, C. P. Dempsey, C. Palmstrøm, and V. S. Pribiag, *Nature Commun*. **14**, 3078 (2023).

National Research Priority: NSF – Quantum Leap

Using Machine Learning to Overcome Interfering Species Interactions in Graphene Sensors

Discriminating between volatile organic compounds (VOCs) for applications including disease diagnosis and environmental monitoring, is often complicated by the presence of interfering compounds such as oxygen. Graphene sensors are effective at detecting VOCs; however, they are also known to be highly sensitive to oxygen. Therefore, the combined effects of each of these gases on graphene sensors must be understood.

In this work performed by the Koester group at the University of Minnesota, machine learning algorithms were developed to allow graphene sensors to distinguish different VOCs despite the introduction of various interfering concentration of oxygen. These results are important for practical applications of graphene sensors for detection of diseases in breath such as lung cancer.

This work was supported the NSF Graduate Research Fellowship Program (GRFP).
N. S. S. Capman, V. R. S. K. Chaganti, L. Simms, C. J. Hogan, Jr., and S. J. Koester, *ACS Appl. Mater. & Interfac.* 16, 7554-7564 (2024).

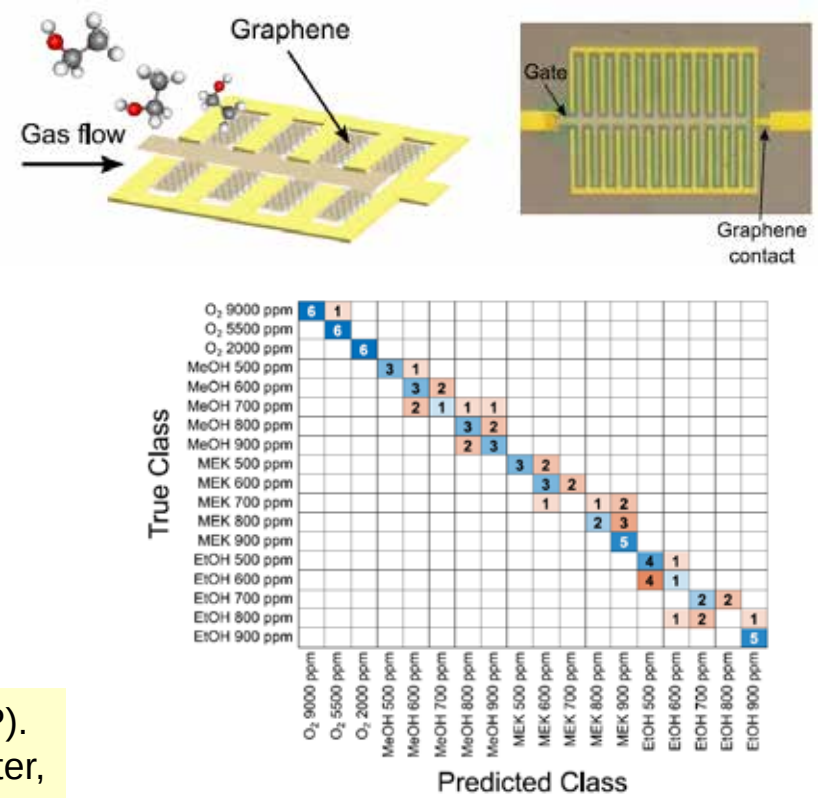

Top: Cartoon and optical micrograph of graphene varactor sensor. Bottom: Confusion matrix after accounting for interfering species interactions showing perfect gas analyte detection and nearest neighbor concentration prediction.

Enhanced Detection of Sickle Cell Disease Using Microfluidics

Sickle cell disease is a disorder where red blood cells (RBCs) become hardened and mis-shapen into a curved "sickle" shape, and is caused polymerization of the abnormal hemoglobin upon deoxygenation which forms fibers in the RBCs. A critical step toward understanding the role of polymer-containing RBCs is quantifying the changes in these cells in physiologically relevant oxygen environments.

In work performed by the David Wood group at the University of Minnesota, the researchers used a microfluidic platform to simultaneously measure single RBC deformability and oxygen saturation under controlled oxygen and shear stress. They found that RBCs with detectable amounts of polymer have decreased oxygen affinity and decreased deformability. This work could be important for understanding the pathophysiology of sickle cell disease, and provide clearer targets for evaluating therapies.

This work was supported by NIH Award No. 3R01HL132906-07S1. Williams, D.C., & Wood, D.K., *Proc. Natl. Acad. Sci.* 120, e2313755120 (2023).

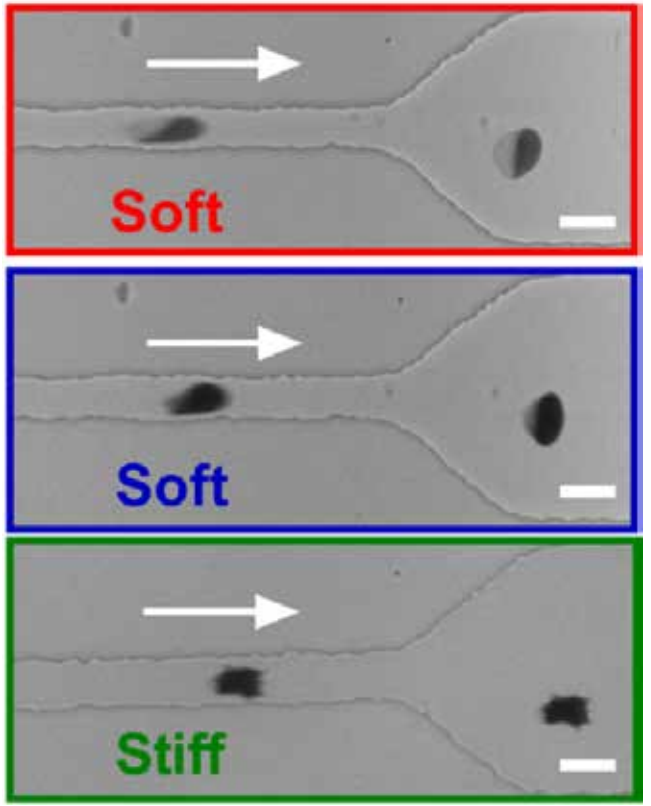

Images of red blood cell transport through microfluidic channels, showing soft oxygenated (red border) and deoxygenated cells (blue border) and stiff deoxygenated cells (green border).

Improved Oxygen Barriers using Polyethylene Microstructures

Linear low-density polyethylene (LLDPE) in packaging applications provides flexibility and toughness but currently requires ethylene-vinyl alcohol (EVOH) additive to improve barrier performance.

In this project, a collaboration between the University of Minnesota (UMN) Characterization Facility staff, the Macosko group at UMN, and Los Alamos National Lab (LANL), the researchers explored blending in 20% high density polyethylene (HDPE) to improve barrier performance without EVOH additive. Photothermal AFM-IR analysis provides stark images of spherulitic crystalline morphologies in both pure HDPE and blended LLDPE/HDPE (80/20%), but essentially absent in pure LLDPE.

The work shows the benefits of photothermal imaging for advanced materials analysis.

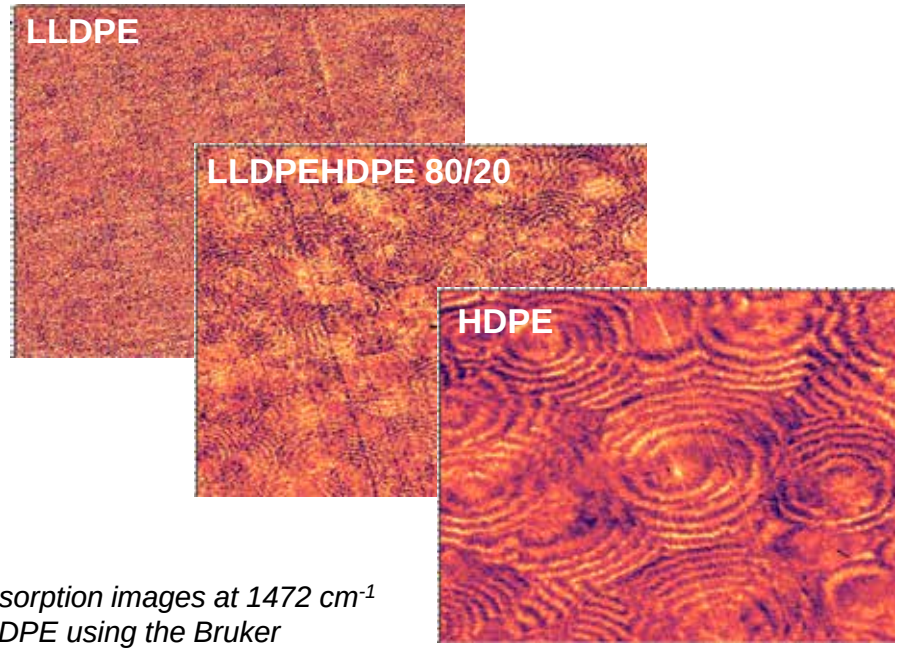

50 x 50-μm^2 photothermal AFM-IR absorption images at 1472 cm^{-1} of LLDPE with and without blended HDPE using the Bruker NanoIR3 system in the Characterization Facility at the University of Minnesota

The work was supported by the Minnesota Industrial Partnership for Research in Interfacial and Materials Engineering (IPRIME) program. Kim, K., Zervoudakis, A. J., LaNasa, J. A., Haugstad G., et al., *ACS Appl. Polymer Mater*. **6**, 524-533 (2023).

MiNIC The Midwest Nano Infrastructure Corridor

Magnetic Tunnel Junction-Based Computational Random-Access Memory

Conventional computing paradigms struggle to fulfill the rapidly growing demands from AI systems due to power consumption associated with data transfer between logic and memory. A new platform called “computational random-access memory (CRAM),” which addresses this fundamental limitation has been developed. CRAM performs logic operations within memory cells themselves, without having the data ever leave the memory.

In this work, led by Prof. Jian-Ping Wang at the University of Minnesota (UMN), in collaboration with the University of Arizona, the CRAM platform based upon magnetic tunnel junctions (MTJs) was demonstrated. The basic logic and memory operations were shown, and a suite of models was developed to characterize functions such as matrix multiplication. This work forms the basis for using CRAM to realize highly power efficient AI applications.

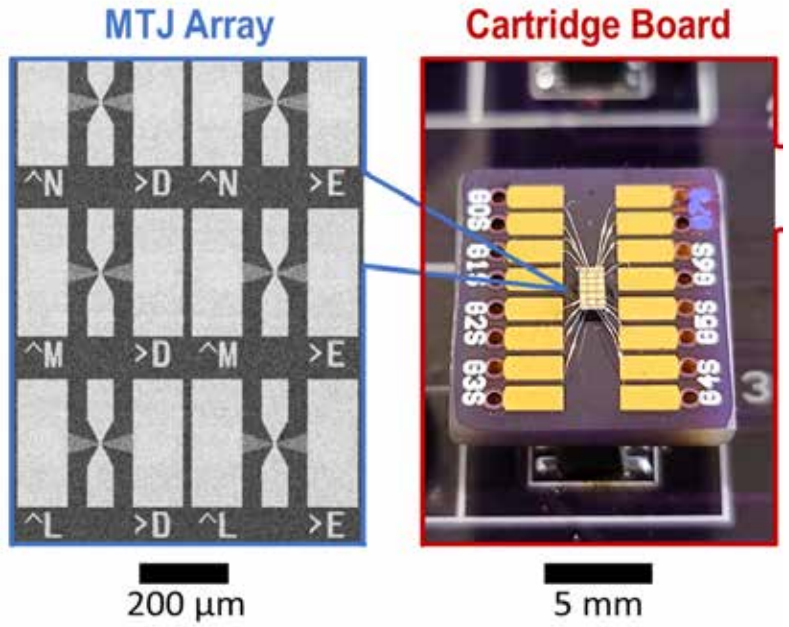

MTJ array on chip and mounted on a circuit board. This hardware demonstrates a fully functioning 1 ✕ 7 CRAM array.

This work was supported by DARPA Award No. HR001117S0056-FP-042, as well as NSF Awards: CCF-1725420, ECCS-2230963, ECCS-2230124. Y. Lv, B. R. Zink, R. P. Bloom, H. Cılasun, P. Khanal, S. Resch, Z. Chowdhury, A. Habiboglu, W. Wang, S. S. Sapatnekar, U. Karpuzcu, and J.-P. Wang, *npj Unconv. Comp*. **1**, 3 (2024).

National Research Priority: DoD – Microelectronics (CHIPS and Science Act)

Atomic Force Microscopy in Cancer Diagnostics

The long-term goal of this research is to integrate rigorous computational, imaging, and deep learning methods to develop tumors in silico, and apply to effective patient-specific therapeutic interventions that can *a priori* predict the patient's response to a specific drug and avoid potential resistance.

In initial work to test the feasibility of AFM methods, arrayed "samples" (2-mm diameter circles) of biopsy human breast cancer were analyzed with atomic force microscopy (AFM) force-distance curves acquired in 50x50-μm^2 "force volume" data cubes under aqueous immersion. Moduli ranging from ~100 kPa to ~20 MPa were measured, dependent on spatial location within a given data set but more significantly between data sets (i.e., different 2-mm sample circles). The example at right is from a sample circle exhibiting notably smaller average modulus than in most of the nine circles. Mappings were generated by special python routines to (i) calculate modulus for a pyramidal indenter (AFM tip) and (ii) measure heights prior to mechanical compliance.

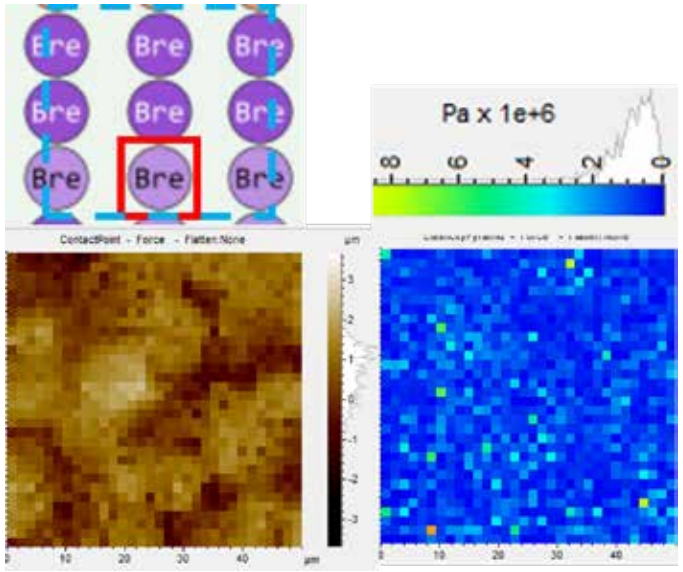

Top left: subset within a larger array of 2-mm sample circles; Bottom left, right: mappings of true topography (compliance-free) and Young's modulus of elasticity (histogram shown above).

Mahsa Dabagh, University of Wisconsin-Milwaukee; Greg Haugstad, College of Science and Engineering Characterization Facility, University of Minnesota.

This work was supported by MiNIC's *Explore Nano* program via the NSF NNCI funding.

National Nanotechnology Coordinated Infrastructure

MiNIC
The Midwest Nano Infrastructure Corridor

Polymer Interdiffusion with Carbon Fiber Occlusions

This project is developing the analytical methodology of photothermal/IR atomic force microscopy (AFM-IR) to probe interfacial mixing of polyetherimide (PEI) and polyether ether ketone (PEEK). Both spatially distributed point spectra and montaged 50-µm images have demonstrated that the ratio of PEI to PEEK can be measured locally and mapped across a >200-µm wide spatial domain, to capture intermixing derived from two widely spaced interfaces. Carbon fibers located in the initial PEEK domain complicate the AFM-IR. The magnitude of the transduced signal (apparent IR absorbance) not only derives from the relative presence of a given material as expected, but also depends on how readily this heat is conducted away. When the AFM tip is near a C fiber this conduction is enhanced, and thereby generates "halos" of reduced signal around the fibers, requiring careful data treatment.

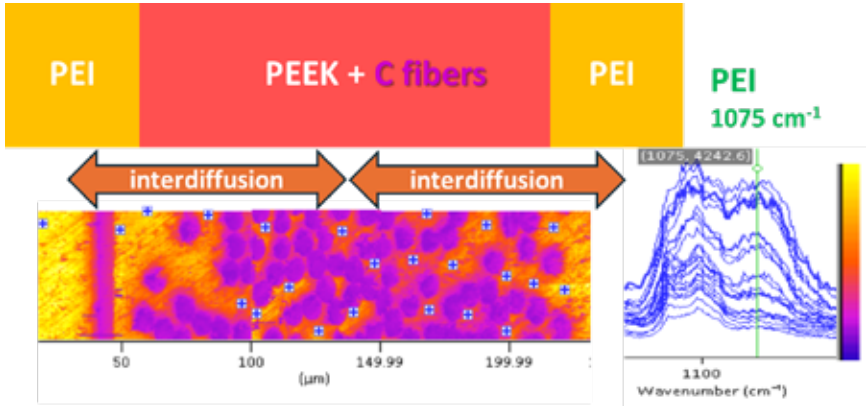

250 x 50-µm² montage of contact resonance AFM-IR absorbance images (lower left) "lighting up" PEI in a cross section that includes two (annealed) interfaces with semicrystalline PEEK (plus C fibers). Spectra at right were acquired at the designated locations atop polymer, wherein there is a variable ratio of PEI:PEEK (from left to center to right in the imaged region).

Joseph Kirchhoff, University of Texas; Mehran Tehrani, University of California San Diego; Tyler B. Hudson, NASA; Greg Haugstad, College of Science and Engineering Characterization Facility, University of Minnesota.

This work was supported by MiNIC's *Explore Nano* program via the NSF NNCI funding.

National Nanotechnology Coordinated Infrastructure

MiNIC
The Midwest Nano Infrastructure Corridor

Montana Nanotechnology Facility (MONT)

National Nanotechnology Coordinated Infrastructure

How the microbiome metabolizes heme for us

- Metabolism is a process in which we feed our microbiomes and they, in turn, feed us.
- Our research aims to discover how gastrointestinal microbes assimilate and safely redistribute iron between themselves and the human host.
- For the first time, we visualized an enzyme that we propose is at the heart of the microbiome's metabolism of heme, the most abundant form of iron in red meat and human cells.
- The structure suggests both how the process might work and how it might be leveraged to support health.

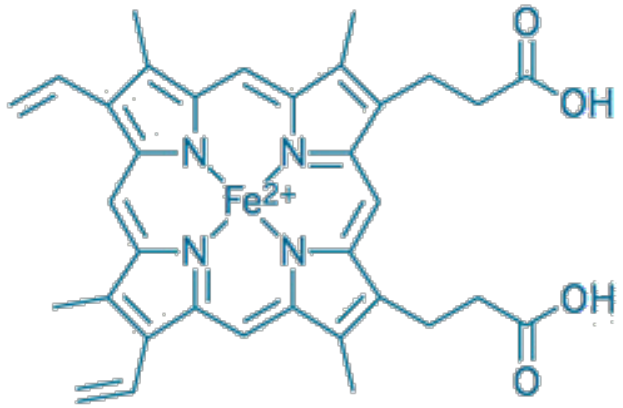

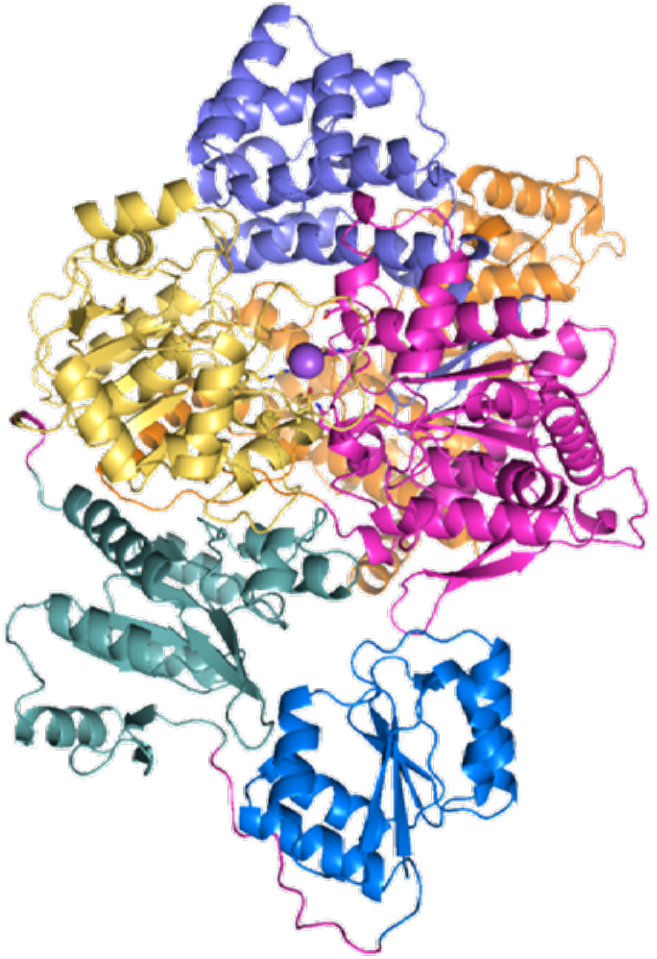

Iron removal from heme (left) by a large protein (right) is an essential function performed by microbiome species.

Arnab Kumar Nath, Colin Gauvin, Emmanuel Akpoto, Martin Lawrence and Jennifer DuBois. Work performed at Montana State University, Biological CryoEM facility.

Supported by NIH-NIGMS R35GM136390.

National Research Priority: NIH - Preventing Disease and Promoting Health

National Nanotechnology Coordinated Infrastructure

MONTANA STATE UNIVERSITY | Montana Nanotechnology Facility

Investigating cell biology of 3D printed biofilms with imaging and image analysis

Biofilm spatial structure often gives rise to emergent properties that are crucial for biofilm behavior and development. However, biofilm structure is difficult to systematically manipulate at relevant spatial scales. Methods of controlling the structure and composition of biofilms are needed. We are developing 3D bioprinting methods that provide control over the structure and composition of living materials at the scale of tens to hundreds of micrometers. We 3D print hydrogels with an encapsulated bacterium and spatially and temporally quantify population dynamics in the hydrogel matrix. We anticipate this technology will advance into a powerful method for engineering complex, spatially structured microbial communities.

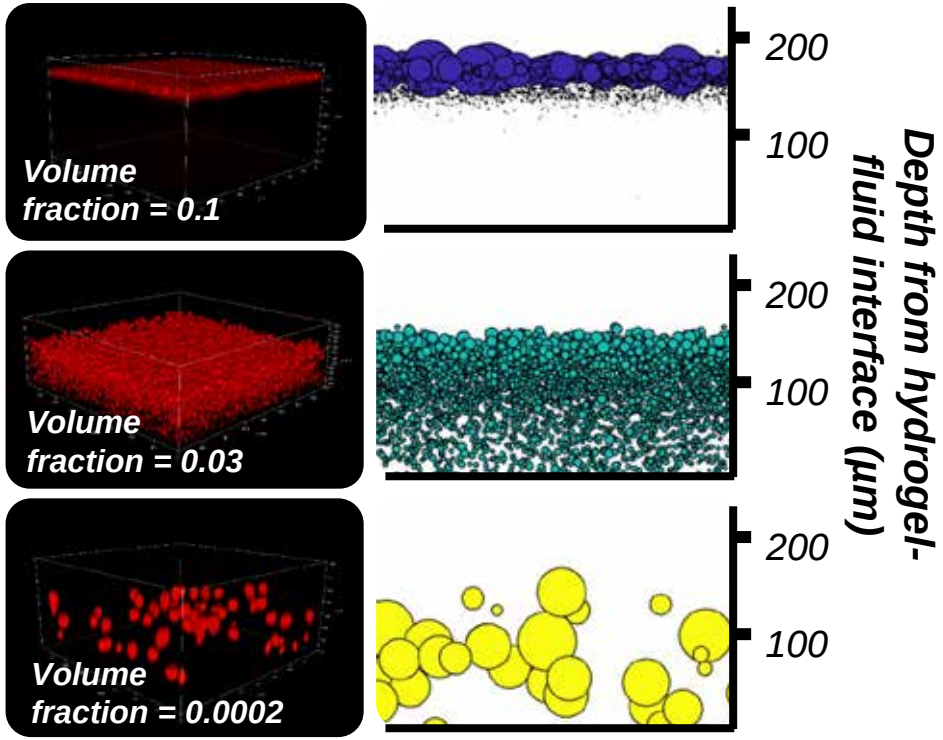

Images of printed biofilms containing Pseudomonas fluorescens at different initial volume fractions reveal emergence of dramatically different synthetic biofilm growth patterns after six days of growth.

Isaak Thornton, Kathryn Zimlich, Chloe Strupulis, Jim Wilking, Heidi Smith, Matthew Fields. Work performed at Montana State University, Center for Biofilm Engineering Bioimaging Facility.

Supported by DOD grant #418-1671.

National Nanotechnology Coordinated Infrastructure

National Research Priority: NSF – Understanding the Rules of Life

MONTANA STATE UNIVERSITY | Montana Nanotechnology Facility

New protein interaction target for treatment of melanoma

Melanoma is the most lethal form of skin cancer and becomes significantly harder to treat if allowed to metastasize. It is the fifth most diagnosed cancer in the U.S. with over 97,000 new cases per year and an even higher incidence in Montana (the fourth most diagnosed cancer). Importantly, we have discovered a novel interaction between a cell surface receptor protein and midkine (MK), also known as MDK, a secreted growth factor named for high expression in mid-gestation. More recently, MDK has been recognized as a marker of cancer and is found to be abnormally elevated in various human malignancies and mediates the acquisition of critical hallmarks of cancer, including cell growth, survival, metastasis, migration, and angiogenesis. Our larger goal is to uncover the immune role of the receptor/MDK interaction, and this leads to our overall hypothesis that interaction interferes with immune cell recognition and may be targetable by additional checkpoint inhibitor therapy. We have designed and fabricated protein sensor arrays, in our local MONT facilities, to test antibody coated nanoparticles as a potential future therapeutic for melanoma and other cancers.

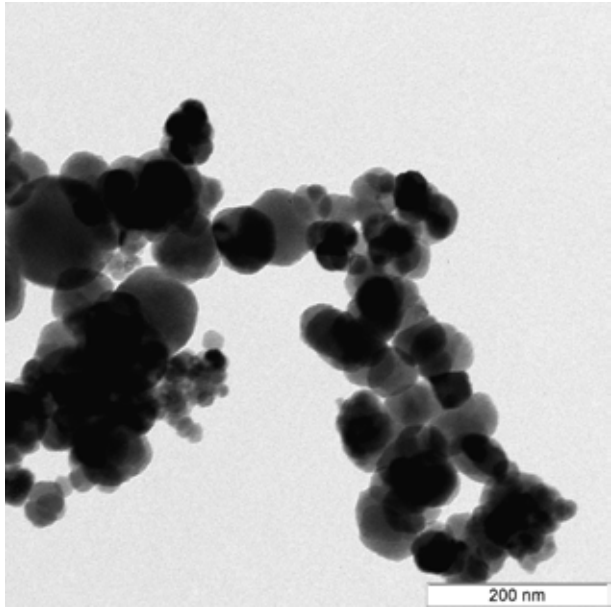

Nanoparticles are used to capture proteins involved in melanoma cancer. The protein coated nanoparticles are then quantified using sensor arrays fabricated in the Montana Microfabrication Facility.

Kestley Lutey, Joshua Heinemann and Richard Warner, Montana State University Billings (MSUB) and Montana State University Bozeman (MSU).

Research supported by the NIH National Institute of General Medical Sciences Award P20GM103474.

National Research Priority: NIH - Develop and Optimize Treatments and Cures and NAE Grand Challenge - Engineer Better Medicines

National Nanotechnology Coordinated Infrastructure

MONTANA STATE UNIVERSITY | Montana Nanotechnology Facility

Fabricating Microfluidic Chips for Magnetic Microrobots Testing

The ultimate goal of this project is to study the underlying mechanism of gravitropism, the growth of plant roots and shoots toward or away from the direction of gravity. It is believed that gravitropism is sensed by statoliths whose sediments change the concentration of auxin which either promotes or suppresses growth of different parts of plants. However, the interaction between statoliths and cell walls is still unclear in the field. We want to study this question by utilizing magnetic microrobots. We built a 3-axis Helmholtz magnetic coil system which can generate arbitrary magnetic fields. As a pilot task, magnetic microparticles will be navigated inside microfluidic chambers to mimic the displacement of statoliths inside plant cells.

So far, we have tested two different designs of microfluidic channels, and successfully navigated magnetic microparticles inside them. The major challenge we have faced is the difficulties to control the distribution of magnetic microparticles due to the hydrodynamic interactions between these microparticles. We just finished our third round of design and have explored a different propulsion method to overcome the hydrodynamic influences.

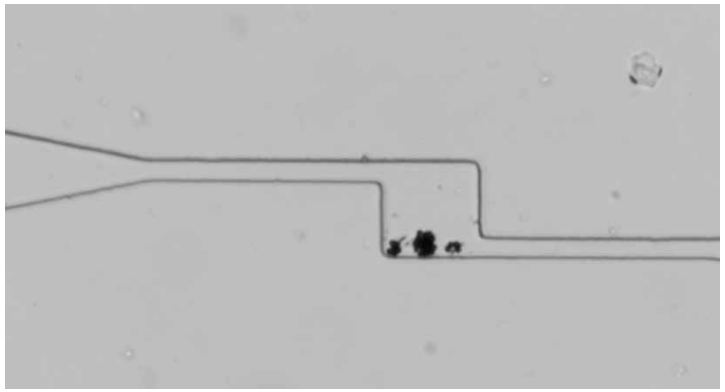

A microscopic image that shows a 100 by 100 μm microfluidic rectangle to mimic plant cells. Magnetic microparticles are navigated into the microfluidic channel through external magnetic manipulation.

Yang Cao, Dewan Sal-Sabil Ahammed, Cyrus Frost. Work performed at Montana State University, MMF Facility.

This work was supported by MONT User Grant, NSF Grant ECCS-2025391

National Research Priority: NSF – Growing Convergence Research and NAE Grand Challenge - Engineer the Tools of Scientific Discovery

Novel Microfluidic Systems for Simulation of Bacterial Transport Through the Subsurface

This work utilizes novel microfluidic systems paired with time lapse microscopy to simulate bacterial transport and partitioning in a contaminated shallow aquifer. This system allows researchers to visualize and quantify the partitioning of key bacterial isolates. This partitioning behavior has been shown to heavily impact rates of biogeochemical cycling within the subsurface and may be influenced by a variety of environmental factors. These microfluidic systems are comprised of glass and SiO_2 and designed to emulate key properties of the aquifer in question. Here, we will utilize these systems to characterize changes in partitioning of key environmental isolates in response to shifts environmental conditions to better understand the forces that drive bacterial localization within the subsurface.

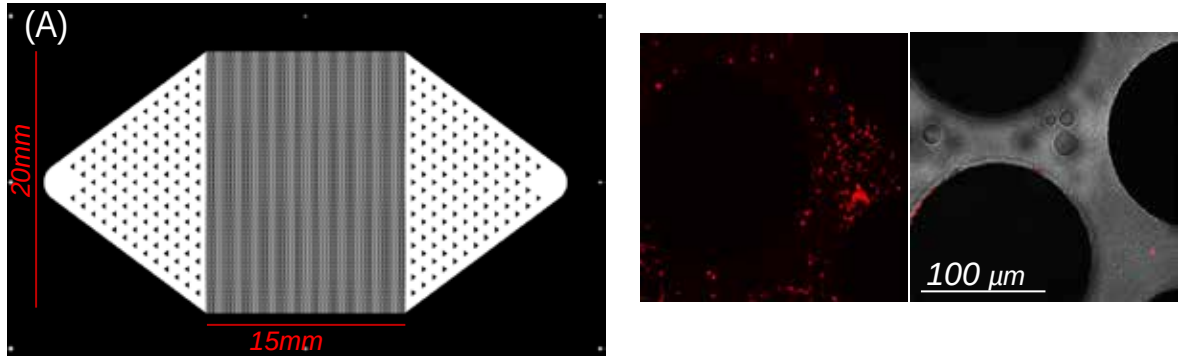

(A) Design file of microfluidic device. (B) Planktonic and attached P. fluorescens cells within device after overnight culture. (C) P. fluorescens within the device after sterile media rinse. Images collected using the Leica Thunder Bioimaging System

James Marquis, Heidi Smith, Yaofa Li, and Matthew Fields, Montana State University. Work performed at Montana State University, Center for Biofilm Engineering Bio-Imaging Facility.

This work was supported by Department of Energy Grant DE-AC02-05CG11231.

National Research Priority: NSF – Growing Convergence Research and NAE Grand Challenge - Provide Access to Clean Water

National Nanotechnology Coordinated Infrastructure

MONTANA STATE UNIVERSITY | Montana Nanotechnology Facility

Identification of Cadmium Corrosion

Corrosion was identified on Commercial Off The Shelf electronics connectors that are cadmium plated and treated with chromium conversion coating in accordance with military specification SAE-AMS-QQ-P-416.

FEM and EDS assisted in determining that the corrosion material has significantly more carbon than the surrounding material and was percolating from cracks in the chromium conversion coating.

In determining the mechanism by which the corrosion was occurring, production processes were able to be adjusted to maintain the integrity of the chromium conversion coating on cadmium plated connectors.

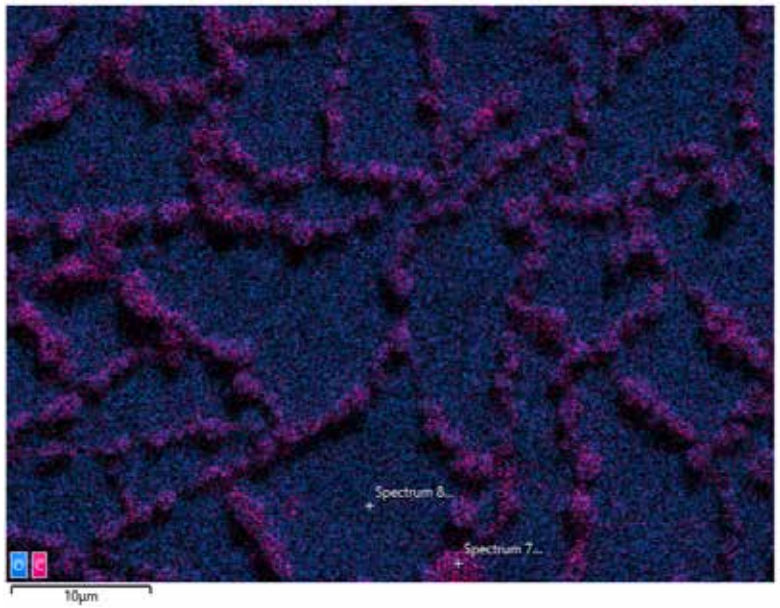

EDS elemental map overlay of O (blue) and C (pink) showing the ridges of material percolating through the surface crack.

Ben Rathman, S&K Electronics, Inc. Work performed at Montana State University, Imaging and Chemical Analysis Laboratory.

This work was supported by S&K Electronics, Inc.

Viral proteins activate PARIS-mediated tRNA degradation and viral tRNAs rescue infection

Viruses compete with each other for limited cellular resources, and some viruses deliver defense mechanisms that protect the host from competing genetic parasites. PARIS is a defense system, often encoded in viral genomes, that is composed of a 53 kDa ABC ATPase (AriA) and a 35 kDa TOPRIM nuclease (AriB). We show that AriA and AriB assemble into a 425 kDa supramolecular immune complex. We use cryo-EM to determine the structure of this complex, explaining how six molecules of AriA assemble into a propeller-shaped scaffold that coordinates three subunits of AriB. ATP-dependent detection of foreign proteins triggers the release of AriB, which assembles into a homodimeric nuclease that blocks infection by cleaving the host tRNA-Lys. Collectively, these data explain how AriA functions as an ATP-dependent sensor that detects viral proteins and activates the AriB toxin. PARIS is one of an emerging set of immune systems that form macromolecular complexes for the recognition of foreign proteins, rather than foreign nucleic acids.

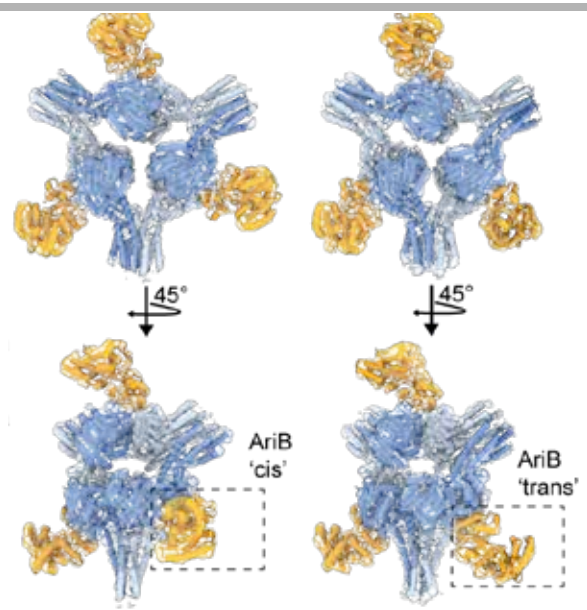

Structures of PARIS determined using Cryo-EM at Montana State University.

Nathaniel Burman, Svetlana Belukhina, Florence Depardieu, Royce A. Wilkinson, Mikhail Skutel, Andrew Santiago-Frangos, Ava B. Graham, Alexei Livenskyi, Anna Chechenina, Natalia Morozova, Trevor Zahl, William S. Henriques, Murat Buyukyoruk, Christophe Rouillon, Lena Shyrokova, Tatsuaki Kurata, Vasili Hauryliuk, Konstantin Severinov, Justine Groseille, Agnès Thierry, Romain Koszul, Florian Tesson, Aude Bernheim, David Bikard, Blake Wiedenheft, Artem Isaev. Work performed at Montana State University, Cryo-EM Core Facility.

Supported by NIH-NIGMS R35GM134867

PFOA Changes Membrane Bilayer Structure

Our work investigates how perfluorooctanoic acid (PFOA) - one of the most common PFAS species, or “forever chemicals” - affects model lipid membrane properties at concentrations approaching regulatory limits. Experiments show that sub-micromolar PFOA concentrations render model membranes more susceptible to bioconcentration of secondary solutes, and these findings have consequences for for how pollutant bioconcentration factors change in the presence of PFAS contaminants.

Cryo-EM images provide critical insight into how PFOA affects bilayer structure and properties. Specifically, PFOA induces multilamellar formation (rather than unilamellar structures) as well as the creation of niosomes. Coupled with fluorescence emission data, we propose that PFOA fluidizes the bilayer structure and destabilizes vesicles.

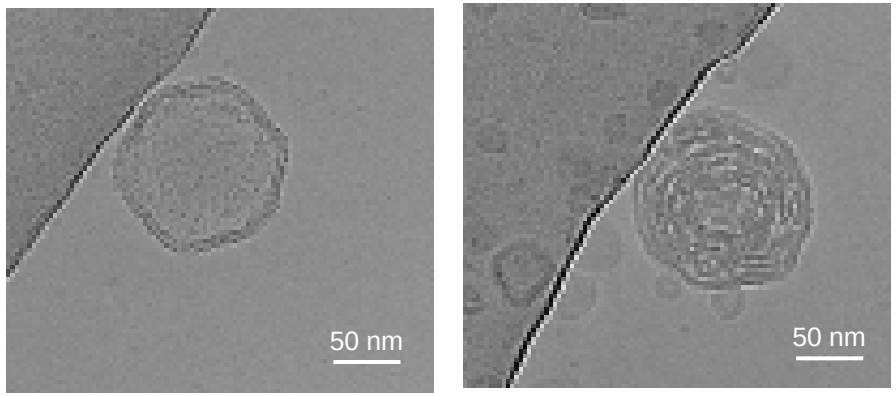

Cryo-EM images of lipid vesicles formed by DPPC in a carbonate buffer (pH 7) solution (left) and in a carbonate buffer solution containing 100 nM PFOA (right). Lipid vesicles formed in the presence of PFOA show complex, compartmentalized structures as well as niosomes, smaller (~35 nm diameter) bilayer structures.

Rhys C. Trousdale, Colin L. Gauvin, Tess N. Sobolewski, C. Martin Lawrence and Robert A. Walker, Montana State Univ. Work performed at Montana State University, Cryo-EM Facility.

Supported by NSF EPSCoR: OIA-1757351. Submitted to *Env. Sci. Tech.* (April 2024)

National Research Priority: NAE Grand Challenge - Provide Access to Clean Water

National Nanotechnology Coordinated Infrastructure

MONTANA STATE UNIVERSITY | Montana Nanotechnology Facility

Fabrication of Calcite-Based Micromodel

The goal of this research is to develop novel fabrication methods to fabricate calcite-based 2D porous microchannels in order to study mineral dissolution and reactive transport in porous media. This work is primarily motivated by CO_2 sequestration – a viable technique to battle against climate change.

In this work, we combined conventional rock sample preparation techniques and microfabrication techniques, enabled by the Sample Prep Lab and Montana Microfabrication Facility (MMF). We have successfully developed a new protocol that has led to novel calcite-based devices and satisfactory test results. The work has led to one journal article (in review), on conference presentation and one external proposal to NSF.

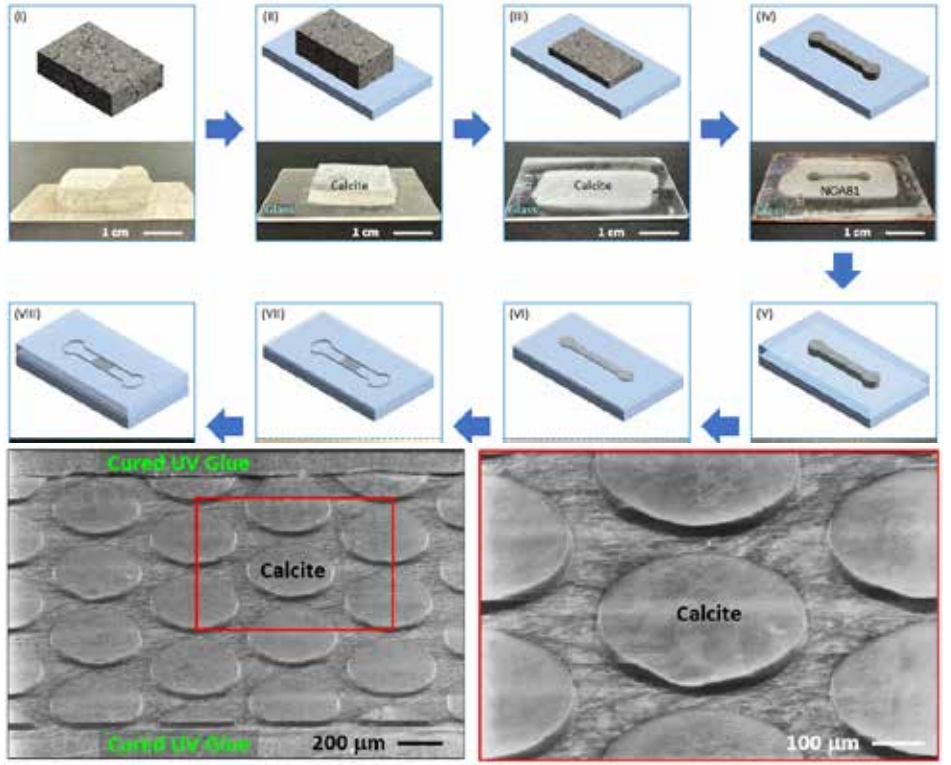

[Top] New fabrication protocols; [Bottom] SEM photos

Rafid Musabbir Rahman and Yaofa Li, Montana State University. Work performed at Montana State University, Montana Microfabrication Facility and Sample Prep Lab.

Supported by NSF (Grant# ECCS-2025391) and ACS PRF (62687- 763DNI9). Rahman, et al. AGU Fall Meeting, San Francisco, December 2023.

National Research Priority: NAE Grand Challenge - Develop Carbon Sequestration Methods

MONT Empower Scholar Student Projects

- ***MONT Supported undergraduate worker in the Mass Spec Facility***: Sample and standards preparation, experiment methodologies for various methods of mass spectrometry.

- Current Projects:
  - Field collection and preparation of water samples for ICP-MS dissolved metals analysis. In progress: working with MSU Geospatial Core Facility to create various visual representations of metal concentration geographically.
  - Commercial ski kick waxes hydrocarbon composition compared with natural source waxes by GC-MS. Prepared and experimented for best sample conditions and data collection. Data analysis in progress.
  - Performed sample preparation and in-depth research of sample origins of over 50 dark chocolate samples in commercial products. Sent externally for comparative analysis before internal ICP-MS experimentation. In progress with goal of undergraduate paper on methodology and learning outcomes.

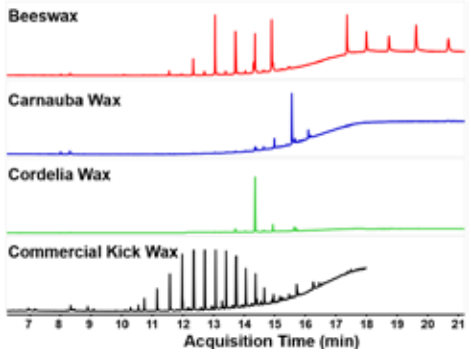

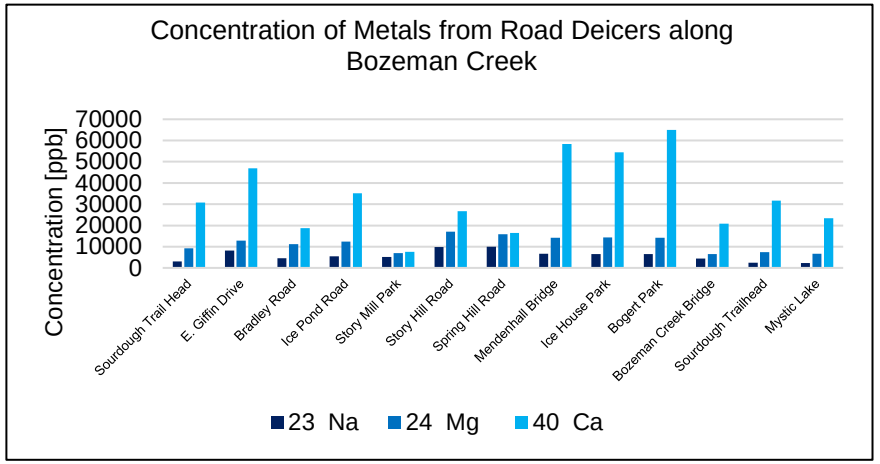

Samantha Roth and Donald F. Smith. Work performed at Montana State University, Mass Spectrometry Facility.

Supported by MONT Empower Scholars Award through NSF Grant ECCS-2025391

Nanotechnology Collaborative Infrastructure Southwest (NCI-SW)

National Nanotechnology Coordinated Infrastructure

Structure of the Inmazeb Cocktail and Resistance to Ebola Virus

Monoclonal antibodies can provide important pre- or post-exposure protection against infectious disease for those not yet vaccinated or in individuals that fail to mount a protective immune response after vaccination. Inmazeb (REGN-EB3), a three-antibody cocktail against Ebola virus, lessened disease and improved survival in a controlled trial. Here, we present the cryo-EM structure at 3.1 A of the Ebola virus glycoprotein, determined without symmetry averaging, in a simultaneous complex with the antibodies in the Inmazeb cocktail. This structure allows the modeling of previously disordered portions of the glycoprotein glycan cap, maps the non-overlapping epitopes of Inmazeb, and illuminates the basis for complementary activities and residues critical for resistance to escape by these and other clinically relevant antibodies. We further provide direct evidence that Inmazeb protects against the rapid emergence of escape mutants, whereas monotherapies even against conserved epitopes do not, supporting the benefit of a cocktail versus a monotherapy approach.

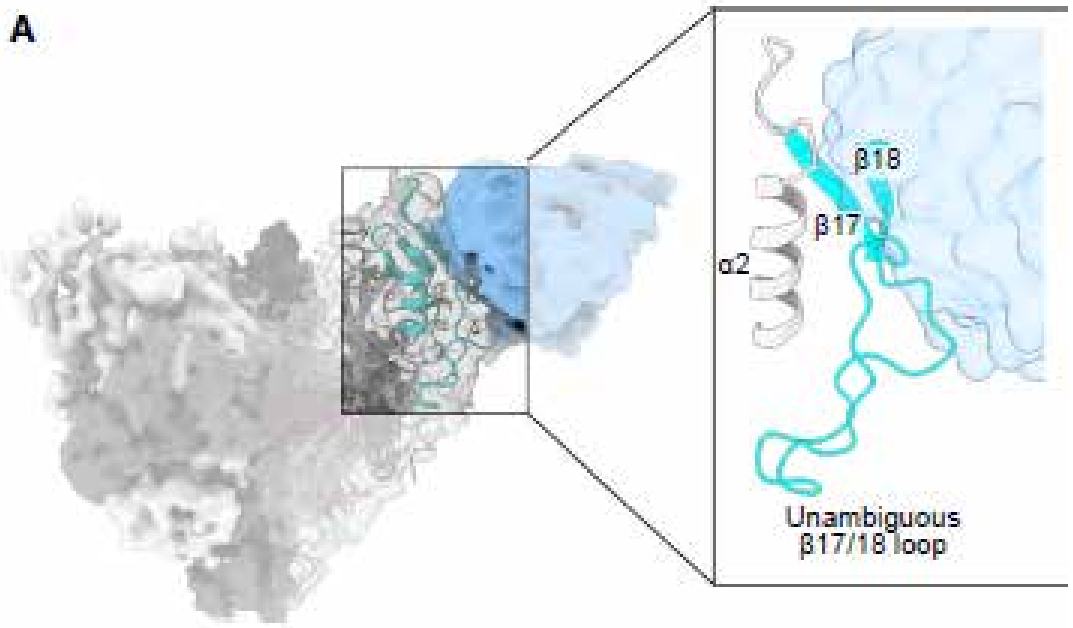

Cryo-EM map of Inmazeb, a three-antibody cocktail against Ebola virus
.

Horacio Bach, Department of Medicine, University of British Columbia, Vancouver. Work performed in part at the NCI-SW site.

This work was supported by NSF Award # ECCS-1542160. *Int. J. Mol. Sci.,* vol. 23, article 13910.
https://doi.org/10.3390/ijms232213910

National Research Priority: NAE Grand Challenge – Engineer Better Medicines

National Nanotechnology Coordinated Infrastructure

NCI Southwest

Spin-Selective Oxygen Evolution Reaction in Chiral Iron Oxide Nanoparticles

Electron spin polarization is identified as a promising avenue for enhancing the oxygen evolution reaction (OER), which is the bottleneck that limits the energy efficiency of water-splitting. Here, we report that both ferrimagnetic (f-Fe_3O_4) and superparamagnetic iron oxide (s-Fe_3O_4) catalysts can exhibit external magnetic field (H_{ext})- induced OER enhancement, and the activity is proportional to their intrinsic magnetic moment. Additionally, the chirality-induced spin selectivity (CISS) effect was utilized in synergy with Hext to get a maximum enhancement of up to 89% improvement in current density (at 1.8 V vs RHE) with a low onset potential of 270 mV in s-Fe_3O_4 catalysts. Spin polarization and the resultant spin selectivity suppress the production of H_2O_2 and promote the formation of ground state triplet O2 during the OER. Furthermore, the design of chiral s-Fe_3O_4 with synergistic spin potential effect demonstrates a high spin polarization of ~42%, as measured using conductive atomic force microscopy (c-AFM).

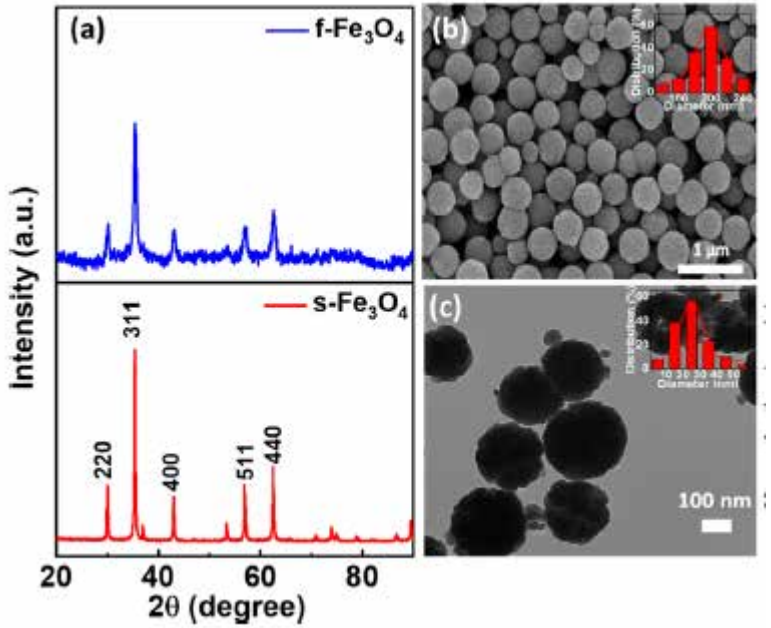

a) XRD of f-Fe_3O_4 (top) and s-Fe_3O_4 (bottom). (b) SEM image of f-Fe_3O_4 and (c) TEM image of s-Fe_3O_4

Sreeprasad Sreenivasan, Department of Chemistry and Biochemistry, The University of Texas at El Paso. Work performed in part at the NCI-SW site.

This work was supported by NSF Award # ECCS-1542160. *Nano Lett.* 2023, 23, 9042−9049

National Research Priority: DOE – Energy Storage Grand Challenge

National Nanotechnology Coordinated Infrastructure

NCI Southwest

Toxicity mechanisms of graphene oxide and cadmium in Microcystis aeruginosa

The potential ecotoxicological hazard of gaphene oxide (GO) is not fully clarified for photoautotrophic organisms.The objective of the current study was to better understand the mechanisms of toxicity of GO in the cyanobacteria Microcystis aeruginosa, and to identify its interactions with cadmium (Cd). The individual and combined contribution of both pollutants in cyanobacteria were evaluated after 96 hours of exposure to GO and/or Cd, using photosynthetic pigments, photo-synthetic parameters, cellular indicators of peroxidative damage, viability, and intracellular ROS formation as indicators of toxicity. Interactions between GO and Cd were evaluated using Toxic Units based on the EC50 of each parameter evaluated. The results of this study indicate that single concentrations ≥ 5 μg mL^{-1} of GO and ≥ 0.1 μg mL^{-1} of Cd induced a decrease in cell biomass and a change in the photosynthetic parameters associated with primary productivity in M. aeruginosa. In the combined experiments, higher GO ratios (≥ 9.1 μg mL^{-1}) in terms of Toxic Units decreased photochemical processes and cellular metabolism, increased oxidative stress, and ultimately affected the size of M. aeruginosa. Finally, the relationship between GO concentration, Cd concentration, and the adsorption capacity of GO with respect to the co pollutant must be taken into account when assessing the environmental risk of GO in aquatic environments.

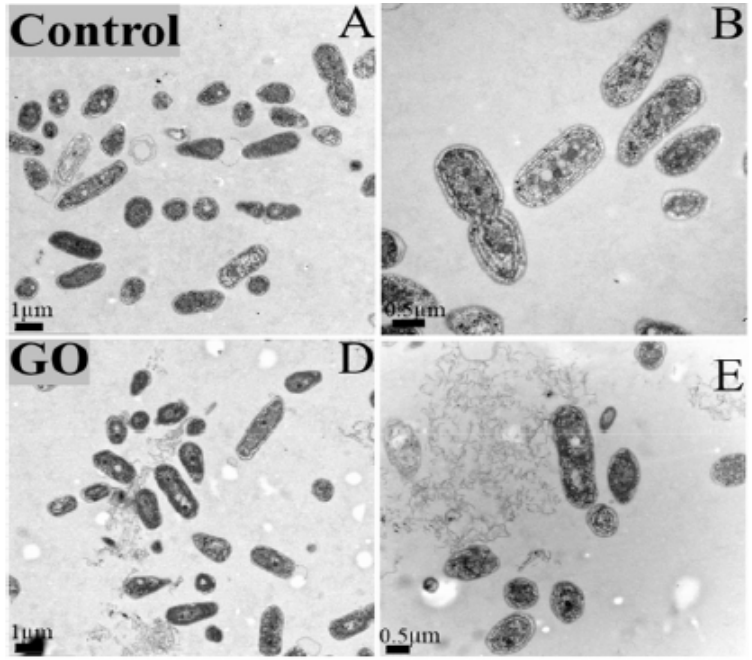

Transmission electron micrographs of M. aeruginosa cells after 96 h incubation

Francois Perreault, Dept. of Chemistry, University of Quebec, Montreal, Canada. Work performed in part at NCI-SW.

This work was supported by NSF Award # ECCS-1542160. *Aquatic Toxicology*, vol. 263, article 106703, 2023
https://doi.org/10.1016/j.aquatox.2023.106703

National Research Priority: NAE Grand Challenge – Provide Access to Clean Water

National Nanotechnology Coordinated Infrastructure

NCI Southwest

Investigation of vertical GaN-on-GaN p–n diode with regrown p-GaN for operation in Venus and other extreme environments

This work reports the performance of vertical GaN-on-GaN p–n diodes with etch-then-regrown p-GaN after exposure to a simulated Venus environment (460 C, 94 bar, containing CO_2/N_2/SO_2 etc., atmosphere) for over 10 days, and compared them to the performance of GaN p–n diodes without the etch-then-regrow process. After the above-mentioned Venus test, temperature-dependent I–V and microscopy investigation were conducted to study the robustness of etch-then-regrow p-GaN and vertical GaN p–n diodes under harsh environments and operation up to 500 C. p-electrode degradation is found to be the main issue of the device's performance. This is the highest temperature at which such characterization has been conducted for vertical GaN p–n diodes, therefore establishing a critical reference for the development of p-GaN regrown and vertical GaN-based electronics for extreme environments.

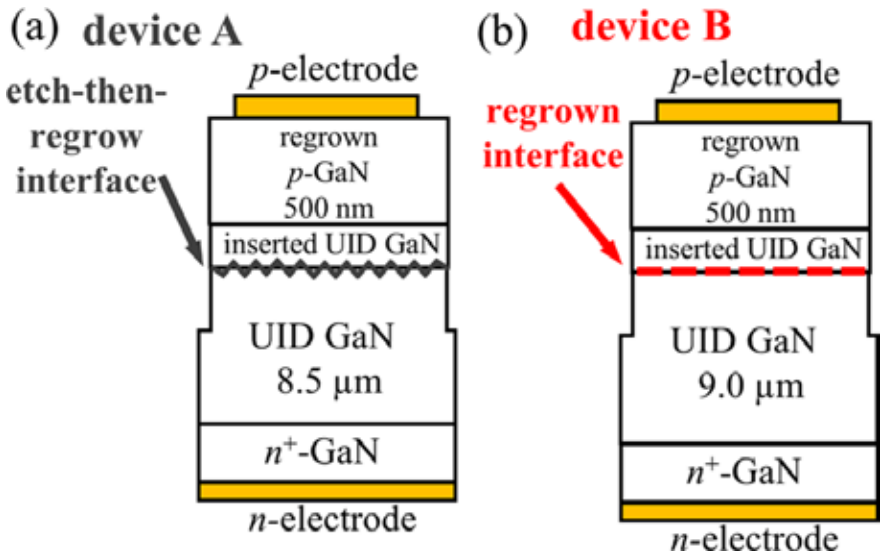

Schematic cross section of (a) device A with the etch-then-regrow process and (b) device B with the regrown process.

Yuji Zhao, Department of Electrical and Computer Engineering, Rice University. Work performed in part at NCI-SW.

This work was supported by NSF Award # ECCS-1542160. *Appl. Phys. Lett.* 123, 243504 (2023); doi: 10.1063/5.0173535.

MoS_2 Nanoflakes based Kilohertz Electrochemical Capacitors

An ultra-fast electrochemical capacitor (EC) designed for efficient ripple current smoothing was fabricated using vertically oriented MoS_2 (VOM) nanoflakes deposited on freestanding carbonized cellulose (CC) sheets as electrodes. The daily used cellulose tissue sheets were transformed into electrode scaffolds through a rapid pyrolysis process within a preheated furnace, on which VOM nanoflakes were formed in a conventional hydro-thermal process. With these ~10 μm thick VOM-CC electrodes, ultrafast ECs with tunable frequency response and specific capacitance density were fabricated. With the facile and easily scaled up process to producing the nanostructured electrode, the miniaturized VOM-CC based ECs have the potential to substitute the bulky aluminum electrolytic capacitors for current smoothing and pulse power applications.

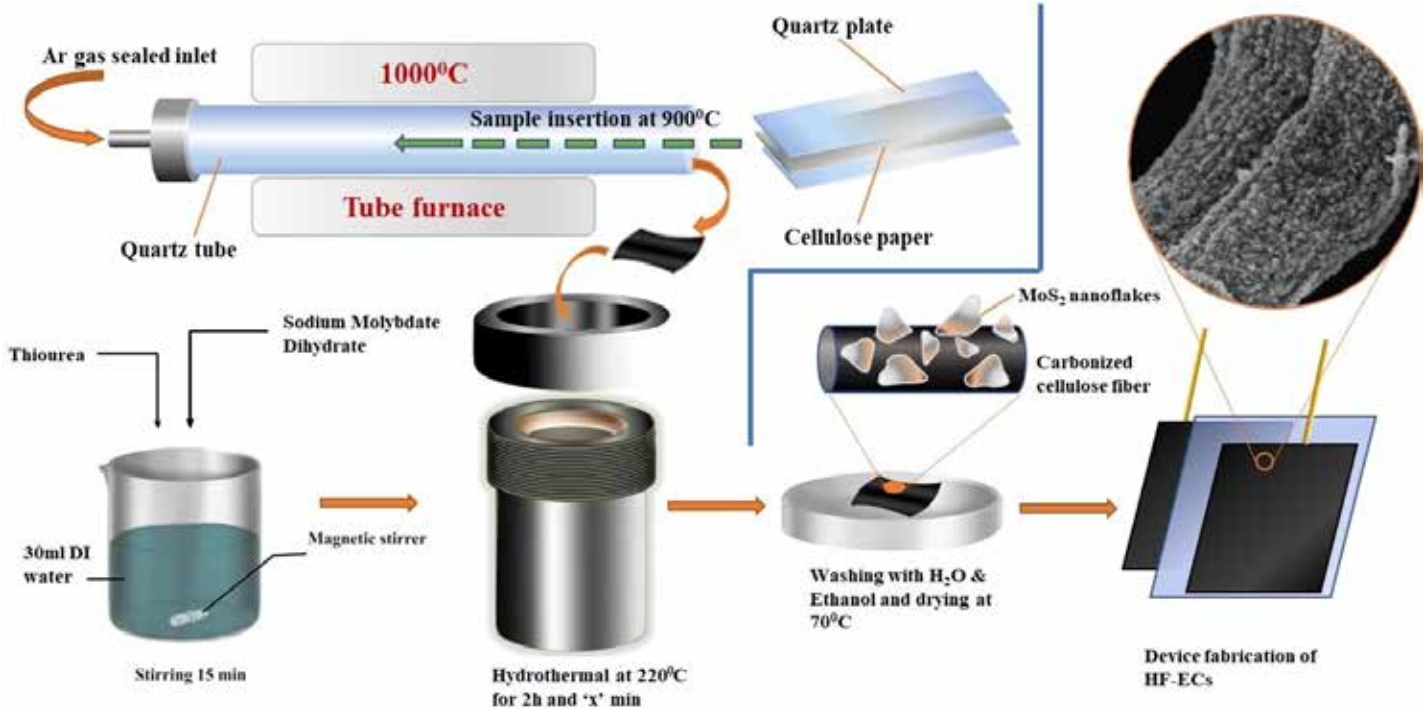

Schematic of the VOM-CC electrode fabrication process

Zhaoyang Fan, School of ECEE, Arizona State University. Work performed in part at NCI-SW.

This work was supported by NSF Award # ECCS-2025490. *Batteries & Supercaps* 2024, 7, e202300363. https://doi.org/10.1002/batt.202300363

National Research Priority: DOE – Energy Storage Grand Challenge

National Nanotechnology Coordinated Infrastructure

NCI Southwest

Self-supported polypyrrole flexible electrodes for electrochemical reduction of nitrite

The efficiency of an electrochemical oxidation/reduction process strongly depends on the working electrode's surface area to volume ratio. By making electrodes flexible and employing different configurations such as rollto- roll membrane, the surface area to volume ratio can be enhanced, therefore improving the overall efficiency of electrochemical processes. Conductive polymers emerge as a new framework to enable alternative electrochemical water treatment cell configurations. Self-standing polypyrrole flexible electrodes were synthesized by electropolymerization and evaluated on the treatment of an oxyanion pollutant: nitrite. Mechanical characterization through stress-strain curves and bending tests demonstrated high electrode resilience that sustained over 1000 bending cycles without impacting mechanical integrity or electrocatalytic responses. The electrocatalytic response towards nitrite reduction was assessed under linear scan voltammetry (LSV) and removal performance evaluated under potentiostatic conditions reaching 79% abatement of initial concentrations of nitrite of 15 mg/L

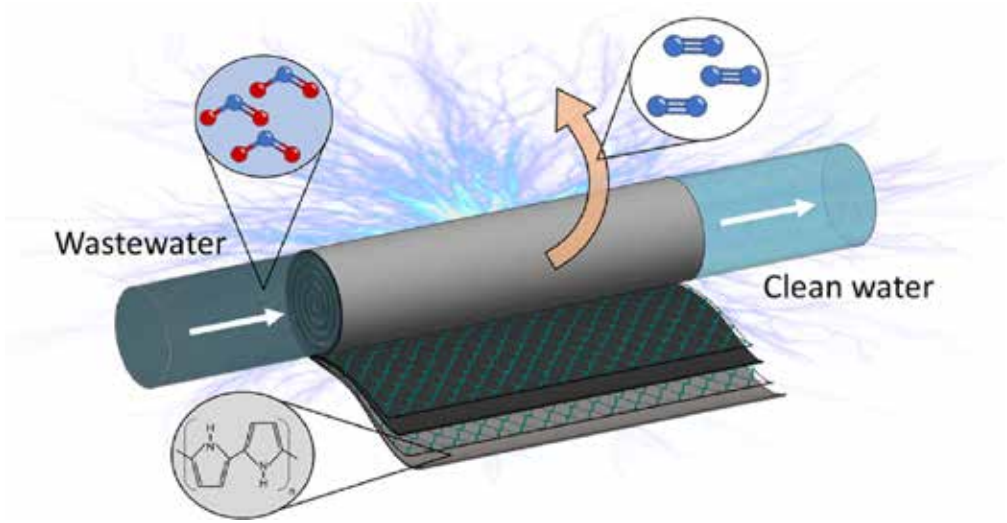

Schematic illustration of the flexible electrodes used for the electrochemical reduction of nitrite.

Sergi Garcia-Segura, School of Sustainable Engineering and the Built Environment, Arizona State University,. Work performed in part at NCI-SW.

This work was supported by NSF Award # ECCS-2025490. *Chemosphere*, vol. 338, article 139582, 2023, https://doi.org/10.1016/j.chemosphere.2023.139582.

National Research Priority: NAE Grand Challenge – Provide Access to Clean Water

Decahedra and Icosahedra Everywhere: The Anomalous Crystallization of Au and Other Metals at the Nanoscale

Throughout history, objects with fivefold symmetry have been a popular topic of interest for artists, philosophers, and scientists. This may be because fivefold symmetry is very conspicuous in nature. In the case of crystals, fivefold rotational symmetry is mathematically forbidden, and macroscopic crystals exhibiting fivefold symmetry have never been shown to exist. Nevertheless, in the nanoworld, nanoparticles are often found with decahedral and icosahedral shapes that have an overall pseudo-fivefold symmetry. These structures are observed at many length scales, from 1 nm up to 1 μm. In this review, several reasons for the stability of fivefold nanoparticles are discussed. These include the formation of twin boundaries, surface reconstruction faceting, and other factors.

Miguel Yacaman, Applied Physics and Materials Science Department, Northern Arizona University. Work performed in part at NCI-SW

Cryst. Res. Technol. 2023, 58, 2200259. https://doi.org/10.1002/crat.202200259

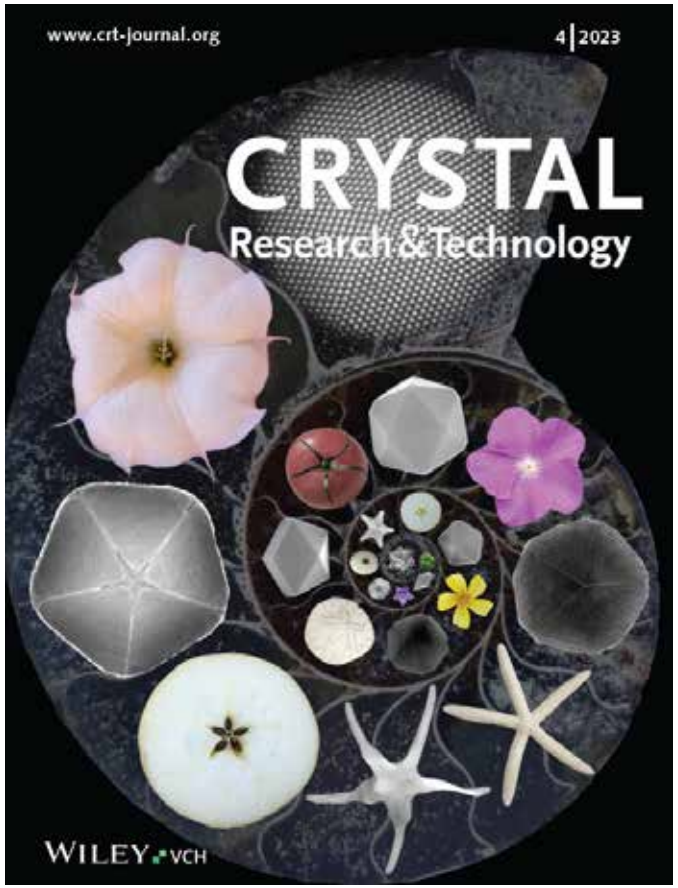

Dr. Yacaman's remarkable images of five-fold symmetry in the nanoworld made the cover of Crystal Research & Technology

National Nanotechnology Coordinated Infrastructure

NCI Southwest

Interface-Mediated Enhancement of Chiroptical Activity in Semiconducting-Metal Hybrid Nanohelices

Strong chiroptical activity has been an active area of research due to potential applications in polarization control and enhanced molecular sensing. However, the creation and investigation of hybrid chiral nanostructures, consisting of multiple active materials, are relatively unexplored areas. In this work, we fabricated nanohelices with a semiconducting material, titanium dioxide, which were “decorated” with a plasmonic material, gold (Au), via physical vapor deposition. Due to the hybrid nature of the samples, we observed broadband chiroptical activity spanning from the ultraviolet through visible wavelengths, which is not observed with either material alone. Remarkably, the magnitude of the visible-wavelength chiroptical activity was found to be highly enhanced and highly sensitive to the amount of Au. This dramatic signal enhancement and high sensitivity cannot be explained by a simple algebraic addition of the optical activities of the two underlying materials and is thus expected to be a result of the plasmonic−semiconducting interface.

John G. Gibbs, Applied Physics and Materials Science Department, Northern Arizona University. Work performed in part at NCI-SW.

ACS Applied Optical Materials **2023** *1* (7), 1320-1325
DOI: 10.1021/acsaom.3c00147

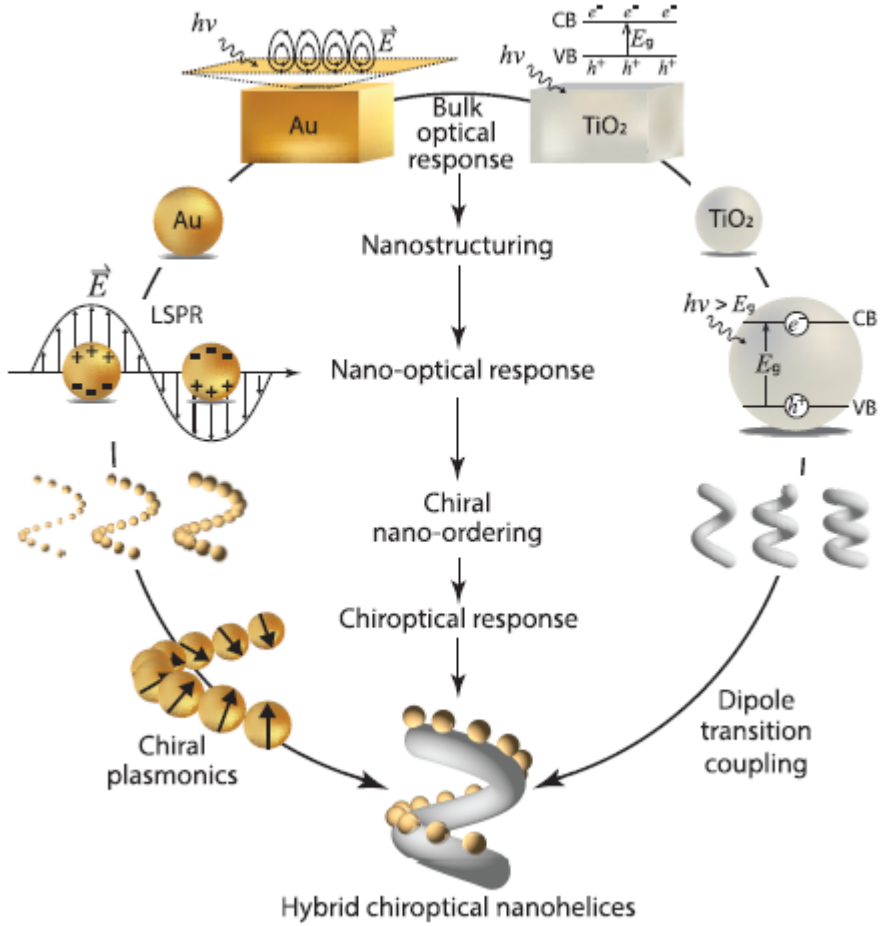

Schematic of how material and geometry are combined to obtain wide-spectrum chiroptical activity spanning UV and visible wavelengths. In practice, TiO2 nanohelices and thin films of Au are deposited using physical vapor deposition.

National Nanotechnology Coordinated Infrastructure

NCI Southwest

Nebraska Nanoscale Facility (NNF)

National Nanotechnology Coordinated Infrastructure

Nitrogen-Vacancy Magnetic Relaxometry of Nanoclustered Cytochrome C Proteins

Nitrogen-vacancy (NV) magnetometry offers an alternative tool to detect paramagnetic centers in cells with a favorable combination of magnetic sensitivity and spatial resolution. Here, Laraoui and coworkers at NNF employ NV magnetic relaxometry to detect cytochrome C (Cyt-C) nanoclusters. Cyt-C is a water-soluble protein that plays a vital role in the electron transport chain of mitochondria. Under ambient conditions, the heme group in Cyt-C remains in the Fe^{3+} state, which is paramagnetic. We vary the concentration of Cyt-C from 6 to 54 μM and observe a reduction of the NV spin–lattice relaxation time (T_1) from 1.2 ms to 150 μs, which is attributed to the spin noise originating from the Fe^{3+} spins. NV T_1 imaging of Cyt-C drop-casted on a nanostructured diamond chip allows us to detect the relaxation rates from the adsorbed Fe^{3+} within Cyt-C.

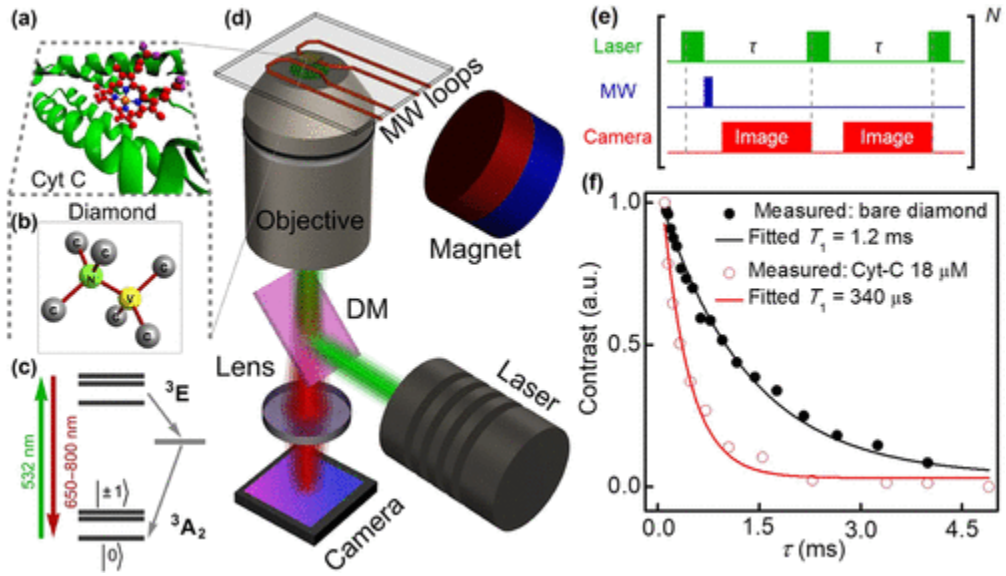

(a) Molecular structure of Cyt-C protein. (b) A schematic of the NV center inside the diamond lattice (nitrogen: green atom; yellow: vacancy). (c) A schematic of the energy levels of the NV center ground ($^3A_2$) and excited (^3E) states with the intermediate metastable state. A green laser (532 nm) initializes the NV center spins and results in fluorescence in a wavelength range of 650–800 nm. (d) A schematic of the widefield NV microscope used for T_1 relaxometry measurements and imaging of Cyt-C nanoclusters. DM is the dichroic mirror. (e) A schematic of a pulse sequence for T_1 relaxometry imaging. (f) T_1 curve measured on a bare diamond (filled circles) and after drop-casting an 18 μM Cyt-C solution on a diamond (open circles). The black and red solid lines are exponential decay function fits of the measured T_1 relaxation curves.

Suvechhya Lamichhane, Rupak Timalsina, Cody Schultz, Ilja Fescenko, Kapildeb Ambal, Sy-Hwang Liou, Rebecca Y. Lai, Abdelghani Laraoui. MME, Dept. Phys and Astr, Dept. of Chem. & NCMN, UNL, Univ of Latvia, Riga, & Dept of Math, Stat, and Phys, Wichita State Univ, Kansas. Part of the work performed at Nebraska Nanoscale Facility (NNF).

Nano Letters, 2024, 24, 873.

National Research Priority: NSF – Quantum Leap and Growing Convergence Research

National Nanotechnology Coordinated Infrastructure

Nebraska Nanoscale Facility

Photografting of Surface-Assembled Hydrogel Prepolymers to Elastomeric Substrates for Production of Stimuli-Responsive Microlens Arrays

A universal strategy for the microfabrication of hydrogel-based devices with robust substrate adhesion amenable to use in liquid environments would enable numerous applications. Morrin and coworkers at NNF reports a general approach for the facile production of covalently attached, ordered arrays of microscale hydrogels (microgels) on silicone supports. Specifically, silicone-based templates are used to: i) drive mechanical assembly of prepolymer droplets into well-defined geometries and morphologies, and ii) present appropriate conjugation moieties to fix gels in place during photoinitiated crosslinking via a “graft from” polymerization scheme. The stimuli-responsive microlensing properties of these arrays, via contractile modulated refractive index, are demonstrated. This process is directly applicable to the fabrication of adaptive optofluidic systems and can be further applied to advanced functional systems such as soft actuators and robotics, and 3D cell culture technologies.

John M. Kapitan, Grayson Minnick, Brennan P. Watts, Nengjian Huang, Mark A. Rose, Ruiguo Yang, Stephen A. Morin, Nebraska Center for Materials and Nanoscience (NCMN), Dept. of Chemistry and Dept. of Mech. & Mater. Eng., University of Nebraska – Lincoln. Part of the work performed at Nebraska Nanoscale Facility (NNF).

Adv. Funct. Mater. 2024, 34, 2305711

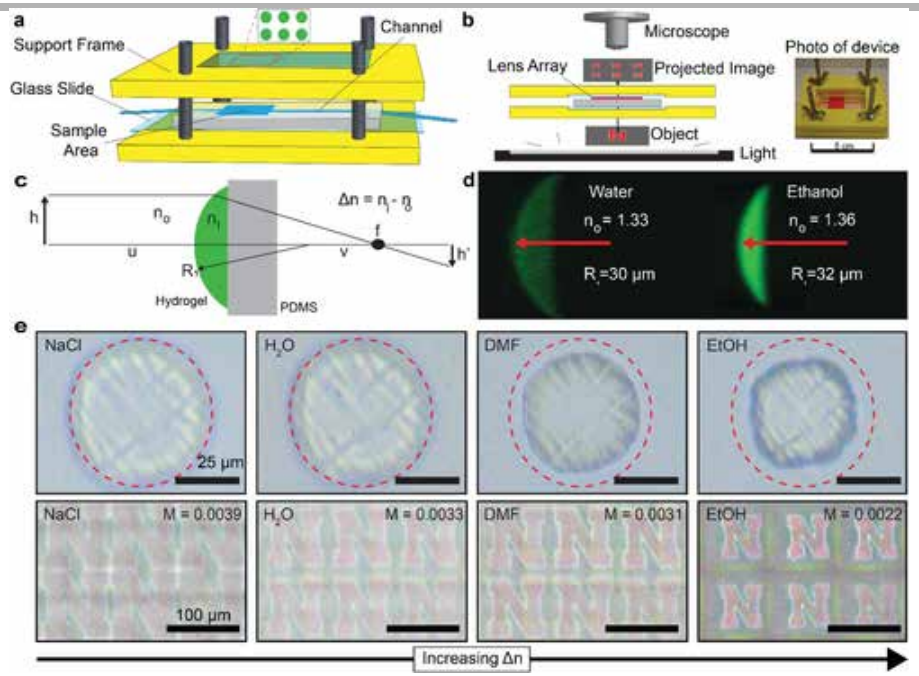

a) Schematic of the flow cell used to exchange submersion fluid for the microgel lens arrays. b) Schematic of the optofluidic lensing experiment. c) Ray diagram of a single microgel acting as a microlens. d) Cross-section of Z-stack images of a microgel in water and ethanol. e) (Top row) Optical micrographs of a PAm microgel in NaCl, water, DMF, and EtOH (annotated dotted red circle provides microgel diameter in water), and (Bottom row) optical micrographs of the projected letter “N”.

National Research Priority: NSF – Growing Convergence Research

National Nanotechnology Coordinated Infrastructure

Nebraska Nanoscale Facility

Record high room temperature resistance switching in ferroelectric-gated Mott transistors unlocked by interfacial charge engineering

The superior size and power scaling potential of ferroelectric-gated Mott transistors makes them promising building blocks for developing energy-efficient memory and logic applications in the post-Moore's Law era. The close to metallic carrier density in the Mott channel, however, imposes the bottleneck for achieving substantial field effect modulation via a solid-state gate. Previous studies have focused on optimizing the thickness, charge mobility, and carrier density of single-layer correlated channels, which have only led to moderate resistance switching at room temperature. Here, Xia Hong and coworkers at NNF, UNL report a record high nonvolatile resistance switching ratio of 38,440% at 300 K in a prototype Mott transistor consisting of a ferroelectric $PbZr_{0.2}Ti_{0.8}O_3$ gate and an $RNiO_3$ (R: rare earth)/$La_{0.67}Sr_{0.33}MnO_3$ composite channel. The ultrathin $La_{0.67}Sr_{0.33}MnO_3$ buffer layer not only tailors the carrier density profile in $RNiO_3$ through interfacial charge transfer, as corroborated by first-principles calculations, but also provides an extended screening layer that reduces the depolarization effect in the ferroelectric gate. Our study points to an effective material strategy for the functional design of complex oxide heterointerfaces that harnesses the competing roles of charge in field effect screening and ferroelectric depolarization effects.

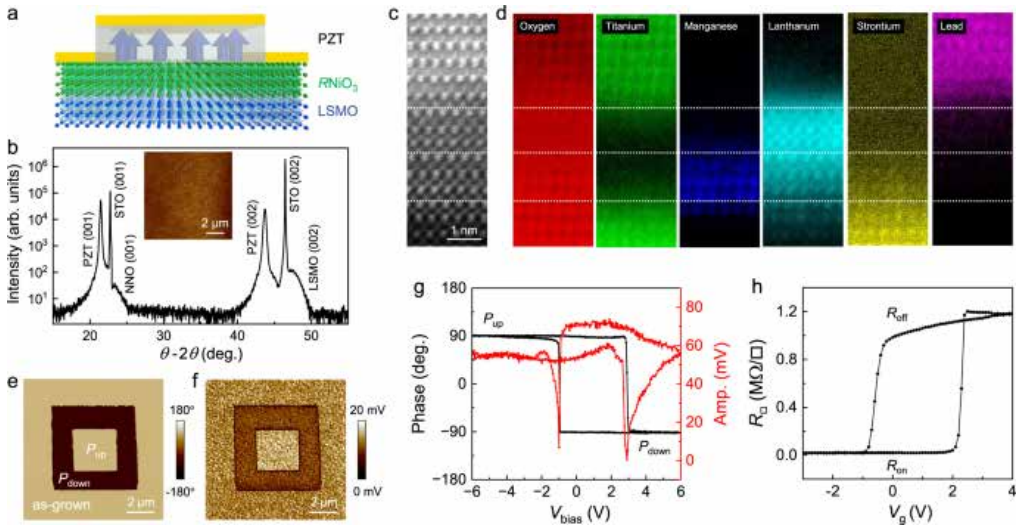

***a** Device schematic. **b** XRD θ −2θ scan taken on a PZT/NNO(4)/LSMO(5) heterostructure deposited on (001) $SrTiO_3$ (STO) substrate. Inset: AFM topography image of the sample. **c** Cross-sectional HRSTEM image and **d**, EELS element mapping taken on a PZT/LNO(3)/LSMO(3) sample. **e**–**h** PFM characterizations and resistance switching taken on a PZT/LNO(4)/LSMO(2) sample. **e** PFM phase and **f** amplitude images of concentric square domains. **g** PFM phase and amplitude switching hysteresis. **h** $R\square$ vs. V_g at 300 K.*

Yifei Hao, Xuegang Chen, Le Zhang, Myung-Geun Han, Wei Wang, Yue-Wen Fang, Hanghui Chen, Yimei Zhu & Xia Hong. Dept. Phys and Astr & NCMN, UNL, Cond Matt Phy & Mat Sci, Brookhaven Nat Lab, UPV/EHU Spain, NYU-ECNU Inst of Phys. China, and Dept of Phy, NY Univ. Part of the work performed at Nebraska Nanoscale Facility (NNF).

Nature Communications, 2023, 14, 8247.

Imaging Local Effects of Voltage and Boron Doping on Spin Reversal in Antiferromagnetic Magnetoelectric Cr_2O_3 Thin Films and Devices

Chromia (Cr_2O_3) is a magnetoelectric oxide that permits voltage-control of the antiferromagnetic (AFM) order, but it suffers technological constraints due to its low Néel Temperature (T_N ≈307 K) and the need of a symmetry-breaking applied magnetic field to achieve reversal of the Néel vector. Recently, boron (B) doping of Cr_2O_3 films led to an increase T_N >400 K and allowed the realization of voltage magnetic-field free controlled Néel vector rotation. Here, Binek and coworkers used NNF Facilities and directly imaged the impact of B doping on the formation of AFM domains in Cr_2O_3 thin films and elucidates the mechanism of voltage-controlled manipulation of the spin structure using nitrogen-vacancy (NV) scanning probe magnetometry. A stark reduction and thickness dependence of domain size in B-doped Cr_2O_3 ($B:Cr_2O_3$) films is found, explained by the increased germ density, likely associated with the B doping. By reconstructing the surface magnetization from the NV stray-field maps, a qualitative distinction between the undoped and B-doped Cr_2O_3 films is found, manifested by the histogram distribution of the AFM ordering, that is, 180 ° domains for pure films, and 90 ° domains for $B:Cr_2O_3$ films. Additionally, NV imaging of voltage-controlled B-doped Cr_2O_3 devices corroborates the 90 ° rotation of the AFM domains observed in magnetotransport measurement.

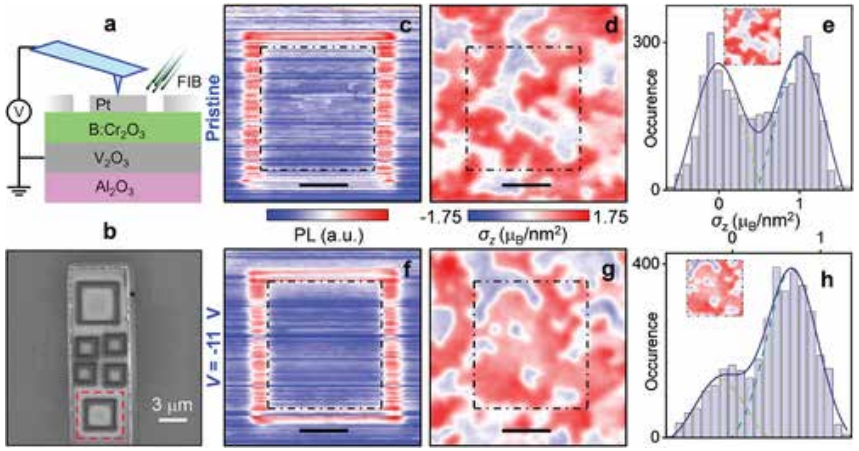

Reorientation of the AFM ordering upon application of electric field. a) Schematic for the application of voltage pulses. b) SEM image of capacitor. The imaged capacitor is denoted by the red dashed square. c) PL image obtained simultaneously during ODMR imaging, revealing the outline of the capacitor due to the lack of quenching associated with the etched platinum region. Reconstructed σ_z map (d) and histogram (e) prior to the application of electric field. PL (f), reconstructed σ_z map (g), and histogram (h) of σ_z after the application of −11 V, respectively. The scale bar in (c, d, f, and g) is 1 μm.

A Erickson, S Q A Shah, A Mahmood, P Buragohain, I Fescenko, A Gruverman, C Binek, A Laraoui, Neb. Cent. for Mater. and Nanosci. (NCMN), Dept. of Phys. and Astron, Dept of Mech. & Mater. Eng., University of Nebraska – Lincoln, Part of the work performed at NNF.

Work was supported by NSF EPSCoR RII Track-1: EQUATE, Award OIA-2044049. *Adv. Funct. Mater.* 2024, 34, 2408542.

National Research Priority: NSF – Quantum Leap

National Nanotechnology Coordinated Infrastructure

Nebraska Nanoscale Facility

Layer-Dependent Gas Sensing Mechanism of 2D Titanium Carbide ($Ti_3C_2T_x$) MXene

When exposed to reducing analytes, monolayer MXene flakes show increased electrical conductivity. On the contrary, both monolayers and bilayers show unidirectional sensing responses with increased resistivity when exposed to oxidizing analytes. Sinitskii and coworkers utilized NNF facilities and investigated the sensing behavior of bulk MXene sensors based on multiflake assemblies, in which this intercalation mechanism results in universal increase in resistance that for many analytes is seemingly inconsistent with the n-type character of the material. By scaling MXene sensors down from multiflake to single-flake level, they disentangled the charge transfer and intercalation effects and unraveled their contributions. In particular, the study shows that the charge transfer has a much faster kinetics than the intercalation process. They demonstrate that the layer-dependent gas sensing properties of MXenes can be employed for the design of sensor devices with enhanced molecular recognition.

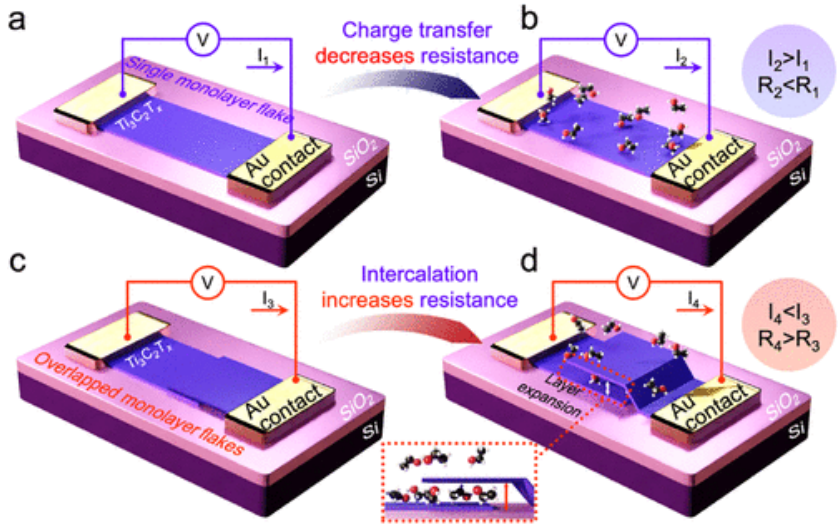

(a) Scheme of an electronic device based on monolayer $Ti_3C_2T_x$ flake. (b) Scheme of the same device as in (a) after the exposure to analyte molecules. (c) Scheme of an electronic device based on two overlapping $Ti_3C_2T_x$ flakes that form a bilayer region in the middle of the channel. (d) Scheme of the same device as in (c) after the exposure to analyte molecules.

Michael J. Loes, Saman Bageri, and Alexander Sinitskii. *Dept. of Chemistry and NCMN,* University of Nebraska – Lincoln. Part of the work performed at Nebraska Nanoscale Facility (NNF).

ACS Nano 2024, 18, 38, 26251.

National Research Priority: NSF – Growing Convergence Research

National Nanotechnology Coordinated Infrastructure

Nebraska Nanoscale Facility

C_{60} Fullerene-Reinforced Silicon Oxycarbide Composite Fiber Mats: Performance as Li-Ion Battery Electrodes

Precursor-derived silicon oxycarbide (SiOC) has emerged as a potential high-capacity anode material for rechargeable Li-ion batteries. The polymer processing and pyrolysis route, a hallmark of polymer-derived ceramics, allows chemical interfacing with a variety of nanoprecursors and nanofiller phases to produce composites with low-dimensional structures such as fibers and coatings not readily attained in traditional sintered ceramics. Here, Gurpreet Singh and coworkers at Kansas State University used NNF Facilities and reported the introduction of buckminsterfullerene or C_{60} as a filler phase in a hybrid precursor of 1,3,5,7-tetramethyl-1,3,5,7-tetravinyl-cyclotetrasiloxane (TTCS) along with polyvinylpyrrolidone or PVP as a spinning agent to fabricate electrospun fiber mats, which upon a high-heat treatment transformed to a C_{60}-reinforced SiOC ceramic composite. Tested as the self-supporting working electrode in a Li-ion half-cell, C_{60}-reinforced fiber mats show a much-improved reversible capacity (825 mA h g^{-1}), nearly 100% Coulombic efficiency, and superior rate capability with low-capacity decay at high currents (only 25.5% decay at 800 mA g^{-1}) compared to neat C_{60} and neat carbonized fiber electrodes.

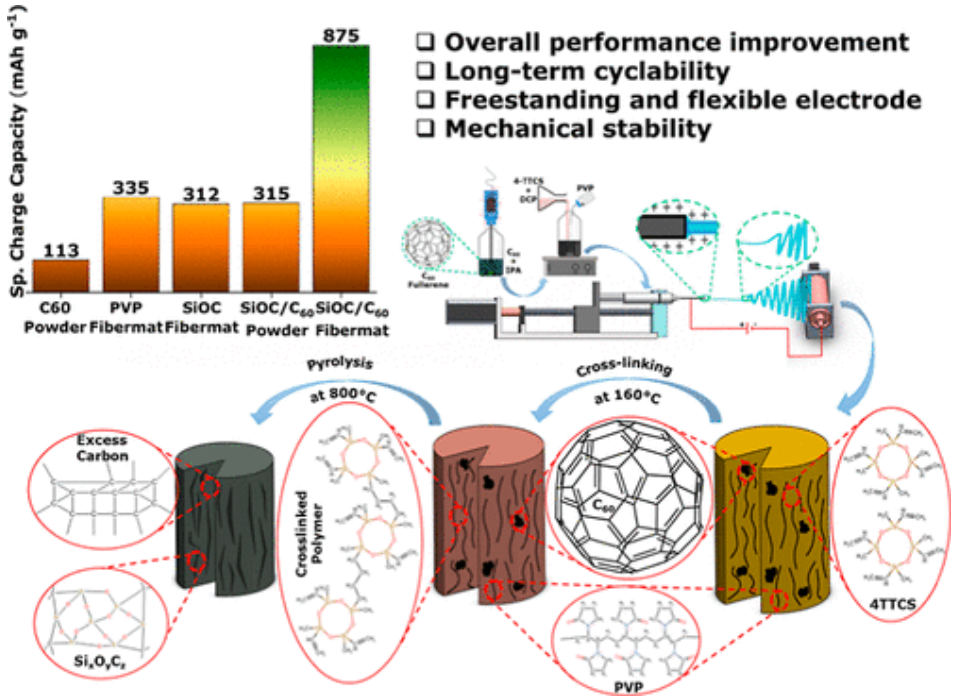

Arijit Roy, Shakir Bin Mujib, and Gurpreet Singh, Dept. of Mech. & Nuclear Eng., Kansas State University, KS. Part of the work performed at Nebraska Nanoscale Facility (NNF).

ACS Omega 2024, 9, 35757.

National Research Priority: NSF – Growing Convergence Research

National Nanotechnology Coordinated Infrastructure

Nebraska Nanoscale Facility

Microplotter-Printed Graphene-Based Electrochemical Sensor for Detecting Phosphates

Enabling an efficient electron transfer from the environment to an atomically thin, two-dimensional material such as graphene and vice versa provides a route to building graphene-based electrochemical sensors. Herein, Suprem Das and coworkers at Kansas State University utilized the NNF Facility and reported the manufacturing of a high-quality graphene nanoink and its use for the first time in fabricating stable and reliable printed phosphate ion electrochemical sensors using a microplotter. These sensors demonstrate a sensitivity of 0.3223 ± 0.025 μA μM^{-1} cm^{-2}, with a limit of detection (LOD) of 2.2 μM and linear sensing range of 1–600 μM. Moreover, they exhibit high selectivity toward phosphates when tested in the presence of NO_3^-, CO_3^-, Cl^-, and SO_4^{2-} interfering ions, affirming their reliability as a sensing platform. Phosphate electrochemical sensing using the proposed printed graphene sensors will pave the way for future development of point-of-care and continuous phosphate monitoring in environmental sensing.

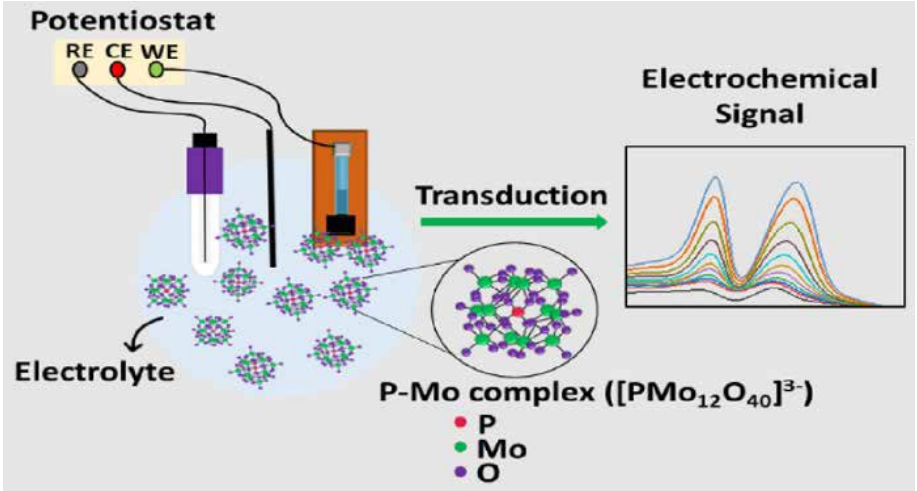

Thiba Nagaraja, Rajavel Krishnamoorthy, Kh M Asif Raihan, Brice Lacroix, and Suprem R. Das. Dept. of Industrial and Manufacturing Systems Eng., Kansas State University, Part of the work performed at Nebraska Nanoscale Facility (NNF), University of Nebraska, Lincoln.

Work supported by NSF Signals in the Soil (SitS) program, # 1935676. *ACS Applied Nano Materials*, 2023, 6, 21, 20288–20297.

National Research Priority: NSF – Growing Convergence Research

National Nanotechnology Coordinated Infrastructure

Nebraska Nanoscale Facility

NNCI Site @ Stanford (nano@stanford)

National Nanotechnology Coordinated Infrastructure

Achieving Optical Transparency in Live Animals

This work demonstrated that strongly absorbing molecules, like tartrazine, can make biological tissue optically transparent. The ***publication gained national attention***, and was featured on NPR News, The Late Show with Stephen Colbert (1.76M viewers), USA Today, and other outlets. It also is ***one of Physics World's top 10 breakthroughs in 2024***. This discovery will enable non-invasive visualization of deep tissues and organs and the observation of biological structure, activity, and function.

- Lorentz Oscillator Model & Kramers-Kronig Relations predicted:
  - dyes with sharp absorption resonances in the near-UV/blue spectral regions could increase the real part of the refractive index in aqueous media at longer wavelengths.
  - dyes could minimize the refractive index contrast between water and lipids to achieve optical transparency.
- Experiments proved these predictions:
  - imaged gut motility, cerebral blood vessels, and muscle sarcomeres.
  - Deep tissue optical imaging through mm of scattering medium was possible with micrometer spatial resolution

Deep-Tissue Optical Imaging of Live Animals

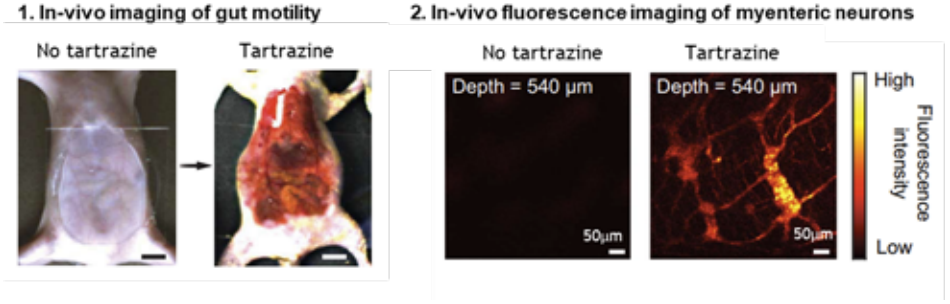

Optical Resolution of 2.2µm Through 1mm of Tissue-Like Material

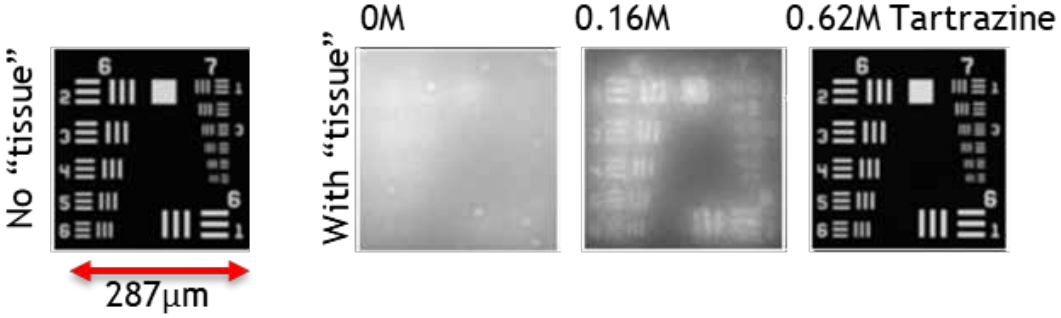

Zihao Ou, Mark Brongersma, Guosong Hong, et. al.,Department of Materials Science & Engineering, Stanford University. Work performed at the Stanford Nanofabrication Facility and elsewhere.

This work was supported by NSF Award #ECCS-2026822. Z. Ou et al., *Science* 385:6713, (2024), 1061. DOI:10.1126/science.adm6869

National Research Priority: NSF – Understanding the Rules of Life

Chip-Scale Ti:sapphire Laser System

To democratize titanium:sapphire technology, this research developed chip-integrated, broadband tunable Ti:sapphire laser systems that are 10,000x smaller and 1,000x cheaper than the existing tabletop systems and can be pumped with a cheap, green laser pointer. This research is ***one of Physics World's top 10 breakthroughs in 2024,*** was the ***2nd place winner in the 2024 NTEC challenge,*** and catalyzed the formation of ***a new startup company, Brightlight Photonics.***

Laser Specifications

- Ti:sapphire (thinned to 100s of nms), on SiO_2, on sapphire crystal (TiSaOI)
- Lasing threshold power=290μW, peak output power=1kW, pulsed amplification below 1μm, footprint= <0.15mm^2

Proof-of-Concept

- Cavity quantum electrodynamics (QED) experiment
  - Diffraction-limited imaging of silicon vacancy color centres
  - Distinguished between artificial atoms and optically active defects
  - Enhanced a quantum system's spontaneous emission rate

Photo & Optical Image of the TiSaOI Laser System Design

2nd place NTEC winner!

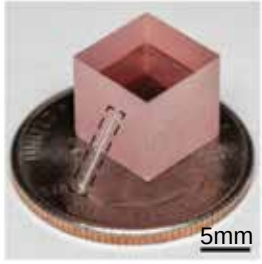

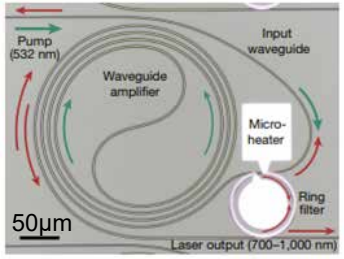

Imaging Artificial Atoms & Optically Active Defects

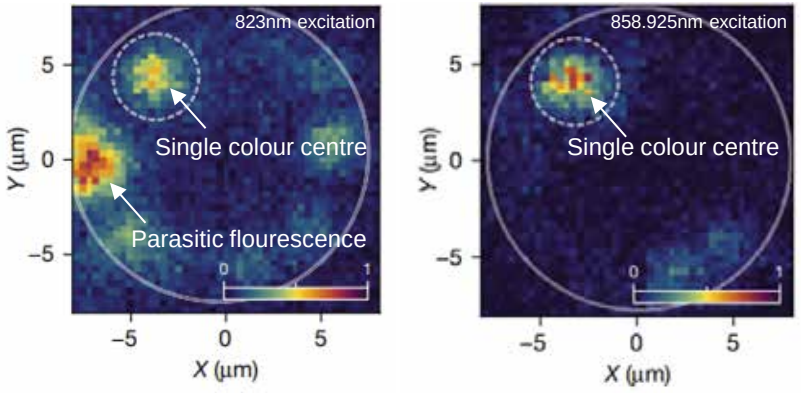

Joshua Yang, Kasper Van Gasse, Jelena Vučković, et. al., Department of Electrical Engineering and E.L. Ginzton Laboratory at Stanford University. Work performed at the Stanford Nano Shared Facilities, the Stanford Nanofabrication Facility, and elsewhere.

This work was supported by NSF Award # ECCS-2026822. J. Yang et.al. *Nature* 630:8018 (2024): 853-859. DOI: 10.1038/s41586-024-07457-2

National Research Priority: NSF – Quantum Leap

Direct Growth of Optically Tunable Transition-Metal Dichalcogenide Nanoribbons

A straightforward, direct growth method for single-crystal transition-metal dichalcogenide (TMC) nanoribbons (NRs) was developed that allowed for control over NR width. The authors were able to tailor the dimensions of MoS_2 and WSe_2 NRs to enable photoluminescence and strain-induced single photon emission. This research may lead to localized quantum dot light sources and advance the field of quantum optoelectronics.

Growth Process

- deposit seed nanoparticles by evaporating a mixture of MoO_2, Ni, and NaBr on fluorophlogopite mica, in the presence of moisture
- expose the nanoparticles to a chalcogen vapor atmosphere
- NR width heavily depended on seed particle diameter and chalcogen vapor pressure

Optical Properties

- strain-induced quantum dot-like states that emit single photons
- width-dependent photoluminescence

AES maps of MoS_2 NR grown from a Na-Mo-Ni Nanoparticle

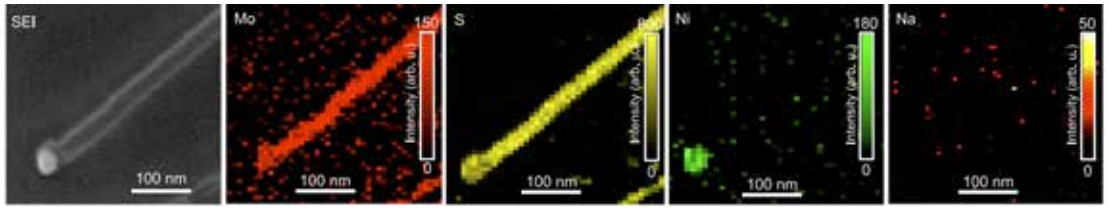

Photoluminescence Spectra of NRs over Au Nanocones

MoS_2

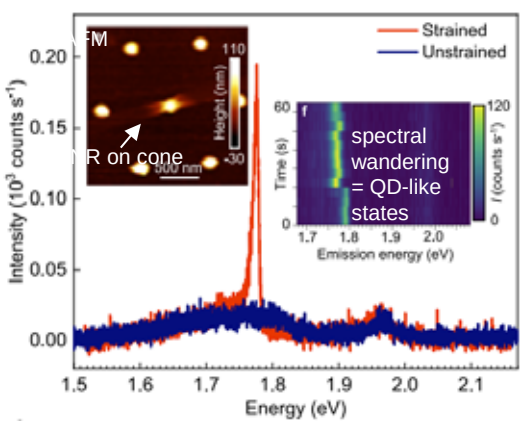

WSe_2

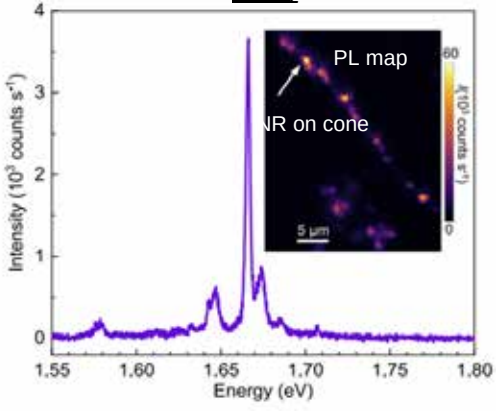

Xufan Li, Samuel Wyss, Avetik Harutyunyan et. al., Honda Research Institute USA, Inc. Work performed at the Stanford Nano Shared Facilities, Oak Ridge National Laboratory, and elsewhere.

This work was supported by NSF Award # ECCS-2026822. Li, X., et al., *Nat Commun* 15, 10080 (2024). e2307380120. DOI: 10.1038/s41467-024-54413-9

National Research Priority: NSF – Quantum Leap

Forming-Free Selectors for Memory Technology

TSMC developed an optimized material (i.e., a thin film of arsenic-free tellurium (Te) in a silicon oxide (SiO_x) matrix) for the low power memory selectors used in data-intensive computing. These forming-free SiO_xTe_y-based selectors will be ideal for low-power, high-density memory technologies and represent a significant step forward in memory development for cross-point array architectures.

Technical need:

- a selector for low-power memory devices that does not need high voltage pre-conditioning (i.e., "forming")

New Selector Properties:

- forming-free behavior (i.e., $V_{FF}=V_{th}=1.2V$) with optimized Te:O ratio (0.45) + film thickness (~5nm)
- low threshold voltage drift (~30 mV/decade), good thermal + air stability, low off-current (3nA at 0.5V), endurance (up to 10^{11} cycles)

Schematic and TEM image of a SiO_xTe_y-based selector

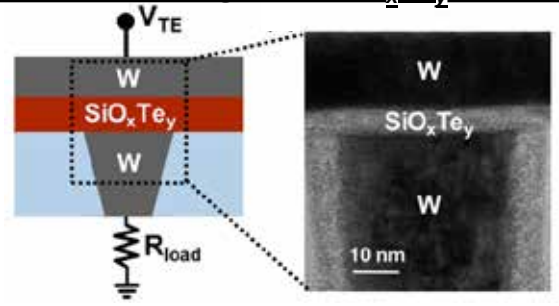

Higher Te:O and Thinner Films resulted in forming-free behavior

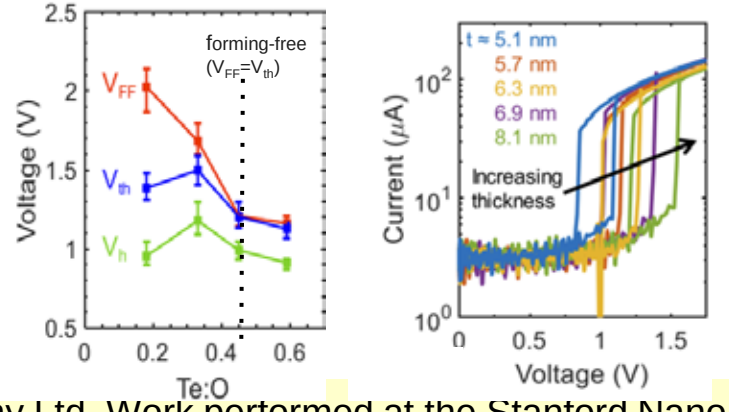

Isha M. Datye, Sam Vaziri, Xinyu Bao, et. al., Taiwan Semiconductor Manufacturing Company Ltd. Work performed at the Stanford Nano Shared Facilities and elsewhere.

This work was supported by NSF Award # ECCS-2026822. M. Datye, et. al., *IEEE Transactions on Electron Devices,* 73:1 (2024), 530-535. DOI: 10.1109/TED.2023.3336629

Molecule-Like Electronic Transitions in Metal Halide Perovskites

Metal halide perovskites are promising photocatalytic materials, with applications such as water splitting, and organic synthesis. This fundamental research investigated the electronic structure and photoexcitation properties of Cs_2TeBr_6 towards the development of improved photocatalytic materials. The results demonstrated that the tunable electronic structures and catalytic centers of perovskites can be leveraged to drive a particular reaction pathway by using different excitation energies.

- SEM-EDS, XPS, and XRD confirmed the chemical composition and crystal structure
- Electronic transitions were studied by UV-vis absorption spectroscopy, VB-XPS, and ***LEIPS (new capability at SNSF)***
- Photocatalytic efficiency was dependent on the excitation energy wavelength
  - UV (365nm) light was most effective for aerobic oxidation of benzyl alcohol
  - At 455nm, excitation occurred from a higher valence band level, leading to a different oxidation pathway

XPS/LEIPS Unraveled Electronic Transitions in Perovskite

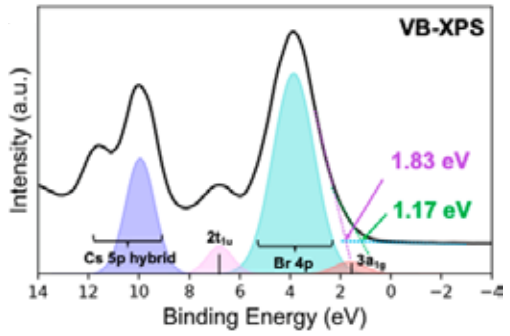

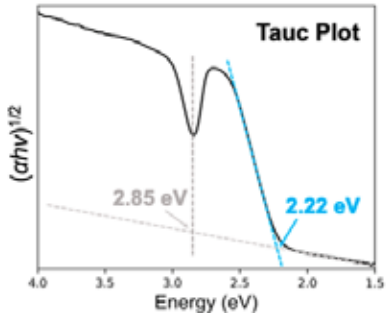

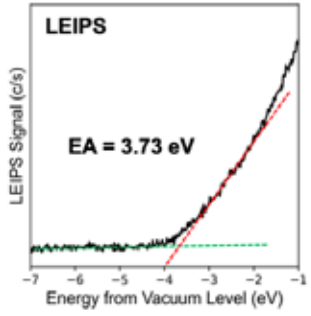

Jianbo Jin, Haowei Huang, Peidong Yang, et. al., Department of Chemistry at the University of California, Berkeley. Work performed at the Stanford Nano Shared Facilities and elsewhere.

This work was supported by NSF Award # ECCS-2026822. J. Jin, et. al., *ACS Photonics* 10:3 (2023), 772-229 DOI: 10.1021/acsphotonics.3c00042

National Research Priority: DoD – Advanced Materials

Efficient Spintronics in Thin Film Ferromagnetic Insulators

This research engineered a new ferromagnetic insulator (FMI) material (i.e., thin film of $Li_{0.5}Al_{1.0}Fe_{1.5}O_4$ (LAFO)) with promising properties (e.g., perpendicular magnetic anisotropy, etc.) for advancing spintronics and enabling faster, more efficient, and smaller electronic devices.

Structural Characterization Results

- high-quality + uniform crystal interfaces, excellent crystallinity + epitaxy
- LAFO unit cell stretched to match MGO crystal size
  - strain in LAFO resulted in perpendicular electron spin orientation

Magnetic Characterization Results

- low-damping
- perpendicular magnetic anisotropy (PMA)
- minimal external magnetic fields to saturate magnetization (~1.5mT)
- lowest reported damping factor (α), compared to similar materials
- lowest critical current density for magnetic switching ($6x10^5$ A/cm^2)
- high spin-orbit torque efficiency

Pt/LAFO/MGO Schematic and TEM Images of Interfaces

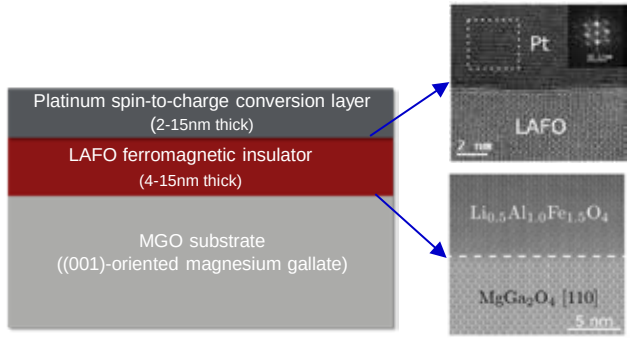

XRD Peak Shift

(LAFO unit cell stretched enabling PMA)

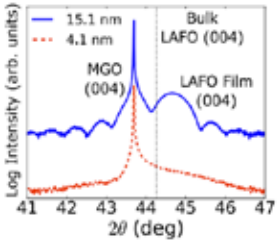

Magnetic Reluctance of Hall Bar

(lowest critical current density)

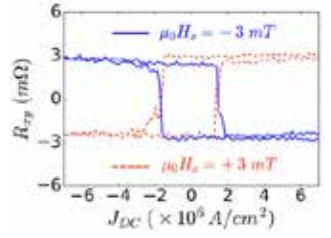

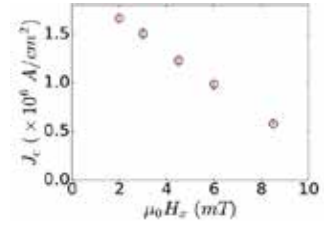

Xin Yu Zheng, Sanyum Channa, Yuri Suzuki, et. al., Departments of Applied Physics and Physics at Stanford University. Work performed at the Stanford Nano Shared Facilities, the Stanford Nanofabrication Facility, Lawrence Berkeley National Labs, and elsewhere.

This work was supported by NSF ECCS-2026822. X.Y. Zheng, et. al., *Nature Comm.* 14:4918, (2023): 1-7. DOI: 10.1038/s41467-023-40733-9

National Research Priority: DoD – Microelectronics

Photovoltaic-based Prosthesis for Vision Restoration

Age-related macular degeneration (AMD) causes severe vision impairment by damaging photoreceptor cells in the retina, but vision can be partially restored using prosthetic devices with photovoltaic pixels to stimulate healthy neurons. This research developed a new photovoltaic-based implant design that had a smaller pixel size (down to 20μm) and a 3D pixel geometry to further improve patient visual acuity compared to the existing benchmark.

- Design used vertical walls to reduce pixel crosstalk & enhance signal efficiency.
- Device was shown to facilitate the migration of bipolar cells into the honeycomb wells, while preventing migration of non-essential retinal cells.
- Device was integrated into the retinal signaling pathway of a rat resulting in a visual resolution comparable to a healthy animal.

Schematics, Simulated Electric Fields, and SEM Images of Pixels

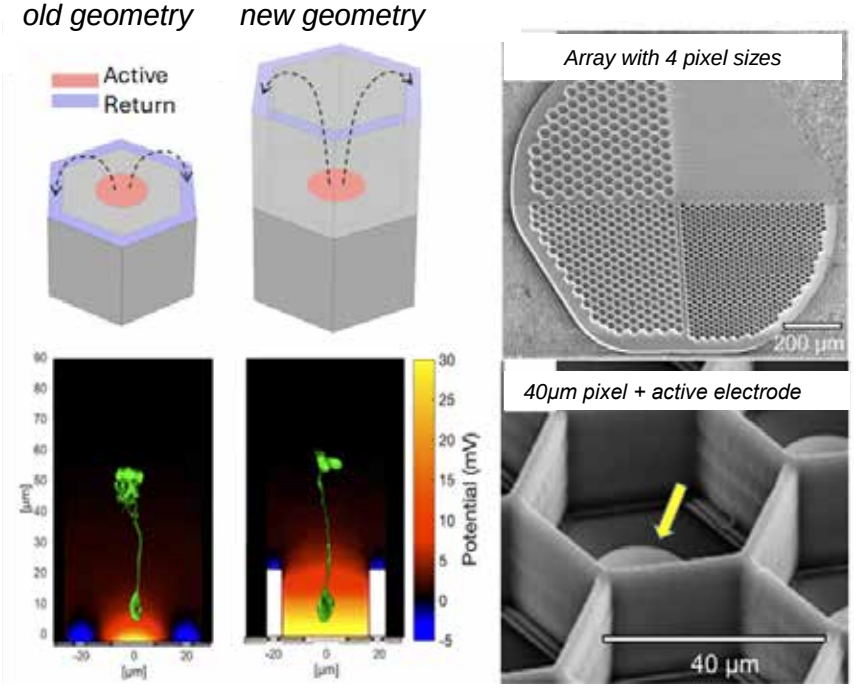

Mohajeet Bhuckory, Bing-Yi Wang, Daniel Palanker, et. al., Departments of Ophthalmology, Physics, Electrical Engineering, and Materials Science at Stanford University. Work performed at the Stanford Nano Shared Facilities, the Stanford Nanofabrication Facility, and elsewhere.

This work was supported by NSF # ECCS-2026822. M.B. Bhuckory, et.al. *PNAS* 120:42 (2023): e2307380120. DOI: 10.1073/pnas.2307380120

National Research Priority: NSF – Growing Convergence Research

A Tiered Approach to Teaching K-14 Students Advanced Materials & SEM

This paper introduced a flexible framework for educators to introduce scanning electron microscopy (SEM) and advanced materials to students ranging in age from elementary school to college. All handouts, lesson plans, and teaching resources are available online. The three-tiered approach allows teachers autonomy to tailor lessons as appropriate for their classroom:

1. Introduction using YouTube videos, an open-access SEM simulation tool (MyScope), and classroom discussion.
2. Hands-on learning (handling graphene aerogels, silica, sponges)
3. SEM imaging with remote tools through the RAIN network and Hitachi. Pore size analysis using ImageJ open-source software.

The efficacy of the teaching framework was evaluated on two cohorts of students (e.g., community college students and 5th graders) using a Hitachi desktop SEM available at nano@stanford. Survey results showed an increase in interest in nanoscience and comprehension of the content.

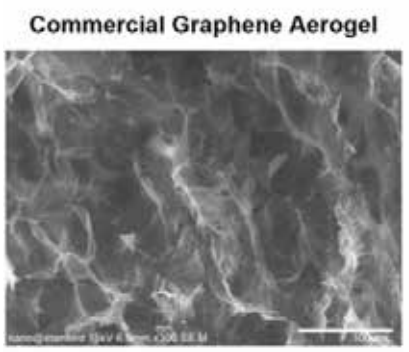

TaNia Donatto, Daniella Duran, Debbie G. Senesky, et. al., Departments of Materials Science and Engineering, Aeronautics & Astronautics, Electrical Engineering, and nano@stanford at Stanford University. Work performed at the Stanford Nano Shared Facilities and elsewhere.

This work was supported by NSF # ECCS-2026822. T. Donatto, et.al., *J. Chem. Ed.* 101:10 (2024): 4502-4509. DOI: 10.1021/acs.jchemed.4c00723

Northwest Nanotechnology Infrastructure (NNI)

National Nanotechnology Coordinated Infrastructure

Frequency-angular resolving (FAR) LiDAR by integrated acousto-optic beam steering

- Light Detection and Ranging (LiDAR) is indispensable for intelligent automation and autonomous vehicles
- Current beam steering systems are bulky and require mechanical parts
- Idea: exploit Brillouin scattering – the interaction of light with acoustic waves – to steer beams at different angles
  - Single-chip gigahertz transducer
  - Frequency-labeled angular direction

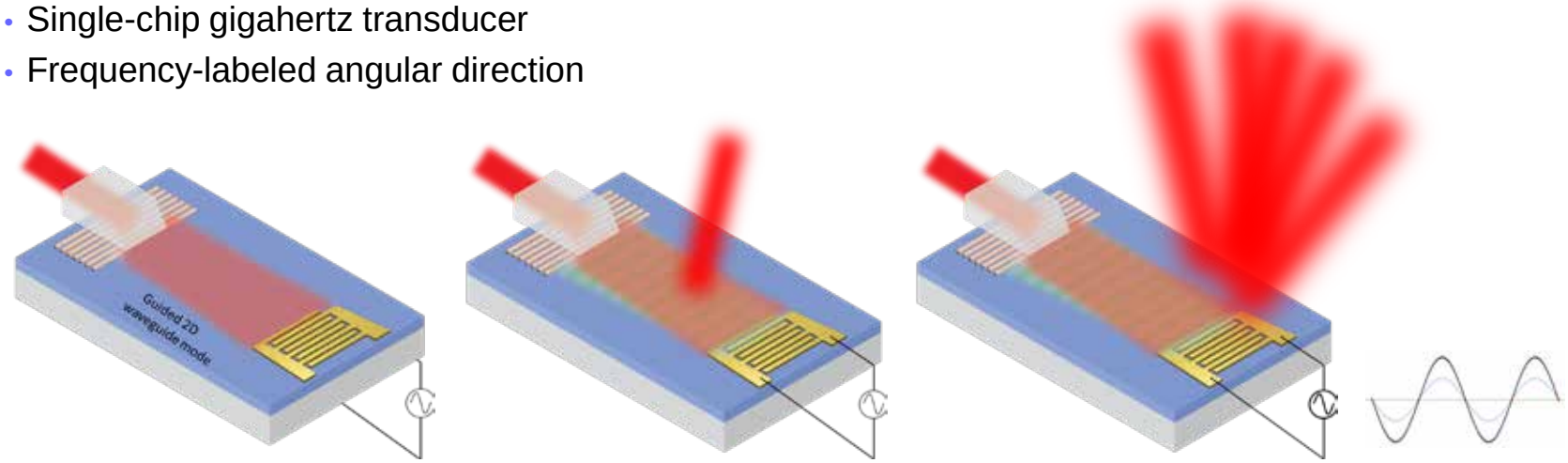

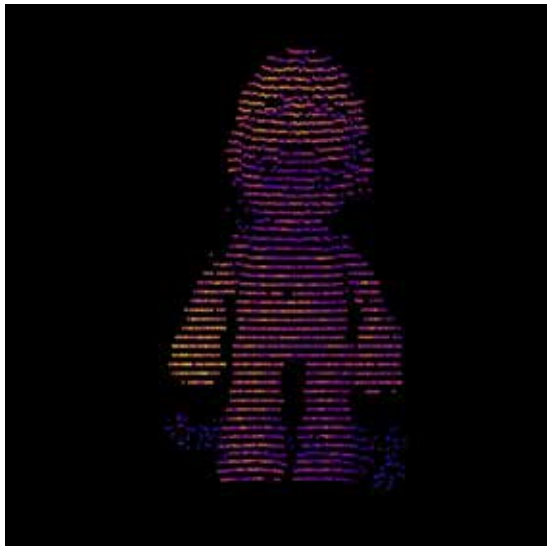

FAR LiDAR image of an object. The position and brightness of each pixel are resolved from the beating frequency and power of the signal, respectively.

Laboratory of Photonic Systems (Mo Li, director), University of Washington. Work performed at the Washington Nanofabrication Facility (WNF).

This work was supported by NSF Convergence Accelerator ITE-2134345 and DARPA. Bingzhao Li, Qixuan Lin, Mo Li, *Nature* 620(7973), 316-322 (2023)

National Research Priority: DoD – Advanced Computing and Software

National Nanotechnology Coordinated Infrastructure

NORTHWEST NANOTECHNOLOGY INFRASTRUCTURE

Programming correlated magnetic states with gate-controlled moiré geometry

Twisted transition metal dichalcogenide bilayers have been predicted to exhibit exotic properties. Two molybdenum ditelluride layers were stacked on top of each other in a rhombohedral configuration and with a twist angle of about 4º, resulting in a moiré structure. By varying the carrier density and an applied electric field, the geometry of the lattice and the nature of magnetic interactions can be tuned. This tunability is expected to enable the realization of a host of correlated states in this system.

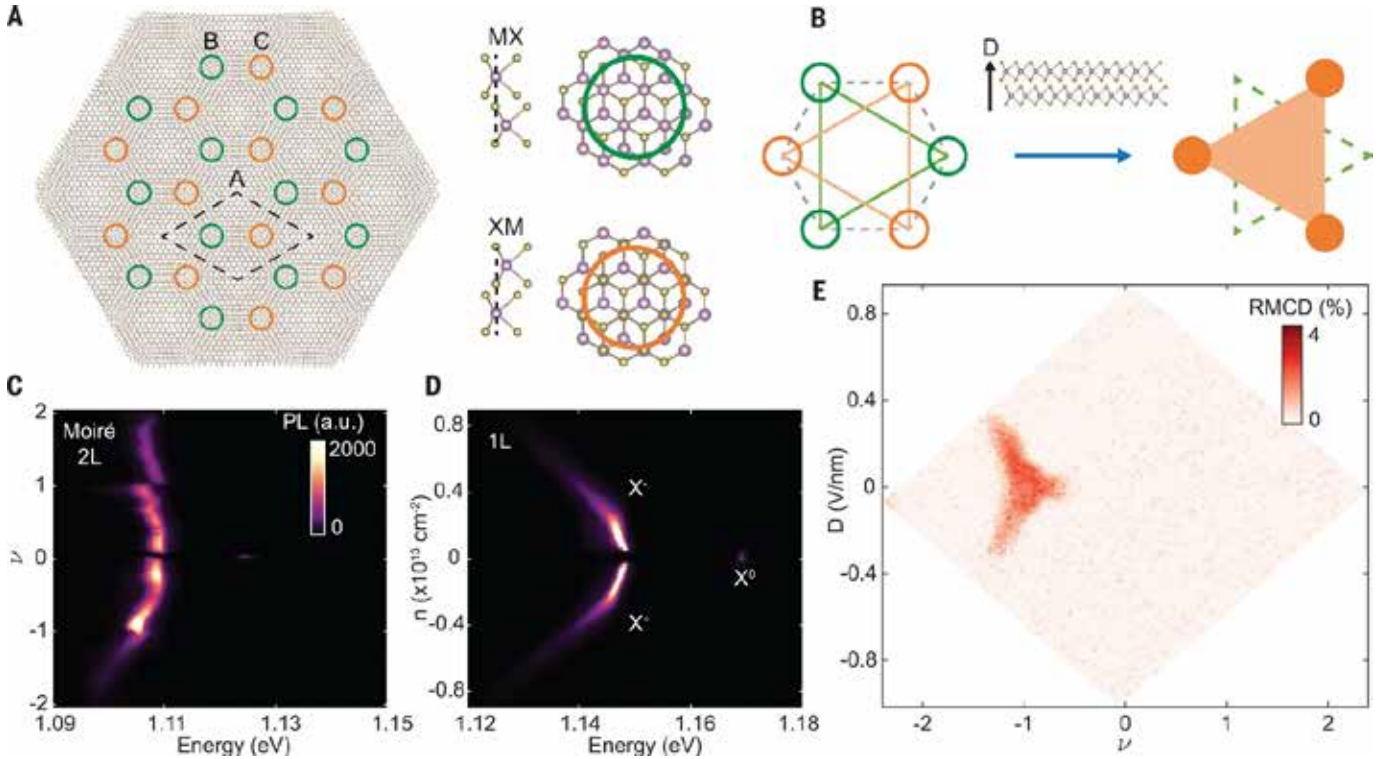

Gate-tunable moiré geometry, correlated states, and magnetic response in twisted $MoTe_2$ bilayer. *(**A**) Cartoons of small-angle-twisted $MoTe_2$ bilayer in R-stacking. High symmetry points with local energy minima are highlighted. The green circles correspond to MX sites (B sublattice), where the metal atom M in the top layer is aligned with the chalcogen atom X in the bottom layer. Orange circles are the corresponding XM sites (C sublattice). Dotted lines indicate a single moiré unit cell. (**B**) Application of vertical electrical field (D) lifts the energy degeneracy of the layers and switches the moiré superlattice geometry from (left) honeycomb to (right) triangular. (**C**) PL intensity plot of the twisted bilayer as a function of moiré filling factor (v) and photon energy. (**D**) Doping-dependent PL of monolayer $MoTe_2$, showing exciton (X^0) and trion (X^+ and X^-) features. (**E**) Reflective magnetic circular dichroism (RMCD) signal intensity plot as a function of v and D of the twisted bilayer without magnetic field. The nonzero RMCD signal was observed close to v = –1 and symmetric in D. The plot represents a 2D ferromagnetic phase diagram. All data were taken at T = 1.6 K.*

Work partially performed at University of Washington (PI: Xiaodong Xu), University of Hong Kong, HKU-UCAS Joint Institute of Theoretical and Computational Physics at Hong Kong, National Institute for Materials Science, Tsukuba, Japan

This work was supported by the US DOE and NSF MRSEC DMR-1719797. E. Anderson et al., *Science* 381:325-330 (2023)

Signatures of fractional quantum anomalous Hall states in twisted $MoTe_2$

- Fractional quantum anomalous Hall (FQAH) states observed in twisted bilayer $MoTe_2$.
- Potential for hosting non-Abelian anyons for quantum computing.
- Fractional conductance values and a QAH state confirmed; electron-doped states are trivial insulators.
- Implications: $MoTe_2$ moiré superlattices are a platform for exploring exotic quantum phases.

***a**, Schematic of dual-gated device structure. **b**, R-stacked homobilayer hosting two degenerate energy minima at high symmetry MX and XM points, forming a honeycomb moiré superlattice. Complex hopping between next-nearest-neighbor sites realizes the Haldane model. **c**, PL intensity plot as a function of hole doping and photon energy. Filling factors v corresponding to the formation of correlated insulating states are indicated. **d**, RMCD signal versus v and perpendicular electric field D at zero magnetic field $\mu_0 H$. The phase space with non-vanishing signal corresponds to the ferromagnetic state. **e**, RMCD signal versus $\mu_0 H$ swept back and forth at selected fillings.*

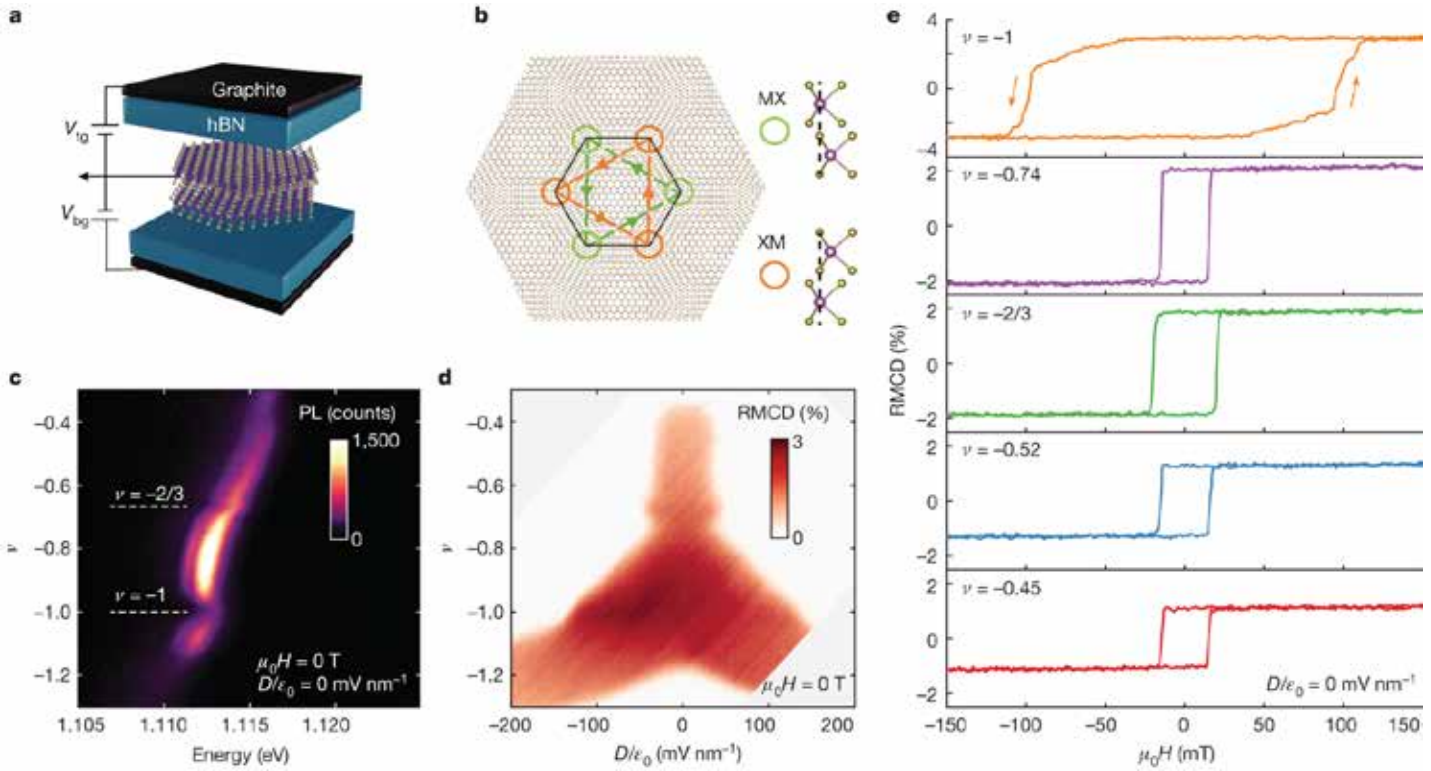

Work partially performed at UW, University of Hong Kong, HKU-UCAS Joint Institute of Theoretical and Computational Physics at Hong Kong

This work was supported by the US DOE, AFOSR, and NSF MRSEC DMR-1719797. JQ Cai et al., *Nature*, 622(7981):1974-1880 (2023)

Artificial neuron transmits chemical signals

An artificial neuron architecture based on antiambipolar organic electrochemical transistors shows responses to biological ions and neurotransmitters akin to real neurons with comparable speed. The soft and more biocompatible nature of organic semiconductors could enable applications in brain-machine interfaces and in vivo sensing.

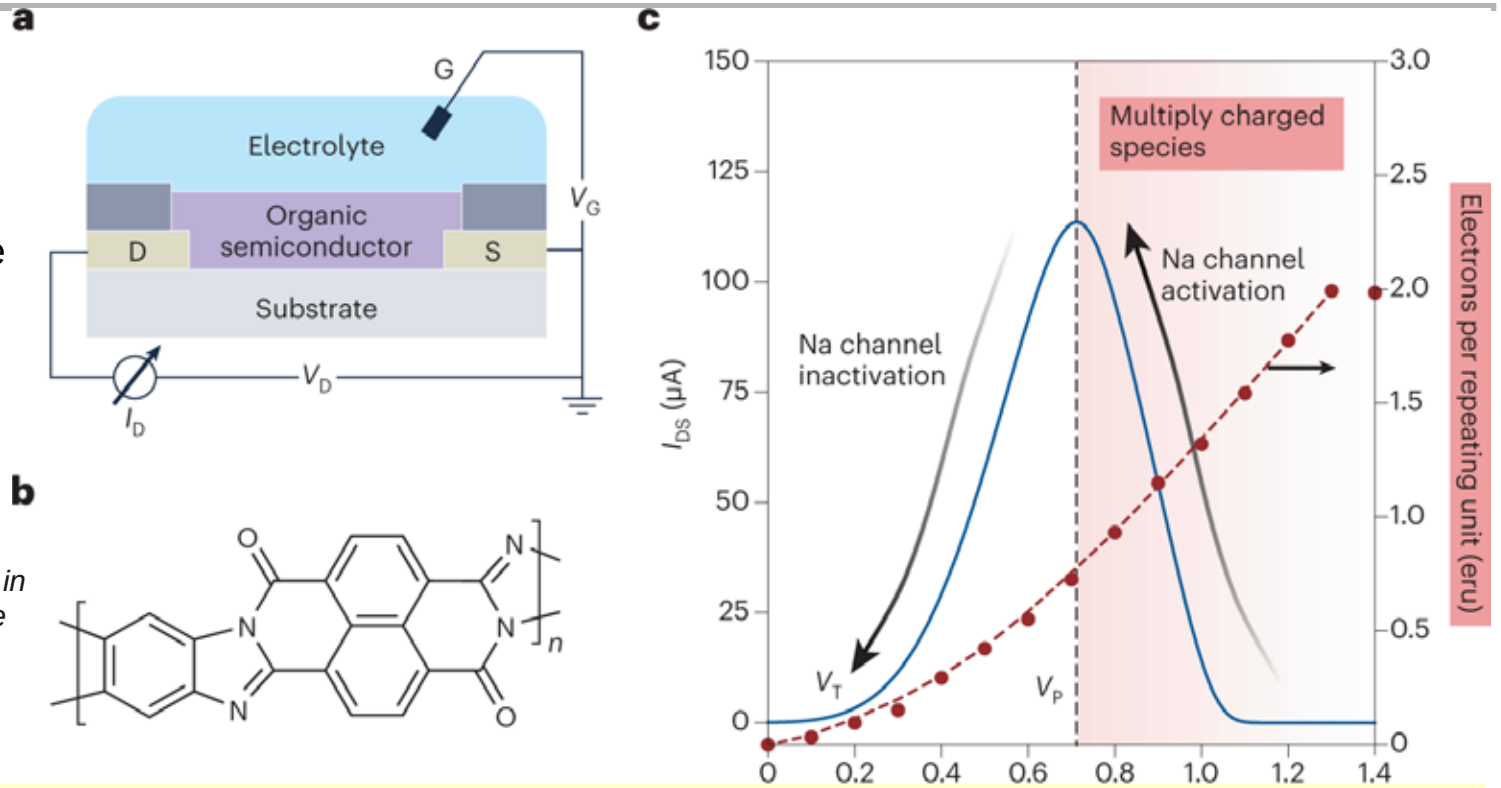

***a**, Device structure of OECT. **b**, Chemical structure of BBL polymer. **c**, The antiambipolar behavior in a BBL-based OECT device resembling the activation and inactivation of Na channels in a neuron. D, drain; S, source; G, gate; V_D, drain voltage; V_G, gate voltage; I_D, drain current; I_{DS}, drain–source current; V_{GS}, gate–source voltage; V_T, threshold voltage; V_P, voltage of the peak current.*

David Ginger Lab, Department of Chemistry, University of Washington. Work performed in part at the Molecular Analysis Facility, University of Washington

Chen, S.E., Giridharagopal, R. & Ginger, D.S., *Nature Materials* 22, 416–418 (2023)

National Research Priority: NSF – Rules of Life and Growing Convergence Research

National Nanotechnology Coordinated Infrastructure

NORTHWEST NANOTECHNOLOGY INFRASTRUCTURE

Directing polymorph specific calcium carbonate formation with de novo protein templates

Biomolecules modulate inorganic crystallization to generate hierarchically structured biominerals, but the atomic structure of the organic-inorganic interfaces that regulate mineralization remain largely unknown. We hypothesized that heterogeneous nucleation of calcium carbonate could be achieved by a structured flat molecular template that pre-organizes calcium ions on its surface. To test this hypothesis, we design helical repeat proteins (DHRs) displaying regularly spaced carboxylate arrays on their surfaces and find that both protein monomers and protein-Ca^{2+} supramolecular assemblies directly nucleate nano-calcite with non-natural {110} or {202} faces while vaterite, which forms first in the absence of the proteins, is bypassed. These protein-stabilized nanocrystals then assemble by oriented attachment into calcite mesocrystals. We find further that nanocrystal size and polymorph can be tuned by varying the length and surface chemistry of the designed protein templates. Thus, bio-mineralization can be programmed using de novo protein design, providing a route to next-generation hybrid materials.

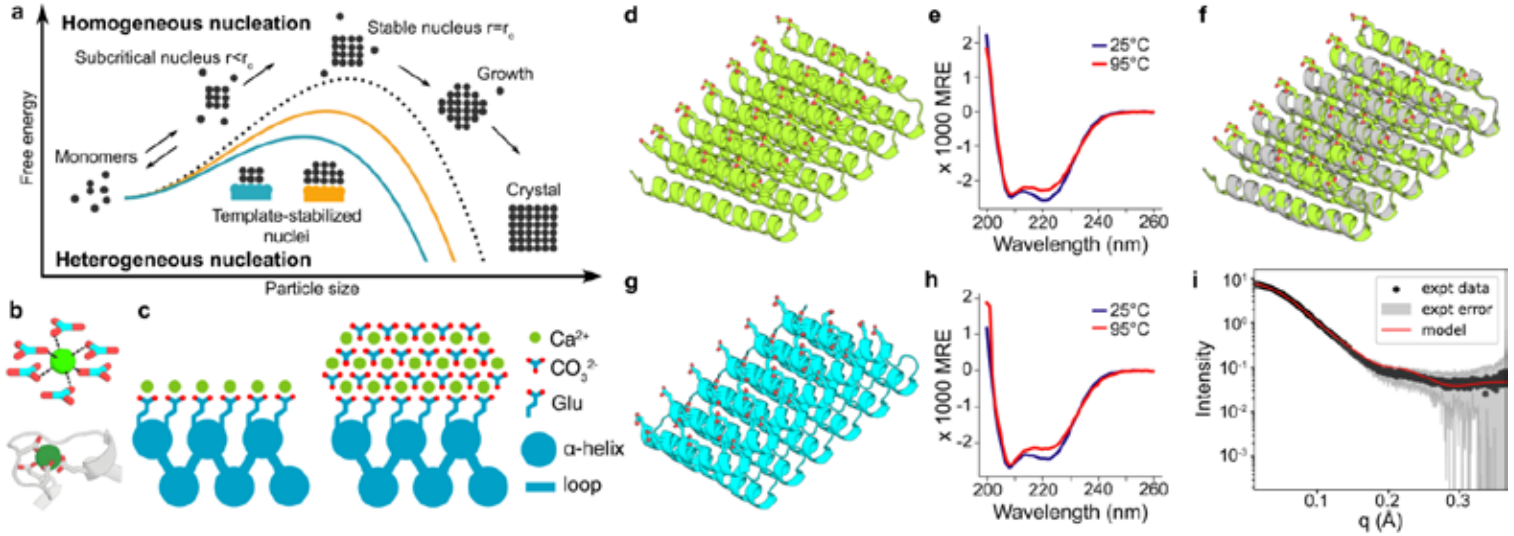

***a** The presence of a template reduces the free energy barrier of nucleation and the critical radius of the nuclei. **b** Coordination of calcium (top) by carbonate ions within a unit cell of calcite, and (bottom) by carboxylate containing glutamate and aspartate residues in the structure of calmodulin (PDB ID: 1A29, residues 18–33). **c** Tessellating binding moieties across repeated α-helices within a designed protein capable of pre-organizing bound calcium ions. **d–i** Biophysical characterization of the designed proteins. **e, h** Their respective circular dichroism scans showing mean residue ellipticity from 200 to 260 nm at 25 °C and 95 °C. **f** The 4 Å resolution crystal structure of FD15 in gray superimposed on the design model in green. **i** Experimental and model SAXS profiles for FD31, scattering vector vs. intensity.*

Institute for Protein Design (David Baker, director), University of Washington. Work performed in part at the Molecular Analysis Facility.

F. A. Davila-Hernandez et al., *Nature Communications* 14:8191 (2023)

National Research Priority: NSF – Understanding the Rules of Life and Growing Convergence Research

National Nanotechnology Coordinated Infrastructure

NORTHWEST NANOTECHNOLOGY INFRASTRUCTURE

Acoustic micro-tapping optical coherence elastography to quantify corneal collagen cross-linking: an ex vivo human study

- This study evaluates changes in the anisotropic elastic properties of ex vivo human cornea treated with ultraviolet cross-linking (CXL) using noncontact acoustic micro-tapping optical coherence elastography (AμT-OCE).
- Cross-linking induced a significant increase in both in-plane and out-of-plane elastic moduli in human cornea. The statistical mean in the paired study (presurgery and postsurgery, n = 7) of the in-plane Young's modulus increased from 19 MPa to 43 MPa, while the out-of-plane shear modulus increased from 188 kPa to 673 kPa.
- The human cornea is a highly anisotropic material where in-plane mechanical properties are very different from those out-of-plane. Noncontact AμT-OCE can measure changes in the anisotropic elastic properties in human cornea as a result of ultraviolet CXL.

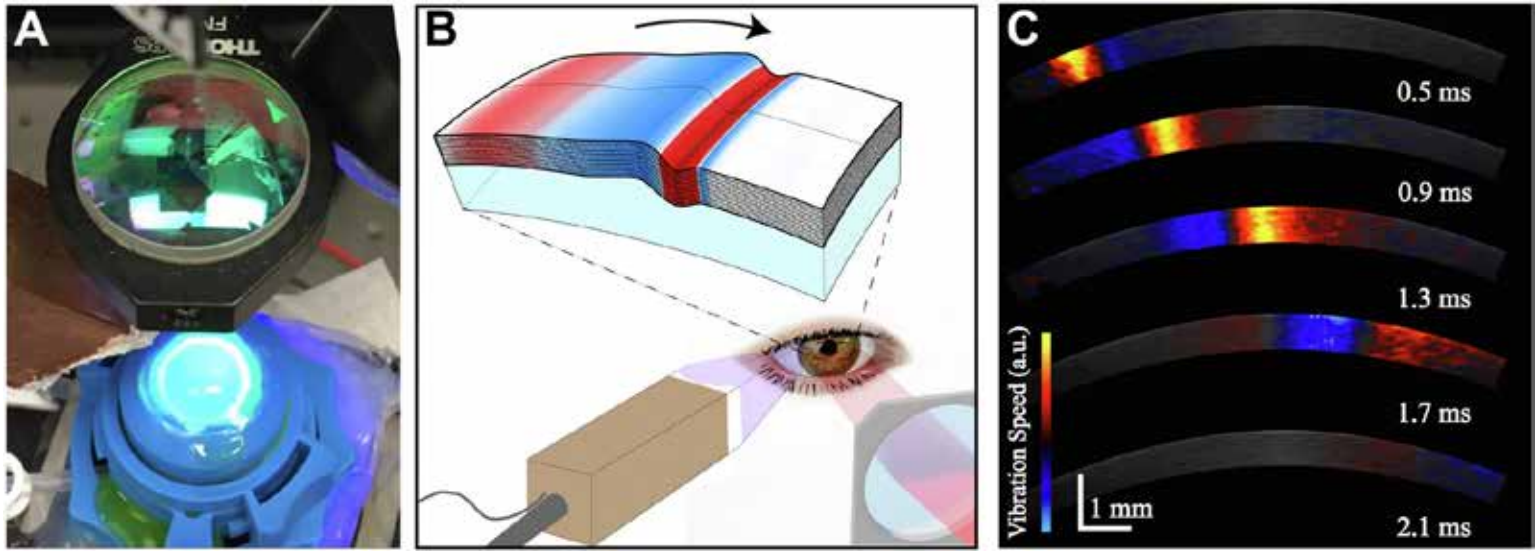

(A) *Acoustic micro-tapping optical coherence elastography imaging system with cornea inflated via artificial anterior chamber undergoing cross-linking treatment.* ***(B)*** *Schematic of mechanical wave propagation within the cornea.* ***(C)*** *Snapshots of elastic transients detected at different time instants using phase-sensitive OCT.*

Vision Science Shen Lab, UW Medicine. Work performed in part at the Molecular Analysis Facility, University of Washington.

This work was supported in part by NIH, Life Sciences Discovery Fund, Coulter Translational Research Partnership Program
Mitchell A. Kirby et al., *Ophthalmology Science* 3(2) (2023)

National Research Priority: Achieve Better Health Outcomes

The role of nonmetallic ion substitution in perovskite $LaCoO_3$ for improved oxygen evolution reaction activity

- Transition metal perovskites are promising but not perfect catalysts for oxygen evolution reactions (OER), which are important for energy technologies like water splitting.
- Traditional theories about how these materials work do not fully explain their behavior.
- This study explores how replacing certain atoms (both metal and non-metal) in a perovskite affects its performance as an OER catalyst, using a specific material ($LaCoO_3$) as a model.
- Methods include advanced experiments (X-ray techniques) and computer simulations (DFT) to study the material.
- Co-doping the material with iron (Fe) and phosphorus (P) improves its catalytic performance by enhancing the bonding between oxygen and metal atoms.
- These insights could help design more efficient, affordable catalysts for clean energy applications.

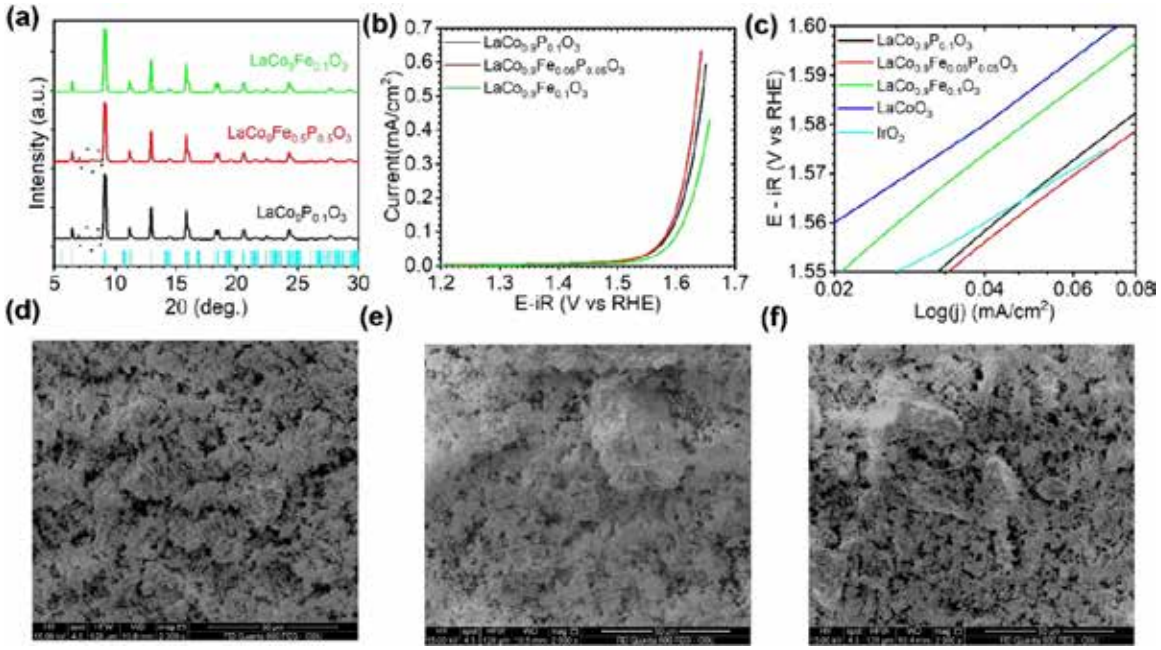

(a) *XRD diffraction with $LaCoO_3$ standard at bottom* ***(b)*** *OER performance of $LaCo_{0.9}P_{0.1}O_3$, $LaCo_{0.9}Fe_{0.05}P_{0.05}O_3$, and $LaCo_{0.9}Fe_{0.1}O_3$* ***(c)*** *Tafel plot of different peroxides compared with unsubstituted $LaCoO_3$ and benchmarked IrO_2; SEM of* ***(d)*** *$LaCo_{0.9}P_{0.1}O_3$,* ***(e)*** *$LaCo_{0.9}Fe_{0.05}P_{0.05}O_3$, and* ***(f)*** *$LaCo_{0.9}Fe_{0.1}O_3$.*

OSU, Argonne Nat. Lab, Pacific Northwest National Lab, Univ. of Louisiana at Lafayette, Lawrence Berkeley Nat. Lab. Work performed in part at the NNCI Northwest Nanotechnology Infrastructure facilities at Oregon State University.

This work was supported in part by NSF CBET, DMR, and CHE. Maoyu Wang et al., *Electrochimica Acta* 466 (2023)

National Research Priority: Global Challenge of Climate Change

National Nanotechnology Coordinated Infrastructure

NORTHWEST NANOTECHNOLOGY INFRASTRUCTURE

Research Triangle Nanotechnology Network (RTNN)

National Nanotechnology Coordinated Infrastructure

NSF

Growth and Characterization of AlInN/GaN Superlattices

AlInN films are widely used in electronic devices like high-electron-mobility transistors (HEMTs) and optical devices such as waveguides and distributed Bragg reflectors.

A key challenge in growing thick AlInN layers is island growth and pitting, leading to poor morphology.

To address this, we developed near-lattice-matched AlInN/GaN superlattices with superior morphology compared to bulk layers.

Grown on free-standing GaN, these superlattices have nearly perfect step-like surfaces and extremely low pit densities.

Refractive index matches the weighted average of the layers, and they emit at 317 nm due to quantum states in the GaN layers.

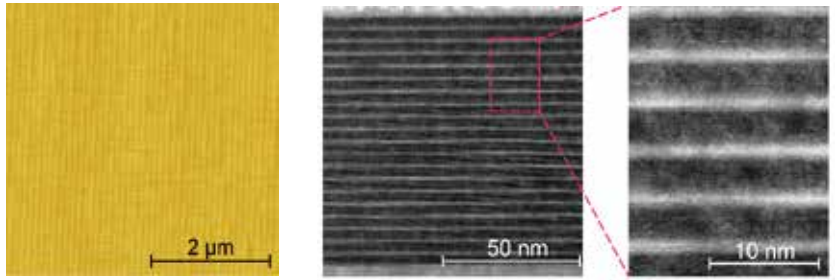

Atomic force microscope (AFM) image of the superlattice surface (left) and scanning transmission electron microscope (STEM) image of the superlattice cross-section (middle/right).

Haotian Xue, Elia Palmese, Ben J. Sekely, Brian D. Little, Fred A. Kish, Jr., John F. Muth, and Jonathan J. Wierer, Jr.; Electrical and Computer Engineering, NC State University; Work performed partially at NC State Analytical Instrumentation Facility and Nanofabrication Facility.

This work supported by NSF Awards #1935295 and #2212639. Xue et al. *Journal of Crystal Growth*, vol. 630 (2024) doi:10.1016/j.jcrysgro.2024.127567

National Research Priority: DoD - Microelectronics

Facile Synthesis of Electrically Conductive Membranes

Endowing membranes with electrical conductivity enhances separation performance via self-cleaning, redox, and electrostatic properties.

However, an effective strategy to fabricate electrically conductive membranes (ECMs) with diverse filtration performance remains unavailable.

A facile method was developed using polyethyleneimine (PEI), glutaraldehyde, and various conductive materials to cast a conductive layer on diverse substrates, from microfiltration to reverse osmosis membranes.

ECMs made with graphite and PVDF were stable, conductive, and effective for solute filtration and electrochemical degradation.

This method also worked with materials like carbon nanotubes, graphene oxide, and silver nanoparticles, yielding ECMs with low resistance, enhanced solute rejection, and reduced water permeance.

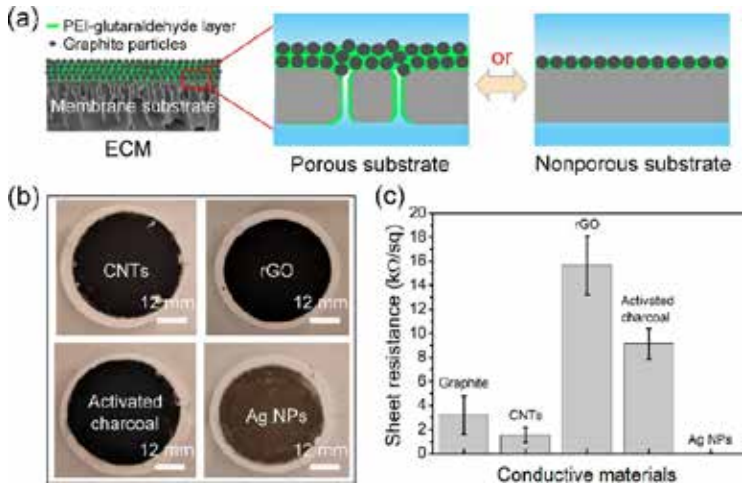

a) *Schematic of proposed physical interlocking between the conductive layer and the substrate in ECMs synthesized using the PEI/glutaraldehyde-based fabrication method.*

b) *Images of ECMs prepared using a PSf 20 kDa membrane as substrate, diverse conductive materials (i.e., CNTs, rGO, activated charcoal, Ag NPs) and the proposed PEI/glutaraldehyde-based fabrication method.*

c) *Sheet resistance of membranes in (b) after stirring.*

Wei Zhang, Nick Guan Pin Chew, Orlando Coronell; Environmental Sciences and Engineering, UNC-Chapel Hill. Work performed partially at Chapel Hill Analytical and Nanofabrication Laboratory.

This work also supported by: National Institute of Environmental Health Sciences (P42ES031007) and CHASE DOE Hub (DE-SC0021173). Zhang et al. *Environmental Science & Technology Letters*, vol. 10, no. 11 ACS (2023) doi:10.1021/acs.estlett.3c00631

Reducing the Vacuum Requirements for Hybrid Thin Film Deposition by Resonant Infrared Matrix-Assisted Pulsed Laser Evaporation (RIR-MAPLE)

- Resonant Infrared Matrix Assisted Pulsed Laser Evaporation (RIR-MAPLE) enables precise film deposition but faces challenges in industrial scalability, including film control and reproducibility.
- Controlling background pressure shows promise, with optimal deposition conditions improving material properties and reducing vacuum requirements. This study examines the effect of background pressure on phenylethyl ammonium lead iodide ($(PEA)_2PbI_4$) films, focusing on morphology, crystallinity, and composition.
- Optimal film quality was observed at 250 mTorr, where X-ray diffraction (XRD) revealed slight crystal rearrangement and minimal linewidth changes.
- Future work will investigate how inert gas environments influence surface composition, roughness, and electrical properties, advancing RIR-MAPLE scalability.

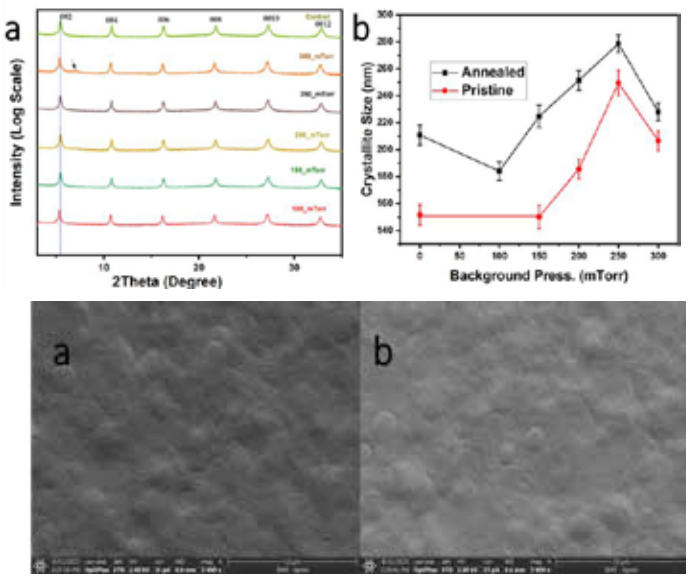

Top: (a) XRD patterns for pristine films deposited at different background pressures (control represents active vacuum). (b) Crystallite size of deposited films (pristine and annealed) as function of background.

Bottom: SEM images of (a) pristine, (b) annealed films deposited under active vacuum and (Scale bar: 10 μm).

Joshua O. Ayeni[1,2] and Adrienne D. Stiff-Roberts[1,2] [1]Materials Science and Engineering, Duke University [2]Electrical and Computer Engineering, Duke University; Work performed partially at Duke Shared Materials Instrumentation Facility

Switching Lead for Tin in $PbHfO_3$: Noncubic Structure of $SnHfO_3$

Developing lead-free dielectric $SnHfO_3$ faces challenges from Sn(II) oxidation during traditional synthesis.

A novel low-temperature ion-exchange method using orthorhombic $PbHfO_3$ as a precursor was developed, employing SnClF flux to produce metastable $SnHfO_3$.

This material shows promising visible-light-driven water oxidation and reversible structural phase transitions, suggesting ferroelectric potential (tracked via in situ XRD). SEM, EDS, and STEM confirm successful Sn substitution, material purity, and polycrystallinity.

Density functional theory reveals a reduced band gap due to valence band changes, with properties comparable to antiferroelectric perovskites. This study provides a pathway for lead-free perovskite oxides with advanced dielectric properties.

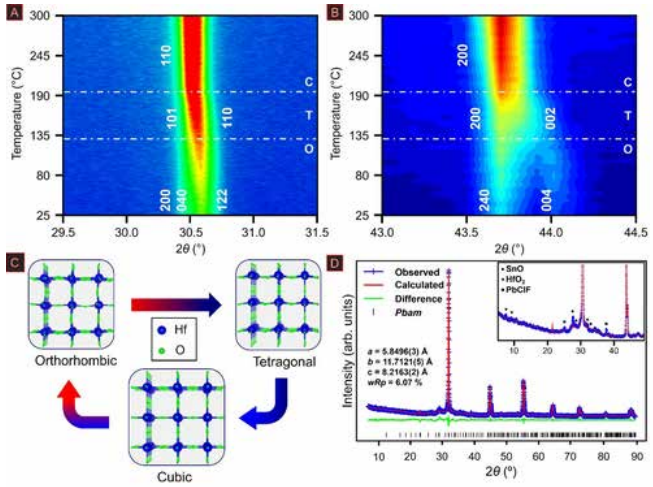

*Selected bulk structural characterization data shown as temperature-dependent XRD of $SnHfO_3$ focused on the {110}-family peak (A) and the {200}-family peak (B), schematic representation of Hf−O substructure phase changes (C), and full-profile Rietveld refinement of $SnHfO_3$ at room temperature with space group Pbam (D). $SnHfO_3$ undergoes a phase transition from Pbam to a higher symmetry phase at ≈130 °C, then to a second phase at ≈200 °C. The phases were assigned based upon previously investigated $PbHfO_3$ phase changes. (D, inset) Secondary phases are marked as • for SnO, ▲ for HfO_2, ▪ for PbClF, and * for the low angle peaks observed in $SnHfO_3$.*

Eric A. Gabilondo[1], Ryan J. Newell[2], Rachel Broughton[2], Aylin Koldemir[3], Rainer Pöttge[3], Jacob L. Jones[2], Paul A. Maggard[3] [1] Chemistry, NC State University, [2]Materials Science and Engineering, NC State University, [3]Universität Münster; Work performed partially at NC State Analytical Instrumentation Facility.

This work also supported by NSF DMR-2004455. Gabilondo et al. *Angewandte Chemie International Edition*, vol. 63, no. 4, (2023) doi:10.1002/anie.202312130

National Nanotechnology Coordinated Infrastructure

RTNN

Chiral Cation Doping for Modulating Structural Symmetry of 2D Perovskites

This work demonstrates a mixed-cation system in two-dimensional (2D) hybrid organic−inorganic perovskites (HOIPs), where a small amount (<10%) of chiral cation S-2-MeBA is doped into (S-BrMBA)$_2$PbI$_4$, modulating structural symmetry.

At low concentrations (1.4 ± 0.6%), the structure remains C2, while 3.9 ± 1.4% doping induces a transition to the lowest symmetry state (P1), stable up to ~7% substitution.

Density functional theory calculations show that this doping modulates spin splitting, important for spintronic applications.

The doping also affects optical properties, bandgap, and melting temperature, offering a strategy to enhance properties sensitive to symmetry breaking.

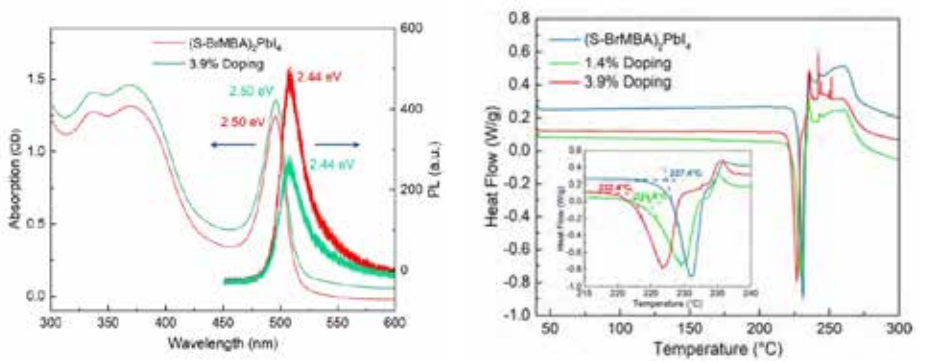

Absorption and Differential scanning calorimetry (DSC) scans of (SBrMBA) $_2PbI_4$ (blue), 1.4% doping material (green), and 3.9% doping material (red) with the heating and cooling rate of 5 °C/min.

Yi Xie,[1,2] Jack Morgenstein,[1] Benjamin G. Bobay,[3] Ruyi Song,[4] Naidel A. M. S. Caturello,[5] Peter C. Sercel,[6] Volker Blum,[1,4] David B. Mitzi[1,4]
[1]Mechanical Engineering and Materials Science, Duke University, [2]Materials Science and Engineering, Duke University, [3]Duke University Medical Center, [4]Chemistry, Duke University, [5]Federal University of ABC, [6]Center for Hybrid Organic Inorganic Semiconductors for Energy.

Work performed partially at Duke Shared Materials Instrumentation Facility.

This work was supported by DOE DEAC02-05CH11231, NSF NSF DMR-1729297, and FAPESP 20/11560-0. Xie et al. *Journal of the American Chemical Society*, vol. 145, no. 32 (2023) doi:10.1021/jacs.3c04832

National Research Priority: DoD - Microelectronics

National Nanotechnology Coordinated Infrastructure

RTNN

Choice of Electrolyte Impacts the Selectivity of Proton-Coupled Electrochemical Reactions on Hydrogen Titanate

- Reactivity of electrolyte protons with transition metal oxides (TMOs) is crucial for electrochemical energy storage and conversion devices using aqueous electrolytes.
- Proton-coupled electron transfer (PCET) reactions, where protons interact with TMOs, affect electrode performance in devices like electrolyzers and fuel cells.
- This study investigates PCET reactions in aqueous acidic electrolytes using layered hydrogen titanate ($H_2Ti_3O_7$).
- Three processes were identified: proton adsorption or insertion, participation in the hydrogen evolution reaction (HER), and dissolution of hydrogen titanate.
- Material characterization and computational results show that phosphate adsorption reduces dissolution in H_3PO_4, improving electrode performance and offering a method to enhance energy storage via electrolyte tuning.

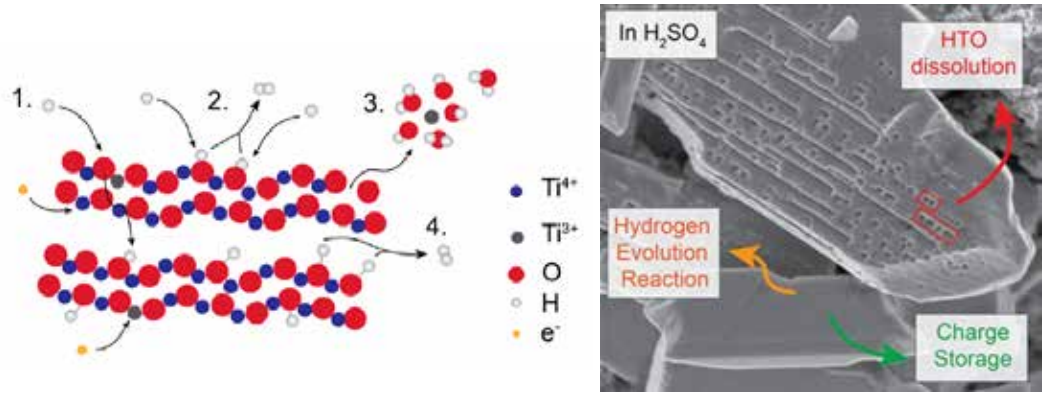

Schematic illustrating three PCET processes that can occur at TMO/aqueous electrolyte interfaces including (1) proton adsorption and insertion, (2) hydrogen evolution reaction, (3) TMO dissolution, and (4) hydrogen evolution from bulk protons and SEM image of $H_2Ti_3O_7$ in H_2SO_4.

Jenelle Fortunato[1], Yun Kyung Shin[2], Michael A. Spencer[1], Adri C. T. van Duin[2], and Veronica Augustyn[1]*, [1]Materials Science and Engineering, NC State University, [2]Mechanical and Nuclear Engineering, Pennsylvania State University ; Work performed partially at NC State Analytical Instrumentation Facility.

This work was supported by ORNL DOE DE-AC0500OR22725. Fortunato et al. *The Journal of Physical Chemistry C*, vol. 127, no. 25 (2023) doi:10.1021/acs.jpcc.3c01057

National Research Priority: DOE Energy Earthshots - Clean Fuels & Products Shot

Acoustic Separation and Concentration of Exosomes for Nucleotide Detection: ASCENDx

Exosomal biomarker isolation is crucial for biomedical applications, but current methods are costly and complex.

ASCENDx, a microfluidic disc, uses acoustics for fast exosome separation and concentration from plasma samples.

Integrated plasmonic nanostars enable label-free detection of exosomes via Surface-enhanced Raman scattering.

ASCENDx achieved 95.8% sensitivity and 100% specificity in colorectal cancer detection from exosomal miRNA.

ASCENDx shows promise for simplifying exosome diagnostics for precision medicine and point-of-care use.

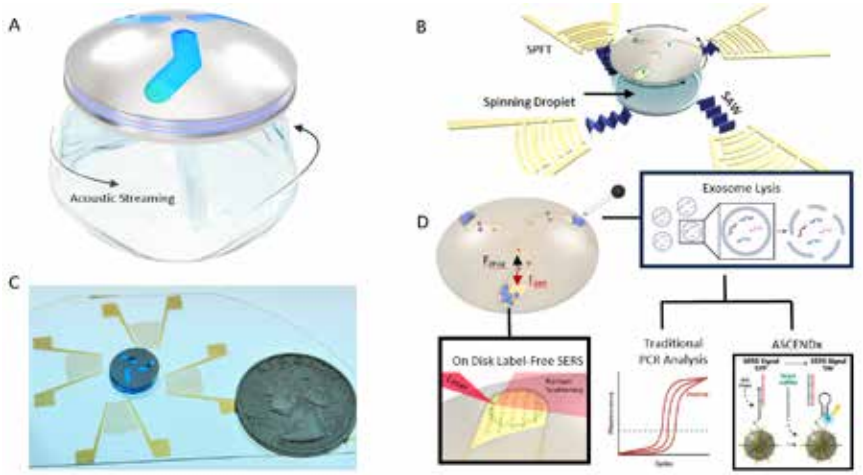

(a) Acoustic streaming within a water droplet deforms the liquid-air interface, causing the droplet to spin. When a disc is placed on top of the droplet, this streaming phenomenon causes the disc to rotate, leading to the concentration and separation of micro/nano objects.
(b) Device photo and
(c) schematic of the acoustofluidic disc unit of the ASCENDx platform. A water droplet is placed within a PDMS ring and situated between four SPFTs. A small disc with microfluidic structures patterned into its surface is placed atop the droplet. As SAWs propagate into the droplet, a helical vortex is formed, causing the droplet-disc system to rotate.
(d) As the disc rotates, larger particles move to the ends of the channel first. In this region, we have immobilized bimetallic nanostars to facilitate SERS analysis of the concentrated sample. The enriched sample can be removed via pipette for PCR analysis and integration with our point-of-care miRNA assay. (D) was made with BioRender.com.

Ty D. Naquin[1], Aidan J. Canning[1], Yuyang Gu[1], Jianing Chen[1], Chloe M Naquin[1], Jianping Xia[1], Brandon Lu[1], Shujie Yang[1], Aleksandra Koroza[1], Katherine Lin[1], Hsin-Neng Wang[1], William R. Jeck[1], Luke P. Lee[2], Tuan Vo-Dinh[1], Tony Jun Huang[1] [1]Mechanical Engineering and Materials Science, Duke University, [2]Harvard Medical School ; Work performed partially at Duke Shared Materials Instrumentation Facility

This work was supported by NIH R01GM135486 and R01GM132603, NSF GFRP DGE 2139754 and CHTN UM1CA239755. Naquin et al. *Science Advances*, vol. 10, no. 10, AAAS (2024) doi:10.1126/sciadv.adm8597.

Development of 4H-SiC Low Gain Avalanche Detectors

- Si-based low gain avalanche detectors (LGADs) are widely used in high energy physics (HEP) for their excellent timing and spatial resolution.
- Research is exploring the use of 4H-SiC in LGADs due to its superior properties, such as higher breakdown voltage, thermal conductivity, and saturation velocity, as well as the ability to operate at or above room temperature.
- This project developed fabrication techniques for 4H-SiC LGADs.
- The first generation showed promising IV and CV behavior and α-particle detection, indicating potential for superior timing resolution.
- SiC LGADs may reduce system cost and mass by eliminating the need for cooling in future collider applications.

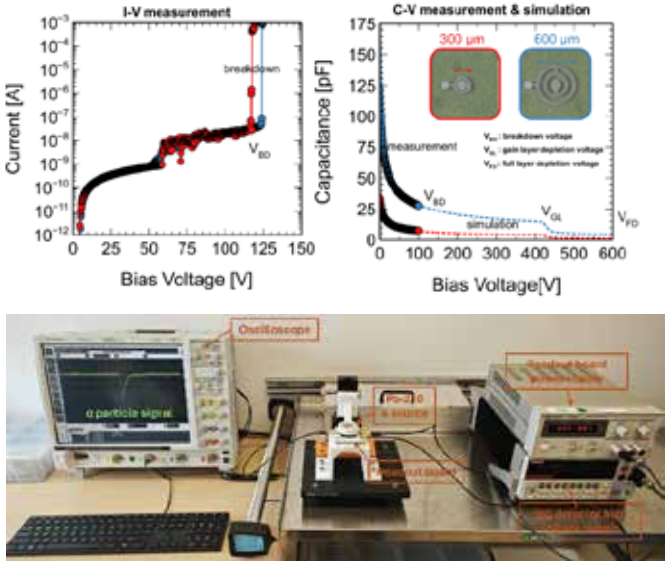

Top: Experimental and simulated IV and CV characteristics from first generation of 4H-SiC devices.; Bottom: 4H-SiC device connected to a readout board while being exposed to α-particles from a Po-210 source

Yashas Satapathy[1], Ben Sekely[1], Tao Yang[4], Greg Allion[3], Philip Barletta[3], Stefania Stucci[5], Stephen Holland[4], Carl Haber[4], John Muth[2], and Spyridon Pavlidis[2] [1]Materials Science and Engineering, NC State University [2]Electrical and Computer Engineering, NC State University [3]NCSU Nanofabrication Facility (NNF), NC State University [4]Physics Division, Lawrence Berkeley National Laboratory [5]Physics Department, Brookhaven National Laboratory; Work performed partially at NC State Nanofabrication Facility

Barletta et al. *Proceedings of the US Community Study on the Future of Particle Physics* (Snowmass 2021) (Published Online: 2022)

National Research Priority: DoD - Microelectronics

Amorphous K–Co–Mo–Sx Chalcogel: A Synergy of Surface Sorption and Ion-Exchange

Chalcogel is a class of meso- to macroporous nanomaterials composed of highly disordered nanoaggregated particles, with applications in energy and environmental fields such as photocatalysis, electrocatalysis, and energy storage.

This work reports the synthesis of an ion-exchangeable amorphous chalcogel with a nominal composition of $K_2CoMo_2S_{10}$ (KCMS) at room temperature. The study demonstrates the stabilization of electrostatically bound K+ ions within the Co–Mo–S covalent network to create K–Co–Mo–S chalcogel.

The research highlights the potential of quaternary chalcogels for advancing separation science, integrating surface sorption and ion-exchange.

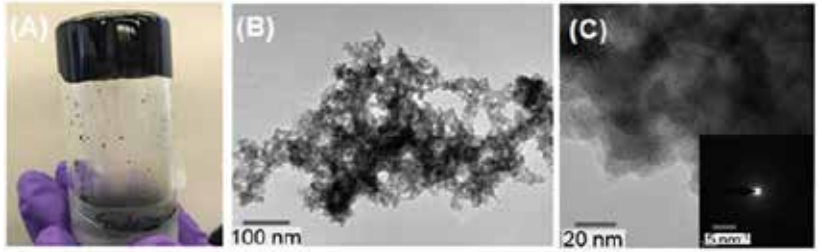

Photograph of the inverted vial showing the strength of the monolith KCMS wet–gels against fragmentation A), TEM image of the aerogels demonstrates the aggregation of the nanoparticles along with diverse range of porosities B), HRTEM image and the SAED image, in the inset of C) showing no evidence of the crystallite's formation.

[1]Jing Nie, [1]Taohedul Islam, [1]Subrata Chandra Roy, [2]Dien Li, [3]Ruhul Amin, [3]Kathryn Taylor-Pashow, [1]Xianchun Zhu, [4]Renfei Feng, [4]Roman Chernikov, [4]Avijit Pramanik, [1]Fengxiang X. Han, [5]Amar S. Kumbhar, [1]Saiful M. Islam, [1]Chemistry and Biochemistry, Jackson State University, [2]Savannah River National Laboratory, [3]Oak Ridge National Laboratory, [4]Canadian Light Source, [5]Chemistry, UNC-Chapel Hill; Work performed partially at UNC Chapel Hill Analytical and Nanofabrication Facility

This work was supported by DOE Contracts No. RFPs 000054252 & 000045835, DE-AC02-06CH11357. Nie et al. *Small* (2024) doi:10.1002/smll.202400679

National Research Priority: DOE Energy Earthshots - Clean Fuels & Products Shot

Photoelectrochemical CO_2 Reduction to CO Enabled by a Molecular Catalyst Attached to High-Surface-Area Porous Silicon

- High-surface-area p-type porous Si photocathode with a covalently immobilized molecular Re catalyst shows high selectivity for photoelectrochemical CO_2 conversion to CO.
- Faradaic efficiencies of up to 90% for CO at −1.7 V (versus ferrocenium/ferrocene) under 1 sun illumination in an acetonitrile solution containing phenol are achieved.
- Photovoltage is approximately 300 mV, based on comparisons with similar n-type porous Si cathodes in dark conditions.
- Porous Si photoelectrode demonstrates greater stability and selectivity for CO production than planar Si wafers with the same Re catalyst.
- Reproducible catalytic performance is confirmed through transmission mode FTIR spectroscopy.

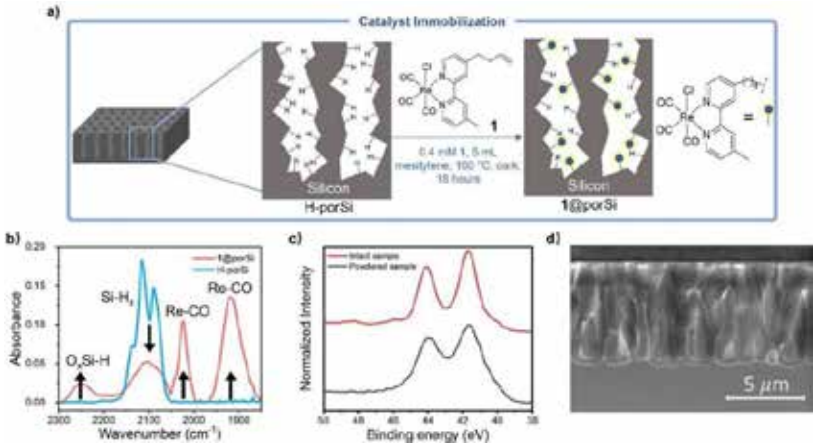

a) Schematic for the immobilization of 1 on porous p-type (1–10 Ω cm–1) Si to form 1@porSi. Characterization of 1@porSi, (b) FTIR and (c) Re 4f region XPS spectra. The XPS spectra are of an intact sample, which is representative of the top 10–15 nm of the surface, and a powdered sample, which was obtained by scratching of the porous material and mixing and is representative of the entire pore. (d) Cross-sectional SEM image (8000× magnification).

Xiaofan Jia [1], Eleanor Stewart-Jones [1], Jose L. Alvarez-Hernandez [1], Gabriella P. Bein [2], Jillian L. Dempsey [2], Carrie L. Donley [2], Nilay Hazari [1*], Madison N. Houck [1], Min Li [1], James M. Mayer [1], Hannah S. Nedzbala [1], Rebecca E. Powers [2] , [1] Chemistry, Yale University, [2] Chemistry, UNC-Chapel Hill, Work performed in part at the UNC Chapel Hill Analytical and Nanofabrication Laboratory.

This work was supported by NSF GFRP 2021315253, NIH R01GM50422, AFOSR FA9550-18-1-0420, DMR-2011924. Jia et al. *Journal of the American Chemical Society*, vol. 146, no. 12 (2024) doi:10.1021/jacs.3c10837

National Research Priority: DOE Energy Earthshots - Carbon Negative Shot

San Diego Nanotechnology Infrastructure (SDNI)

National Nanotechnology Coordinated Infrastructure

NSF

Healable and Conductive Sulfur Iodide for Solid-State Li-S Batteries

Breakthrough in Convergence Research: The development of lithium-sulfur solid-state batteries has been historically plagued by the inherent characteristics of sulfur cathodes. To overcome these challenges, the team developed a new cathode material: a crystal composed of sulfur and iodine. Iodine introduces new states into the band gap of sulfur and promotes the formation of reactive polysulfides during electrochemical cycling. This discovery has the potential to solve one of the biggest challenges to the introduction of solid-state lithium-sulfur batteries by dramatically increasing the useful life of a battery.

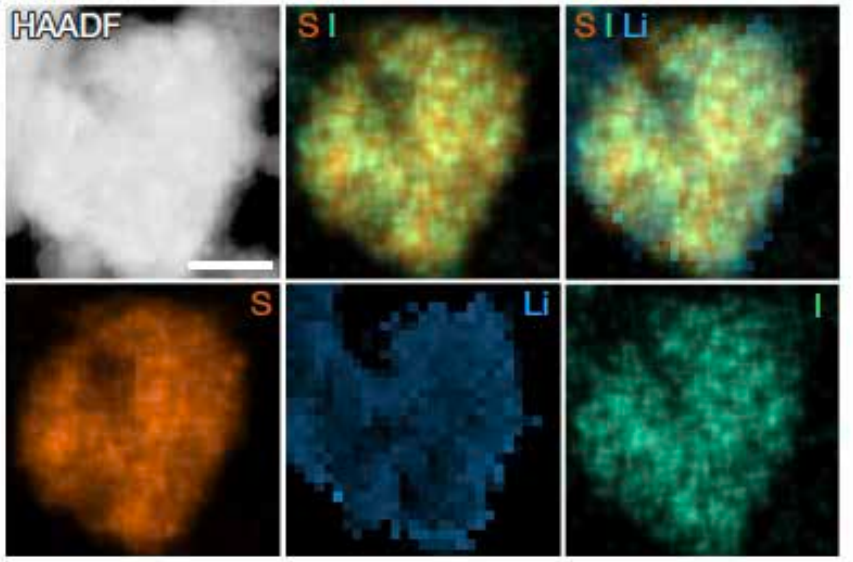

Brookhaven National Laboratory, University of Houston, UCSB, Johns Hopkins University, Pacific Northwest National Laboratory, Honda Research Institute USA, and UCSD.

Nature (2024) (https://doi.org/10.1038/s41586-024-07101-z).

National Research Priority: NSF – Growing Convergence Research

An electroencephalogram microdisplay to visualize neuronal activity on the brain surface

Breakthrough in nano medical device: an intracranial electroencephalogram (iEEG) microdisplay to address limitations in current functional brain mapping.

The iEEG consists of free-standing arrays of 2048 GaN light-emitting diodes (μLEDs) laminated on the back of micro-electrocorticography (μECoG) electrode grids. With a series of proof-of-concept experiments in rats and pigs the team demonstrated that these iEEG-microdisplays allowed to perform real-time iEEG recordings and display cortical activities by spatially corresponding light patterns on the surface of the brain in the surgical field. The iEEG-microdisplay holds promise to facilitate monitoring of pathological brain activity in clinical settings.

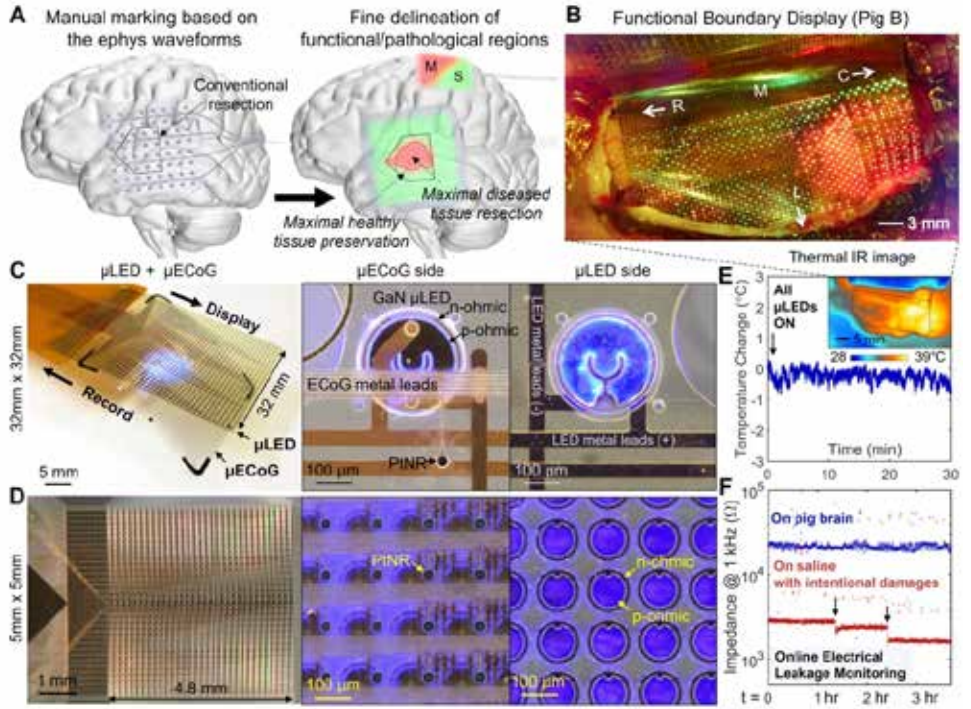

Oregon Health & Science University, Massachusetts General Hospital, Ohio State University, and UCSD

Science Translational Medicine (doi: 10.1126/scitranslmed.adj7257)

National Research Priority: NSF – Growing Convergence Research

Understanding the rules of life: 3D bioprinting

Advances in understanding the rules of life via 3D bioprinting: 3D bioprinting uses cells and biopolymer to create biological structures and tissues. 3D-engineered tissues—lab-created yet functional human-like tissues made of living cells and biomaterial scaffolds—have great potential for biomedical applications, including drug testing and development, organ transplants, regenerative medicine, personalized medicine, disease modeling, and more.

The 3D bioprinting technology has been successfully commercialized and its application has been extended to studies of the ecology of coral reef and living organisms-on-a-chip, helping scientists to understand the rules of life.

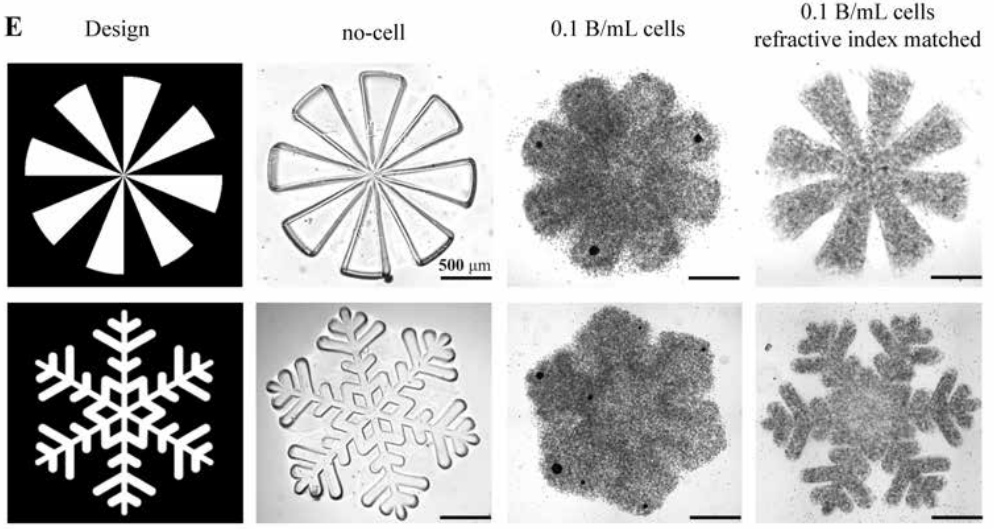

Scripps Institution of Oceanography and UCSD

Science Advances, 2023. doi/10.1126/sciadv.ade7923)

National Research Priority: NSF – Understanding the Rules of Life

A fully integrated wearable ultrasound system to monitor deep tissues in moving subjects

Advance in nano medical device: A fully integrated wearable ultrasound system to monitor deep tissues in moving subjects.

The USoP allows continuous tracking of physiological signals from tissues as deep as 164 mm, continuously measuring central blood pressure, heart rate, cardiac output, and other physiological signals for up to 12 hours at a time.

- *A fully integrated autonomous wearable ultrasonic-system-on-patch (USoP).*
- *Machine learning is used to track moving tissue targets and assist the data interpretation.*
- *Continuous tracking of physiological signals from tissues as deep as 164 mm.*
- *IoMT: internet-of-medical-things.*

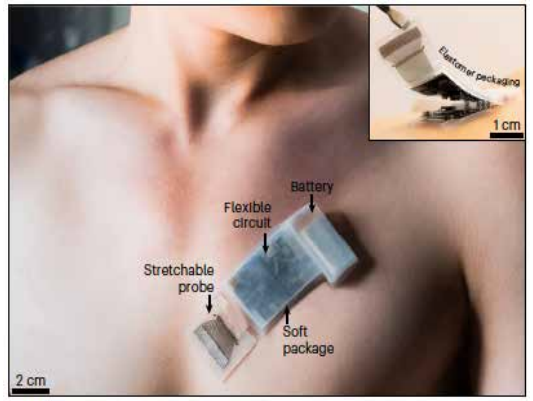

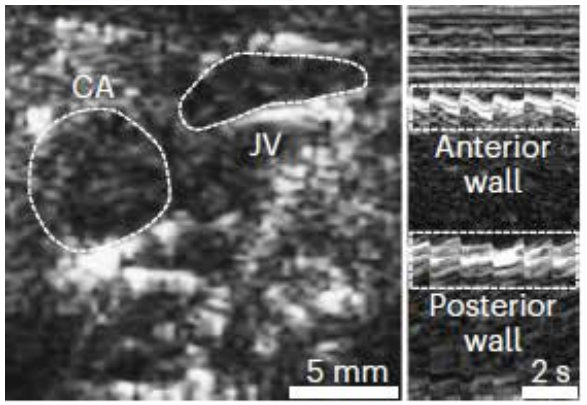

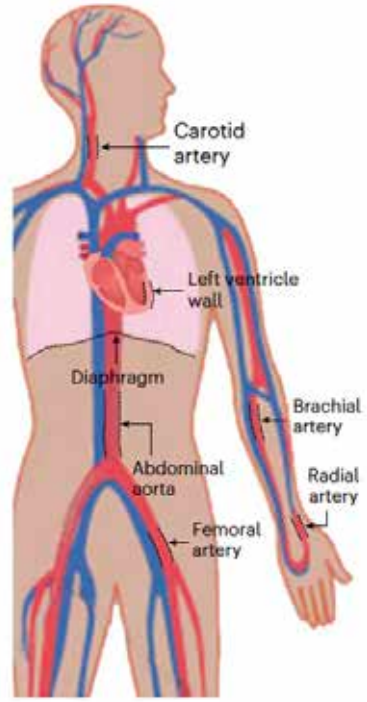

UCSD, Massachusetts Institute of Technology, Yale University, Stanford University

Nature Biotechnology (2023)
https://doi.org/10.1038/s41587-023-01800-0

National Research Priority: NSF – Growing Convergence Research

National Nanotechnology Coordinated Infrastructure

sdni San Diego Nanotechnology Infrastructure

A fingertip-wearable microgrid system for autonomous energy management and metabolic monitoring

Advances in nano biomedical device: The work reports an autonomous and continuous sweat sensing system that operates on a fingertip. The system uses a self-voltage-regulated wearable microgrid based on enzymatic biofuel cells and AgCl-Zn batteries to harvest and store bioenergy from sweat. It relies on osmosis to continuously supply sweat to the sensor array for on-demand multi-metabolite sensing and is combined with low-power electronics for signal acquisition and wireless data transmission. The wearable system is powered solely by fingertip perspiration and can detect glucose, vitamin C, lactate and levodopa over extended periods of time.

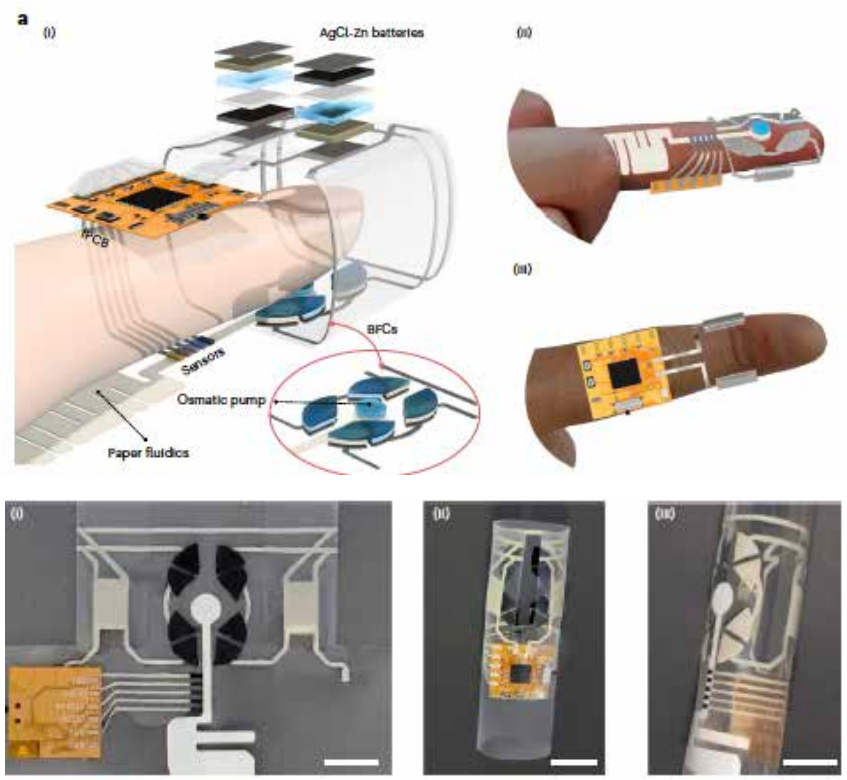

UCSD, Samsung Electronics

Nature Electronics (2024) doi.org/10.1038/s41928-024-01236-7

National Research Priority: NSF – Growing Convergence Research

National Nanotechnology Coordinated Infrastructure

sdni San Diego Nanotechnology Infrastructure

Soft and Hybrid Nanotechnology Experimental (SHyNE) Resource

National Nanotechnology Coordinated Infrastructure

Earth and Planetary Sciences

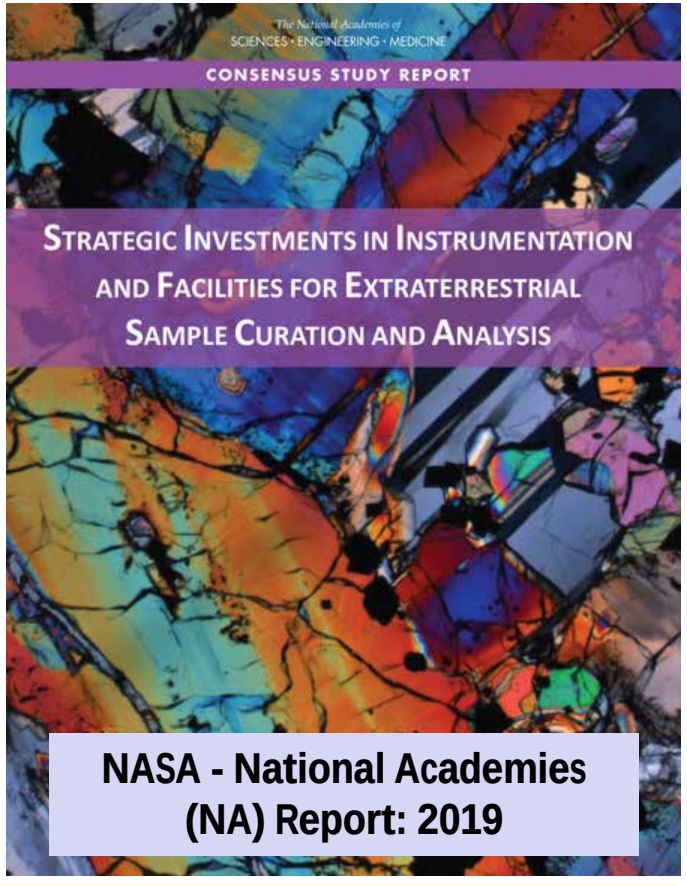

NASA - National Academies (NA) Report: 2019

Extra-Terrestrial Materials Analysis; PI Dravid helped developed this seminal NASA – National Academies report.

Spring 2024 HEALTH & SCIENCE

Turning Moon Dust Into Building Blocks

Northwestern mineralogist analyzes lunar soil for moon-based, 3D-printed construction.

Research lead by Prof. Steve Jacobsen at Northwestern University in collaboration with NASA and ICON Technology Inc., aimed at developing technology to construct a lunar base using moon dust. NASA's Artemis program requires a durable landing pad to prevent moon dust, which is highly abrasive, from damaging equipment and habitats. ICON plans to use 3D printing technology to convert lunar soil into ceramic material for construction. Researchers are currently studying the varying properties of simulated moon dust using electron microscopy at the NUANCE Center to ensure the 3D printer can adjust to differences in soil composition, aiding in the successful construction of moon-based structures.

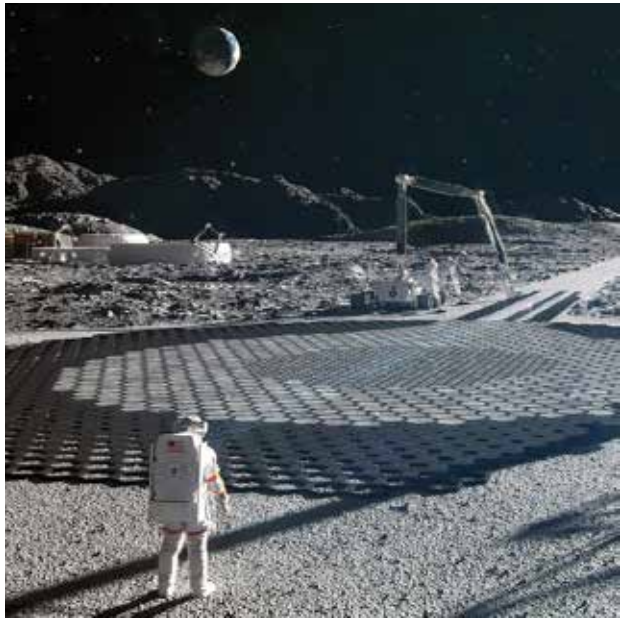

Jacobsen, Steve; Earth and Planetary Sciences (EPS), Northwestern University; Abbott, Tirzah, SHyNE staff member and EPS graduate student.

Supported by NASA SBIR Phase III award.

National Research Priority: NSF - Growing Convergence Research

National Nanotechnology Coordinated Infrastructure

SHyNE Soft Hybrid Nanotechnology Experimental Resource

Rapid Detection of Diverse HIV-1 variants using monoclonal antibodies immobilized on Microcantilevers

Concentration dependent response curves for p24 detection on 1:1 ratio of mAbs functionalized microcantilevers.

a) Deflection plots of p24 detection of diverse HIV-1 subtype A.

b) Deflection plots of p24 detection of diverse HIV-1 subtype B.

c) Deflection plots of p24 detection of diverse HIV-1 subtype C.

d) Deflection plots of p24 detection of diverse HIV-1 subtype D.

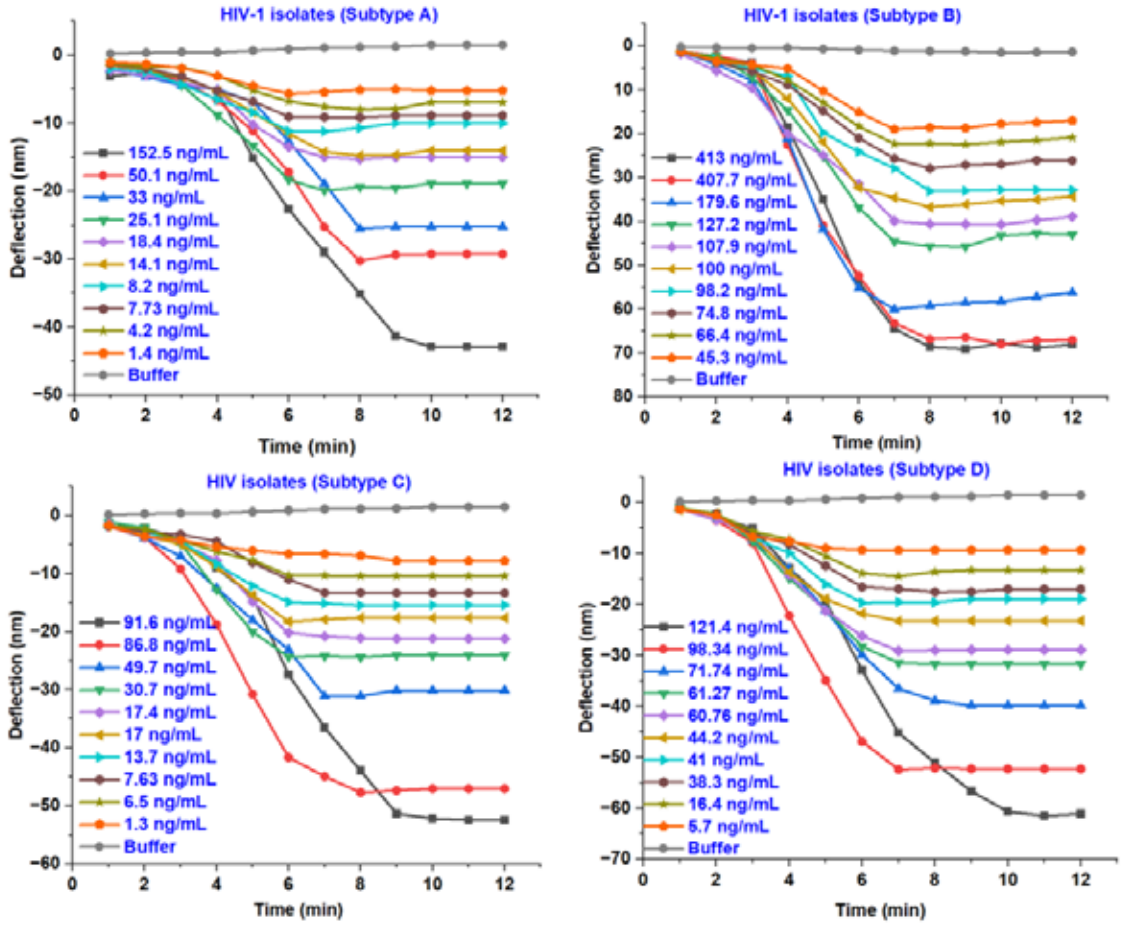

Vinayak Dravid and Gajendra Shekhawat, Northwestern University. Work performed at SHyNE Resource.

National Research Priority: NSF - Understanding the Rules of Life

Ga Zircons Anchor Chronology of Lunar Magma Ocean

Zircon crystals (center circle) extracted from lunar rocks returned to Earth by the Apollo 17 mission in 1972 are subjected to atomic-scale analysis by atom-probe tomography (atom-by-atom 3D elemental map displayed in the right-hand side circle) to capture the exact distribution of lead (Pb) isotopes generated by radioactive decay of uranium (U) isotopes intrinsic to the zircon crystal. The concentration ratio of the respective lead and uranium isotopes is used for determining a concordant average uranium-lead radiometric date of 4460 ± 31 Ma, the oldest lunar zircon yet reported.

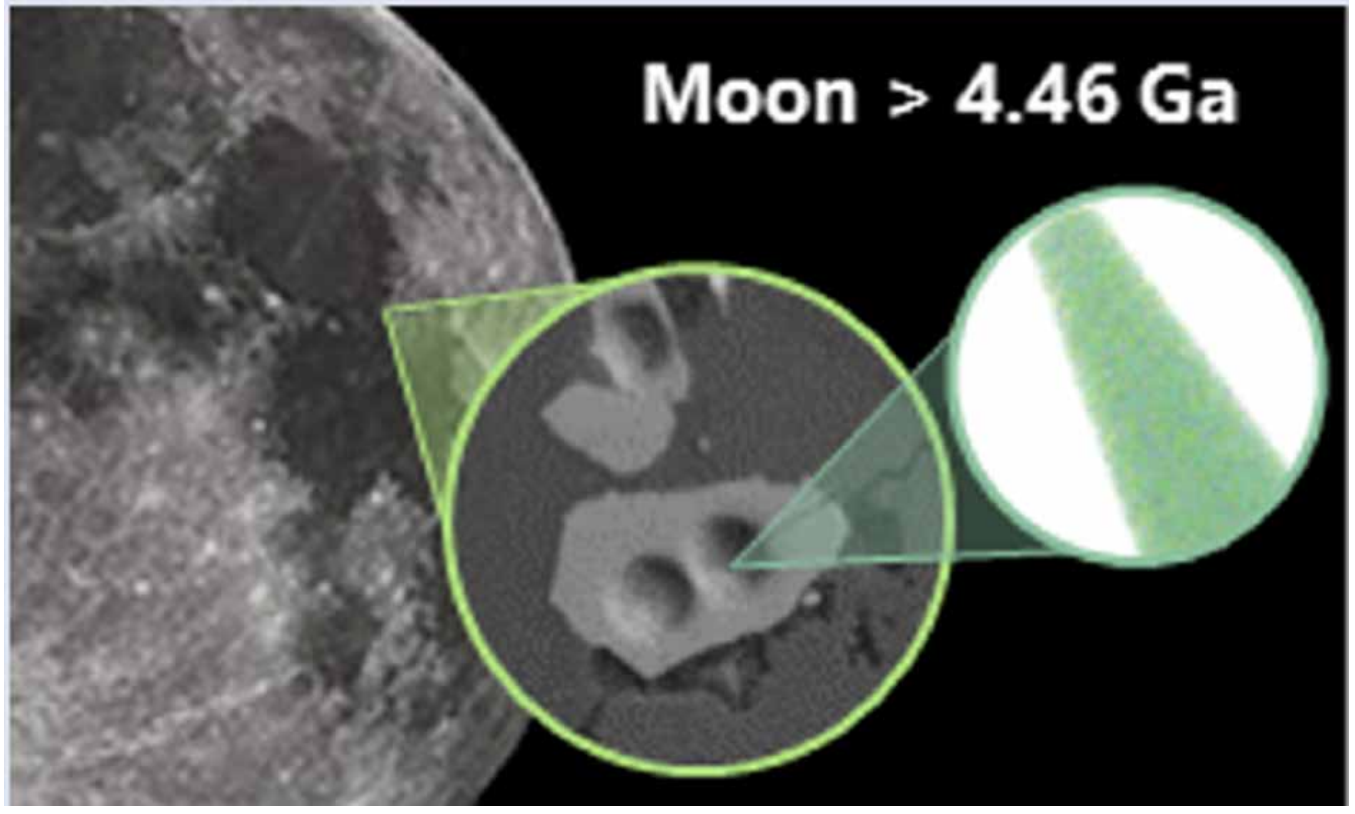

Supported by NSF-MRI (DMR-0420532), ONR-DURIP (N00014-0400798, N00014-0610539, N00014-0910781, N00014-1712870), NU MRSEC (NSF DMR-2308691),SHyNE Resource (NSF ECCS-2025633). J. Greer, B. Zhang, D. Isheim, D.N. Seidman, A. Bouvier, P.R. Heck, *Geochemical Perspectives Letters* 27 (2023) 49-53.

National Research Priority: NSF - Growing Convergence Research

An Electric Molecular Motor

Graphical representations for the reduced state of the [3]catenane molecular motor [3]CMM7+6• with key superstructural formulas showing the radical-pairing interactions between the CBPQT2(+•) rings and the V+• units. Positive charges are balanced by PF6− counterions, which are omitted for the sake of clarity

•Design and Structure: The motor comprises a [3]catenane with two cyclobis(paraquat-p-phenylene) (CBPQT^{4+}) rings encircling a 50-membered loop, engineered to facilitate controlled, directional movement.

•Mechanism of Motion: Utilizing a flashing energy ratchet mechanism, the system converts electrical energy into mechanical motion, guiding the rings to move unidirectionally around the loop with approximately 85% efficiency.

•Energy Landscape: Interactions between the two rings create a two-dimensional potential energy surface analogous to that of F_0F_1 ATP synthase, enabling coordinated movement.

•Electrical Activation: The motor operates under an oscillating voltage or external modulation of the redox potential, demonstrating the feasibility of electrically driven molecular machines in solution.

•Advancement Over [2]catenane: Initial studies with a [2]catenane revealed insufficient kinetic asymmetry for unidirectional motion, leading to the development of the [3]catenane system to achieve the desired mechanical behavior.

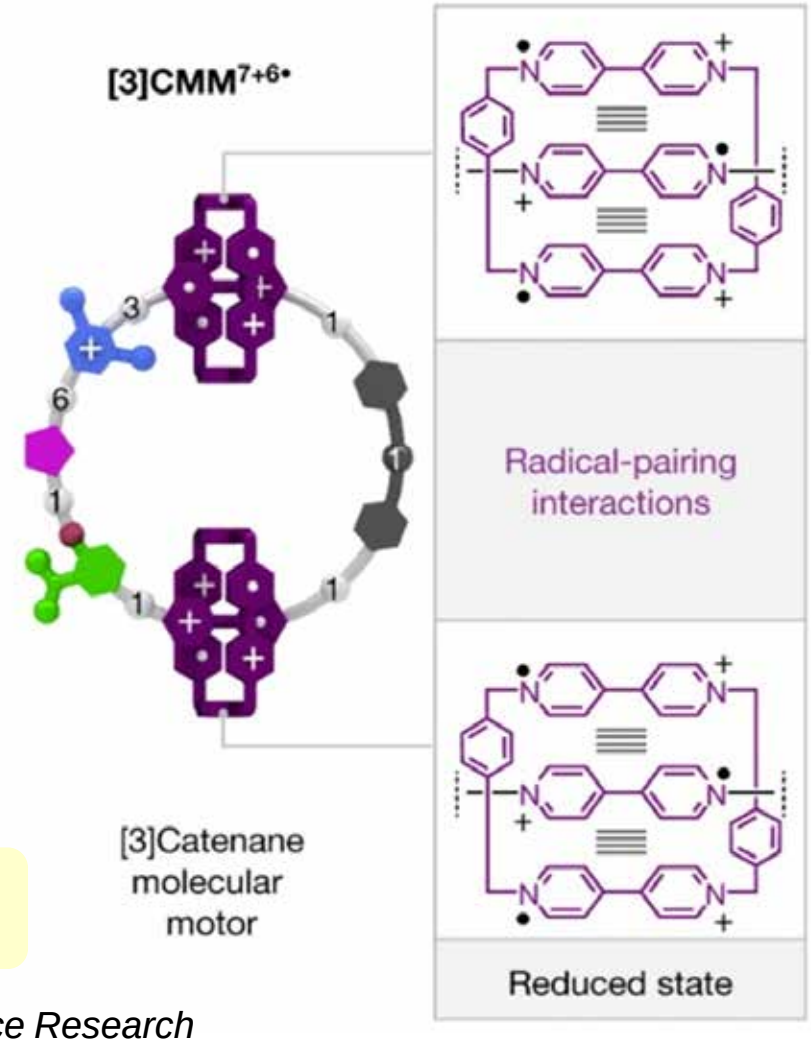

Supported by NSF Award # CBET-2005250 and SHyNE Resource NSF ECCS-2025633.
Zhang, L., et al., *Nature* 2023, volume 613, pages 280–286.

National Research Priority: NSF - Growing Convergence Research

Ultrathin silicon nitride microchip, in-situ/operando microscopy w/ high spatial resolution & spectral visibility

Fabrication and physical characterizations of the ultrathin SiNx membrane with back-supporting structure. (A) Fabrication process of the UT SiNx membranes. (B) Digital photograph of fabricated membrane chips with thickness ranging from 50 nm to 5 nm. The scale bar is 10 mm. (C) Optical micrograph (top) and the bright field TEM image of the UT microchip with honeycomb patterns. The scale bar is 100 μm. (D) Pressure-resistance of the SiNx membrane with different thickness. Dashed line indicates the averaged pressure tolerance and orange-colored box indicates the general operation pressure. (E) Breakdown electron dose of SiNx membrane under a focused illumination in STEM mode. (F) Correlation of membrane thickness and inelastic mean free path (IMFP: t/λi) of SiNx membrane measured with TEM-EELS. The black dots indicate the t/λi of single membrane and blue dots indicate the t/λi of assembled closed cells with 760 Torr Ar gas.

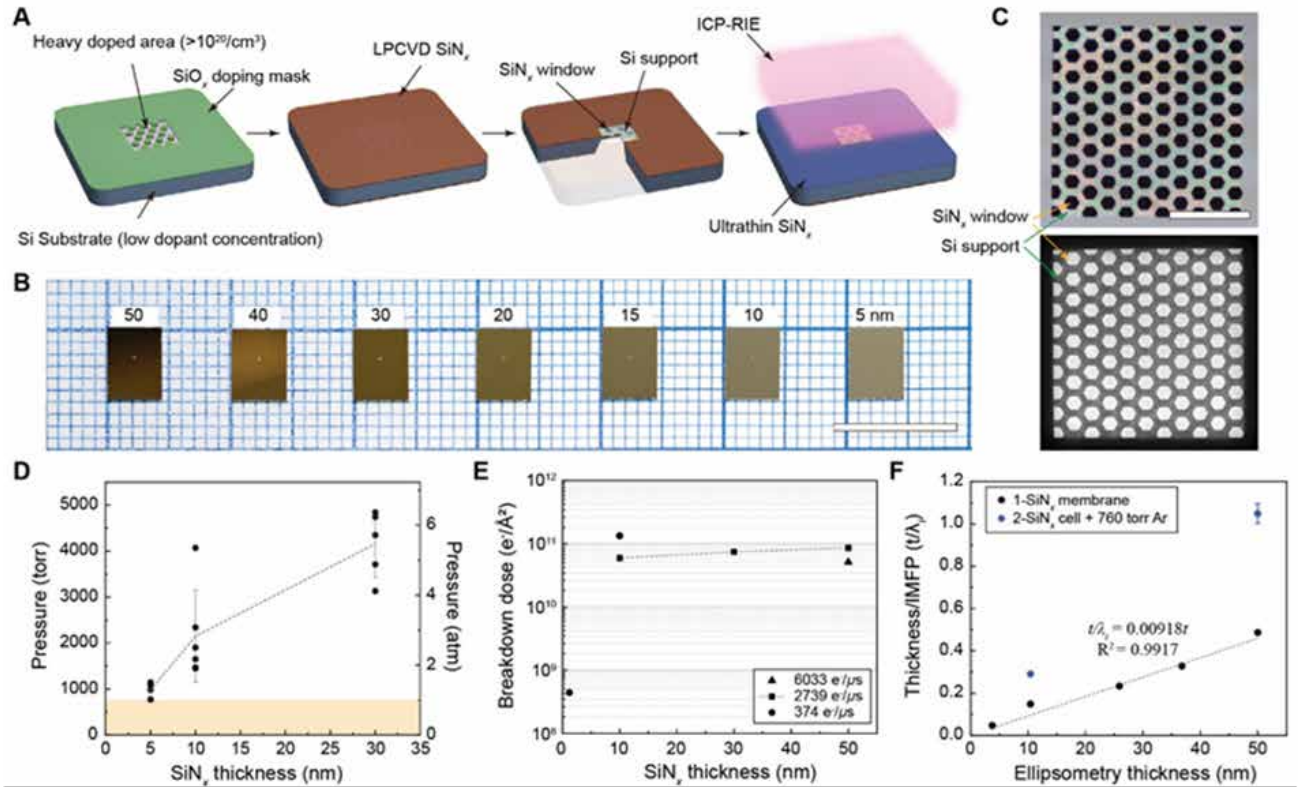

Supported by ARO MURI program W911NF-18-1-0200, AFOSR FA9550-22-1-0300, National Research Foundation of Korea 2022R1A6A3A03059199, NRF-2022R1A2C2008929, SHyNE Resource NSF ECCS-2025633, The IIN, NU MRSEC NSF DMR-2308691.
Kunmo Koo, et al., *Science Advances* 10, eadj6417 (2024). DOI:10.1126/sciadv. adj6417.

National Research Priority: NSF - Growing Convergence Research

Design concept of ref-OECT-based E-AB sensor

Design concept of ref-OECT-based E-AB sensor.
a.) Schematic image of the ref-OECT-based E-AB sensor.
b.) Testing scheme of the ref-OECT-based E-AB sensor. Output of channel current inOECT can be monitored during the operation of E-AB sensor in the 3-electrode setup.
c.) Sensing mechanism of the ref-OECT-based E-AB sensor for TGF-β1. Without the existence of TGF-β1, themethylene blue (MB) redox reporter is closer to the gate electrode surface, which results in a high gate current (IG) as well as a larger channel current modulation (IDS). In the presence of TGF-β1, a conformational change occurs in the aptamer, and the MB redox reporter moves further from the gate electrode surface, which results in low gate current and smaller channel current modulation.

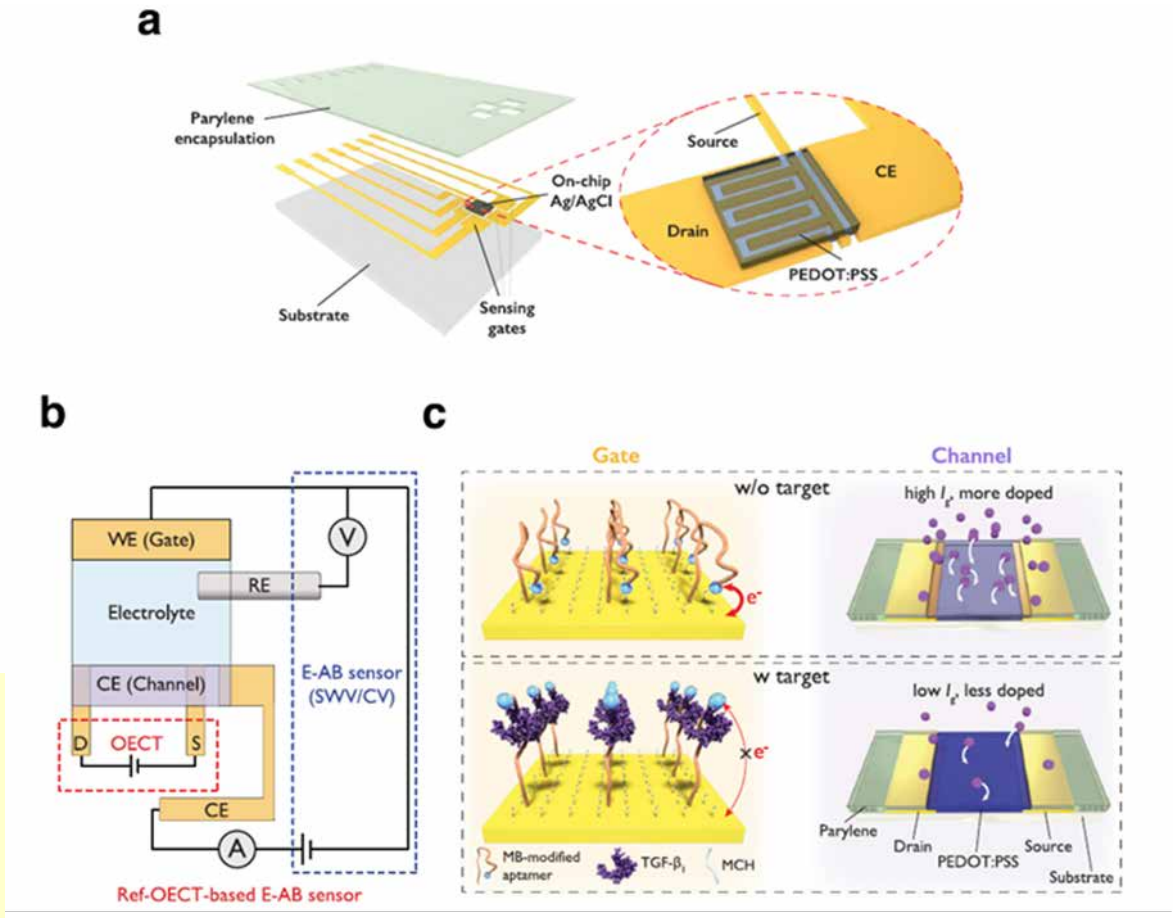

Supported by Defense Advanced Research Projects Agency (DARPA) through Cooperative Agreement D20AC00002. SHyNE Resource (NSF ECCS-2025633), The IIN, and Northwestern's MRSEC program (NSF DMR-1720139). Xudong Ji, Xuanyi Lin and Jonathan Rivnay. *Nature Communications* (2023) 14:1665.

National Research Priority: NSF - Growing Convergence Research

SHyNE Resource Research Highlights from UChicago

Fermilab researchers improve superconducting qubit coherence through materials integration

- 1000X decrease in deleterious niobium oxide
- 3X improvement in qubit coherence times
- Excellent substrate-metal interface

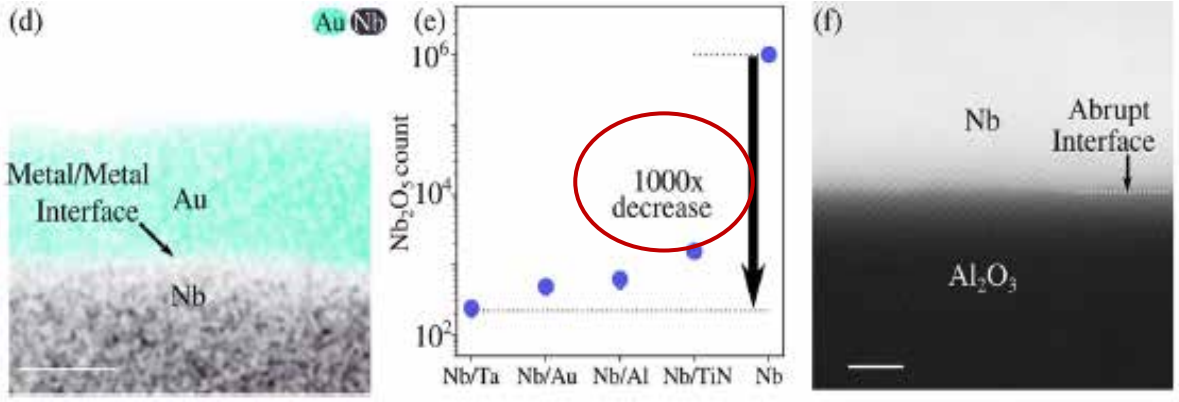

Work performed at UChicago's Pritzker Nanofabrication Facility, supported by NSF Award # NNCI ECCS-2025633. M. Bal, A. Murthy, S. Zhu et al., *npj Quantum Inf.* 10, 43 (2024)

UChicago researchers build atom-photonics integrated chip

- Enables direct loading of individual atoms into photonics chip
- 64 optical tweezers and 100 optical nanocavities
- Applies to quantum communication & simulation

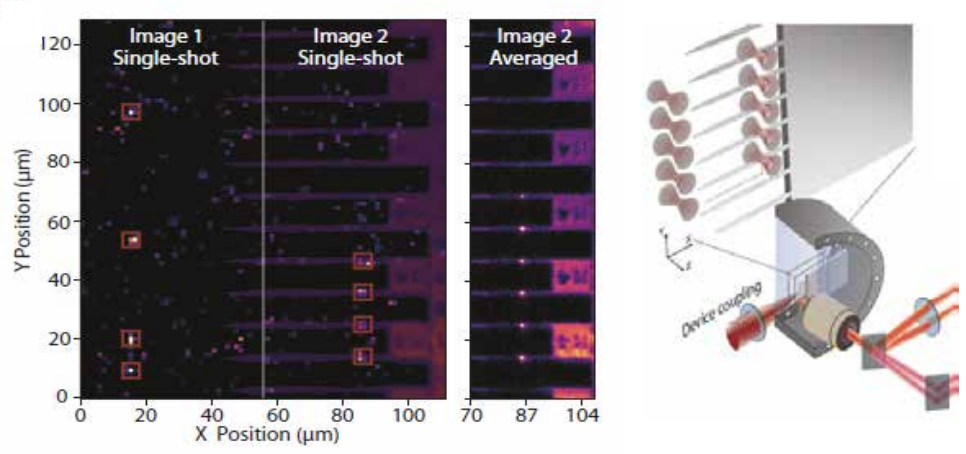

Work performed at Uchicago's Pritzker Nanofabrication Facility, supported by NSF Award # NNCI ECCS-2025633. S. G. Menon et al., *Nature Comm* 15, 6156 (2024)

National Research Priority: NSF - Quantum Leap

SHyNE Resource Education and Outreach

Midwest Microscopy & Microscopy Spring Meeting: Frontiers in AI-ML and computationally-mediated microscopy

ü 90+ attendees

ü 8 Speakers

ü Vendor Fair

ü Facilities Tours

"[The event was] Well organized and good variety of activity"
-anonymous attendee

"[I liked the] variety of speakers, engaging sponsors. Close community with new attendees"
-anonymous attendee

ü 220+ attendees

ü 36+ countries

ü 9 Speakers

ü Physical & Biological Sciences Talks

ü Panels: Career Pathways, Amplifying Voices, Overcoming Imposter Syndrome

"Participation was possible for people from various backgrounds, not just from the academic environment (I am a high school student). The topics were interesting and discussed in an accessible way. A good option was joining subgroups on topics that interested the person the most." - anonymous attendee

"Loved connecting with other women in microscopy. The panel sessions were enticing and interactive." - anonymous attendee

SHyNE staff organized these events in partnership with Microscopy Society of America, with support from NSF Award # NNCI ECCS-2025633 and Northwestern University Materials Research Center, Award # NSF DMR-2308691.

National Research Priority: NSF - NSF INCLUDES

SHyNE Resource Computation

Globus - Transfer for High-Volume Data Transfer

- Globus is a reliable, high-performance data transfer tool tailored for researchers.
- Designed for transferring and sharing large volumes of data between facilities, clouds, and personal computers.

Benefits to the user community:

1. Speed - Transfers large datasets quickly.
2. Security - Encryption methods to ensure data protection.
3. Automation - Provides automated retries, synchronization, and failover.
4. Usability - Offers an intuitive web-based interface.

Cloud Environment – User Access for Data Analysis

- Problem: Users struggle accessing computing resources for efficient data analysis.
- Solution:
  - Pre-installed software ensures users can analyze data without worrying about licensing restrictions
  - Cloud-based virtual machines offer scalable solutions, meeting diverse data analysis needs

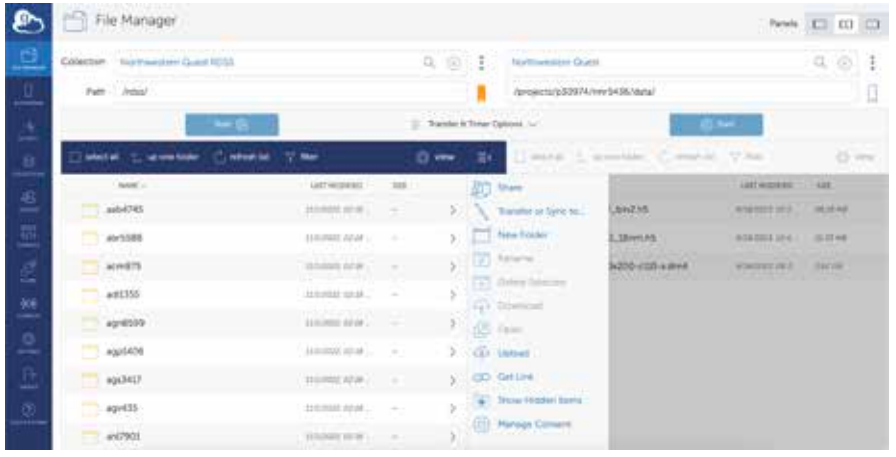

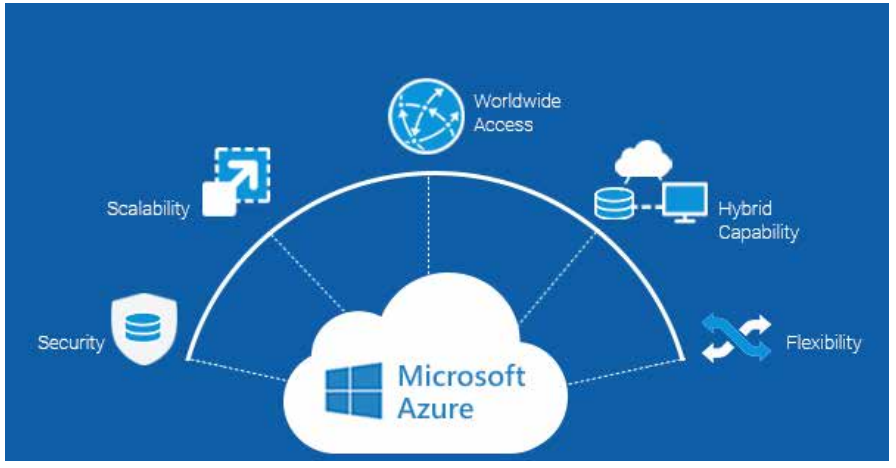

Dos Reis, Roberto; Abbott, Tirzah; Jia, Ying, SHyNE Resources, Northwestern University.

This work is supported by NSF Award # NNCI ECCS-2025633.

National Research Priority: NSF - Harnessing the Data Revolution

Southeastern Nanotechnology Infrastructure Corridor (SENIC)

National Nanotechnology Coordinated Infrastructure

Deposition of ultrathin HfO_2 dielectrics on epigraphene

Goal: integrate ultrathin Hafnium Dioxide (HfO_2) dielectrics onto graphene devices grown on atomically flat silicon carbide surfaces.

Methods: 2.2nm of thermal ALD on the Cambridge Nanotech followed by 3.2nm plasma assisted ALD on the same machine are grown on the PTCDA (organic molecule) seeded graphene surface (epigraphene lab).

Results: The thermal ALD layers protect the graphene from the plasma, while using the plasma ALD reduced gate leakage by about 100x 1600μm^2 devices.

•The resulting devices have an acceptable leakage current of less than 200μA/cm^2 at 0.5V and allow a total swing in charge density of over 10^{13} electrons/cm^2.

•In addition, a resist-free technique using nickel stencil masks was developed to define structures in graphene without exposing the surface to resist residues.

•Finally, the graphene growth process was optimized to produce atomically flat terraces more than a millimeter in length and hundreds of microns wide.

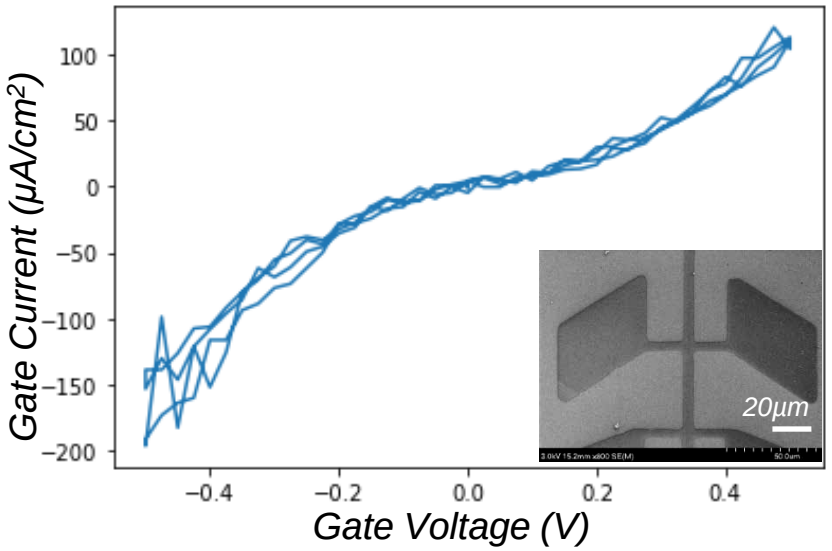

Graph of gate leakage current vs gate voltage for a 5.7-6nm thick HfO_2/PTCDA dielectric on graphene. Inset SEM image of graphene device fabricated with resist-free processing, and smooth 7μm features. Dark gray is the graphene structure, light gray is silicon carbide.

William Griffin, Amira Bencherif, Noel Dudeck, Bladen Le Clus, Peter Mcgoron, Walt de Heer, and Claire Berger, School of Physics, Georgia Institute of Technology. Work performed at Georgia Tech's Institute for Matter and Systems (SENIC).

This work was partially supported by a Georgia Tech Institute for Matter and Systems Facility Seed Grant.

National Research Priority: DoD – Advanced Materials

National Nanotechnology Coordinated Infrastructure

SENIC Southeastern Nanotechnology Infrastructure Corridor

Deposition of $P6_3cm$ $ScFeO_3$ for Ferroelectric Photovoltaic Measurements

The goal of this research project is to develop synthesis methods for narrow band gap materials with polar crystal structures to enable next-generation photovoltaic technologies. Many established materials with polar crystal structures have wide band gaps (>3 eV), limiting light absorption and thus efficiency. We are depositing thin films (<50 nm) of $ScFeO_3$, targeting the polar hexagonal phase, which has a predicted narrow band gap, using pulsed laser deposition on Al_2O_3. This phase is not the ground-state phase but using pulsed laser deposition at 900 °C we were able to stabilize the phase. We have measured the optical band gap to be ~1.4 eV, which is approximately the band gap for theoretical maximum energy conversion efficiency in solar cells. Using scanning transmission electron microscopy (STEM) tools available in the Materials Characterization Facility at Georgia Tech, we found that an iron-oxide interlayer stabilizes the polar phase of $ScFeO_3$, shown in the figure. This discovery enabled the growth of hexagonal $ScFeO_3$ on conductive substrates by intentionally depositing an iron interlayer, enabling electrical and photovoltaic measurements. This work also unveils a mechanism to grow similar materials that aren't the ground state.

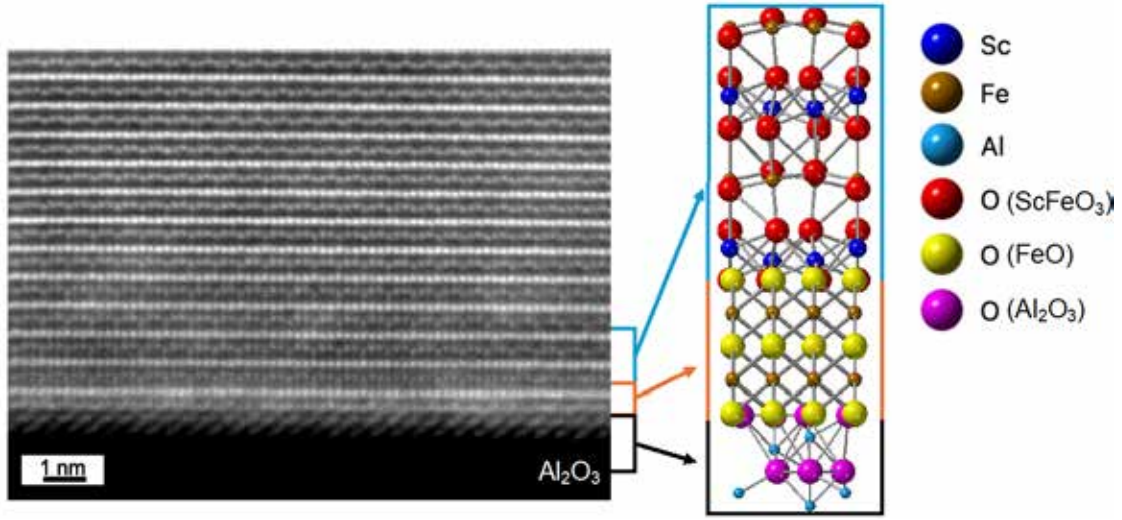

STEM micrograph of a $ScFeO_3$ sample grown on Al_2O_3 and a schematic of the crystal structure at the interface.

Marshall Frye and Lauren Garten, School of Materials Science and Engineering, Georgia Institute of Technology. Work performed at Georgia Tech's Institute for Matter and Systems (SENIC).

This work was partially supported by a Georgia Tech Institute for Matter and Systems Facility Seed Grant. Frye, M.B.; Chin, J.; Barone, M.; Zeltmann, S.; Garten, L.M, *Scr. Mater.* 2025.

National Research Priority: NAE Grand Challenge – Make Solar Energy Economical

Measurement of Mechanical Strength of Feather Barbules Using Nanoindentation

To understand the mechanical and structural properties of sandgrouse ventral feather barbules, we utilized a nanoindentation technique at the IMS facility to measure the reduced elastic modulus of cross-sections of barbules. We first immobilized clean feathers within epoxy resin, then cut the hardened epoxy using a wet saw into the cross-sectional view of barbules. The cut epoxy surface was sanded four times using an automatic wet polisher from 100-micron scale to the 100-nanometer scale. The smooth cross-sections of barbules were indented by a cantilever tip of the triboindenter. Acquired force – displacement curves were transformed to yield the elastic modulus (E) value of barbules. Through this technique, we have for the first time the E values of both helical (E=3.6 GPa) and straight (E=3.4 GPa) barbules. It also demonstrates that the sandgrouse barbules have the similar E value compared to previous feather dataset, E ~ 4GPa. This reveals a picture of barbules as strong materials composed of stacked keratinous nano-filaments.

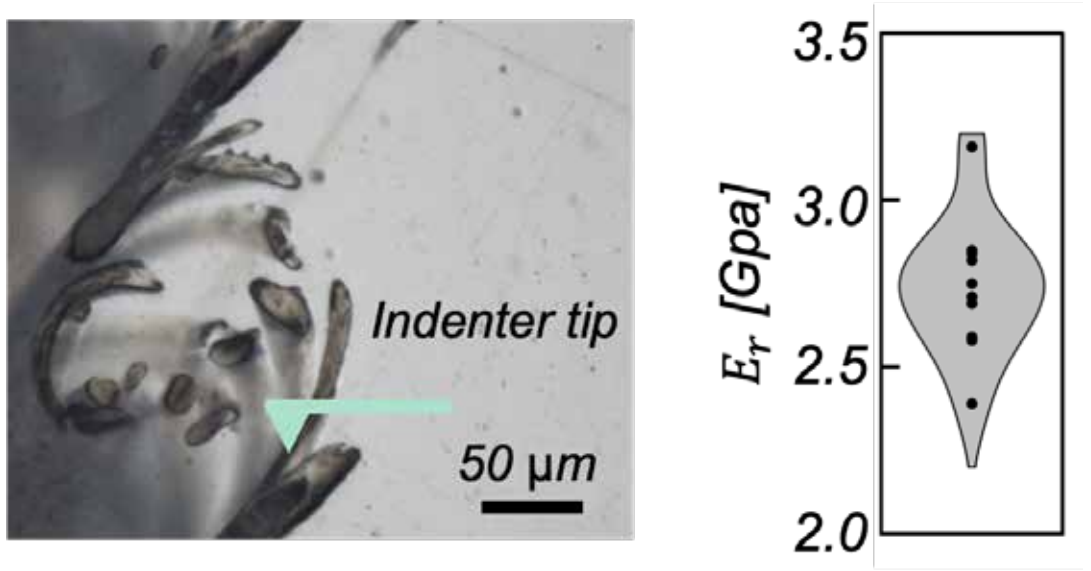

Characterization of barbules to understand the hydration-driven coiling/uncoiling principle

Nami Ha and Saad Bhamla, Department of Chemical and Biomolecular Engineering, Georgia Institute of Technology. Work performed at Georgia Tech's Institute for Matter and Systems (IMS).

This work was partially supported by a Georgia Tech Institute for Matter and Systems Facility Seed Grant.

National Research Priority: NSF – Growing Convergence Research

Effective Electrophysical Antimicrobial Surfaces Based on Electric Field Treatment Induced by Interdigitated Electrodes

This work targets an interdigitated electrodes (IDEs)-induced electroporation-based antimicrobial surfaces, exhibiting excellent antibiofilm efficiency. Intensive electric field is produced among the IDEs surfaces and then electroporation is induced to inactivate bacteria and inhibit biofilms. The role of electric field is confirmed by the consistence of distribution and intensity of electric field simulated with COMSOL and microbial inactivation. The microbial inactivation is observed and quantified with microscopes and fluorescent dye. The inactivation efficiency increases from 15.58% ± 1.35 to 96.45% ± 9.26 when increasing voltage from 20 V to 30 V at 5 μm gap/width and 200 μm length IDEs surface. It shows excellent antibiofilm efficiency after enlarging the effective antimicrobial areas, with the biomass is 18.67 times larger in glass and electrode pads areas compared to IDEs areas. This study pave an electrophysical approach to control biofilms which can be applied to integrate with other platforms.

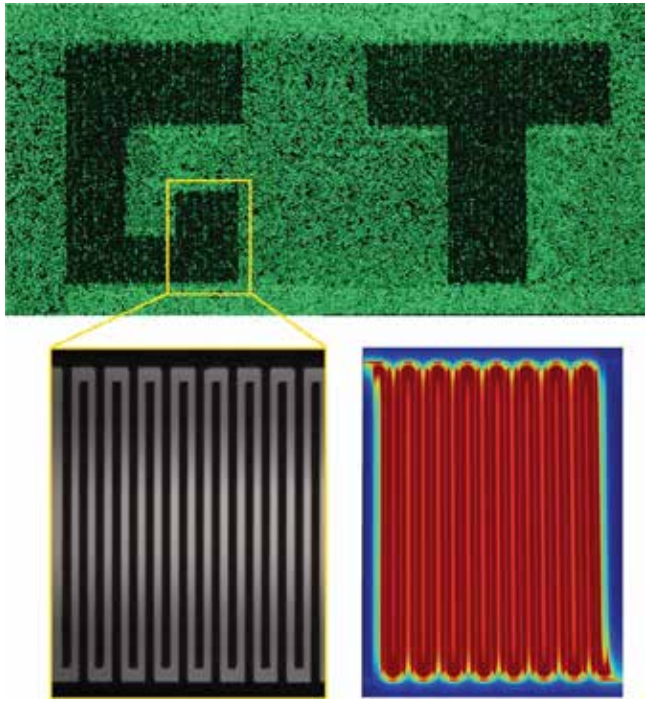

Top microscopy images represent the antibiofilm efficiency of IDEs-surface. Bottom left microscope image show the structure of IDEs while bottom right indicate the electric field distribution among electrodes.

Feifei Liu, Durga GaJula, Xing Xie; School of Civil and Environmental Engineering, Georgia Institute of Technology. Work performed at Georgia Tech's Institute of Electronics and Nanotechnology.

This work was partially supported by a Georgia Tech Institute for Matter and Systems Facility Seed Grant.

National Research Priority: NSF – Growing Convergence Research and NAE Grand Challenge - Provide Access to Clean Water

Empowering Mass Spec through Rapid Sample Prep using Anodic Aluminum Oxide filtration

This technology exploits the tunable, uniform pore structure of anodic aluminum oxide thin films to facilitate sample preparation for mass spectrometry (MS). By integrating the film with channels, and with wafer-to-wafer-bonding, both sides of the filter are accessible to the system. This allows pressure matching to efficiently and effectively maximize sample filtration with a buffer solution. A target market is native mass spectrometry (nMS) - which retains biologically relevant protein structure and non-covalent interactions for analysis. For nMS, samples are often introduced to the MS via nano-electrospray ionization (nano-ESI), which enhances data quality through improved ionization efficiency, higher signal-to-noise ratios, and better salt tolerance. Due to the complexity of sample prep and low sample throughput, nMS applications in today's market are limited. The system built around this filtration technology overcomes these limitations, bringing sample prep to an operator level.

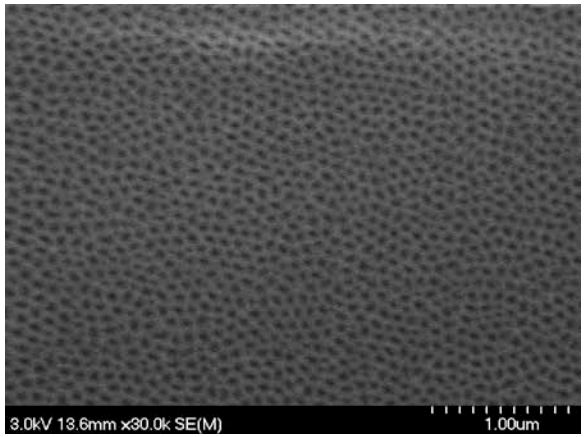

SEM of surface of AAO filter that will be integrated with channels into a bonded Si system

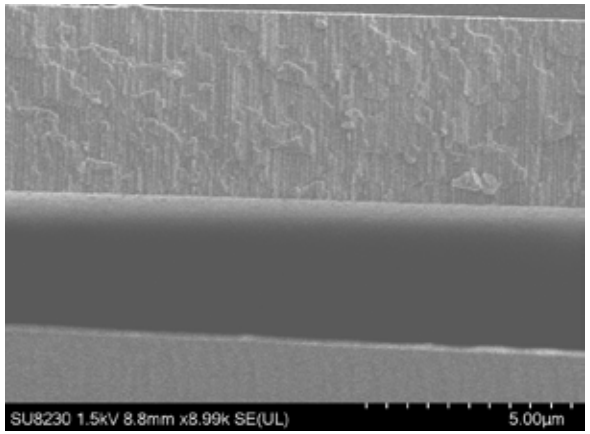

Cross section of AAO filter suspended over an open channel

Suzanne Bock, Andson Biotech. Work performed at Georgia Tech's Institute for Matter and Systems (SENIC).

National Research Priority: NAE Grand Challenge - Engineer the Tools of Scientific Discovery

Heterogeneous Integration Enabled by3D Stitch-Chips

To address the limitations of existing interconnection methods, this paper proposes a three-dimensional (3D) stitch-chip technology for chip-to-chip and chip-to-package interconnections over varying transition lengths and heights. Building on architectures like flip-chip interconnects and foil-based stitch-chips, this approach features low-loss, impedance-matched waveguides for customizable integration of commercial off-the-shelf (COTS) components such as MMICs. By incorporating through-silicon vias (TSVs), the 3D stitch-chip enables vertical signal transitions, accommodates vertical step heights without die-embedding cavities, and allows face-up mounting with minimal detuning. This design achieves high electrical performance, simplifies assembly, enhances thermal dissipation via direct die-to-package contact, and eliminates the need for solder bumps, offering improved efficiency for RF applications. Its modular design and flexible pitch adaptation also make it suitable for complex multi-chip modules (MCMs), establishing a versatile solution for advanced electronic packaging.

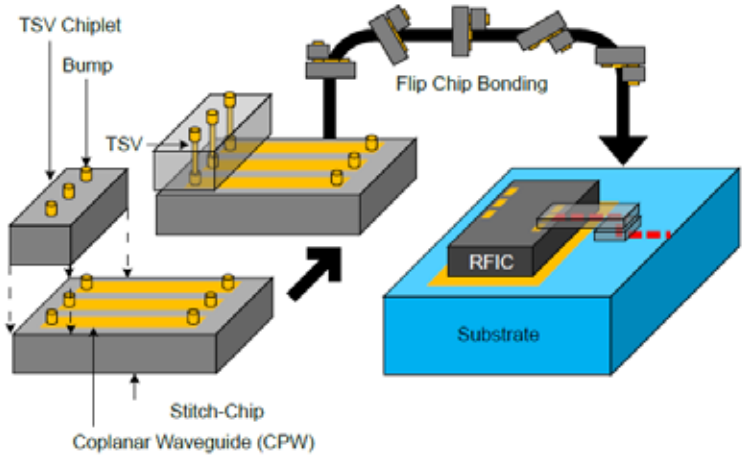

The constituent components of the 3D stitch-chip and its assembly.
The 3DSC is a versatile interconnection technology for the various functions, materials, and form factors of the chiplet being integrated.

Shane Oh, Zhonghao Zhang, Geyu Yan, Paul K. Jo, and Muhannad S. Bakir, School of Electrical and Computer Engineering, Georgia Institute of Technology. Work performed at Georgia Tech's Institute for Matter and Systems.

IEEE Transactions on Components, Packaging and Manufacturing Technology. pp 1-1. 10.1109/TCPMT.2024.3507552.

National Research Priority: DoD – Microelectronics

Superior Asymmetric Visibility Using Obscurants Formed by Reconfigurable Metasurfaces

This study presents an innovative approach to significantly enhancing asymmetric visibility using reconfigurable metasurfaces, designed to outperform traditional nanosphere-based scattering and absorption methods. By integrating phase-change materials such as VO_2 into the metasurface design, we enable dynamic, real-time control over optical properties, leading to superior asymmetric light management. Our metasurfaces allow for adjustable scattering and absorption profiles, achieving lower transmission rates and improved detection performance. Additionally, we incorporate an antenna directly fabricated beneath the metasurface layer, further enhancing the structure's reconfiguration capabilities. This work offers a more efficient and adaptable solution for advanced optical applications by optimizing light manipulation and reducing total transmission.

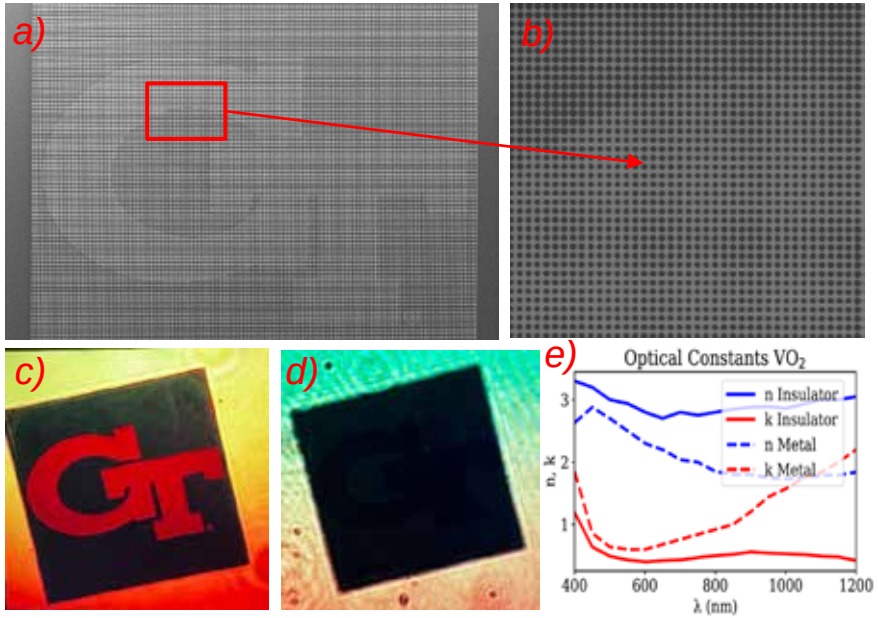

SEM Image of the fabricated device on VO_2 (a,b), Captured image of Dynamic Transformation of Georgia Tech Log in Insulator (c) and Metallic (d) Phase of VO_2 showcasing the meta surface's capability to modulate its properties based on the state of VO_2. oscillations. Wavelength dispersions of refractive index and extinction coefficient of VO_2 in both phases.

Hamed Abiri, Reza Marzban, Oliver Pierson, Amin Khavasi, Ashkan Zandi, Brent Wagner, Ali Adibi, School of Electrical and Computer Engineering, Georgia Institute of Technology. Work performed at Georgia Tech's Institute for Matter and Systems.

This work was supported by Coded Visibility (CV), a DARPA program. A.Khavasi, et al. 2024 *Photonic and Phononic Properties of Engineered Nanostructures XIV.*

National Research Priority: DoD – Advanced Materials

Gate Stack Engineering to achieve QLC compatible Memory Window for FE-NAND applications

In this work, we investigate Hafnium Zirconium Oxide (HZO)-based ferroelectric gate stacks for FE-NAND applications. To achieve a QLC-compatible memory window (MW > 7.5 V) for NAND storage, we inserted various dielectric materials, such as SiO_2, HfO_2, Si_3N_4, and Al_2O_3, into the gate stack. The dielectric materials and their positions within the gate stack were systematically varied while maintaining a constant overall thickness of 18nm to understand their impact on memory window performance. Our findings reveal that inserting Al_2O_3 between the HZO layers and SiO_2 between the top HZO layer and the metal electrode significantly enhances MW performance. Furthermore, combining the middle Al_2O_3 layer and the top SiO_2 layer to create a hybrid gate stack achieves a memory window as high as 11 V.

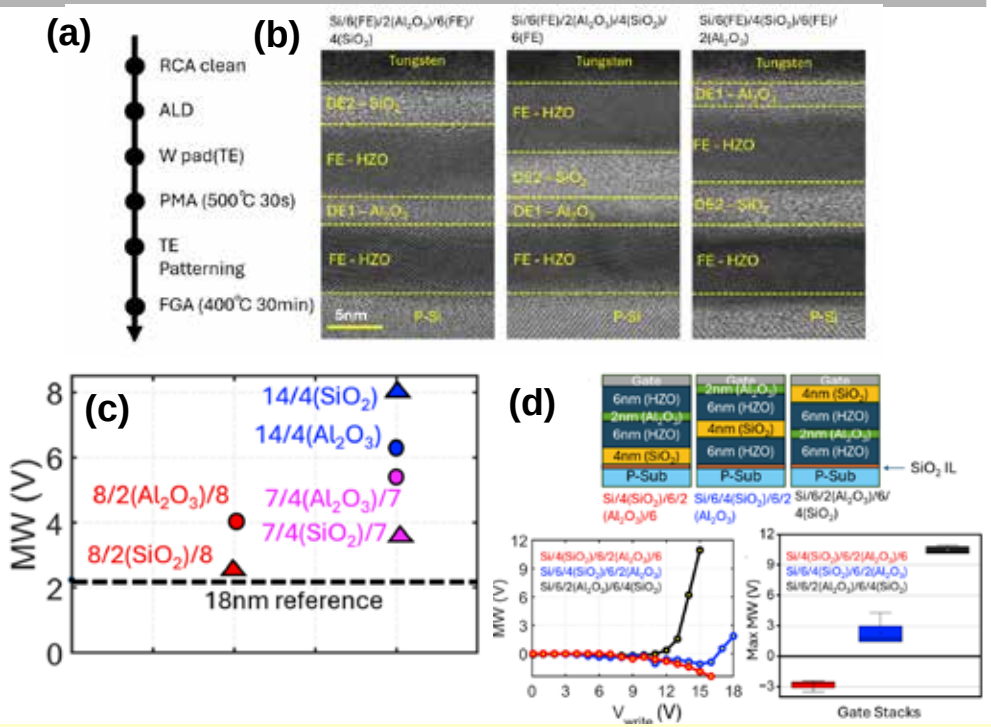

(a) Fabrication Process flow (b) TEM image of the Hybrid gate stacks (c) MW for stacks with Al_2O_3 and SiO_2 inserted at different positions
(d) MW for hybrid stacks with both *Al_2O_3 and SiO_2* enabling a 11V MW

Lance Fernandes, Asif Khan, School of Electrical and Computer Engineering, Georgia Institute of Technology. Work performed at Georgia Tech's Institute for Matter and Systems.

This work was supported by Samsung Electronics and SUPREME, a SRC/DARPA JUMP 2.0 center. L Fernandes, et al. 2024 *IEEE Electron Device Letters* (doi: 10.1109/LED.2024.3437239). L. Fernandes, et al., 2024 *IEEE Transaction on Electron Devices* (doi: 10.1109/TED.2024.3504475)

National Research Priority: DoD – Microelectronics

Exploring the "Carpenter" as a substrate for green synthesis: Biosynthesis and antimicrobial potential

The frequent use of antibiotics has created favorable conditions for bacteria to develop resistance. The use of nanoparticles (NPs) including Silver as alternatives to conventional antibiotics may have the potential to combat bacterial resistance. Conventionally, silver nanoparticles have been synthesized through physical, chemical, and biological processes. However, the biosynthesis of Ag NPs from the wings of carpenter bees (Xylocopa virginica), abundantly available in summer, is yet to be explored. We report the synthesis of Ag NPs using wing extracts from X. virginica. We investigated the antimicrobial activity of the biosynthesized Ag NPs against two common Gram-negative and Gram-positive pathogenic bacteria. Biosynthesized Ag NPs exhibited antimicrobial activity against all tested bacteria, signifying their potential in biomedical, pharmaceutical, and agricultural applications.

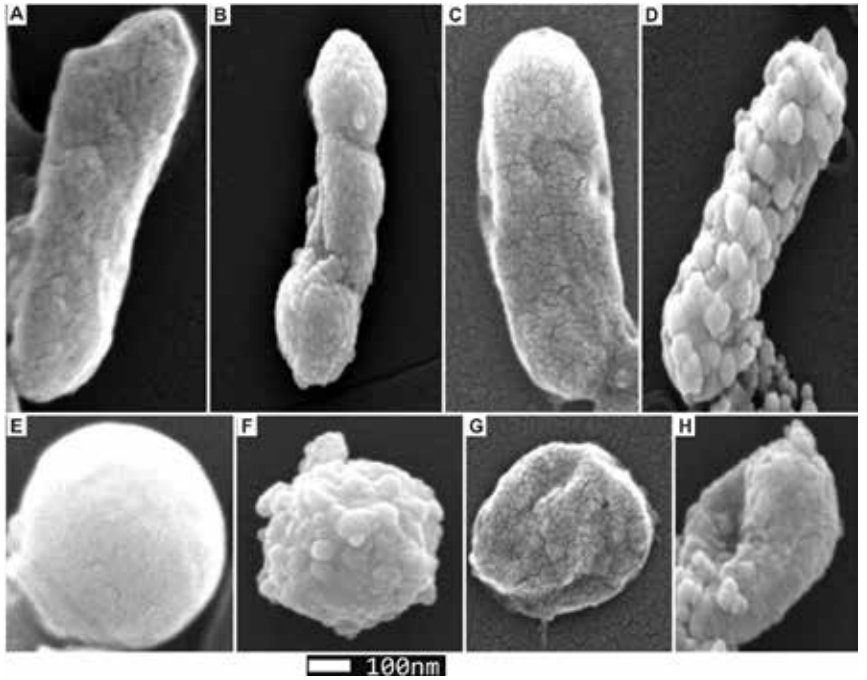

SEM bacterial cells in treated and control groups after incubation with Xylocopa virginica-derived biosynthesized Ag NPs at 24 h. (A), (C), (E), (G) different bacteria Controlc and (B), (D) , (F) and (G) after treatment with Ag NPs.

Akamu Ewunkem and Zahirah Williams, Faculty of Natural and Physical Sciences, Winston Salem State University. Part of the work performed at Joint School of Nanoscience and Nanoengineering.

A. J. Ewunkem, Z. J. Williams, N. S. Niore S. Johnson, J. L. Brittany, A. Maselugbo, K. Nowlin, (2023), *Gene & Protein in Disease*, 2(4), 2155.

National Research Priority: Environmental Sustainability

3D-Printed Mechanical Metamaterial for Fluidic Control in Vertically Stacked Valve Array

Microfluidic systems are often limited to planar structures, thereby presenting challenges in the control of fluids within 3D structures. This work addresses control of fluids within 3D structures by incorporating mechanical metamaterials that exhibit spatially adjustable mechanical properties. A systematic computational and experimental characterization of a modified re-entrant honeycomb structure was performed to generate a modular metamaterial for an active device that allowed for direct regulation of flow through integrated, multiplexed fluidic channels “one-at-a-time,” in a manner that is highly scalable. It is expected that mechanical metamaterials in 3D fluidic systems will enable new biotechnological and biomedical applications for 3D printed devices.

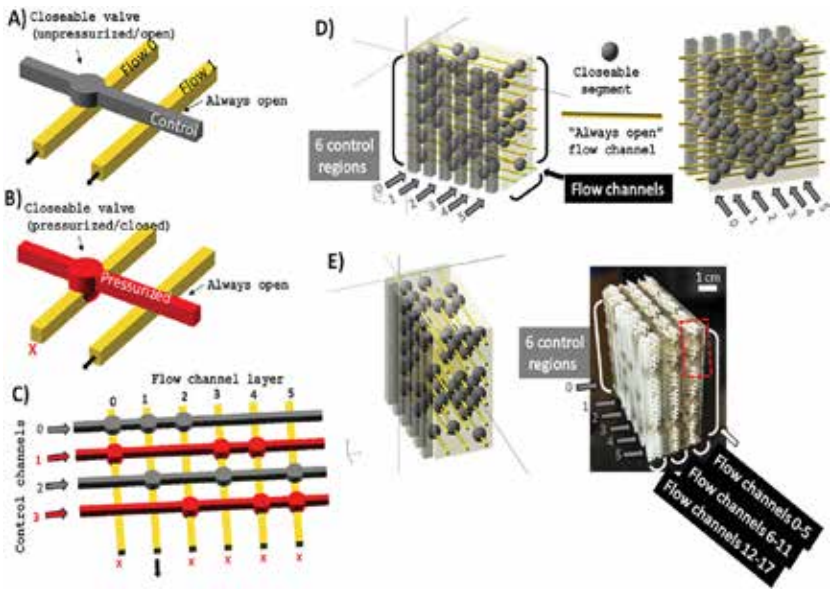

A 3D-printed, vertically stacked valve array for fluidic control. E) Schematic and 3D printed valve array manifold, engineered using a mechanical metamaterial design.

Jeff Alston and Eric Josephs, Departments of Nanoscience and Nanoengineering, North Carolina A&T State University and UNCG. Work performed at Joint School of Nanoscience and Nanotechnology.

This work was supported by NIH #1R35GM133483 and NSF #32027738. Supakar, T….. Josephs, E. A. (2024), *Advanced Functional Materials*, 2315419.

National Research Priority: NSF - Growing Convergence Research

Photocatalytic Hydrogen Evolution Using Mesoporous Honeycomb Iron Titanate

In this work, mesoporous honeycomb iron titanate using a sol-gel, evaporation-induced self-assembly method is synthesized. A triblock copolymer, F127, serves as a structure-directing agents, with iron chloride and titanium (IV) isopropoxide as inorganic precursors. The study of physicochemical properties using different techniques reveals the formation of microstructures with a remarkable degree of porosity. The amorphous iron titanate outperforms the photochemical generation of H2 due to its disorderly structural arrangement and incomplete crystal formation. The high amount of hydrogen gas, 40.66 mmolg−1h−1, is observed in the investigation over 3 h of activity for the iron titanate honeycomb sample. The iron titanate materials synthesized with low-cost materials and methods are very effective and have the potential for hydrogen generation.

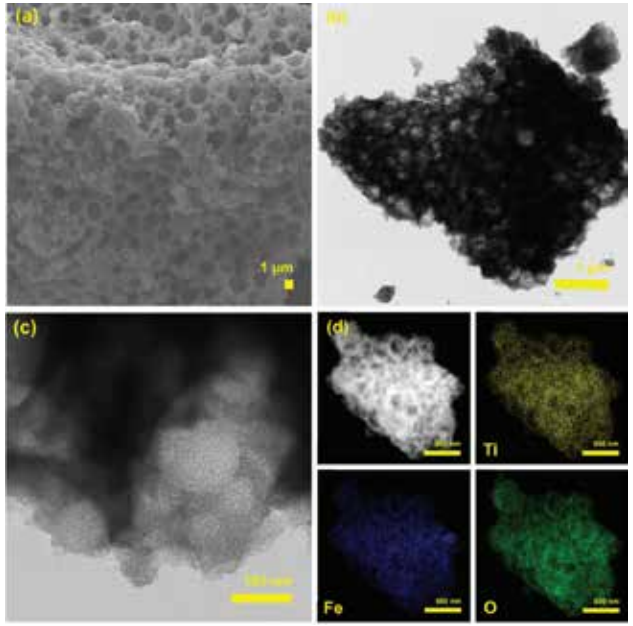

a) SEM image b,c) TEM images, and d) High-angle annular dark-field scanning transmission electron microscopy images with EDS analysis mapping of calcined iron titanate

M. D. Ashie, B. P. Bastakoti, Department of Chemistry, NC A&T. Work performed in part at Joint School of Nanoscience and Nanoengineering

This work was supported by NSF RIA-2000310, DMR-2122067, and DOE DE-SC0023415. Ashie, M. D., & Bastakoti, B. P. (2024), *Small*, 2310927.

National Research Priority: DOE Energy Earthshots – Hydrogen Shot

Compartmentalized CRISPR for High-Throughput Screening of Guide RNA Potency and Specificity

CRISPR ribonucleoproteins (RNPs) use a variable segment in their guide RNA (gRNA) called a spacer to determine the DNA sequence at which the effector protein will exhibit nuclease activity and generate target-specific genetic mutations. However, nuclease activity with different gRNAs can vary considerably in a spacer sequence-dependent manner that can be difficult to predict. Here, the study presents compartmentalized CRISPR reactions (CCR) for screening large numbers of spacer/target/off-target combinations simultaneously in vitro for both CRISPR effector activity and specificity. Results shows that CCR can be used to screen hundreds of thousands of extended gRNA variants that can completely block cleavage at off-target sequences while maintaining high levels of on-target activity.

Tinku Supakar, Ashley Herring-Nicholas, and Eric Josephs, Nanoscience, UNCG. Work performed at Joint School of Nanoscience and Nanoengineering

This work was supported by NIH NIBIB R21EB033595, NSF #202773 and DoD #W911QY2220006. Supakar, T., Herring-Nicholas, A., & Josephs, E. A. (2024), *Small*, 2403496.

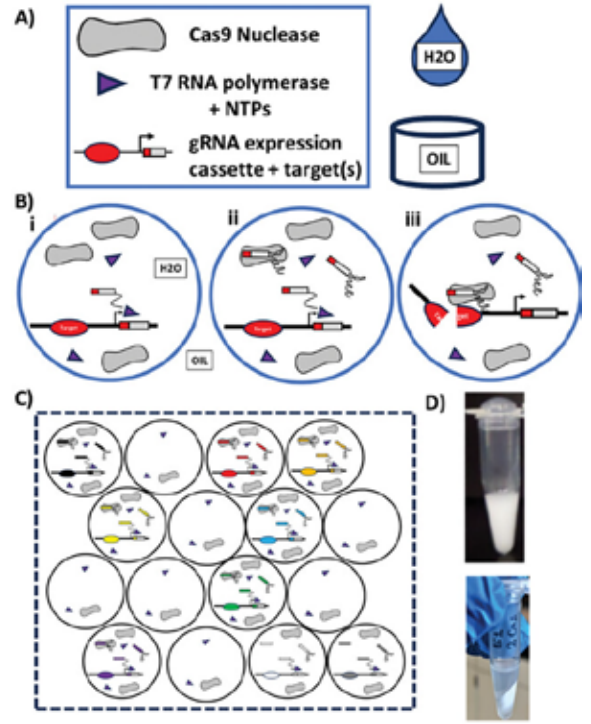

A) Compartmentalized CRISPR Reactions are performed in water-in-oil emulsions, B) Within each emulsion, unique gRNAs can be i) transcribed and ii) assembled into RNPs, then iii) either demonstrate or fail to demonstrate cleavage. C) library of DNA molecules with different gRNA/target/off-target. D) water-in-oil emulsions in a microcentrifuge tube

National Research Priority: NSF – Understanding the Rules of Life

Texas Nanofabrication Facility (TNF)

National Nanotechnology Coordinated Infrastructure

NSF

Quantum Conductance in Vertical HBN Memristors with Graphene-Edge Contacts

Two-dimensional materials (2DMs) have gained significant interest for resistive-switching memory toward neuro-morphic and in-memory computing (IMC). To achieve atomic-level miniaturization, the researchers introduced vertical hexagonal boron nitride (h-BN) memristors with graphene edge contacts. In addition to enabling three-dimensional (3D) integration (i.e., vertical stacking) for ultimate scalability, the proposed structure delivers ultralow power by isolating single conductive nanofilaments (CNFs) in ultrasmall active areas with negligible leakage thanks to atomically thin (~0.3 nm) graphene edge contacts. Moreover, it facilitates studying fundamental resistive-switching behavior of single CNFs in CVD-grown 2DMs that was previously unattainable with planar devices. They studied their programming characteristics and observed a consistent single quantum step in conductance attributed to unique atomically constrained nanofilament behavior in CVD-grown 2DMs. This resistive-switching property was previously suggested for h-BN memristors and linked to potential improvements in stability (robustness of CNFs). This study shows experimental evidence of this, including superior retention of quantized conductance.

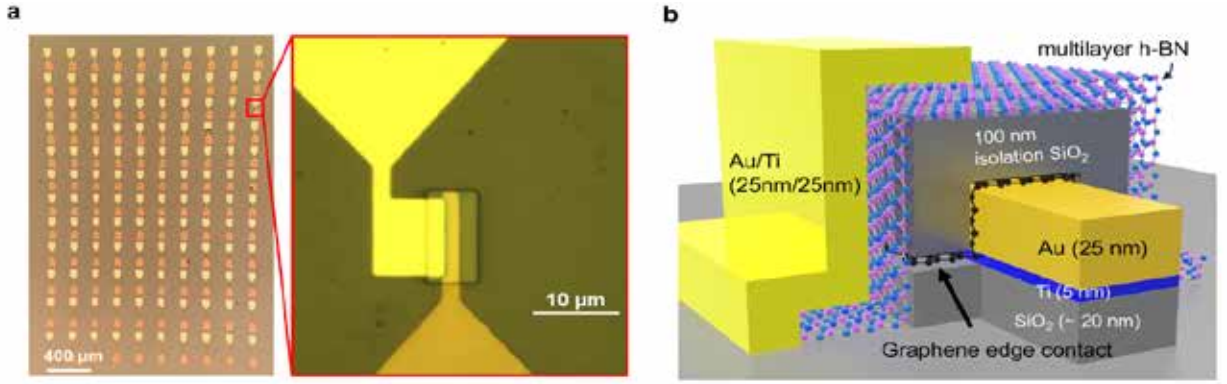

(a) Optical micrograph of a fully fabricated device array with different active widths. The insert in the red box shows the single device with active widths equal to 10 µm. (b) Schematic of the vertical h-BN memristor with graphene-edge contact. (c) Annular dark field scanning transmission electron microscopy (ADF-STEM) and (d, e) bright-field (BF)-STEM images at different magnification levels revealing the layered h-BN switching medium as well as the graphene edge contact and surrounding materials (i.e., SiO2 isolation and the Ti/Au top contact).

Prof. Deji Akinwande, Univ. of Texas and Jing Xie, Prof. Ivan Esqueda, Arizona State University. Work performed at TNF.

Funded by NSF and Applied Materials. *Nano. Lett.* (2024).

National Research Priority: NSF - Growing Convergence Research

Radiation Response of Domain-Wall Magnetic Tunnel Junction Logic Devices

Domain-wall magnetic tunnel junctions are a new spintronic device family that may be exploited in resilient edge logic processors or neuromorphic edge accelerators in the future. Here, domain-wall magnetic tunnel junction logic devices were exposed to large total ionizing doses, heavy ion displacement damage, or both. The parts demonstrated complete resilience to the ionizing radiation, but ion-irradiated parts followed a similar degradation curve to previously tested tunnel junction parts in response to heavy ion irradiation. Microscopy and spectroscopy methods confirm significant damage in some devices.

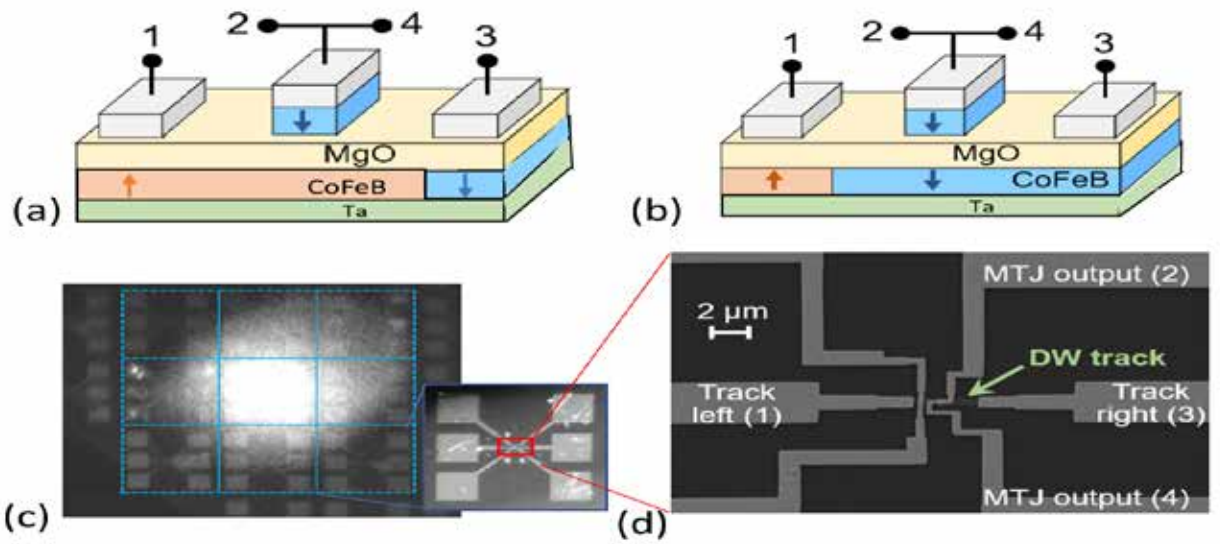

(a) Schematic of a SOT DW-MTJ device that is in the anti-parallel configuration (Bit: 0), where the up (+z)orientation of the domain wall in the free layer has propagated past the junction; (b) similar schematic of a DW-MJT in the parallel configuration (Bit: 1), where the domain wall has not propagated past the junction (–z orientation under the tunnel junction) (c) View of chiplet while in the QASPR-III chamber , and sub-view of a single bare device , both via optical microscopy; (d) SEM image of parts with pads and active device noted.

C. Bennett, (Sandia), Incorvia group (UT Austin). Work performed at TNF.

Funded by DOE. *IEEE Trans. Nuclear Science* (2023)

National Research Priority: NSF - Quantum Leap

Power FETs with low subthreshold slope and ON resistance

Previously, we had reported a new class of Si power MOSFET technology (ANDFET) with sub-30um substrate developed by AND partly using the NNCI facilities at UT-Austin. We have further advanced the technology using the UT-Austin NNCI labs to develop a polyimide passivation module, which is compatible with pick and place die level packaging approaches as well wafer level chip scale packages such as ANDPACK. In addition, dicing experiments were carried out to develop a dicing process for thin Si on thick metal foils that eliminates peeling and constrains any chipping to be within the dicing streets (wafer 2)

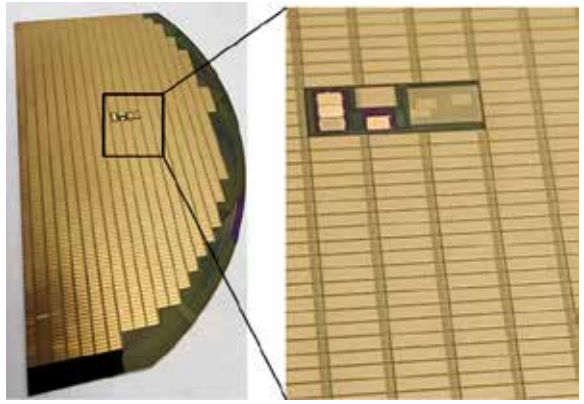

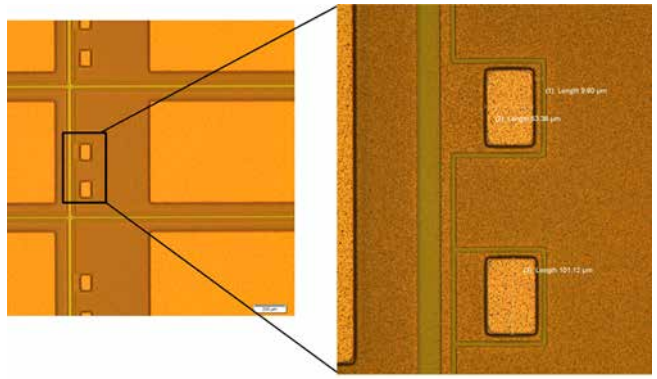

Wafer	Topside (x100) Good area	Topside (x100) Bad area	Sidewall (x100)	Sidewall (x300)
1	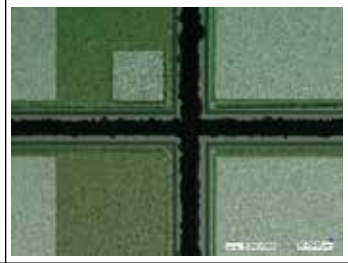	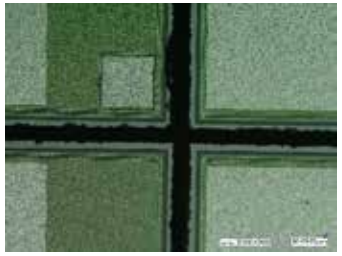		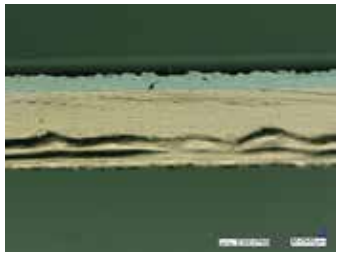
2	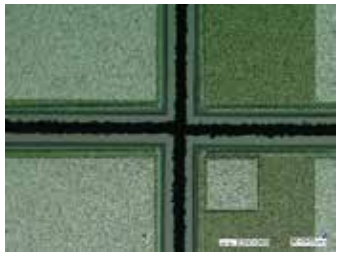	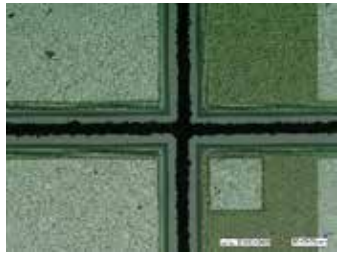	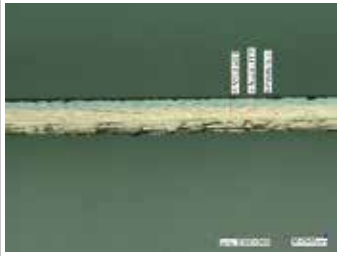	

Leo Mathew, Dr. Rajesh Rao, FET Fabrication

National Research Priority: NSF - Growing Convergence Research

National Nanotechnology Coordinated Infrastructure

TNF TEXAS

Optically Functional Nanopatterns

With the help of the UT-MRC fabrication facility we are able to prototype, test and optimize nanopatterns for waveguides and other optical components such as Anti-Reflective structures into Master Templates which once replicated through Nanoimprint in High Volume (>10,000's) can give >99.9% Tr% at targeted wavelengths with ability to modulate this at different wavelengths. The plot shows how the min. Ref% can be tuned for the desired Tr% response.

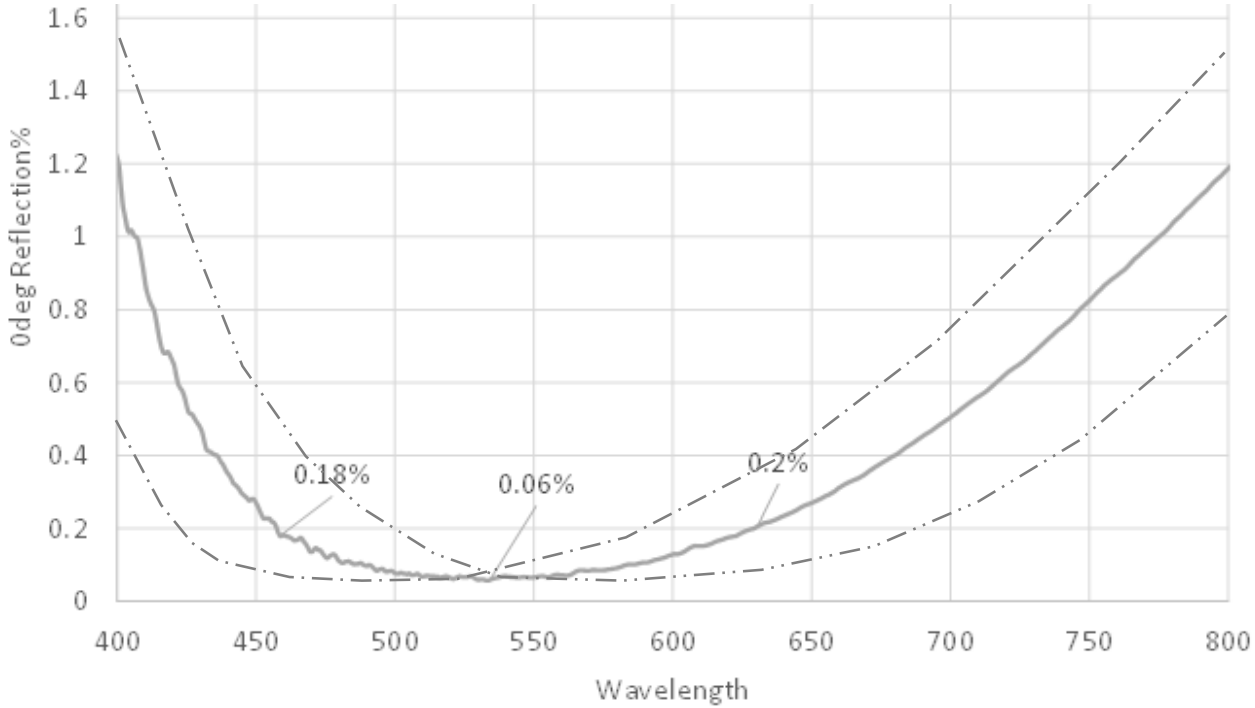

Vik Singh, Shuqiang Yang, Julie Frish, Magic Leap. Test Template Fabrication Performed at UT-MRC.

National Research Priority: NSF - Quantum Leap

Metasurface detection device for food safety

Low-cost optical sensor for rapid screening of foodborne pathogens

- Farm-to-fork screening for food safety using the MetaDot portable, low-cost reader and single-use test chips
- Test is fast, easy, and highly sensitive
- Screens for 36 pathogens simultaneously – all for a low cost
- Test chips will have a high profit margin
  - Like selling ink (instead of just printers)
  - Small, cheap, disposable embossed plastic strip with a metasurface coated with binding agent, such as antibody or aptamer
- Can be extended to other point-of-care (PoC) screening:
  - Infectious disease
  - Water and soil microbes
  - Trauma and ER infection
  - Oral health

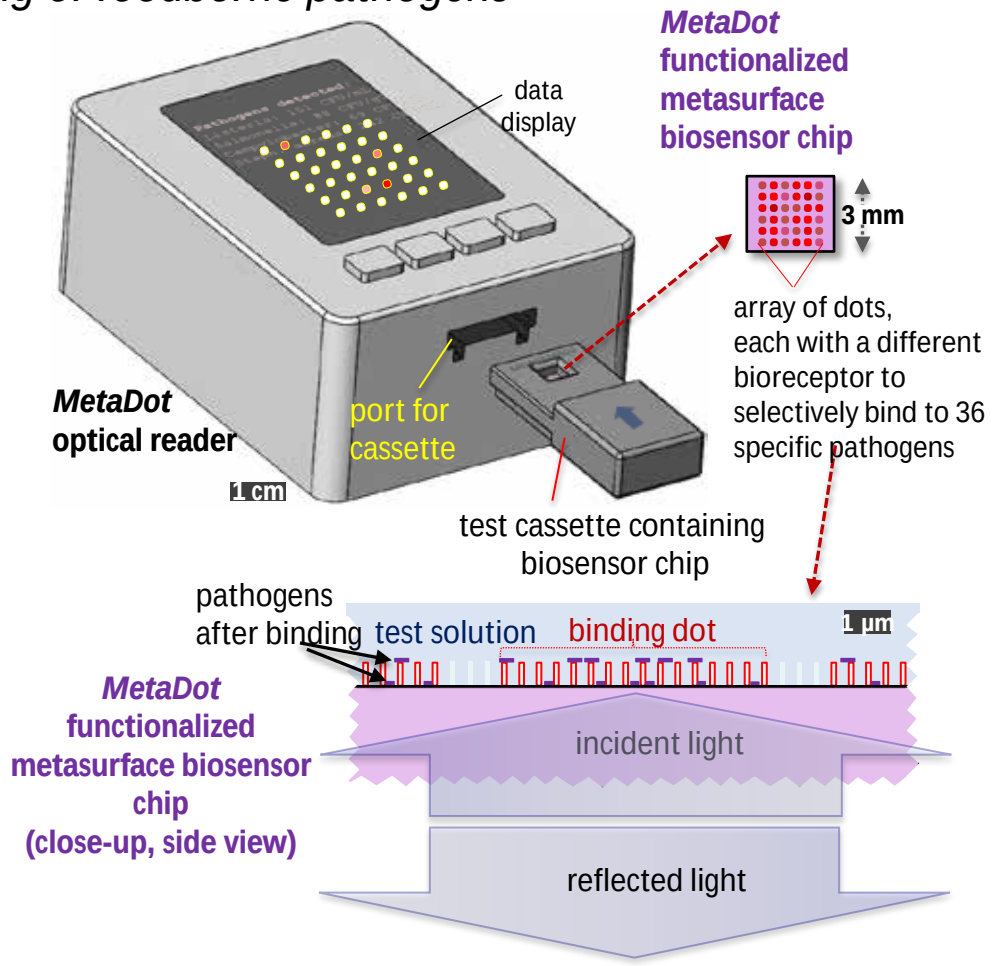

Mark Lucente, Nanohmics. Work performed at Texas Nanofabrication Facility.

This work was supported by FDA/NIH SBIR Phase II, Grant 2R44FD006910-02

NIR/SWIR FPA Sensors Based On Graphene + CMOS

Ultrasensitive NIR/SWIR FPAs based on sensitized graphene

- Compatible with CMOS ROICs: low-cost scale-up
- Low noise, achieving specific detectivity of D* = 10^{11} - 10^{12} cm(√Hz)/W even in uncooled operation
- High internal device gain: ~10^7 or more
- High responsivity, $\mathcal{R}$ ~ 10^5 A/W or more
- Fast response times ~1 ms
- Graphene acts as channel of gFET phototransistor in each pixel: single layer graphene serves as a high-speed carrier transport channel, in direct contact with a layer of sensitizers with strong IR absorption
- Graphene is sensitized by a thin film of one or more absorptive compounds
- Sensitizers, such as nanocrystals (NCs), quantum dots (QDs), or other nanoparticles, are chosen for specific spectral ranges, such as near-infrared (NIR), SWIR, MWIR, LWIR
- Low-SWaP: Ideal for soldier-borne night vision applications as well as vehicle-mounted, UAV, etc.
- Extensible to other IR bands

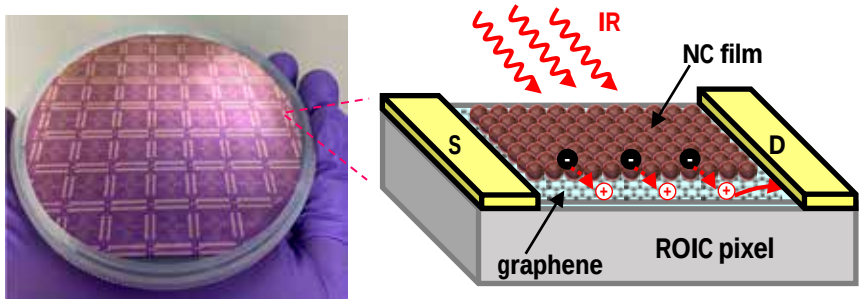

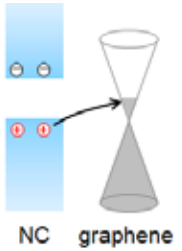

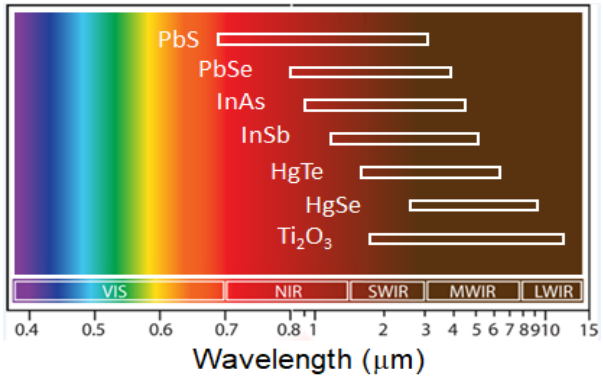

Mark Lucente, Nanohmics. Work performed at Texas Nanofabrication Facility.

This work was supported by Army STTR Phase II, W909MY23C0008.

National Research Priority: NSF - Quantum Leap

Compact Imaging Spectropolarimeter Based On Multifunction Meta-optic

Compact, light-weight instrument for suborbital measurements

- Imaging spectropolarimeter uses a single multifunction meta-optic that analyzes both the spectrum and polarization state of collected light
- Cost-effective orbital and suborbital Earth science data collection such as atmospheric aerosol absorption and scattering
- Low-cost suborbital monitoring for NASA's Earth Science Division (ESD) and Science Mission Directorate (SMD), including for Earth science atmospheric composition monitoring
- Operating bands demonstrated to-date include NIR and SWIR; easily scalable to other spectral bands such as visible, MWIR, LWIR
- Light-weight, low-cost, high-performance optics based on microfabricated metasurfaces, a key component of many imaging, remote sensing, and optical communication subsystems with small size, weight and power consumption (SWaP)
- Team includes Andrea Alù and researchers at CUNY Advanced Science Research Center (ASRC)

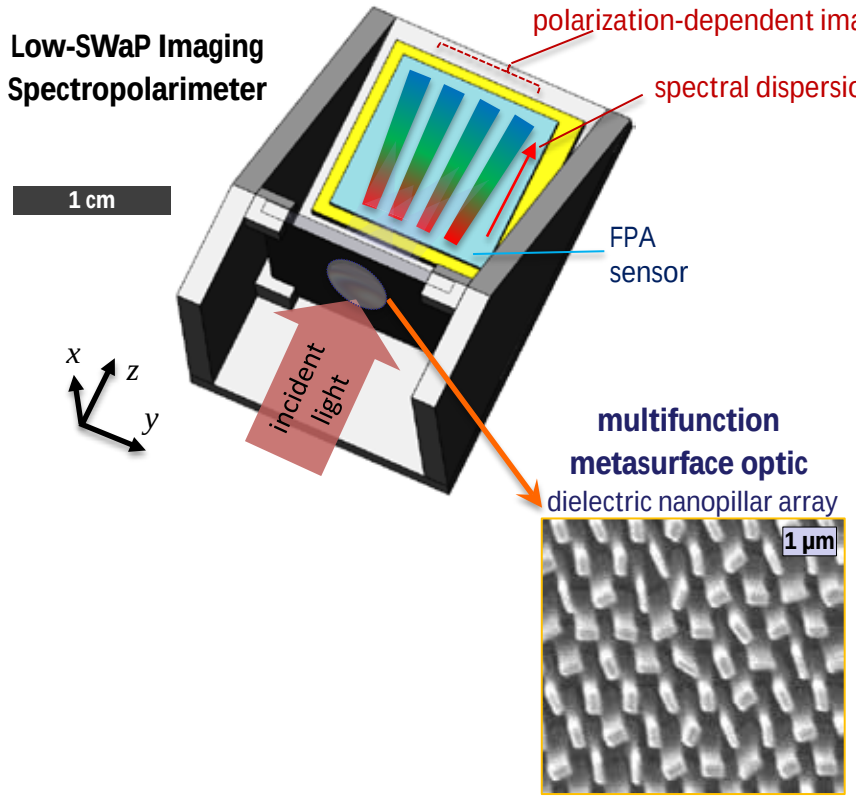

Mark Lucente, Nanohmics. Work performed at Texas Nanofabrication Facility.

This work was supported by NASA SBIR Phase II, 80NSSC21C0302

High Power Vertical Photoconductive Semiconductor Switches

Nanohmics Inc. (Austin, TX) is developing high-power vertical photoconductive switches (PCSS) designed with a microlens array trigger assembly. The devices are designed to be used in low-jitter, ultra-broadband pulsed power systems. The key innovation is achieving filament scaling and efficient optical delivery using the microlens array (MLA), which can simultaneously control the location and density of filaments, and efficiently couple light through tight windows patterned in the semiconductor's anode. Proof-of-concept device fabrication has been done on semi-insulating gallium arsenide (GaAs).. DoD is interested in pulsed power systems for remote detonation of IEDs, immobilization of vehicles, directed energy weapons, linear accelerators, and ultrawideband sources.

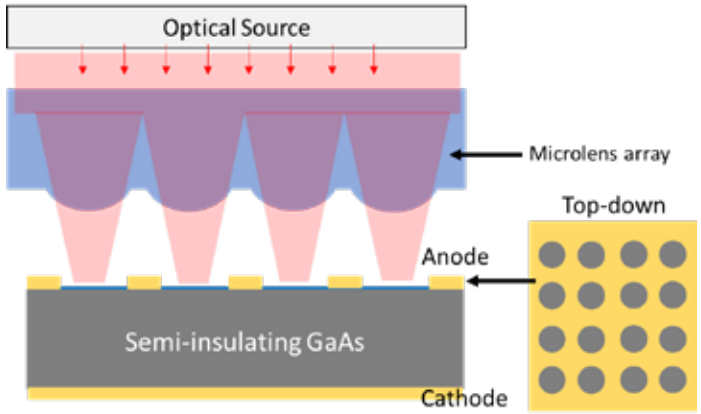

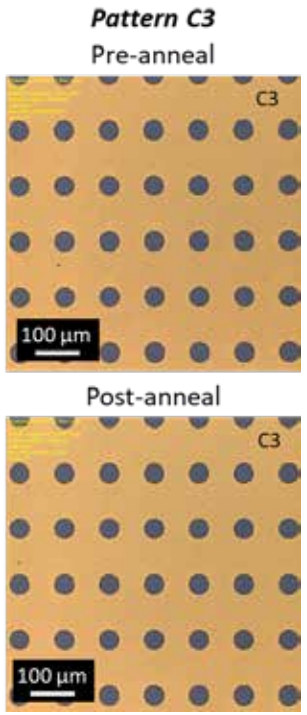

PI: Dr. Karun Vijayraghavan, Nanohmics Inc. Part of this work was performed at the Texas Nanofabrication Facility.

This work was supported by a DMEA SBIR Phase I grant HQ072723P0026

National Research Priority: NSF - Quantum Leap

On-demand Single-photon Pair Source for Correlated Calibration Application

Correlated-photon metrology using correlated single-photon pairs provide a straightforward means to directly measure detection efficiency of single photon detectors (SPDs) in the photon regime without relying on external standards. To fulfill the need of primary standard, high-efficiency single-photon pair sources with high brightness that can provide correlated calibration for SPDs, Nanohmics, Inc. is developing a laser-pumped on-demand single-photon pair source based on single colloidal semiconductor quantum dot (QD) nanocrystals coupled to a hybrid plasmonic bullseye cavity.

The photon pair generation is based on high biexciton cascade emission quantum yield of single QD nanocrystals. Relative to the laser-pumped spontaneous parametric down-conversion (SPDC), Nanohmics technology has potential advantages of on-demand photon pair generation, low-cost, and low pump power operation. The bullseye cavity fabrication is carried out in The University of Texas at Austin Microelectronics Research Center facilities.

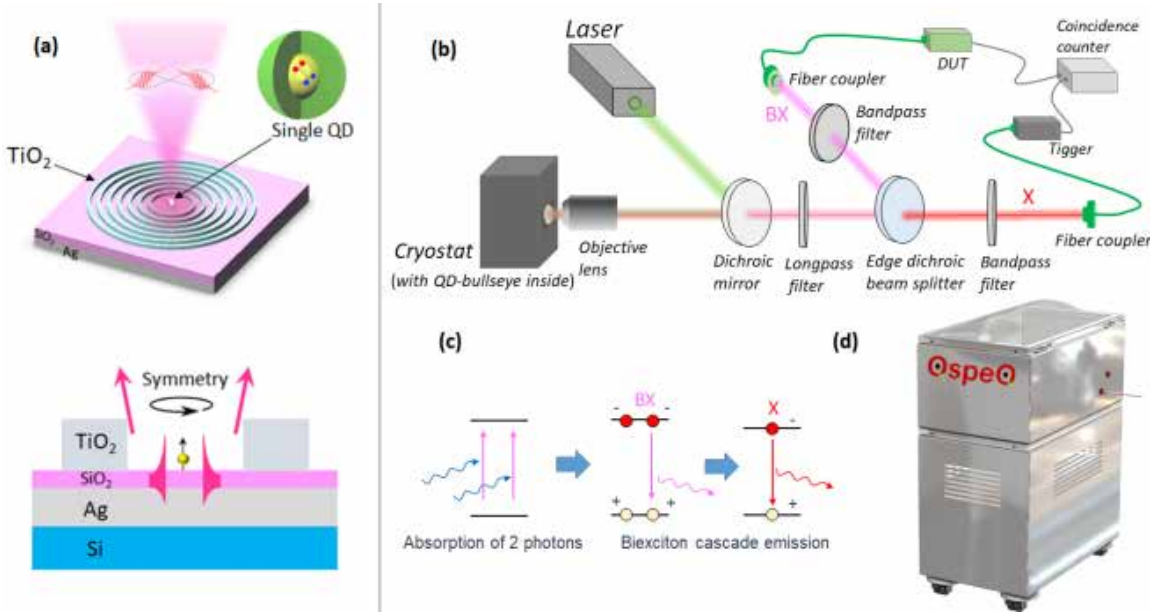

Steve Savory & Zhongjian Hu, Nanohmics. Work performed at Texas Nanofabrication Facility.

This work was supported by NASA Phase II, 80NSSC22CA029.

National Research Priority: NSF - Quantum Leap

Virginia Tech National Center for Earth and Environmental Nanotechnology Infrastructure (NanoEarth)

National Nanotechnology Coordinated Infrastructure

NSF

Wildland-urban interface (WUI) fire ashes as a major source of incidental nanomaterials (INMs)

- Fires generate numerous combustion products
  - Wildland fires tend to consume organic material
  - Urban fires consume a wide variety of substances from building materials to household items to industrial solvents and more
  - The nature of the products of wildland-urban interface (WUI) fires has not been investigated in detail
- Ti, Cu, Fe, Zn, Mn, Pb, and Cr-bearing INMs were detected in WUI fire ash with sizes varying from <50 nm to a few hundred nm in the initial work.
- Further work detected original and transformed Cr, Cu, and As INMs in WUI fire ash and studied their concentrations and compositions.
- The source of Cr, Cu, and As-bearing INMs in WUI fire ashes is treated wood.

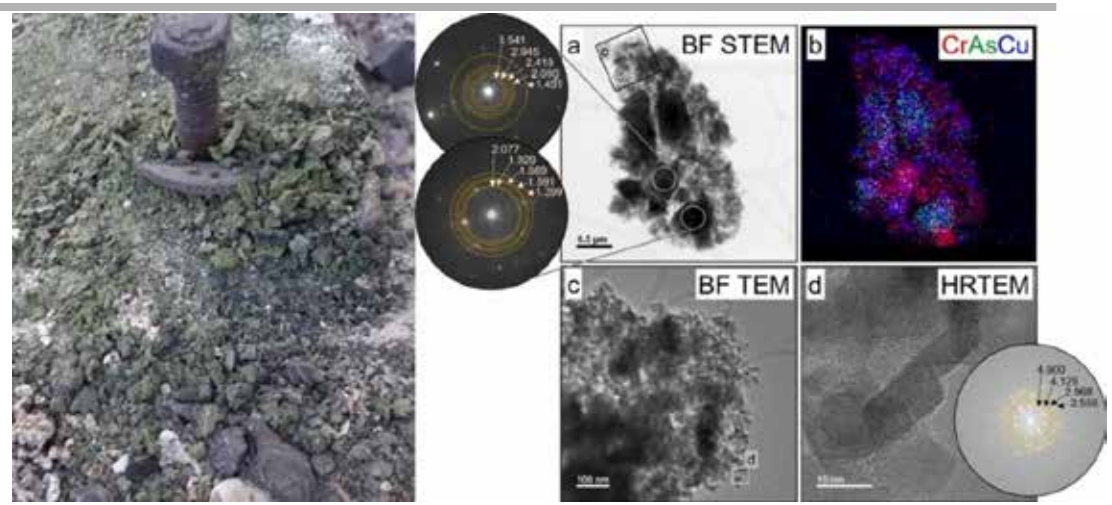

(left) Wildland-urban interface fire ashes. (right) TEM, EDS, and electron diffraction from Cr-, Cu-, and As-bearing nanomaterials in an aggregate from ash A125.

PI Mohammed Baalousha, University of South Carolina.

This work was supported by NSF Awards CBET-2101983, CBET-1828055, & ECCS-2025151 and the U.S. Geological Survey (USGS) Toxic Substances Hydrology Program, Minerals Integrated Science Team, under the Environmental Health Program of the USGS Ecosystem Mission Area. Alam, M., Alshehri, T., Wang, J., Singerling, S. A., Alpers, C. N., & Baalousha, M. (2023), *Journal of Hazardous Materials*, 445, 130608. https://doi.org/10.1016/j.jhazmat.2022.130608; Alshehri, T., Wang, J., Singerling, S. A., Gigault, J., Webster, J. P., Matiasek, S. J., Alpers, C. N., and Baalousha, M. (2023), *Journal of Hazardous Materials*, 443, 130311. https://doi.org/10.1016/j.jhazmat.2022.130311

National Research Priority: EPA Goal 7 – Chemicals Environmental Health and Safety

Estimating lung carcinogenicity of 3D printer emissions

- Use of 3D printing is expanding, but methods to assess the risk of lung carcinogenesis have not been developed. This study demonstrates a methodology for modeling lung cancer risk related to specific exposure levels as derived from an experimental study of 3D printer emissions for various types of filaments (ABS, PLA, and PETG).
- The emissions of 15 filaments were assessed at varying extrusion temperatures for a total of 23 conditions.
- Three approaches were utilized for cancer risk estimation: (a) calculation based on PM2.5 and PM10 concentrations, (b) a proximity assessment based on the pulmonary deposition fraction, and (c) modeling based on the mass weighted aerodynamic diameter of particles.
- The central tendency estimation of lung cancer risk for 3D printer emissions was found at the level of 14.74 cases per 10,000 workers in a typical exposure scenario (average cumulative exposure of 0.3 mg/m3 – years), with the lowest risks for PLA filaments, and the highest for PETG type.

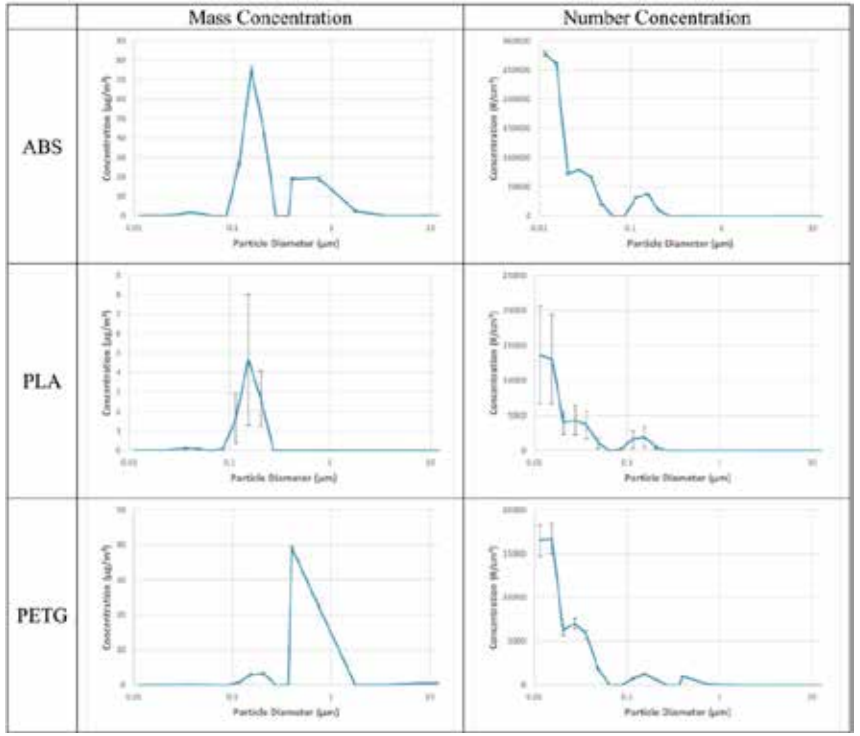

Size distribution characteristics of particulates released from natural ABS, PLA, and PETG filament exhibited similar trends with slight differences in peak particle diameter. Data presented were recorded during the stable emissive period at an extrusion temperature of 240ºC. The increased variability in emissions released from PLA may be related to the relatively high extrusion temperature; manufacturer recommendations typically prescribe printing of PLA at 220ºC or lower, while 240ºC is suggested for ABS and PETG.

PI Andrey Korchevskiy, Chemical & Industrial Hygiene, Inc.

This work was supported by NIH award R44ES030650, the Safe and Rapid Advanced Materials for Resilient Sensors CI Project from the USACE Engineer Research and Development Center Environmental Laboratory under Contract W912HZ21C0061, and the NSF ECCS-2025151.

Korchevskiy, A. A., Hill, W. C., Hull, M., & Korchevskiy, A. (2023), *Journal of Applied Toxicology*, 1-18. https://doi.org/10.1002/jat.4561

National Research Priority: EPA Goal 4 – Air Environmental Health and Safety

Differentiation between humic and non-humic substances using alkaline extraction and ultraviolet spectroscopy

Although humic substances are the principal ingredients in processed humic products, there has been no practical way to determine if a material is humified, allowing fake products to be used by farmers instead of genuine humic substances. The objective of this research was to develop a test method using conventional laboratory techniques to determine if a material is humified. In the tested method, a neutralized extract is prepared using the standardized extraction protocols specified in ISO 19822:2018(E). A portion of the extract is used to determine the concentration of dissolved organic matter on an ash-free basis. A portion of the remaining neutralized extract is diluted to a concentration of 30mg/kg of dissolved organic matter and transferred to a quartz UV cuvette for ultraviolet-visible (UV-Vis) spectroscopy. UV-Vis absorbance is recorded over a wavelength range of 220–500nm at 5nm intervals. The absorbance data are normalized by conversion to scaled absorbance, which is compared to a reference scaled absorbance spectral curve for humic substances to determine if the tested material is humic or non-humic. In a multiple-laboratory validation study, this method was able to differentiate legitimate humic substances from non-humic adulterants in materials intended to be used as ingredients in commercial humic products or for research in a multiple-laboratory validation study.

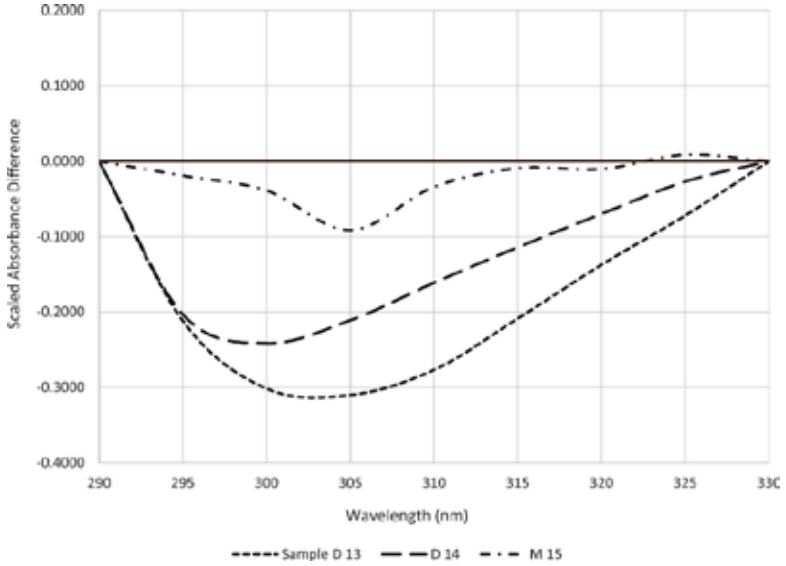

Scaled absorbance difference relative to the humic standard curve for humified materials (orange line at 0.0) and non-humified materials at 30 mg/L concentration of dissolved organic matter (DOM), suggesting there is a measurable difference between humic and non-humic materials.

PI Lawrence Mayhew, EAM Consulting, LLC. Work completed in Virginia Tech Center for Sustainable Nanotechnology (VTSuN) Laboratory.

This work was supported by NSF ECCS-2025151. Mayhew, L., Singh, A. P., Li, P., & Perdue, E. M. (2023), *Journal of AOAC International*, 106(3), 748-759. https://doi.org/10.1093/jaoacint/qsad001

National Research Priority: USDA Global Food Supply and Security

Antimicrobial Coatings

Initially spurred by the COVID-19 pandemic, this research focuses on antimicrobial coatings that can be used to reduce the transmission of infectious agents that are spread by contact. The aim is to coat a variety of common-use objects such as doorknobs, shopping cart handles, gas pump handles, and the buttons of a credit card readers to quickly inactivate any virus particles that end up on those objects. The multifaceted research has investigated effective coating strategies, coating active agents and their antimicrobial mechanisms with a focus on cuprous oxide, and the need to reapply coatings after their finite lifetime. The three 2023 publications below highlight recent breakthroughs in these areas.

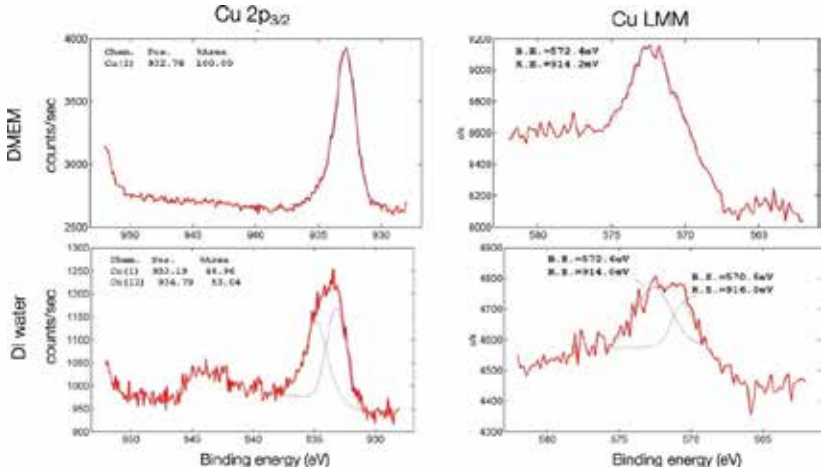

XPS spectra of an aqueous droplet dried onto polyethylene (red lines). Each droplet contained leachate from Cu_2O into DMEM (top) or DI water (bottom). For DMEM, the leachates are Cu^+, whereas for DI water, the leachates are a mixture of Cu^+ and Cu^{2+}. Blue lines are fitted Cu(I) spectra and the green lines are fitted Cu(II) spectra.

PI William Ducker, Virginia Tech. Work completed in Virginia Tech's Nanoscale Characterization and Fabrication Laboratory (NCFL).

This work was supported by NSF Awards CBET-1902364 and CHE-1531834, Virginia Tech's Proof of Concept program under Grant 238079, and by Virginia Tech GRDP program under Grant 118965. Behzadinasab, S., Williams, M. D., Aktuglu, M., Falkinham III, J. O., & Ducker, W. A. (2023), *ACS Applied Materials & Interfaces*, 15(12), 15120-15128. https://doi.org/10.1021/acsami.2c22240

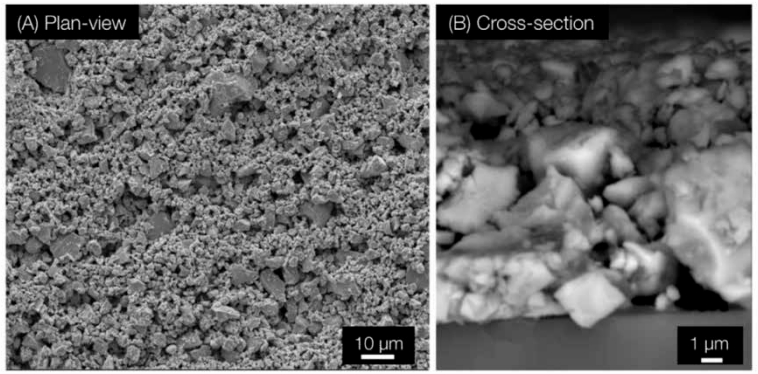

(A) Plan-view and (B) cross-section SEM images of PU/Cu_2O wrap. The thickness of the coating was approximately 12 µm. For SEM imaging, the coating was prepared on glass.

National Research Priority: NIH Goal 2 - Health Conditions and Outcomes Environmental Health and Safety

Quantification of the emission of atmospheric microplastics and nanoplastics via sea spray

There is growing interest in the transfer of micro- and nanoplastics (MNP) to the atmosphere from the ocean via sea spray, and a limited number of studies have quantified this emission. This study addresses the uncertainty surrounding existing global oceanic MNP emission estimates by developing an experimentally based emission parametrization. We conducted systematic laboratory experiments to understand the impact of MNP size, density, and concentration in water on their aerosolization. The results show that the MNP considered in this study, with a diameter of ≤10 μm, can be emitted via bubble bursting, with the aerosolization increasing monotonically with an increase in the concentration in water and decreasing with an increase in the particle size. Floating polyethylene MNP are observed to be less effectively aerosolized than polystyrene MNP dispersed in bulk water. Using the developed emission parametrization, we estimate that the upper limit of yearly MNP oceanic emission is 50.7 (14.2–93.4) quadrillion (1015) pieces $year^{-1}$ and 1.66 (0.72–4.13) t $year^{-1}$. The experimental measurements and ensuing parametrization developed in this study are a timely contribution to the atmospheric microplastic modeling community and will help in further constraining the oceanic source of atmospheric MNP and their potential climatic, environmental, and health implications.

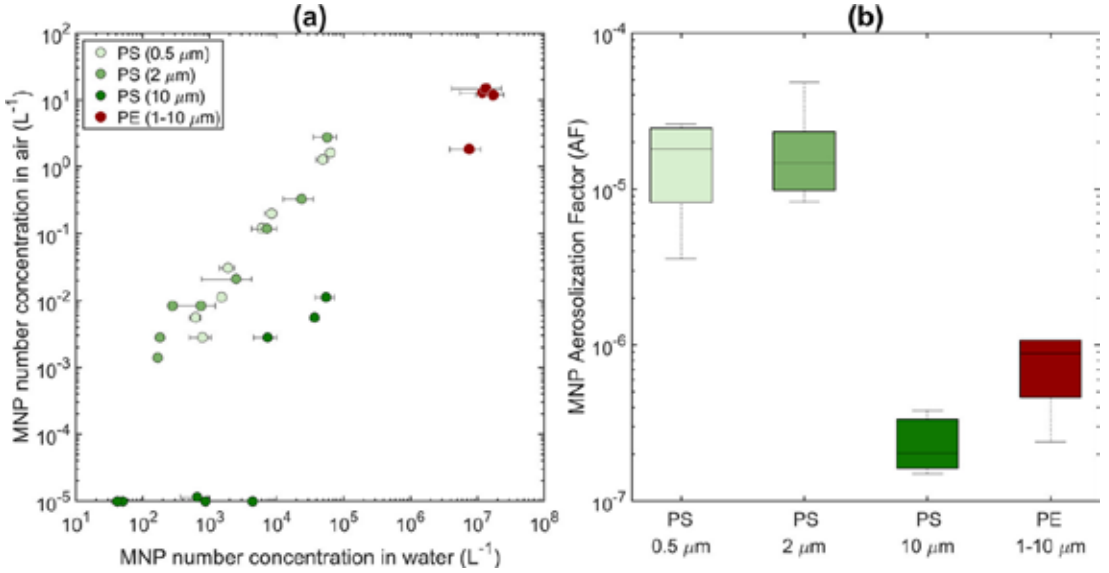

(a) Aerosolized PS and PE MNP concentrations plotted vs the corresponding average concentration in the bulk water and the surface microlayer (SML), respectively, for each aerosolization experiment. (b) Average aerosolization factor (AF), defined as the air-to-water MNP concentration ratio, for each MNP size and type.

PI Hosein Foroutan, Virginia Tech. Work completed in Virginia Tech Center for Sustainable Nanotechnology (VTSuN) Laboratory.

This work was supported by NSF Award CBET-2145532. Harb, C., Pokhrel, N., & Foroutan, H. (2023), *Environmental Science & Technology Letters*, 10(6), 513-519. https://doi.org/10.1021/acs.estlett.3c00164

Colloidal stability of hematite nanoparticles in the presence of a common quaternary ammonium compound at environmentally-relevant concentrations

The fate and behavior of environmental nanomaterials can be strongly affected by organic molecules, including surfactants. Quaternary ammonium compounds (QACs) are surfactants used daily in personal care products, cleaners, and as disinfectants. Due to increasing use worldwide, they are continuously released into water and soils via waste streams and sludge. Hematite (iron oxide, α-Fe_2O_3) nanoparticles (~38 nm) were exposed to a commonly-used QAC, cetyltrimethylammonium chloride (CTAC). At concentrations representative of wastewater influent (100 μg L^{-1}) and sources of concentrated QAC discharge (1000 μg L^{-1}), CTAC limited NP aggregation at air–water interfaces (AWIs). Changing the stability of iron oxide NPs may significantly impact microbial ecosystems and pollutant transport. The study results suggest that in areas with limited wastewater treatment, QACs may significantly affect the mobility and fate of iron oxide NPs, particularly in non-saturated porous zones and turbulent waters.

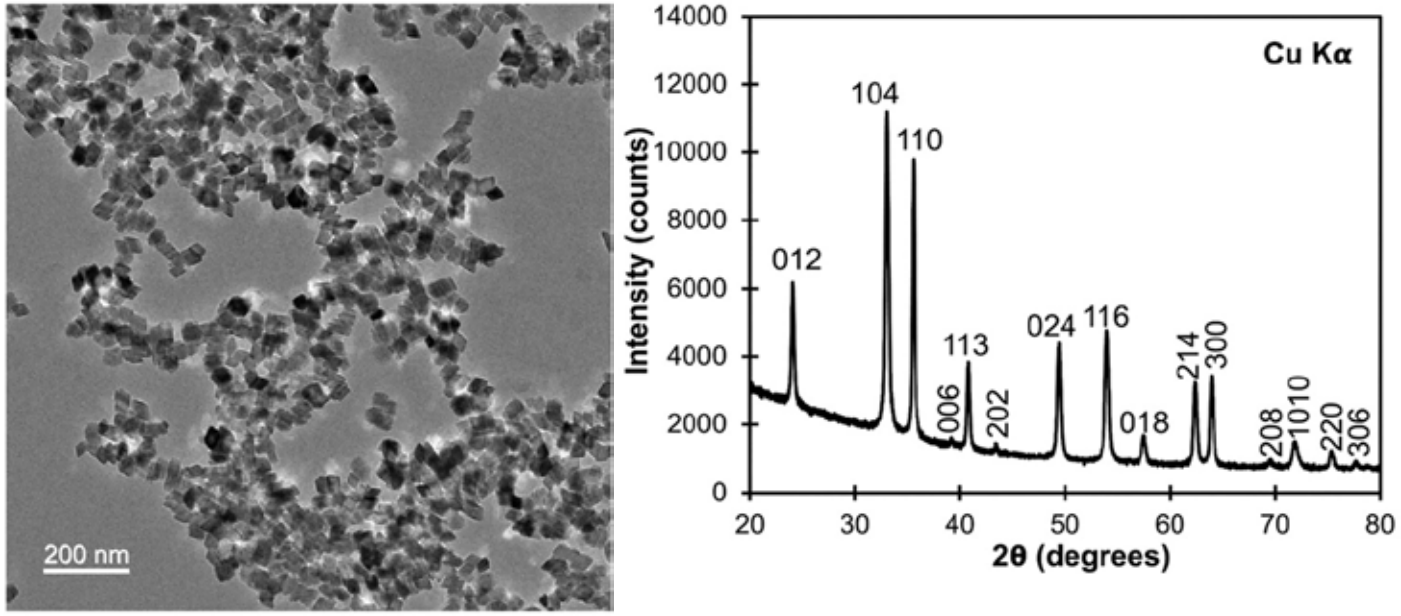

(left) TEM image of hematite nanoparticles; note the rhombohedral morphology. (right) Powder XRD from hematite nanoparticles, indexed.

PI Deborah Aruguete, Penn State Behrend.

This work was supported by Penn State Behrend startup funding and summer undergraduate research grants, Orris C. Hirtzel and Beatrice Dewey Hirtzel Memorial Foundation and Lake Erie Research Institutes, and NSF Award ECCS-2025151. Aruguete, D. M., Zhang, A., Canonaco, C., Sheckler, T., Schmidt, C., & Borgohain, R. (2023). *Environmental Science: Nano*, 10(12), 3476-3485. https://doi.org/10.1039/D3EN00544E

NanoEarth: Education and Outreach
Virginia Tech College of Science Explore Physical Sciences Camp

- Campers: 47 rising 11th & 12th graders from 8 different states and 3 different countries
- 7 Undergraduate and Graduate Student Volunteers: Supported logistics, hands-on demos, engaging campers *(It has been challenging to find volunteers after the pandemic, so having 7 during the summer was a great success)*
- With volunteer support, NanoEarth team focused on instrumentation demos with hands-on time for campers
- As for their time with NanoEarth, 97% of campers agreed or strongly agreed that: a) the activity was interesting to me; b) the activity was intellectually stimulating, and I was able to understand the material, and c) I learned something new.



Student Volunteers


Half of the campers


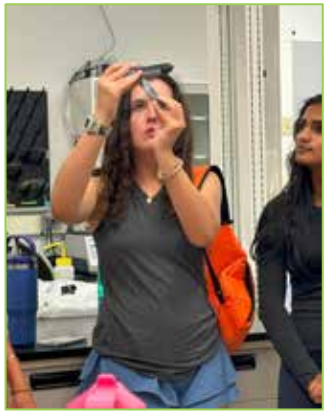



National Nanotechnology Coordinated Infrastructure

NanoEarth

NanoEarth: Education and Outreach
Workforce Development Pilot Programs

- **NanoTrain (Nanotechnology Instrumentation Training Program)**
  - Two undergraduates in Nanoscience Degree Program trained to independently operate the SEM
  - Supported NanoEarth users with SEM analysis
- **New River Community College**
  - Started with tours and demos
  - Two NRCC students were hired as interns
- **Undergraduate Professional Development**
  - New NanoCareers course with NNCI alumni panel
  - Pilot seminar series with MONT

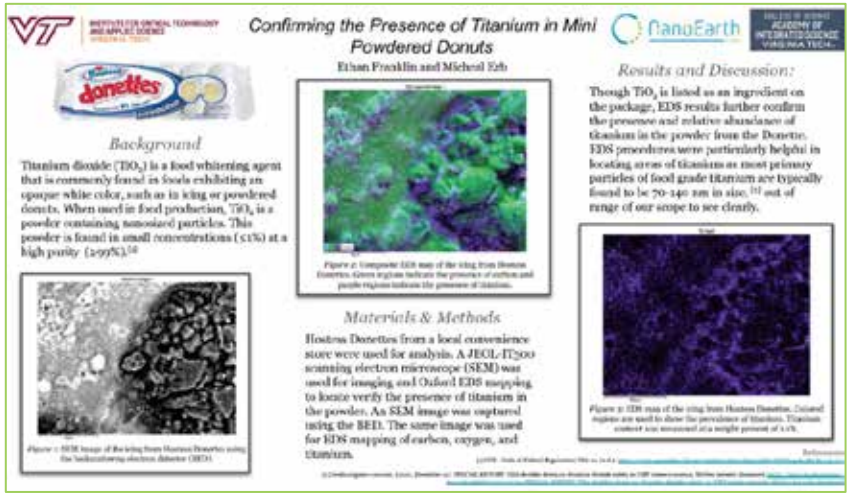

National Nanotechnology Coordinated Infrastructure

NanoEarth